

University of Szeged
Faculty of Pharmacy
Institute of Pharmaceutical Technology and Regulatory Affairs
Head: Prof. Dr. Ildikó Csóka, Ph.D.

Ph.D. thesis

**DEVELOPMENT OF MELOXICAM CONTAINING CARRIER-FREE
“NANO-IN-MICRO” DRY POWDER INHALER SYSTEMS**

By
dr. Petra Party
Pharmacist

Supervisor:

Dr. habil. Rita Ambrus, Ph.D.

SZEGED
2024

PUBLICATIONS RELATED TO THE SUBJECT OF THE THESIS

- I. **Party, P.**; Bartos, Cs.; Farkas, Á.; Szabó-Révész, P.; Ambrus, R.; Formulation and In Vitro and In Silico Characterization of “Nano-in-Micro” Dry Powder Inhalers Containing Meloxicam, *Pharmaceutics*, 13:2, Paper: 211, 18 p. 2021.
(Q1, IF: 6.525)
- II. **Party, P.**; Kókai, D.; Burián, K.; Nagy, A.; Hopp, B.; Ambrus, R.; Development of extra-fine particles containing nanosized meloxicam for deep pulmonary delivery: in vitro aerodynamic and cell line measurements, *European Journal of Pharmaceutical Sciences*, 176, Paper: 106247, 13 p. 2022.
(Q1, IF: 4.6)
- III. **Party, P.**; Ambrus, R.; Investigation of Physico-Chemical Stability and Aerodynamic Properties of Novel “Nano-in-Micro” Structured Dry Powder Inhaler System, *Micromachines*, 14:7, Paper: 1348, 14 p. 2023.
(Q2, IF: 3.4)

PUBLICATIONS NOT RELATED TO THE SUBJECT OF THE THESIS

- I. Chvatal, A.; **Party, P.**; Katona, G.; Jójárt-Laczkovich, O.; Szabó-Révész, P.; Fattal, E.; Tsapis, N.; Ambrus, R.; Formulation and comparison of spray dried non-porous and large porous particles containing meloxicam for pulmonary drug delivery, *International Journal of Pharmaceutics*, 559 pp. 68-75., 8 p. .2019.
(D1, IF: 4.845)
- II. Party, P.; Klement, ML.; Szabó-Révész, P.; Ambrus, R.; Preparation and Characterization of Ibuprofen Containing Nano-Embedded-Microparticles for Pulmonary Delivery *Pharmaceutics*, 15:2, Paper: 545, 15 p. 2023.
(Q1; IF: 5.4)

PRESENTATIONS RELATED TO THE SUBJECT OF THE THESIS

Oral presentation:

- I. Ambrus, R., Chvatal, A., Benke, E., Bartos, Cs., **Party, P.**, Szabóné Révész P. Porlasztva-szárításos eljárás alkalmazása "nano in micro" száraz porinhalációs rendszerek fejlesztése céljából. Gyógyszerkémiai és Gyógyszertechnológiai Szimpózium, Szeged, 2018.
- II. **Party, P.** "Nano-in-micro" száraz porinhalációs készítmények előállítása és vizsgálata, SZTE ÁOK-FOK-GYTK-ETSZK TDK Konferencia, Szeged, 2018.
- III. **Party, P.**, Ambrus, R. Meloxikám tartalmú „nano-in-micro” száraz porinhalációs készítmények formulálása XVI. János Szentágothai Multidisciplinary Conference, Pécs 2019.
- IV. **Party, P.**, Ambrus, R. Nanonizált hatóanyag alkalmazásával száraz porinhalációs készítmények formulálása, 26. Tudományos Diákköri Konferencia, Románia, Marosvásárhely, 2019.
- V. **Party, P.** "Nano-in-micro" száraz porinhalációs készítmények előállítása és vizsgálata, XXXIV. Országos Tudományos Diákköri Konferencia, Debrecen, 2019.
- VI. **Party, P.**, Benke E., Szabóné Révész P., Ambrus, R. Új szerkezet, új lehetőségek a száraz porinhalációs rendszerek fejlesztésében, XIV. Magyar Aeroszol Konferencia, Visegrád, 2019.
- VII. **Party, P.** Nano porlasztva-szárítás alkalmazása porinhalációs rendszerek előállítása céljából, SZTE ÁOK-FOK-GYTK-ETSZK TDK Konferencia, Szeged, 2019.
- VIII. **Party, P.**, Ambrus, R. II. Móra Szakkollégiumi Interdiszciplináris Konferencia, Nanoméretű száraz porinhalációs rendszerek fejlesztése, Szeged, 2019.
- IX. **Party, P.**, Ambrus, R. Száraz porinhalációs készítmények formulálása nano porlasztva-szárító berendezéssel, IX. Eötvözet Konferencia, Szeged, 2020.
- X. **Party, P.**, Ambrus, R. Preparation and characterization of carrier-free dry powder inhalers containing nanosized active ingredient, III. Symposium of Young Researchers on Pharmaceutical Technology, Biotechnology and Regulatory Science, Szeged, 2021.
- XI. **Party, P.** Nano porlasztva-szárítás alkalmazása porinhalációs rendszerek előállítása céljából, 35. Országos Tudományos Diákköri Konferencia, Szeged, 2021.
- XII. **Party P.**, Ambrus R. Száraz porinhalációs készítmények formulálása alveoláris depozíció elérése céljából, XXIV. Tavaszi Szél Konferencia, Miskolc 2021.

- XIII. **Party, P.** Nano porlasztva-szárítás alkalmazása porinhalációs rendszerek előállítására céljából, OTDK PLUSZ, Szeged, 2021.
- XIV. **Party P.,** Kókai D., Burián K., Ambrus R. Meloxicam tartalmú szub-mikronos száraz porinhalációs rendszerek aerodinamikai és sejtvonalas vizsgálata, MKE Kristályosítási és Gyógyszerformulálási Szakosztály, 16. Kerekasztal Konferenciája, Balatonszemes, 2021.
- XV. **Party P.,** Ambrus R. Nanonizált meloxicam tartalmú hordozómentes porinhalációs rendszerek stabilitás vizsgálata, XV. Magyar Aeroszol Konferencia, Hévíz, 2022.

Poster presentations:

- I. Ambrus R., **Party P.,** Chvatal A., Benke E., Szabó-Révész P. Nano-in-micro formulation for further pulmonary administration of meloxicam in lung diseases, 3rd European Conference on Pharmaceutics, Bologna, Olaszország, 2019.
- II. **Party P.,** Ambrus R. Development of nanonized dry powders inhalers to treat different respiratory diseases, EUGLOH Annual Student Research Conference, Szeged, 2020.
- III. **Party P.,** Ambrus R. Development of nanosized active ingredient containing powders for pulmonary drug delivery, EUFEPS Annual meeting 2021, Stockholm, Svédország, 2021.
- IV. **Party P.,** Ambrus R. Development of nanosized drug containing extra-fine powder aerosols: stability aspects, European Aerosol Conference 2023, Malaga, Spanyolország, 2023.

PRESENTATIONS NOT RELATED TO THE SUBJECT OF THE THESIS

Oral presentations:

- I. **Party P.,** Klement M. L., Ambrus R. Formulation and investigation of ibuprofen containing inhalable nanocrystals to treat cystic fibrosis, IV. Symposium of Young Researchers on Pharmaceutical Technology, Biotechnology and Regulatory Science, Szeged, 2022.
- II. **Party P.,** Pisman Z. I., Ambrus R. High-dose ibuprofen containing carrier-free dry powder inhalers for the therapy of cystic fibrosis, V. Symposium of Young Researchers on Pharmaceutical Technology, Biotechnology and Regulatory Science, Szeged, 2023.

- III. Piszman Z. I., **Party P.**, Ambrus R. Ibuprofén és mannit tartalmú száraz porinhalációs rendszerek fejlesztése cisztás fibrózis kezelése céljából, VI. Fiatal Technológusok Fóruma, Budapest, 2023.
- IV. **Party P.**, Klement M. L., Ambrus R. Integráló technológiák alkalmazása ibuprofén tartalmú inhalációra alkalmas „nano-in-micro” szemcsék képzése céljából, MKE Kristályosítási és Gyógyszerformulálási Szakosztály, 14. Kerekasztal Konferenciája, Balatonszemes, 2023.
- V. **Party P.**, Sümegi S. S., Ambrus R. Formulation and investigation of nanosized piroxicam containing orodispersible lyophilisate, V. Symposium of Young Researchers on Pharmaceutical Technology, Biotechnology and Regulatory Science, Szeged, 2024.

Poster presentations:

- I. Chvatal A., **Party P.**, Farkas Á., Balásházy I., Ambrus R., Szabó-Révész P., Fattal, E., Tsapis M. In vitro and in silico evaluation of carrier-free porous inhalable particles, 12th Central European Symposium on Pharmaceutical Technology and Regulatory Affairs, Szeged, 2018.
- II. **Party P.**, Ambrus R. Development of ibuprofen containing innovative dry powder inhalers for the treatment of cystic fibrosis, 13th World Meeting on Pharmaceutics, Biopharmaceutics and Pharmaceutical Technology, Rotterdam, Hollandia, 2022.
- III. **Party P.**, Ambrus R. Development of combined inhalable formulation of ibuprofen and mannitol for the treatment of cystic fibrosis, 9th BBBB International Conference on Pharmaceutical Sciences, Ljubljana, Szlovénia, 2022.
- IV. **Party P.**, Ambrus R. Hordozómentes ibuprofén tartalmú száraz porinhalációs rendszerek fejlesztése cisztás fibrózis kezelésének céljából, Gyógyszertechnológiai és Ipari Gyógyszerészeti Konferencia, Siófok, 2022.

ABBREVIATIONS

A	Area under the curve
A549 cells	Adenocarcinomic human alveolar basal epithelial cells
ACI	Andersen cascade impactor
Actb	Actin beta
A _m	Surface area of the membrane
ANOVA	Analysis of Variance
API	Active pharmaceutical ingredient
APS	Aerodynamic particle sizer
BCS	Biopharmaceutical Classification System
C _d	Concentration of the donor phase
CF	Cystic fibrosis
CI	Carr index
COPD	Chronic obstructive pulmonary disease
COVID-19	Coronavirus disease of 2019
COX-2	Cyclooxygenase-2 enzyme
C _t	Threshold cycles
D[0.1]	10% of the volume distribution is below this value
D[0.5]	50% of the volume distribution is below this value
D[0.9]	90% of the volume distribution is below this value
D _{ae}	Aerodynamic diameter
DLS	Dynamic light scattering
DMSO	Dimethyl sulfoxide
DPI	Dry powder inhaler
DSC	Differential scanning calorimetry
EF	Emitted fraction
ELISA	Enzyme-linked immunosorbent assay
EMA	European Medicines Agency
EU	European Union
FDA	U. S. Food and Drug Administration
FPF	Fine particle fraction
HR	Hausner ratio
ICH	The International Council for Harmonization of Technical Requirements for Pharmaceuticals for Human Use
IL-6	Interleukin 6
IUPAC	International Union of Pure and Applied Chemistry
IV	Inhalation volume

J	Flux
K _p	Permeability coefficient
LEU	L-leucine
LPS	Lipopolysaccharide
MDI	Metered dose inhaler
MMAD	Mass median aerodynamic diameter
MTT	3-(4,5-dimethyl-2-thiazolyl)-2,5-diphenyl-2H-tetrazolium bromide
M _w	Molecular weight
MX	Meloxicam
NSAID	Non-steroidal anti-inflammatory drug
NSCLC	Non-small cell lung cancer
NTA	Nanoparticle tracking analysis
OCA	Optical contact angle
OD	Optical density
PdI	Polydispersity index
PM	Physical mixture
PSD	Particle size distribution
PVA	Polyvinyl alcohol
qPCR	Quantitative polymerase chain reaction
RI	Refractive index
RNA	Ribonucleic acid
S.D.	Standard deviation
SEM	Scanning electron microscopy
SPD	Spray dried
SSA	Specific surface area
ST	Surface tension
T _g	Glass transition temperature
t _{in}	Inhalation time
X _c	Degree of crystallinity
XRPD	X-ray powder diffraction
Z-average	Average hydrodynamic diameter
ZrO ₂	Zirconium-dioxide
ζ pot.	Zeta potential
ρ _b	Bulk density
ρ _t	Tapped density

TABLE OF CONTENTS

1. Introduction	1
2. Aim of the work	2
3. Literature background	3
3.1. Burden of the chronic respiratory diseases	3
3.2. Advantages of the local treatment of the airway conditions	3
3.3. Dry powder inhalers, as an effective drug delivery system	3
3.4. Deposition of the medications in the respiratory system	5
3.5. Advantages of the nanoparticles in the pulmonary drug delivery	7
3.6. Particle engineering techniques for “nano-in-micro” DPIs	8
3.7. Stability aspects of the novel DPIs	10
3.8. Meloxicam in the pulmonary therapy	11
4. Materials	13
4.1. Active pharmaceutical ingredient	13
4.2. Excipients	13
5. Preparation methods of the “nano-in-micro” DPI systems	14
5.1. Production of the nanosuspension by wet milling	14
5.2. DPI formulations by spray drying	15
5.2.1. Mini spray drying method	15
5.2.2. Nano spray drying method	16
5.3. Preparation of the physical mixtures	17
6. Characterization of the nanosuspension	18
6.1. Particle size analysis	18
6.1.1. Laser diffraction based particle size measurement	18
6.1.2. Dynamic light scattering investigations	18
6.1.3. Nanoparticle tracking analysis	18
6.2. Determination of the surface tension	18

7.	Solid phase characterization	19
7.1.	Particle size analysis	19
7.1.1.	Laser diffraction based particle size measurement	19
7.1.2.	Dynamic light scattering analysis	19
7.2.	Morphology investigation	19
7.3.	Density and powder flow measurement	19
7.4.	Determination of the crystallinity	20
7.4.1.	Thermoanalytical measurement	20
7.4.2.	Analysis of the crystalline structure	20
7.5.	Solubility test	20
7.6.	<i>In vitro</i> and <i>in silico</i> aerodynamic characterization of the DPI systems	21
7.6.1.	Andersen cascade impactor measurement	21
7.6.2.	<i>In silico</i> aerodynamic characterization	22
7.6.3.	Aerodynamic particle size analysis using the Spraytec® device	22
7.6.4.	Aerodynamic particle size analysis with particle counter	23
7.7.	<i>In vitro</i> investigations of the pulmonary dosage form	24
7.7.1.	<i>In vitro</i> dissolution test using the conventional paddle method	24
7.7.2.	<i>In vitro</i> dissolution test using the paddle method combined with ACI	24
7.7.3.	<i>In vitro</i> permeability investigation	25
7.7.4.	<i>In vitro</i> cell line investigations	26
7.8.	Stability test	27
7.9.	Statistical analysis	27
8.	Result of the characterization of the nanosuspension	28
8.1.	Particle size analysis	28
8.1.1.	Results of the laser diffraction based particle size distribution	28
8.1.2.	Outcomes of dynamic light scattering investigation	28

8.1.3.	Results of the nanoparticle tracking analysis.....	28
8.2.	Surface tension results of the nanosuspension.....	29
9.	Results of the solid phase characterization.....	29
9.1.	Particle size analysis	29
9.1.1.	Results of the laser diffraction based particle size distribution	29
9.1.2.	Outcomes of the dynamic light scattering investigation.....	30
9.2.	Findings of the morphology investigation	30
9.3.	Results of the density and powder flow test	31
9.4.	Analysis of the crystallinity	32
9.4.1.	Results of the thermoanalytical measurement	32
9.4.2.	Findings of the crystalline structure investigation.....	32
9.5.	Effects of the formulation on the solubility of MX	33
9.6.	Evaluation of the <i>in vitro</i> and <i>in silico</i> aerodynamic tests	34
9.6.1.	Outcomes of the Andersen cascade impactor measurement.....	34
9.6.2.	Findings of the <i>in silico</i> aerodynamic characterization	36
9.6.3.	Results of the characterization by Spraytec® device.....	37
9.6.4.	Particle size results according to particle counter.....	37
9.7.	Results of the <i>in vitro</i> investigations of the pulmonary dosage form	39
9.7.1.	Conclusion of the <i>in vitro</i> dissolution test	39
9.7.2.	Results of the <i>in vitro</i> permeability test.....	40
9.7.3.	Consequences of the <i>in vitro</i> cell line investigations.....	41
9.8.	Results of the stability test	42
10.	Conclusions	44
11.	Novelty and practical relevance of the work	46

1. Introduction

The burden of chronic lung diseases has increased dramatically over the past decades. In terms of prevalence, the five most prominent lung diseases are asthma, tuberculosis, chronic obstructive pulmonary disease (COPD), lung cancer and pneumonia caused by various infections. Local treatment of the conditions compared to oral or parenteral drug delivery could be more efficient with better patient compliance.

Among the pulmonary drug delivery systems, the application of dry powder inhalers (DPIs) continues to grow in therapy due to their outstanding stability, ease of use and low production costs. Advantages compared to propellant aerosols are that the inhaled air stream delivers the drug to the airways, which can significantly reduce greenhouse gas emissions. Compared to conventional carrier-based DPIs, carrier-free DPIs are more effective, because the active pharmaceutical ingredient (API) creates a complex system with additives. Due to their special morphology, structure, and better aerodynamic properties, even low respiratory function is enough for proper lung deposition.

The majority of APIs used today are poorly water-soluble. Nanosized drugs can provide higher bioavailability due to their smaller particle size and larger specific surface. The various size reduction methods include bottom-up and top-down approaches. Water-solubility can be improved by applying particle engineering techniques that also enable new, alternative administration routes.

Although pulmonary therapy would benefit from the use of nanoparticles, there is no commercially available formulation yet. The main challenge is that the required aerodynamic particle size should be between 1-5 μm . For this, the “nano-in-micro” structure could be a solution, having the advantages of nanosized drugs while providing adequate aerodynamic properties. The combination of wet milling, as a top-down particle size reduction method, and spray drying, as a bottom-up technology, could be suitable for their preparation. These systems deposit deeper into the respiratory tract compared to the conventional formulations, while overcoming its elimination mechanisms.

It is difficult in pharmaceutical technology to find organic solvent-free, scalable, cost-effective and time-saving techniques that are suitable for the preparation of the “nano-in-micro” DPIs. This thesis reports the development of DPIs containing the non-steroidal anti-inflammatory agent (NSAID) meloxicam (MX) using a combined preparation technique with the aim of effective pulmonary delivery.

2. Aim of the work

This Ph.D. work aimed to develop innovative MX containing carrier-free “nano-in-micro” DPIs for pulmonary delivery. Efficiency in the lungs is based on the appropriate particle properties, aerodynamic diameter and proper drug release. The research work was planned considering the development requirements [1,2] according to the following steps:

- I. To review the literature on basic properties, suitable excipients, preparation techniques, and mechanism of action of “nano-in-micro” DPI systems and identify the available NSAID containing DPI formulations.
- II. To develop the formulation strategy and composition without organic solvent to achieve MX nanosuspension *via* wet milling, with particle size below 200 nm.
- III. To optimize the preparation method and composition of MX-containing “nano-in-micro” particles, with proper particle size, narrow size distribution and spherical morphology, using mini and nano spray drying devices. The DPIs were designed to have a particle size in the 2–5 μm range and particles smaller than 2 μm respectively. A comparison study was conducted to establish the advantages and disadvantages of the two spray drying methods, while the performance of the selected additives was observed during the investigations.
- IV. To determine the *in vitro* and *in silico* aerodynamic properties of DPIs at different flow rates using the Andersen cascade impactor (ACI) and the stochastic lung model to prove the proper lung deposition.
- V. To describe the pulmonary applicability of the formulation, *in vitro* drug release study and *in vitro* permeability study were performed under pulmonary conditions. In addition, *in vitro* cytotoxicity and anti-inflammatory tests were implemented.
- VI. Lastly, our aim was to test the physical stability of the DPI in a long-term study according to the International Council for Harmonization (ICH) Q1A guideline.

In overall, the goal was to provide novel MX containing “nano-in-micro” DPIs for the treatment of respiratory diseases by implementing the therapeutic advantages of nanoparticles and an alternative delivery route. In addition to the application of modern particle engineering techniques, the development of a comprehensive investigation protocol for DPIs was also aimed. The formulation strategy could be easily adapted to existing APIs, therefore opening up modified therapeutic protocols and advanced treatments, which could lead to long-term cost reduction in chronic treatments.

3. Literature background

3.1. Burden of the chronic respiratory diseases

Chronic lung diseases are a significant issue worldwide and the primary source of both morbidity and mortality. The five most severe lung diseases in terms of prevalence are lung cancer, COPD, pneumonia caused by different infections, asthma, and tuberculosis. Due to the fact that the majority of the affected people live in low- and middle-income countries, the true prevalence and burden of these conditions in adults is unknown. Of all cancers, lung cancer accounts for nearly 20% of deaths. Lower respiratory infections are among the top 3 causes of death in adults and children. Infection in youth may also predicts chronic lung disease later in life. More than 200 million people are affected by COPD, 65 million of whom are already in advanced stages. Moreover, the disease is extremely underdiagnosed. Nearly 3 million people die from COPD every year, and this number is continually increasing. Two major risk factors of COPD are air pollution and smoking. In addition to influenza, the current spread of a new type of coronavirus shows how serious a problem these diseases are in health, social and economic terms. Currently, symptomatic managements are available to improve quality of life, which represents a significant financial burden. In view of these facts, the development of effective therapeutic protocols, innovative and safe medications is considered a current challenge [3–5].

3.2. Advantages of the local treatment of the airway conditions

Pulmonary administration is one of the most utilized treatments for local respiratory disorders. It is considered a non-invasive approach with enhanced patient compliance. Lungs are characterized by their large surface area (100 m²), abundant blood supply, high permeability of the thin epithelial layer (0.2–0.7 μm), low enzymatic activity, and the ability to avoid first-pass metabolism [6–8]. The beneficial characteristics of the lung enable the administration of larger drug concentrations to the airways for enhanced efficacy and to limit adverse effects. This makes pulmonary delivery an attractive route for targeting and achieving rapid onset of action [9–11].

3.3. Dry powder inhalers, as an effective drug delivery system

Nebulizers, MDIs (metered dose inhalers), soft mist inhalers and DPIs are the most frequently used pulmonary medication delivery devices. In terms of environmental aspects, MDIs have a larger carbon footprint than DPIs [12]. Hydrofluorocarbon propellants are used in MDIs, which are greenhouse gases that persist in the atmosphere for years. As in

DPIs the drug delivery is driven by the inhalation flow; therefore, they are absent of these propellants. This combined with the fact that they only have a carbon footprint of 20 g CO₂ per dose compared to 500 g CO₂ for MDIs results in them having a lower greenhouse gas emission potential [13]. DPIs are also cost-effective and portable tools that make it simple for the patient to administer the medication. DPIs do not require the need of hand-breath-coordination as MDIs, which makes them attractive for long-term therapy in chronic lung diseases. On the other hand, education is essential for the correct use of the products. Furthermore, due to their solid form, DPIs have superior long-term stability and do not require cold chain storage [10,14,15].

DPIs can be categorized, as carrier-based and carrier-free systems. The APIs in carrier-based DPI systems are attached to the surface of a large carrier (50–100 µm), which is typically lactose, mannitol or glucose [16]. During inhalation the API reaches the lungs, while the large carrier deposits in the upper airways. Typically, a significant amount of API remains in the carrier, resulting in inadequate lung deposition. Optimizing the aerosolization of the products is essential for proper dispersion and deposition in the airways. To improve the therapeutic effect, new carrier-free DPIs have been developed. Two main groups are distinguished: dense and non-dense particles (Figure 1.).

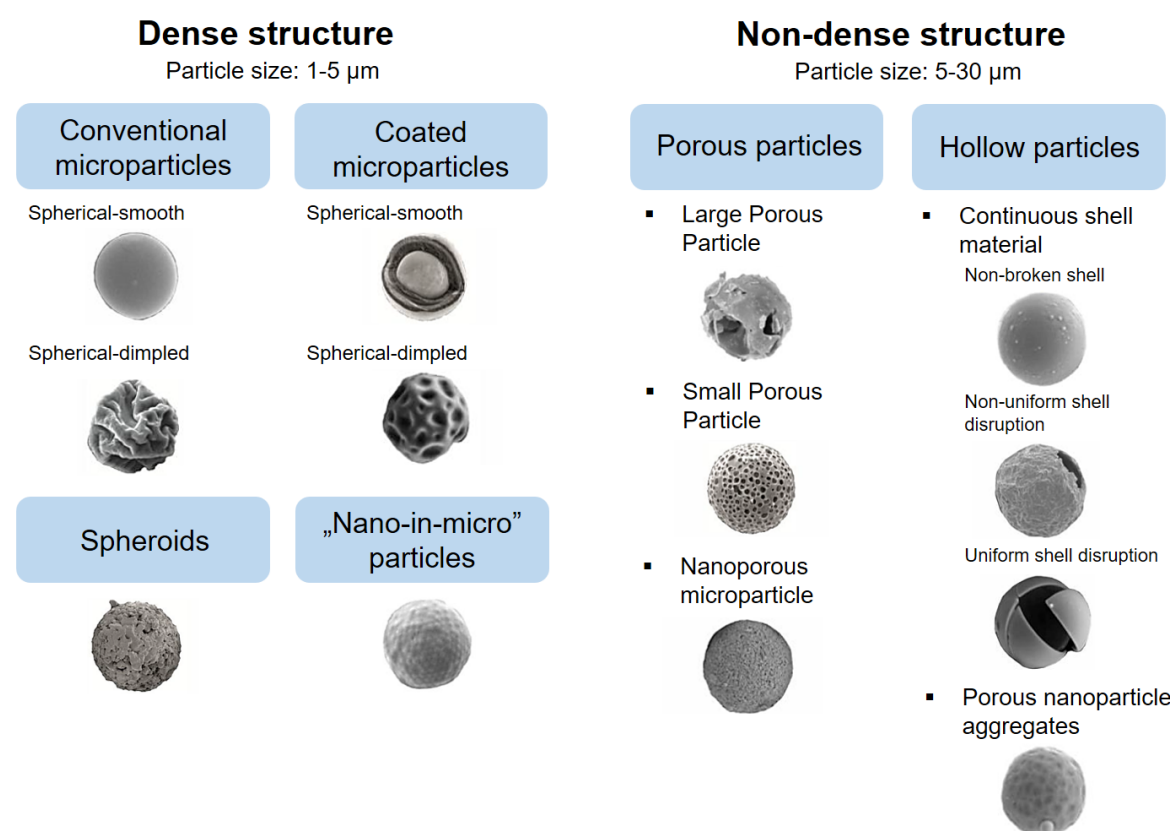


Figure 1. Different types of carrier-free DPIs [17].

The carrier-free formulations aimed to reduce the intrinsic cohesion of the particles, thus increasing the dispersion and helping to deliver from the inhaler. In this case, a complex powder is formulated by combining API with appropriate excipients, leading to optimal aerodynamic properties [18–20]. Additives for carrier-free DPI formulations are hydrophobic materials protecting against moisture, lipids for coating, amino acids for improved aerosol efficiency and biodegradable polymers (Table 1.) [11,21]. The excipients used in oral products are mostly not suitable, due to the different conditions in the airways compared to the intestines. Additionally, exogenous materials in the lungs can cause disadvantageous accumulation [22,23]. Therefore, the approved excipients are limited and new materials have to undergo costly toxicity evaluations, adding extra uncertainty to the development [11,24].

Table 1. Examples of the most frequently used excipients of carrier-free DPI formulations.

Type	Example	Functions
Amino acids	D or L-leucine, glycine, alanine	Enhance dispersibility and aerosolization properties, moisture protection [25–28]
Polymers	Poly(lactic-co-glycolic acid), poly vinyl alcohol, polyethylene glycol, polyvinylpyrrolidone	Matrix former, film former, stabilizer, prolonged drug release [29–32]
Lipids	Cholesterol phosphatidylcholine, dipalmitoylphosphatidylcholine, Distearoylglycerophosphocholine,	Natural lung surfactant, matrix former, coating, absorption enhancer [33–35]
Cellulose derivatives	Carboxy methyl cellulose, hydroxypropyl methyl cellulose, hydroxypropyl cellulose	Matrix former [36,37]
Other additives	Alginates	Matrix former, mucoadhesive [38,39]
	Ammonium carbonate	Enhance porosity, reduce density [40–42]
	Chitosan	Mucoadhesive polymer, bioavailability enhancer, fine carrier [43–45]
	Cyclodextrin	Solubility and permeability enhancer, improve dispersibility [46,47]
	Magnesium stearate	Moisture protection, lubricant [48,49]

3.4. Deposition of the medications in the respiratory system

In addition to the components, the particle size of DPIs plays a key role in the deposition pattern. To understand the deposition, the structure of the airways must be known. The respiratory area and the conducting airways are the two main parts, which could be further divided into generations. The conducting airways region is found in the

upper part and splits into the respiratory region after 17 bifurcations from the trachea. It is made up of the mouth, nose, trachea, bronchi, bronchioles, and terminal bronchioles. The alveolar ducts, alveolar sacs, and respiratory bronchioles make up the respiratory area. Moving from the trachea to the distal airways, the diameter of the airways decreases and their number simultaneously increases (Figure 2.) [50,51].

The deposition of inhaled particles depends on the distinct structural parts of the airways [52]. There are three principal mechanisms of deposition. Inertial impaction affects particles that are larger than 5 μm . These particles are unable to follow the changes of gas flow. Therefore, they impact on walls of the upper airways. Gravitational sedimentation is based on the settling of particles under the action of gravity and occurs in the smaller airways. This deposition mechanism can be observed for particles sized 1–5 μm in diameter. Random motions of the particles caused by their collisions with gas molecules result in deposition by Brownian diffusion. It becomes the dominant deposition mechanism for particles less than 1 μm in diameter. These particles are the most effective in the alveolar region (Figure 2.) however they have the highest chance for exhalation. [53,54].

Consequently, controlling the aerodynamic diameter at 1–5 μm is required for the transportation of particles to the desired area in the lungs [55]. Particles in the 0.5-1.5 μm size range are ideal for deposition in the smaller airways, due to their low deposition in upper regions [56–58]. The application of micronized particles (2-5 μm) and extra-fine particles ($< 2 \mu\text{m}$) could be beneficial for the treatment of different lung segments [59–62].

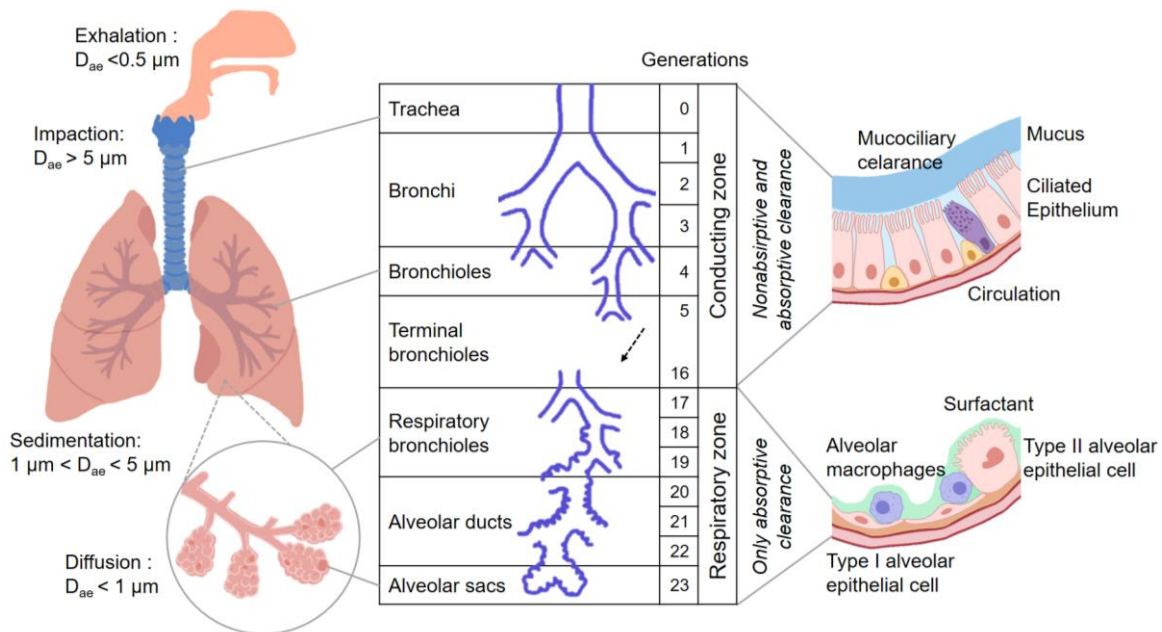


Figure 2. Mechanism of the particles, structure and defensive mechanism of the respiratory system.

3.5. Advantages of the nanoparticles in the pulmonary drug delivery

Nanotechnology is currently revolutionizing drug delivery, including the field of pulmonary administration. The definition of nanomaterials according to the European Union (EU) requires the particle size to be under 100 nm [63]. Pharmaceutical nanoparticles are defined as individual particles with a size below 1 μm . This met the definition of products prepared by nanotechnology according to the U. S. Food and Drug Administration (FDA) [64]. Typically the mean particle diameter is between 200 and 500 nm [65,66]. The reduced size and larger specific surface area enhance the dissolution rate of poorly water-soluble drugs, where this is the rate-limiting step for absorption. Therefore, nanoparticles increase intracellular drug delivery, resulting in higher bioavailability [66,67].

The fate of the inhaled drug nanoparticles could be characterized according to the Inhalation-Based Biopharmaceutics Classification System (iBCS). It differs from the conventional Biopharmaceutics Classification System (BCS, giBCS), as giBCS focuses on systemic drug absorption and activity outside of the gastrointestinal tract, while the iBCS system focuses on local, pulmonary drug delivery. The residence time in the lung for drugs depends on non-absorptive and absorptive clearance mechanisms as well as the physicochemical properties of the drug and the formulation (Figure 2.). The border between high and low permeability in the iBCS grid is established by considering absorption through passive transcellular permeability (Table 2.) [68–70].

Table 2. Characteristics of oral and inhaled drugs based on BCS.

Class	Solu- bility	Permea- bility	giBCS	iBCS
I.	high	high	complete dissolution, complete absorption	complete dissolution, rapid absorptive clearance e.g. terbutaline-sulfate
II.	low	high	incomplete dissolution, complete absorption	incomplete dissolution, dissolution dependent absorptive and non-absorptive clearance and retention e.g. mometasone-fluorate
III.	high	low	complete dissolution, incomplete absorption	complete dissolution, permeability dependent absorptive clearance and retention e.g. ipratropium-bromide
IV.	low	low	incomplete dissolution, incomplete absorption	incomplete dissolution, dissolution and/or permeability dependent absorptive, non-absorptive clearance and retention

Proper formulation is essential for efficient transport of the nanosized API to the respiratory system. The development of “nano-in-micro” or nano-embedded microparticles for pulmonary application can harmonize the advantages of nanoparticles with the aerodynamics of microparticles and could achieve an improved bioavailability and aerosolization behavior [71,72]. If the powders come into contact with the lung lining fluid in the appropriate parts of the airways, the particles can disintegrate to their nano-subunits and spread on the epithelial surface, resulting in an increased absorption and more homogenous distribution [73]. Due to the large surface area of the lungs dissolution and penetration are exceptionally fast. Because of their size nanoparticles can easily enter through the mucus, eliminating the mechanism of mucociliary clearance. The systems could prolong the retention time of inhaled nanoparticles, providing a sufficient duration of time for drug release, leading to improved bioavailability. The liberated nanosized drug can effectively reach the epithelium, because they are not eliminated by the size-dependent uptake of the alveolar macrophages (Figure 2.) [52,57,73]. Nanoparticles have advantages to get through the biological barriers and can improve drug uptake into cells through various endocytosis-based pathways as well [71,74,75]. In general, the required dosage can be reduced due to enhanced drug transport [76].

However, the prolonged residence of the particles in the lung may lead to cellular injury, biological responses and undesired effects. The impacts (e.g. increased reactivity, oxidative stress, cellular injury and interruption of cellular processes) of nanoparticles are significantly influenced by their properties. Therefore, to characterize nanoparticles for toxicological investigations, a number of nanomaterial characteristics must be considered including size distribution, surface area, morphology, solubility, chemical composition and particle agglomeration [77–79].

3.6. Particle engineering techniques for “nano-in-micro” DPIs

Despite the growing number of research works devoted to the development of inhalable “nano-in-micro” particles (Table 3.), only a few formulations have entered clinical trials so far (e.g. formulations containing nanosized atropine sulfate [80], remdesivir [81] and silver [82]). There are no “nano-in-micro” DPI products that have been approved to date as individually applicable medications, only a nebulizer formulation (Arikayce[®], an amikacin containing liposome) [76,83,84].

Table 3. Examples for studies on the development of nanoparticle based dry powders for local delivery.

API	Indication	Type of the nanoparticle
Cefixime	Pulmonary infections	Polymeric nanoparticle [85]
Ciprofloxacin	Pulmonary infections	Polymeric micelle [86]
	Bronchiectasis	Nanoparticle complex [87]
Docetaxel	Lung cancer	Polymeric nanoparticle [88]
Ethambutol	Tuberculosis	Solid lipid nanoparticle [89]
Gefitinib	Lung cancer	Solid lipid nanoparticle [90]
Ibuprofen	Cystic fibrosis	Polymeric nanoparticle [91]
Isoniazid	Tuberculosis	Polymeric nanoparticle [92]
Itraconazole	Aspergillosis	Polymeric nanoparticle [93]
Ivacraftor	Cystic fibrosis	Polymeric nanoparticle [94]
Ketoprofen	Cystic fibrosis	Polymeric nanoparticle [95]
Ketotifen	Asthma	Core-shell complex [96]
Levofloxacin	Tuberculosis	Polymer-lipid hybrid nanoparticle [97]
	Biofilm infection	Polymeric nanoparticle [98]
Methotrexate	Lung cancer	Polymeric nanoparticle [99]
miRNA	COPD	Polymeric nanoparticle [100]
N-acetylcisteyne	Tuberculosis	Polymeric nanoparticle [101]
Paclitaxel	Lung cancer	Polymeric micelle [102]
Pneumococcal surface protein A	Pneumonia	Polymeric nanoparticle [103]
Rapamycin	Lung inflammation	Lipid/polymer hybrid nanoparticle [104]
Rifampicin	Tuberculosis	Polymeric nanoparticle [105]
Salbutamol	Asthma	Liposome [106]
Sodium cromoglicate	Allergy	Pure drug nanoparticle [107]
Thymoquine	COVID-19	Polymer-amino acid nanoparticle [108]
TNF- α siRNA	Lung inflammation	Polymer-lipid hybrid nanoparticle [109]

A major challenge is the reproducible and scalable production of nanoparticle based DPIs. A prosperous technique for them is the preparation of a nanosuspension by wet milling followed by solidification, using spray drying [37,110]. Usually, this combination is environmentally friendly because it does not require any kind of organic solvent.

Milling is a common, scalable, cost and time-effective method used in the pharmaceutical industry to reduce particle size to improve the solubility and subsequently the bioavailability of poorly water-soluble APIs [111–113]. During wet milling the drug is suspended in a liquid medium, such as surfactants and/or polymers, to stabilize the drug

particles [114]. The high surface energy of nanoparticles in suspension form, would promote their aggregation by Ostwald ripening and recrystallization [115]. Therefore, the solidification of the suspension is beneficial, because it combines the advantages of liquid nanosuspension (e.g. enhanced dissolution and solubility) with the benefits of solid formulation formulations (e.g. stability and easy handling) by producing microsized nanoparticle agglomerates suitable for pulmonary delivery [116].

Spray drying is a particle-engineering technique that is used to produce respirable powders for drug delivery to the lung [117], which is utilized in laboratory and industrial environments. Its main advantage is the ability to precisely control the particle size, which would be crucial for effective aerosol performance. Compared to other popular drying methods, such as lyophilization, it is less expensive, requires less time and energy [118]. The spray dried (SPD) powders have enhanced resistance to various environmental factors (such as light, oxidation, and temperature) [119]. The frequently used laboratory spray dryers, the Nano Spray Dryer and the Mini Spray Dryer are easily scalable to industrial level [118].

3.7. Stability aspects of the novel DPIs

One of the most important factors for ensuring the safety and efficacy of pharmaceutical products is stability [120]. The physicochemical integrity of API and/or excipients, along with any quantitative change that exceeds acceptable limits, could affect the drug delivery profile and potentially cause adverse effects or counteract the therapeutic benefit. Stability testing generally aims to demonstrate that a product remains within the specifications for the expected shelf life when stored under suggested circumstances [2].

Drug nanoparticle stability issues such as crystal formation, sedimentation and agglomeration may occur during production, transportation, storage and application [121]. For efficient therapy it is necessary to maintain the quality-influencing properties of the products. Proper attention should be paid to drug nanocrystal stability difficulties during the development of pharmaceutical products [122]. In general, liquid formulations are less stable than solid dosage forms. However, when nanosized APIs are applied, including "nano-in-micro" DPIs, the risk of aggregation should be taken into consideration.

The preparation methods have a significant impact on the stability of the DPIs. During milling, recrystallization may occur as a result of mechanical activation and the formation of local amorphous sites at the surface of the particle. The solutions to this issue

are to coat the surface of the particles and/or maintain a controlled storage environment in terms of temperature and relative humidity. For amorphous materials, recrystallization could be a challenge during spray drying. Controlling the process parameters and the composition of the formulation maintain the physical stability and optimal aerosol performance of DPIs [10]. Application of hydrophobic excipients (e.g. metal stearates, amino acids) and amorphous additives with high glass transition temperature (T_g) (e.g. isoleucine, trehalose) could be beneficial; however, their safety profile for pulmonary delivery may be a limitation. In addition to the excipients, the packaging of the DPI (e.g. the type of the device, blisters, capsules) may also affect the stability. It is essential to select the right materials to prevent moisture uptake, which may modify the surface characteristics and crystallinity of the powder [123].

3.8. Meloxicam in the pulmonary therapy

The application of NSAIDs in the pulmonary therapy is not common, due to their bronchoconstrictive side effect. However, their application could be useful in different lung diseases [124]. There are a few NSAID containing DPI in the literature (e.g. ibuprofen and ketoprofen in cystic fibrosis (CF) [37,91,95,125,126], celecoxib in non-small cell lung cancer (NSCLC) and coronavirus disease of 2019 (COVID-19) caused inflammation [127], acetylsalicylic acid in tuberculosis and other lung inflammation [128]). Furthermore, DPIs could be used to induce the systemic anti-inflammatory effect of diclofenac [129] or indomethacin, while reducing side effects compared to oral application [130].

MX is a poorly water-soluble selective cyclooxygenase-2 (COX-2) inhibitor, NSAID [131]. Currently, the main indications of MX are arthritis and osteoarthritis in human therapy. MX is commercially available only in oral, intravenous and intralesional delivery routes [132]. The development of novel delivery systems and/or changes in administration routes is an alternative way to reposition drugs that is widely used by the pharmaceutical industry due to the notable cost and time reduction. A great amount of experience with MX and different additives was collected in the research group. Previous studies were concerned with the particle size reduction of MX *via* wet milling [133,134]. Carrier-based [135,136] and carrier-free DPIs [137,138] have been developed by spray drying using different APIs including MX.

Pharmacological studies demonstrated its antioxidant, antifibrotic and analgesic activity, therefore MX containing “nano-in-micro” DPIs could be advantageous to improve

the condition of patients with CF, COPD, NSCLC and lung inflammation (Figure 3.) [139–144]. In CF the right upper lobe is most likely to develop inflammation and bronchiectasis, in comparison to this, in the lower lobes, mucus plugging and air trapping more frequent [145,146]. In the treatment of CF, nanosized MX particles reach the apical part of the lung and can go through the more viscous mucus. Although COPD affects not only small airways but also large airways, but the condition is more prominent in the proximal airways and it is even more pronounced in its peripheral airway tree [147–149]. In case of COPD, the tighter respiratory tracts, the increased amount of mucus and the inflammatory macrophages impact the nanoformulation less, compared to conventional formulations. In NSCLC the expression of the COX-2 is high during carcinogenesis; therefore, MX can be used in combination with cytostatic agents. The disease can be localized in every lobes of the lung; however, the nanosized API can target specifically the tumor cells [150,151]. The deep respiratory deposition of drugs is also important in the treatment of COVID-19. When the aerosol particles of coronavirus contact the airways, the virus can travel down to the deeper segments, resulting in a higher deposited fraction in the acinar airways than in the bronchi [152]. The virus replicates in type II pneumocytes. They induce the release of proinflammatory cytokines, leading to the common symptoms: acute respiratory distress syndrome, pneumonia, fever, multiple organ system failure and coughing [153]. Since the virus replicates in alveolar epithelial cells, inhalation as deeply as possible is believed to enhance the therapeutic effect of the inhaled drug [154]. Inhibition of COX-2 by MX may play a role in lung inflammation [144]. Therefore, MX could be important in the adjuvant therapy of COVID-19, as a repositioned drug [155].

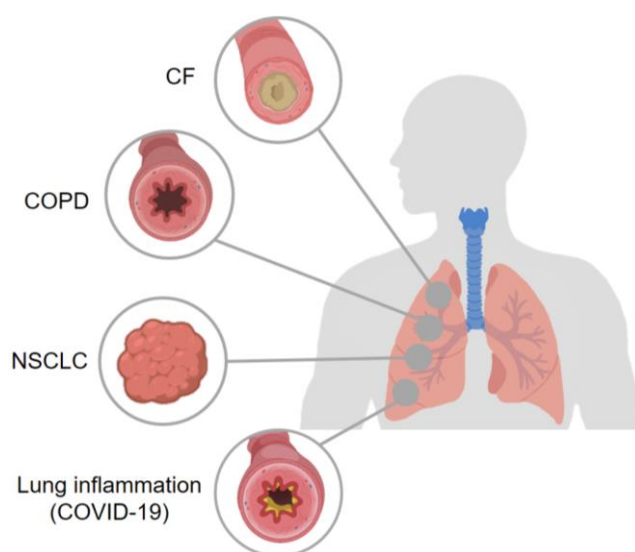


Figure 3. Possible therapeutic applications of MX.

4. Materials

4.1. Active pharmaceutical ingredient

MX (International Union of Pure and Applied Chemistry, IUPAC name: 4-hydroxy-2-methyl-N-(5-methyl-1,3-thiazol-2-yl)-1,1-dioxo-1λ6,2-benzothiazine-3-carboxamide, (Figure 4.) was used as the API (Egis Pharmaceuticals PLC., Budapest, Hungary), which is a poorly water-soluble NSAID (in water, 7.15 mg/l at 25 °C).

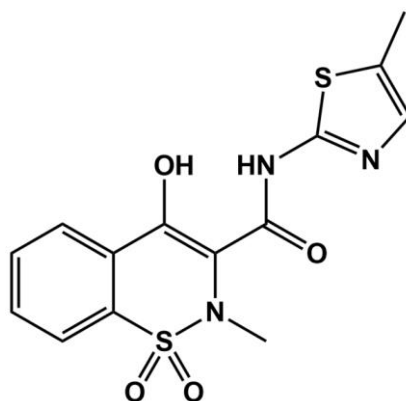


Figure 4. Structure of the MX [131].

4.2. Excipients

The additives were chosen according to the most important requirements of DPI formulations to obtain good aerodynamic properties [8]. Poly-vinyl-alcohol 4–98 (PVA, $M_w \sim 27.000$ g/mol, Sigma-Aldrich, St. Louis, MO, USA) was used to stabilize the samples [156]. L-Leucine (LEU, M_w : 131.17 g/mol, AppliChem GmbH, Darmstadt, Germany) was applied to enhance the dispersity of the particles, thereby improving the aerosolization and decreasing the hygroscopicity of the powder (Figure 5.) [28,157]. Although PVA and LEU have been combined before to create DPIs [47,137], they have not been utilized or studied as additives to create polymeric “nano-in-micro” DPIs; instead, they have only been employed to create lipid–polymer hybrid nanoparticles [97,104,109].

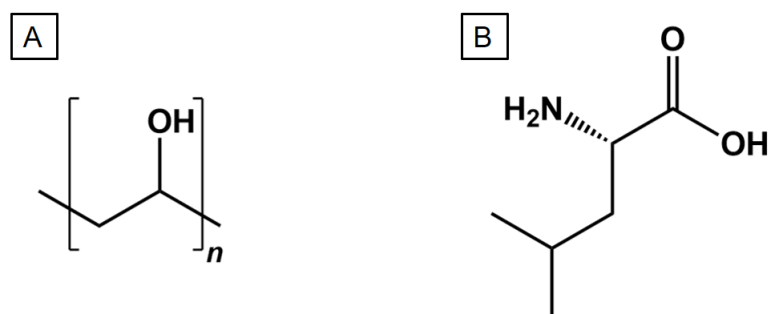


Figure 5. Structure of PVA (A) [158] and LEU (B) [159].

5. Preparation methods of the “nano-in-micro” DPI systems

5.1. Production of the nanosuspension by wet milling

During the particle size reduction process a wet and ball milling techniques were combined [160]. Planetary ball milling is a high-energy method that is suitable for wet grinding, when the raw material is broken down *via* mechanical forces, while a concentrated dispersion of drug particles in an aqueous or non-aqueous liquid is applied. It is capable of nanonization using pearl milling. The grinding beads cause mechanical attrition and impaction. The medium prevents adhesion and subsequent compaction of the drug particles on the wall of the vessel and/or the surfaces of the milling beads [134,161].

The MX containing nanosuspension was prepared as follows: 2.00 g of MX and 18.00 g of 2.5% (w/w%) PVA solution were added to a planetary ball mill (Retsch PM 100; Retsch GmbH, Haan, Germany). The following conditions were used: 20.00 g of zirconium-dioxide (ZrO_2) beads ($d = 0.3 \text{ mm}$), 500 rpm, 60 min. As a result, predispersion containing MX was achieved. It was diluted with purified water to 500 ml. This nanosuspension was used during the following spray drying processes.

The MX concentration was based on earlier research that resulted in low success rates due to the contact between MX and the grinding medium when the MX concentration was lower than 10%. However, a higher MX content resulted in a higher sample density and a lower grinding efficiency [162]. The particle size was influenced by the quantity of beads and the milling time. In the case of a ratio of 1:0.5, the milling efficiency was not sufficient; however, it increased linearly with increasing milling media and milling duration. The concentrated pre-dispersion to beads ratio was optimized to be 1:1, because using the minimum efficient grinding medium, was reducing the product loss. Although in a previous experiment, the most advantageous particle size distribution (PSD) was produced with a milling period of 45 min at 437 rpm at PVA concentrations between 4.0% and 5.5% [162], the 2.5% concentration of PVA was selected. Because using this concentration, a suitable PSD was achieved by extending the milling time to 60 minutes at 500 rpm. Therefore, the PVA concentration was reduced as low as possible to create nanoparticles, which is crucial to avoid the possible lung toxicity of the polymer.

5.2. DPI formulations by spray drying

5.2.1. Mini spray drying method

During the mini spray drying process (Figure 6.) the liquid is fed to the two-fluid nozzle by a pump and then atomized to generate fine droplets. The nozzle is made of steel and it is equipped with an *in situ* nozzle cleaning needle. After atomization the droplets go through the drying chamber, where the air is heated up by an electrical heater and circulated through the system by an aspirator, resulting in rapid evaporation of the liquid. Cyclone technology collects the dry particles [163]. The procedure is capable of preparing particles between 2 and 25 μm at yields typically around 60% [164,165].

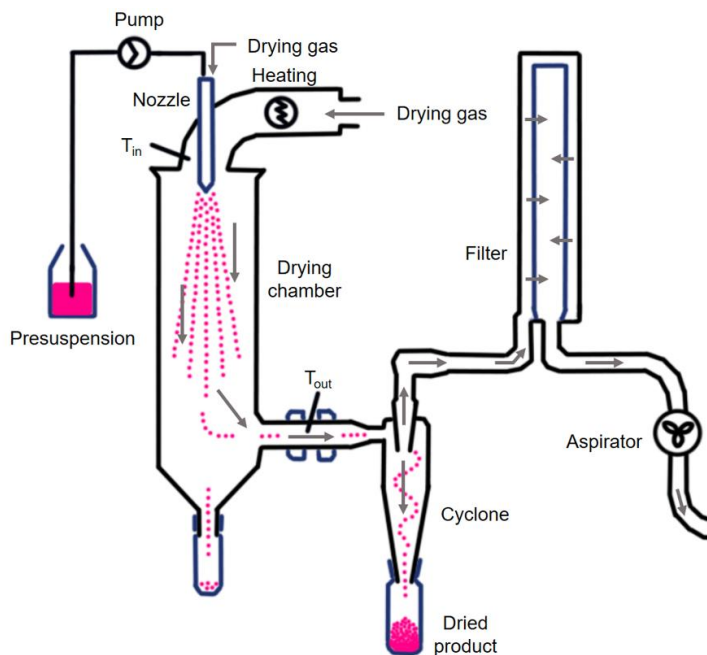


Figure 6. Schematic figure of the mini spray dryer.

Three compositions were prepared by adding various amounts of LEU to the MX nanosuspension (Table 4.). A magnetic stirrer was used for sample homogenization (AREC.X heating magnetic stirrer, Velp Scientifica Srl., Usmate Velate, Italy). Inhalable microparticles were produced using a spray dryer equipped with a two-fluid nozzle of 0.7 mm (Büchi Mini Spray Dryer B-191, Büchi, Flawil, Switzerland). The spray drying properties were as follows: inlet temperature: 165 °C, outlet temperature: 100 °C, aspirator capacity: 85%, airflow rate 500 l/h, and feed pump rate: 10%.

The properties of the MX allowed the application of high temperature, with which the yield could be improved. The applied aspirator capacity also helped to reach a higher yield. The outlet temperature indicated the maximum temperature of the product achieved during the drying process. This reduction was the result of the relatively rapid rate of the

feed pump and the airflow rate. The parameters were based on the preliminary experiments, where the particle size, PSD and the morphology of the dried particles were observed. The application of PVA would minimize the nanoparticle fusions during drying as well as milling. Its decreasing effect on surface tension could result in smaller particles. PVA produces particles with low moisture content, despite its high hydrophilicity [97]. The yield was calculated as the ratio of the mass of the particles collected after spray drying to the mass of the solid content of the initial suspension. Low spray drying yields are indicative of cohesive powders. LEU reduced the cohesion between the particles; therefore, the application of LEU improved the yield of the spray drying (Table 4.) [166].

5.2.2. Nano spray drying method

The novelty of nano spray drying (Figure 7.) lies in the vibration mesh spray technology, which includes a piezoelectric actuator in the spray head [116]. A spray cap is attached to the nozzle, which is made of a stainless-steel mesh with perforated micron-sized holes. Electricity drives the piezoelectric actuator at an ultrasonic frequency. The vibration draws the fluid through the holes to form droplets into the drying chamber. The drying gas flow directs the electrostatically charged particles to the electrostatic particle collector. The high voltage applied between the electrodes sets up an electrostatic field that accelerates the deposition of particles onto the collecting electrode. The method has the advantage of collecting micron to sub-micron sized particles (300 nm to 5 μm) effectively at high yields (up to 90 %) even in small sample quantities (1-200 ml) [165,167–169].

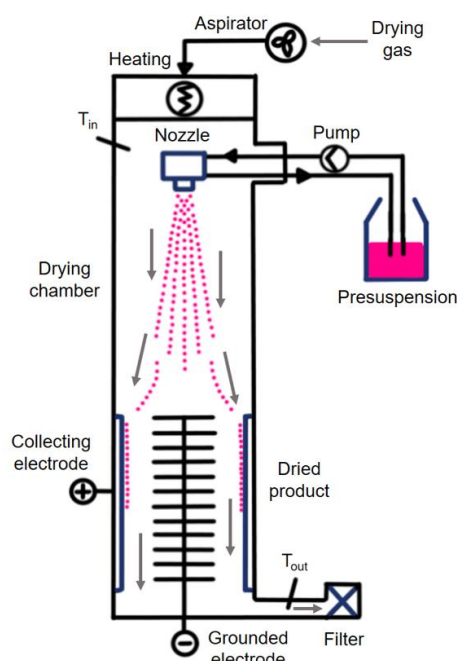


Figure 7. Schematic figure of the nano spray dryer.

Three similar compositions were formulated from the MX nanosuspension by adding different amounts of LEU (Table 4.). A magnetic stirrer was used for homogenization. The inhalable powders were produced with a nano spray dryer (Büchi Nano Spray Dryer B-90 HP, Büchi, Flawil, Switzerland). To produce particles under 2 µm the device was equipped with a small nebulizer (hole size: 4 µm). The drying parameters were derived from the preliminary data: inlet temperature: 80 °C, aspirator capacity: 100%, airflow rate: 120 ml/min, pump rate: 20%.

In this case, a gentler spraying technique was used, which could potentially be implemented for more heat-sensitive APIs as well. Furthermore, it would not be optimal if the particle size increased due to the higher temperature. The aforementioned parameters were utilized in the preparation of the desired particles based on scanning electron microscopy and laser diffraction studies. Despite a greater temperature would produce a better yield, using 80 °C as inlet temperature the nano spray dryer still outperformed the mini spray drying process (Table 4.) [170].

5.3. Preparation of the physical mixtures

A physical mixture (PM) was created from the raw materials to observe the effect of the excipients. The composition of the PM was equal to the SPD samples (Table 4.). During the experiments, the different qualities of the SPD samples were compared to the PM. The API content of the final powders was determined (see Section 7.6.1.).

Table 4. Composition of the SPD samples and the PMs, yield of the spray drying methods and API content results of the formulations.

Sample name	MX (g)	PVA (g)	LEU (g)	Yield (%)	API content (%)
mini[MX1_PVA_LEU0]	2.00	0.45	0.00	45.41 ± 5.10	93.81 ± 2.99
mini[MX1_PVA_LEU0.5]	2.00	0.45	1.00	57.56 ± 1.36	55.48 ± 0.78
mini[MX1_PVA_LEU1]	2.00	0.45	2.00	58.43 ± 6.36	51.46 ± 2.99
nano[MX1_PVA_LEU0]	2.00	0.45	0.00	61.44 ± 3.34	72.50 ± 3.55
nano[MX1_PVA_LEU0.5]	2.00	0.45	1.00	63.29 ± 2.38	51.26 ± 3.19
nano[MX1_PVA_LEU1]	2.00	0.45	2.00	62.44 ± 5.86	42.65 ± 1.33
pm[MX1_PVA_LEU0]	2.00	0.45	0.00	-	81.63
pm[MX1_PVA_LEU0.5]	2.00	0.45	1.00	-	57.97
pm[MX1_PVA_LEU1]	2.00	0.45	2.00	-	44.94

6. Characterization of the nanosuspension

6.1. Particle size analysis

6.1.1. Laser diffraction based particle size measurement

The particle size, PSD, and specific surface area (SSA) of the nanosuspension were determined by laser diffraction (Mastersizer Scirocco 2000, Malvern Instruments Ltd., Worcestershire, UK). The wet dispersion unit was used. The refractive index (RI) of the MX was adjusted to 1.720. The suspension was measured three times in purified water with stirring at 2000 rpm.

6.1.2. Dynamic light scattering investigations

The average hydrodynamic diameter (Z-average), polydispersity index (Pdl), and zeta potential (ζ potential) were analyzed *via* dynamic light scattering (DLS) using a Zetasizer Nano ZS (Malvern Instruments, Worcestershire, UK). The suspension was diluted in purified water and measured at 25 °C in folded capillary cells. The RI of MX was set to 1.720. Measurements were made in triplicate.

6.1.3. Nanoparticle tracking analysis

The NanoSight NS 3000 device (Malvern Instruments, Worcestershire, UK) for nanoparticle tracking analysis (NTA) was used to obtain high-resolution particle size information. The instrument was equipped with a 565 nm laser, a high sensitivity sCMOS camera and a syringe pump. The MX suspension was diluted 1000 times and loaded into the device using syringe pump speed of 50. The experiment videos were analyzed using NTA 3.4 Build 3.4.4 after capture in script control mode (3 videos of 30 s per measurement). A total of 1500 frames per sample were examined.

6.2. Determination of the surface tension

Surface tension (ST) measurements of the PVA solution and the MX nanosuspension were performed using the pendant drop technique with an optical contact angle (OCA) apparatus (OCA 20, Dataphysics Instrument GmbH, Filderstadt, Germany). The density values of the samples were established for the calculations. Drop images were collected at 25 °C and the profiles were fitted using the Young-Laplace equation [171]. For each experiment, ten subsequent images were collected and the average ST was determined.

7. Solid phase characterization

7.1. Particle size analysis

7.1.1. Laser diffraction based particle size measurement

Laser diffraction was applied to determine the particle size, PSD and SSA of the SPD samples. The dry dispersion unit was used. The dispersion air pressure was set to 3.0 bar and a vibration feed was applied. The RI was set to 1.720. Each sample was measured three times. PSD was characterized by the values of D[0.1] (10% of the volume distribution is below this value), D[0.5] (50% of the volume distribution is below this value), and D[0.9] (90% of the volume distribution is below this value), (Equation 1.). The SSA was derived from the PSD data under the assumption of spherical particles.

$$\text{Span} = \frac{D[0.9]-D[0.1]}{D[0.5]} \quad (1)$$

7.1.2. Dynamic light scattering analysis

The Z-average, PdI, and ζ potential were analyzed *via* DLS. The SPD formulations were suspended in purified water and measured at 25 °C in folded capillary cells. The RI of MX was set to 1.720. Each measurement was carried out in triplicate.

7.2. Morphology investigation

The shape of the particles was analyzed using scanning electron microscopy (SEM, Hitachi S4700; Hitachi Ltd., Tokyo, Japan). The investigation conditions were the following: 10 kV high voltage, 10 mA amperage, and 1.3–13.1 mPa air pressure. A high vacuum evaporator and argon atmosphere were applied to make the sputter-coated samples conductive with gold-palladium (Bio-Rad SC 502; VG Microtech, Uckfield, UK).

7.3. Density and powder flow measurement

The bulk and tapped densities of the formulations were measured using a tap density tester (ETD-1020x, Electrolab, Mumbai, India) [172]. A cylinder was filled with 1.5-2.0 cm³ of powders to calculate the bulk density (ρ_b). It was tapped 1000 times. The tapped density (ρ_t) was calculated compared to the volume of the powder before and after the taps. The measurements were performed three times. The Hausner ratio (HR) and Carr index (CI) values of the samples were evaluated from the bulk density and the tapped density (Equation 2., 3.) [173].

$$\text{HR} = \frac{\rho_t}{\rho_b} \quad (2)$$

$$\text{CI} = \frac{(\rho_t - \rho_b)}{\rho_t} * 100 \quad (3)$$

7.4. Determination of the crystallinity

7.4.1. Thermoanalytical measurement

Differential scanning calorimetry (DSC) measurements were performed with a Mettler Toledo DSC 821e thermal analysis system with the STARE thermal analysis program V9.1 (Mettler Inc., Schwerzenbach, Switzerland). The samples (3 to 5 mg) were heated to temperatures between 25 and 300 °C at a rate of 10 °C/min while maintaining a steady flow of argon at a rate of 10 l/h.

7.4.2. Analysis of the crystalline structure

The crystalline structure was investigated using X-ray powder diffraction (XRPD). The Bruker D8 advance diffractometer and the VANTEC-1 detector (Bruker AXS GmbH, Karlsruhe, Germany) were used with Cu K α I radiation. The powders were placed on a flat quartz glass with an etched square. Scanning was performed at a uniform voltage of 40 kV and a current of 40 mA from 3° to 40°, scanning time constant was 0.1°/min, angular step was 0.01°. DIFFRACplus EVA program was used for the evaluation. The degree of crystallinity (X_c) were determined (Equation 4.). A symbolizes the area under the curve: The PM sample was considered 100% crystalline.

$$X_c = \frac{A_{crystalline}}{A_{crystalline} + A_{amorphous}} * 100 \quad (4)$$

7.5. Solubility test

The solubility tests of the SPD products were implemented in 3 ml of artificial lung fluid (0.68 g/l NaCl, 2.27 g/l NaHCO₃, 0.02 g/l CaCl₂, 0.1391 g/l NaH₂PO₄, 0.37 g/l glycine and 5.56 ml/l 0.1 M H₂SO₄) [174]. The pH of the medium was 7.4 \pm 0.1. The samples were stirred with a magnetic stirrer at 25 °C for 24 h, filtered (pore size = 0.45 μ m, Millex-HV filter unit, Millipore Corporation, Bedford, MS, USA) and the drug content was analyzed using a UV/VIS spectrophotometer, (ATI-Unicam, Cambridge, UK) at a wavelength of 362 nm. The samples were measured in triplicate.

7.6. *In vitro* and *in silico* aerodynamic characterization of the DPI systems

7.6.1. *Andersen cascade impactor measurement*

The aerosolization properties of the SPD formulations were evaluated *in vitro*, using an Andersen cascade impactor (Figure 8., ACI, Apparatus D, Copley Scientific Ltd., Nottingham, UK) [175]. The inhalation flow rate was set at 28.3 l/min and 60 l/min (High-capacity pump model HCP5, Critical flow controller model TPK, Copley Scientific Ltd., Nottingham, UK). The actual airflow through the impactor was measured by a mass flow meter (Flow meter model DFM 2000, Copley Scientific Ltd., Nottingham, UK). The inhalation time was 4 s. Using the flow rate of 60 l/min, the breathing pattern with a 4 l inhalation volume was simulated. The application of 28.3 l/min led to an inhalation volume of 1.89 l, which is in concordance with the inhalation volume of patients with COPD [176]. Furthermore, the use of different flow rates can take into account the large variability of pulmonary function of the patients, which is an important aspect in the preclinical development. The Breezhaler[®] single-dose device (Novartis International AG, Basel, Switzerland) was applied, which is classified as a low-resistance inhalator. It requires a weaker inspiratory effort to achieve high flow rates across the device [177,178]. Transparent size 3 gelatin capsules (Capsugel, Bornem, Belgium) were filled with the powders, containing the pulmonary dose (1.5 mg) of MX. The API contents (Table 2) of the different DPIs were determined by solving 1.0 mg of powder in 25 ml of methanol and pH 7.4 phosphate buffer (60+40 V/V%) and analyzed by UV/Vis spectrophotometry at a wavelength of 362 nm. Measurements were carried out in triplicate. To simulate the pulmonary adhesive conditions, the collection plates were coated with a mixture of span 85 and cyclohexane (1 + 99 w/w%). After the measurement, the device, capsules, induction port, plates and the filter (A/E glass fiber filter, Pall Corporation, NY, USA) were washed with methanol and pH 7.4 phosphate buffer (60+40 V/V%) to dissolve the deposited amount of MX. The API was quantified by UV/Vis spectrophotometry at a wavelength of 362 nm. Aerodynamic properties were evaluated using Inhalytix[™] software (Copley Scientific Ltd., Nottingham, UK). The fine particle fraction (FPF) and mass median aerodynamic diameter (MMAD) values were determined. FPF is defined as the percentage of mass of the particles consisting of API with an MMAD of less than 5 µm divided by the emitted dose of the formulations. The emitted fraction (EF) was also calculated, which is the released fraction from the DPI device.

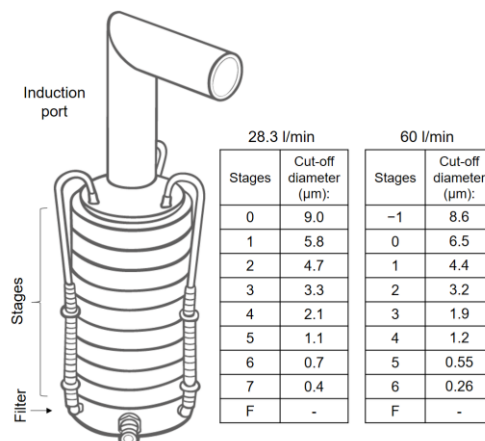


Figure 8. Conformation of ACI and the cut-off diameters at the two different flow rates.

7.6.2. *In silico aerodynamic characterization*

The *in silico* simulations were performed using the stochastic lung model, which tracks the inhaled particles until their deposition or exhalation and computes the fraction of the particles deposited in each anatomical part of the airways [179]. The particle trajectories were simulated in an asymmetrical branching airway structure, mimicking realistic airways by selecting adequate morphometric parameters [180]. The input of the computational model can be different parameters characterizing aerosol particles like density, shape, or size, as well as the breathing parameters of the patient. In our work, the aerodynamic PSD of the samples measured by the ACI served as input for the numerical model of airway deposition. The inhalation parameters corresponded to the inhalation of a COPD patient through Breezhaler[®], whose inhaled volume ($IV = 1.7$ l) and inhalation time ($t_{in} = 3.2$ s) corresponded to the best flow rate of the impactor measurements. Two different (5 s and 10 s) breath-holding times were used. The computational deposition model was validated in earlier works [181,182]. The test was carried out in cooperation with the Center for Energy Research of Hungarian Academy of Sciences.

7.6.3. *Aerodynamic particle size analysis using the Spraytec[®] device*

The aerodynamic diameter was determined using a Spraytec[®] laser diffractometer equipped with an inhalation cell (Malvern Instruments Ltd., Worcestershire, UK) and ACI. The investigation accounts for the EF of the DPI formulation and measures PSD directly from the inhalation device. SPD formulations were aerosolized from 3 gelatin capsule inserted into a Breezhaler[®] device connected to an induction port of the inhalation cell. The assembly was attached to an ACI, which created a closed system that allowed measurement of the size under controlled circumstances [183]. The inhalation flow rate was set at 60 l/min. The inhalation time was 4 s. Measurements were made in triplicate.

7.6.4. Aerodynamic particle size analysis with particle counter

During particle counter measurement, the products were loaded into gelatin capsules and a Breezhaler[®] inhaler. The set-up consisted of a breathing simulator, an induction port, a vacuum pump with a critical flow controller and an aerodynamic particle sizer (APS, TSI 3321, TSI Incorporated, Shoreview, MN, USA, Figure 9.). The breathing simulator produced the flow profile that activated the DPI unit through the mixing inlet (Copley Scientific Ltd., Nottingham, UK), which provided an interface between the flow that activated the DPI and the main stream that transfers particles to the APS. The APS sampled particles from the main stream using an isokinetic nozzle. The instrument measured the number size distributions and determined the aerodynamic size of the particles by time-of-flight measurement in an accelerated flow. The sample flow rate of the APS was 1 l/min and the sampling time was set at 5 s without pause. The IV range was 0.1 to 6800 cm³. The time resolution of the inhalation profile can be set to 20, 50, and 100 ms. For the measurements, the inhalation waveform programmed into the breathing simulator was constructed based on data from the literature [184,185]. The flow controller was used to set a flow rate of 60 l/min, which was regularly checked during the measurements with a TSI 4000 thermal mass flow meter (TSI Incorporated, Shoreview, MN, USA); the measuring range is 0.5-200 NI/min.). The test was carried out in cooperation with the Wigner Research Center for Physics of Hungarian Academy of Sciences.

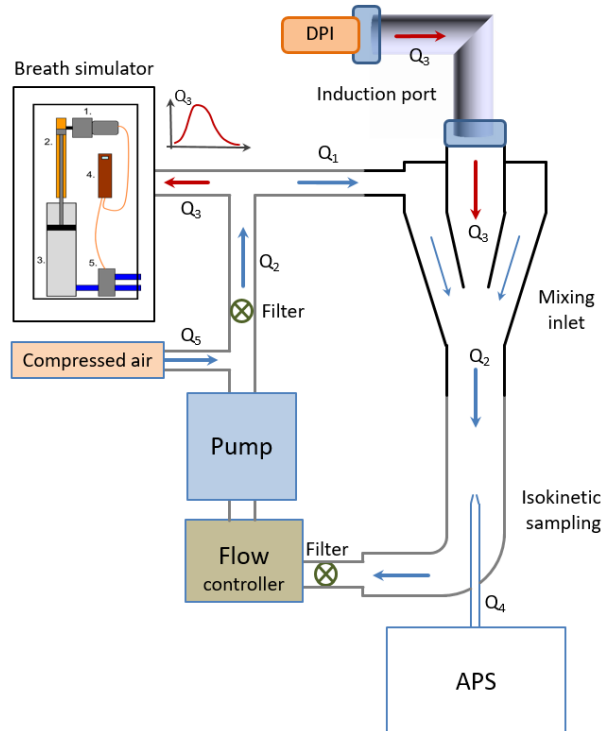


Figure 9. Set-up of the particle size counter.

7.7. *In vitro* investigations of the pulmonary dosage form

7.7.1. *In vitro* dissolution test using the conventional paddle method

Currently, there are no regulatory requirements for the *in vitro* dissolution testing of inhaled products [8,186,187]. A modified paddle method (Hanson SR8 Plus, Teledyne Hanson Research, Chatsworth, CA, USA) of the European Pharmacopeia [188] was used to define the release of MX from the dosage form. The samples contained 1.5 mg of MX, which is the tenth of the highest oral dose of MX [131] and the estimated dose of MX for pulmonary delivery. The estimated value of the lung lining fluid is between 10 and 70 ml [189]. Considering the limitation of the dissolution setup, 50 ml of the previously mentioned simulated lung medium was applied [174,190]. The paddle was rotated at 100 rpm and the measurement was performed up to 60 min at 37 °C [156]. Samples of 5 ml were taken after 5, 10, 15, 30, and 60 min. The medium was replenished in all cases. After filtration (pore size: 0.45 µm, Millex-HV syringe-driven filter unit, Millipore Corporation, Bedford, MA, USA), the dissolved quantity of MX was determined spectrophotometrically at a wavelength of 362 nm. The measurement was performed three times.

7.7.2. *In vitro* dissolution test using the paddle method combined with ACI

The release profile of MX was determined from the respirable fraction of the formulations, which is recommended for better *in vivo* correlation [183]. The inhalation flow rate was set at 60 l/min. The inhalation time was 4 s. The stages of ACI were used, as a Fast Screening Impactor to collect particles between 1 and 5 µm [190]. Between the number one stage, and the number four stage a plate was applied covered with a polycarbonate (PCTE) membrane filter (Sterlitech, Auburn, WA, USA). On the last stage a filter (A/E glass fiber filter, Pall Corporation, NY, USA) was applied to catch the smallest particles. A mass of each DPI formulation, equivalent to a dose of 1.5 mg of MX, was filled into a gelatin capsule of size 3. A Breezhaler[®] device was used for actuation. After inhalation, the filters were individually fixed on a watch glass-PTFE disk assembly (Copley Scientific Ltd., Nottingham, UK) with clips and a PTFE mesh screen [186]. The disk assembly was then immersed in a dissolution vessel of a Hanson SR8 Plus dissolution apparatus with 400 ml of artificial lung fluid [174,189]. Measurement was carried out for up to 60 min at 37 °C and the paddle was rotated at 100 rpm [39]. Samples of 2 ml were taken after 5, 10, 15, 30, and 60 min. The medium was replenished in all cases. The dissolution tests were performed in triplicate for each DPI formulation.

7.7.3. *In vitro* permeability investigation

A 3D printed horizontal diffusion cell was used to investigate the *in vitro* permeability of the samples (Figure 10.) [191]. 9 ml of artificial lung medium [174] was used as the donor phase. As the volume of the lung lining fluid is 10 to 70 ml [189], which is divided for the different generations of lung, 9 ml was ideal choice to model the absorption of the drug in different parts of the airways. The acceptor phase was 9 ml of phosphate buffer (pH = 7.4), simulating the circumstances of the lung epithelium. Between the two phases, a cellulose membrane (RC 55 Whatman™ GE Healthcare Life Sciences, Buckinghamshire, UK) was applied, which was impregnated with isopropyl myristate. The pore size of the membrane was 0.5 µm, its thickness was 0.75 µm. The diffusion surface was 0.785 cm². The rotation of the stirring bar was set to 300 rpm. The magnetic stir bars were moved by a CS-DSD1 digital magnetic stirrer (CS-Smartlab Devices Ltd., Kozármiszlény, Hungary). The temperature was set at 37 °C during the investigation, which is the usual temperature inside the human lung. Samples containing 1.5 mg of MX were investigated. The design of the chambers was suitable for real-time analysis with the input of an immersion probe. The amount of API diffused to the acceptor phase was determined at a wavelength of 362 nm, for 60 minutes with a spectrophotometric sonda (FDP-7UV200-VAR, Avaspec-ULS2048-USB2, Avantes, Apeldoorn, The Netherlands). Three parallel measurements were made. The flux (J) [µg/cm²/h] was calculated from the quantity of MX, which permeated through the membrane (m), divided by the surface of the membrane (A_m) and the duration time (t) (Equation 6.). The permeability coefficient (K_p) [cm/h] was determined as flux and MX concentration in the donor phase [µg/cm³] (Equation. 7.)

$$J = \frac{m}{A_m \cdot t} \quad (6)$$

$$K_p = \frac{J}{C_d} \quad (7)$$

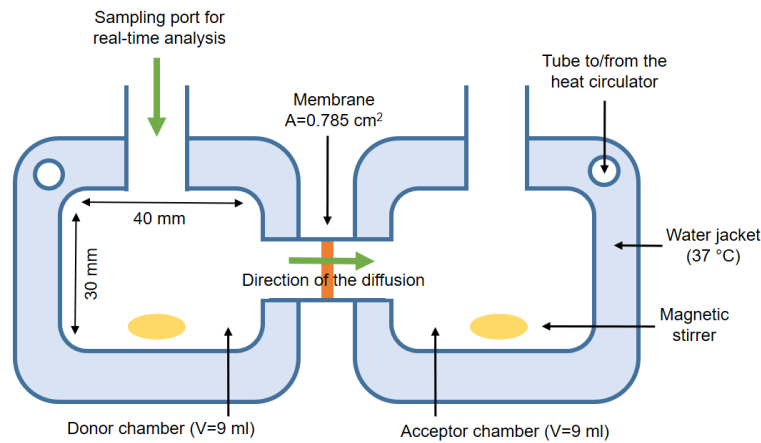


Figure 10. Structure of the *in vitro* permeability test chambers.

7.7.4. *In vitro cell line investigations*

7.7.4.1. Cytotoxicity measurement

The SPD samples were dissolved in dimethyl sulfoxide (DMSO, VWR Chemicals, Leuven, Belgium), a concentration of 0.1 mg/ml was applied. This concentration of MX is adequate for pulmonary administration, for 1.5 mg of drug dose in approximately 15 ml of lung fluid volume. Further diluted concentrations of 0.05 and 0.025 mg/ml were tested. Mitochondrial activity as a measure of cell viability was performed using MTT (3-(4,5-dimethylthiazol-2-yl)-2,5-diphenyltetrazolium bromide) assay in 96-well cell culture microplates using A549 (adenocarcinomic human alveolar basal epithelial cells, ATCC). A549 cells were seeded at a density of 4×10^4 cells/well. The cells were treated with either MX or nano SPD compositions. Furthermore, 5 µg/ml lipopolysaccharide (LPS; ThermoFisher Scientific, Waltham, MA, USA) cytotoxicity was also measured. LPS was used to induce inflammation in cells during the anti-inflammatory effect investigations. Cells were incubated at 37 °C for 48 h. Subsequently, 20 µl of thiazolyl blue tetrazolium bromide (Sigma, St. Louis, MO, USA) was added to each well. After additional incubation at 37 °C for 4 h, a sodium dodecyl sulfate solution (Sigma, St. Louis, MO, USA, 10 % in 0.01 M HCl) was added and incubated overnight. The cytotoxicity was then determined by measuring the optical density (OD) at 550 nm (ref. 630 nm) with an EZ READ 400 ELISA reader (Biochrom, Cambridge, UK). The assay was replicated four times for each concentration [192]. Cell viability was concluded on the following Equation 8.

$$\text{Cell viability} = 100 - \frac{(\text{OD}_{\text{sample}} - \text{OD}_{\text{medium control}})}{(\text{OD}_{\text{control}} - \text{OD}_{\text{medium control}})} \times 100 \quad (8)$$

7.7.4.2. Measurement of the anti-inflammatory effect

Cells were propagated in minimum essential medium with Earle's salt (Sigma, St. Louis, MO, USA) and were supplemented with 25 µg/ml gentamycin, 10 % of fetal calf serum, 0.5 % w/vol of glucose, 0.3 mg/ml of l-glutamine and 4 mM HEPES. A549 cells were seeded in 6-well plates at a density of 1×10^6 cells/well and treated with 0.1 mg/ml of MX or DPI formulations and 5 µg/ml of LPS or only 5 µg/ml of LPS or left untreated, then the cells were incubated for 48 h at 37 °C.

After the treatment, ribonucleic acid (RNA) was extracted using the TRI reagent (Sigma-Aldrich, St. Louis, MS, USA) according to the protocol of the manufacturer. Subsequently, 0.1 µg of mRNA was reverse transcribed using Maxima reverse transcriptase according to the instructions using oligo(dT) primers (ThermoFisher Scientific, Waltham,

MA, USA). Quantitative polymerase chain reaction (qPCR) was performed using a Bio-Rad CFX96 real-time system with the 5x HOT FIREPol® EvaGreen® qPCR Supermix (Solis BioDyne, Tartu, Estonia) and the following pairs of human-specific primers: interleukin-6 (IL-6) and Actb (actin beta). Primers were designed using the Primer Quest Tool software and synthesized by Integrated DNA Technologies Inc. (Montreal, Quebec, Canada). Threshold cycles (Ct) were determined for IL-6 and Actb, and the relative gene expression was calculated *via* the 2-($\Delta\Delta C_t$) method [193].

After 48 h of treatment, the supernatant of the cells was collected and a standard sandwich human IL-6 enzyme-linked immunosorbent assay ELISA kits Legend Max™ (BioLegend, San Diego, CA, USA) was used to determine the IL-6 concentration. The supernatant of the LPS-treated cells was diluted 10 times. The assay was performed according to the manufacturer's instructions. The dynamic range of the kit was between 7.8 and 500 pg/ml. The plates were analyzed using the Biochrom Anthos 2010 microplate reader (Biochrom, Cambridge, UK). Samples were assayed in duplicate.

The *in vitro* cell line investigations were performed with the help of the Department of Medical Microbiology of University of Szeged.

7.8. Stability test

The stability of the nano[MX1_PVA_LEU1] sample was investigated. The results could also be extended to the other formulations, due to their similar composition. The stability test was performed at 25 ± 2 °C with $50 \pm 5\%$ relative humidity to mimic the room conditions in a desiccator. The samples were taken and measured after 1 day, 6 months and 12 months [194,195].

7.9. Statistical analysis

All the described data indicate the standard deviation (\pm SD) of three parallel measurements ($n = 3$). Statistical analysis was performed using Student's t test and one-way analysis of variance (ANOVA) using GraphPad Prism 8.0.1. software (GraphPad Software, CA, USA). P-values < 0.05 indicated statistically significant differences.

8. Result of the characterization of the nanosuspension

8.1. Particle size analysis

8.1.1. Results of the laser diffraction based particle size distribution

The initial diameter of the API was in the micrometric size range ($D[0.5] = 9.91 \pm 0.37 \mu\text{m}$), which was successfully reduced by wet milling to $D[0.5] = 137.70 \pm 4.97 \text{ nm}$. SSA increased from $1.09 \pm 0.03 \text{ m}^2/\text{g}$ to $43.65 \pm 5.32 \text{ m}^2/\text{g}$. PVA coated the MX particles, which inhibited particle aggregation during size reduction [134]. The enhanced SSA predicted a higher rate of dissolution compared to the raw MX [196].

8.1.2. Outcomes of dynamic light scattering investigation

The DLS method is more accurate than the laser diffraction to determine the size of nanoparticles [197]. However, the method is sensitive to the presence of large particles. Therefore, in polydisperse formulations, the proportion of small particles is underestimated due to the fact that larger particles scatter more light than smaller particles [198]. The DLS test showed that the Z-average of the suspension was $359.75 \pm 12 \text{ nm}$ and the PDI was 0.34 ± 0.06 . In addition, it proved that the diameter of MX was reduced under 500 nm . Therefore, the drug could avoid the uptake by alveolar macrophages [57]. The ζ potential was -23.70 ± 0.85 , demonstrating a stable suspension [199].

8.1.3. Results of the nanoparticle tracking analysis

NTA is comparable to DLS and successfully minimizes its drawbacks. The technique uses nanoparticle light scattering and Brownian motion to determine the size distribution of the sample. NTA simultaneously detects large and small particles, resulting in a more precise particle distribution [198,200]. According to NTA, $D[0.5]$ of the MX nanosuspension was $124.90 \pm 8.60 \text{ nm}$ and PSD was monodisperse (Figure 11.).

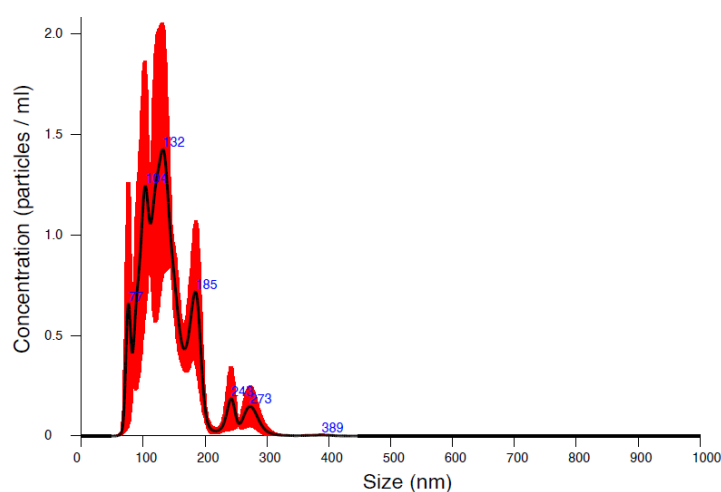


Figure 11. The particle size result of the suspension according to the NTA.

8.2. Surface tension results of the nanosuspension

The ST of the 2.5% (w/w) PVA solution was 51.78 ± 1.32 mN/M, which means that the polymer decreased the ST of the water (71.99 ± 0.36 mN/m at 25 °C) [201]. The ST value of the nanosuspension was increased to 66.07 ± 0.54 mN/M compared to the polymer solution. Adding LEU could further increase ST [202]. The energy introduced during milling led to an increase in ST, which was associated with a higher dissolution pressure, which could lead to improved saturation solubility [203]. Generally, low-ST fluids produce smaller particle size during spray drying [119,168]. Therefore, the application of LEU forms larger droplets compared to the LEU-free products.

9. Results of the solid phase characterization

9.1. Particle size analysis

9.1.1. Results of the laser diffraction based particle size distribution

After solidification, the size of the particles was applicable for pulmonary delivery, since the D[0.5] values were in the 1-5 μm range in all cases (Table 5.). The geometric diameter of the mini SPD samples was between 3.2-4.4 μm . After nano spray drying, the D[0.5] values of the samples were between 1–1.5 μm . The results met the initial aim, which was to produce particles above and below 2 μm using the two different spray drying techniques. Nano spray drying was capable of producing smaller particles, especially using the small nebulizer, compared to the mini spray dryer. In all cases, the incorporation of LEU increased the geometric size of the SPD particles, leading to a decrease in SSA. The reason behind this is that the particle-particle interaction forced to alter the diameter of the particle [204]. The higher the Span value, the broader is the distribution [205]. PSD was monodisperse (Span < 2.0) in the case of mini SPD and LEU containing nano SPD products, which is an important factor for accurate doses [137].

Table 5. The particle size, Span and SSA values of the DPIs. Data are means \pm S.D. (n = 3 measurements).

Sample name	D[0.5] (μm)	Span	SSA (m^2/g)
mini[MX1_PVA_LEU0]	3.19 ± 0.02	1.56 ± 0.07	2.22 ± 0.03
mini[MX1_PVA_LEU0.5]	3.80 ± 0.01	1.46 ± 0.00	1.88 ± 0.02
mini[MX1_PVA_LEU1]	4.40 ± 0.03	1.58 ± 0.08	1.71 ± 0.05
nano[MX1_PVA_LEU0]	1.17 ± 0.00	5.42 ± 1.49	6.60 ± 0.03
nano[MX1_PVA_LEU0.5]	1.31 ± 0.04	1.68 ± 0.30	5.19 ± 0.06
nano[MX1_PVA_LEU1]	1.43 ± 0.09	1.59 ± 0.12	4.39 ± 0.01

9.1.2. Outcomes of the dynamic light scattering investigation

Table 6. showed the outcomes of the DLS investigation. The average diameter of the dispersed mini SPD products was between 1200-1900 nm. The diameters of the dispersed nano SPD particles were between 500-700 nm. It predicted that as the dry particles deposit in the lung fluid, they disintegrate into nanoparticles, which is required in the case of “nano-in-micro” systems, resulting in greater dissolution and cellular absorption [50]. According to the results, the mini SPD samples will disintegrate slower than the nano SPD particles, due to their larger particle size. However, as mentioned previously in Section 8.2., the larger particles may have disturbed the scattering method, resulting in a larger Z-average. The inhomogeneous distribution was shown by the relatively high PdI results (PdI > 0.3). However, it is not considered a problem if it does not negatively affect the drug release [91]. All systems were more degradable and less retentive in the airways due to the negative ζ potential values of the products. It is beneficial, since the particles are unlikely to trigger further fibrosis, infection, or inflammation [206].

Table 6. Z average, PdI, and ζ potential of DPIs. Data are means \pm SD (n = 3 independent measurements).

Sample name	Z average (nm)	PdI	ζ potential (mV)
mini[MX1_PVA_LEU0]	1852.00 \pm 126	0.552 \pm 0.056	-2.15 \pm 0.25
mini[MX1_PVA_LEU0.5]	1292.00 \pm 231	0.653 \pm 0.065	-18.63 \pm 2.06
mini[MX1_PVA_LEU1]	1386.00 \pm 142	0.706 \pm 0.074	-23.83 \pm 1.19
nano[MX1_PVA_LEU0]	676.70 \pm 47	0.543 \pm 0.055	-21.35 \pm 5.27
nano[MX1_PVA_LEU0.5]	743.25 \pm 27	0.502 \pm 0.074	-23.30 \pm 2.74
nano[MX1_PVA_LEU1]	526.90 \pm 20	0.381 \pm 0.031	-24.50 \pm 1.47

9.2. Findings of the morphology investigation

On the SEM images (Figure 12.) of the DPIs, the size differences between the different batches can be easily seen. A nearly spherical shape was observed, which was the result of the optimized spray drying methods [207]. The spherical form met the requirements of DPIs [208]. PVA prevented the aggregation of the particles because it created a hydrophilic layer around the drug particles. However, smooth surfaces are not preferred for pulmonary delivery because they tend to increase the interaction between particles, while rough surfaces enhance aerosolization efficiency. When LEU was present in the systems, preferable wrinkled particles were established [209] and the spherical morphology shifted to a shell-shaped appearance [210]. The low diffusion coefficient of LEU increased particle enrichment on the droplet surface during spray drying. The rough

surface was formed as the rapidly drying core crumpled [138]. LEU developed a crystalline layer, which reduced surface energy while improving surface rugosity [117]. Therefore, LEU can reduce the adhesion between particles and the attachment to the capsule, resulting in higher EF and FPF values. The samples containing the highest amount of LEU demonstrated an internal hollow structure, reflecting a low density [138]. LEU enrichment can also result in moisture protection, therefore improving their physical storage stability [211]. In overall, particles containing LEU predicted a proper powder dispersion during inhalation, therefore improving drug delivery to the bronchial and acinar regions as well [58,138,212].

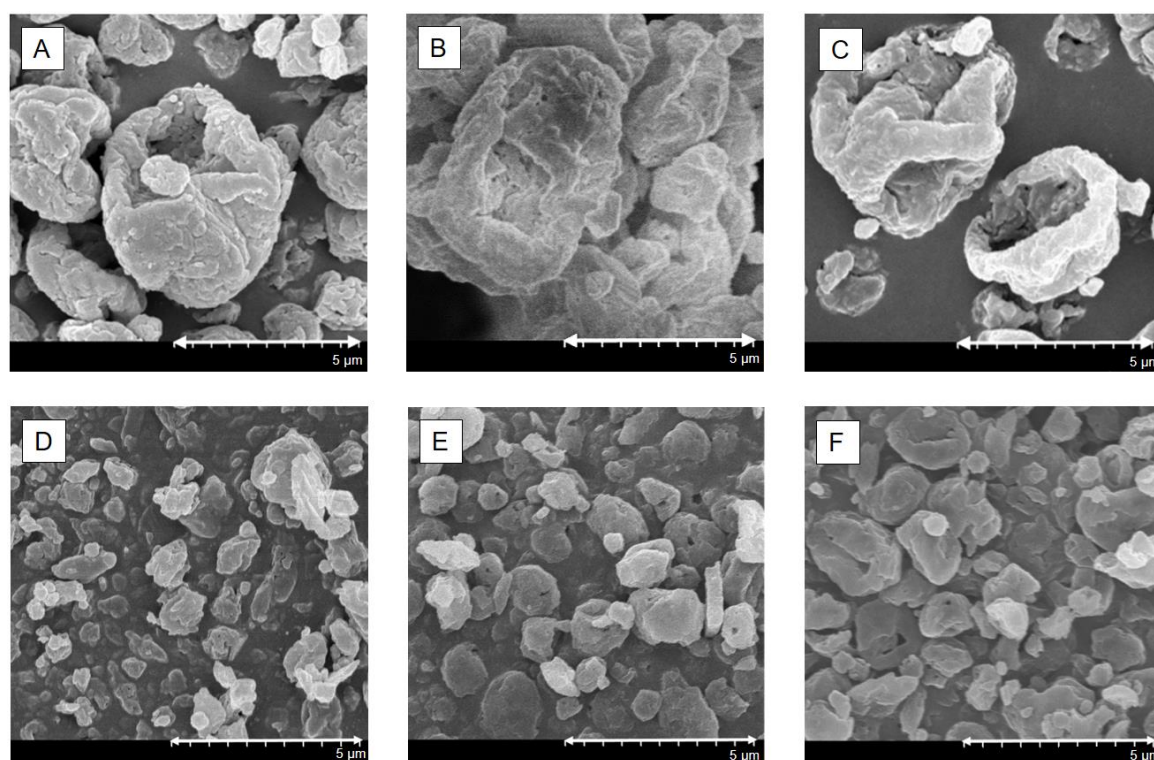


Figure 12. SEM pictures of the SPD samples: A: mini[MX1_PVA_LEU0], B: mini[MX1_PVA_LEU0.5], C: mini [MX1_PVA_LEU1], D: nano[MX1_PVA_LEU0], E: nano[MX1_PVA_LEU0.5], F: nano[MX1_PVA_LEU1].

9.3. Results of the density and powder flow test

The low density of the DPIs could offer better deposition in the airways. The ρ_t of the products was lower than or around 0.3 g/cm^3 . The density of the commercially available DPIs is approximately 1 g/cm^3 , therefore, the samples can be considered as low-density formulations. Favorably, the lower the ρ_t is, the higher the FPF is [213]. The application of a larger amount of LEU was reduced the ρ_b , therefore improved powder dispersibility [54]. The HR and CI results (Table 7.) were similar to other carrier-free formulations [214]. The HR and CI values indicated powder flow, which is also responsible for aerosolization.

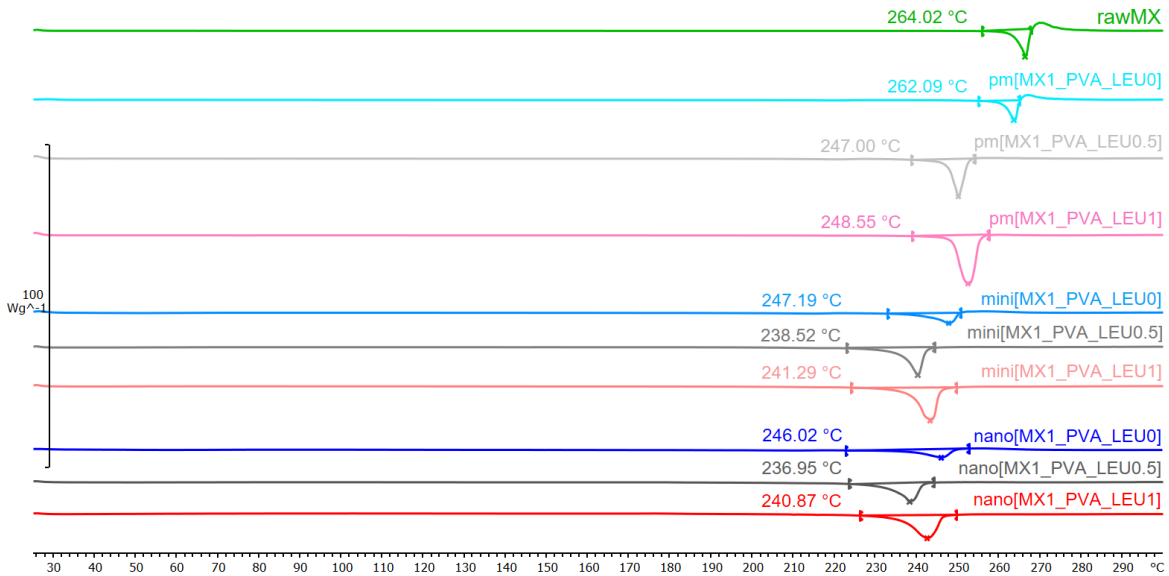
Table 7. Density, HI and CI results of the DPIs. Data are means \pm SD (n = 3 independent measurements).

Sample name	$\rho_b(\text{g/cm}^3)$	$\rho_t(\text{g/cm}^3)$	HR	CI
mini[MX1_PVA_LEU0]	0.18 ± 0.02	0.26 ± 0.00	1.49 ± 0.05	32.39 ± 7.23
mini[MX1_PVA_LEU0.5]	0.16 ± 0.01	0.27 ± 0.00	1.76 ± 0.08	43.09 ± 2.70
mini[MX1_PVA_LEU1]	0.15 ± 0.01	0.20 ± 0.01	1.40 ± 0.21	27.65 ± 10.8
nano[MX1_PVA_LEU0]	0.22 ± 0.01	0.31 ± 0.01	1.33 ± 0.09	27.27 ± 4.55
nano[MX1_PVA_LEU0.5]	0.22 ± 0.01	0.32 ± 0.02	1.43 ± 0.10	30.00 ± 5.00
nano[MX1_PVA_LEU1]	0.21 ± 0.00	0.32 ± 0.01	1.50 ± 0.08	33.33 ± 3.33

9.4. Analysis of the crystallinity

9.4.1. Results of the thermoanalytical measurement

DSC was employed to investigate the MX melting process in the case of the raw form, PM and dried products (Figure 13.). The raw MX showed a sharp endothermic peak at 264.03 °C, reflecting its melting point and crystallinity. After the preparation methods, the curves showed broader endothermic peaks of MX, indicating a decrease in their crystallinity. The residual MX crystals in the products were melted at a lower temperature than the raw MX due to the smaller particle size and amorphization. This was promoted by PVA, which has a T_g value at 85 °C [134].

**Figure 13.** DSC curves of the initial MX, PM and SPD samples.

9.4.2. Findings of the crystalline structure investigation

XRPD was used to characterize the crystalline state of MX before and after the preparation process. The XRPD pattern of the raw material demonstrated the crystalline structure of MX, which has characteristic peaks with the highest intensities at 6.6°, 11.4°, 13.1°, 13.5°, 15.1°, 18.7°, 19.3°, 25.9° and 26.4° 2-theta peaks [215]. In the case of the

products, the intensities of the characteristic peaks decreased, due to milling and spray drying (Figure 14.). After treatment, 73.23 % of the MX remained crystalline of the mini[MX1_PVA_LEU0], 51.81 % of the mini[MX1_PVA_LEU0.5] and 54.14 % of the mini[MX1_PVA_LEU1]. The other part of the API became amorphous during the preparation process. In nano[MX1_PVA_LEU0], nano[MX1_PVA_LEU0.5] and nano[MX1_PVA_LEU1] 68.19 %, 66.11% and 54.04 % of MX became amorphous, respectively [133].

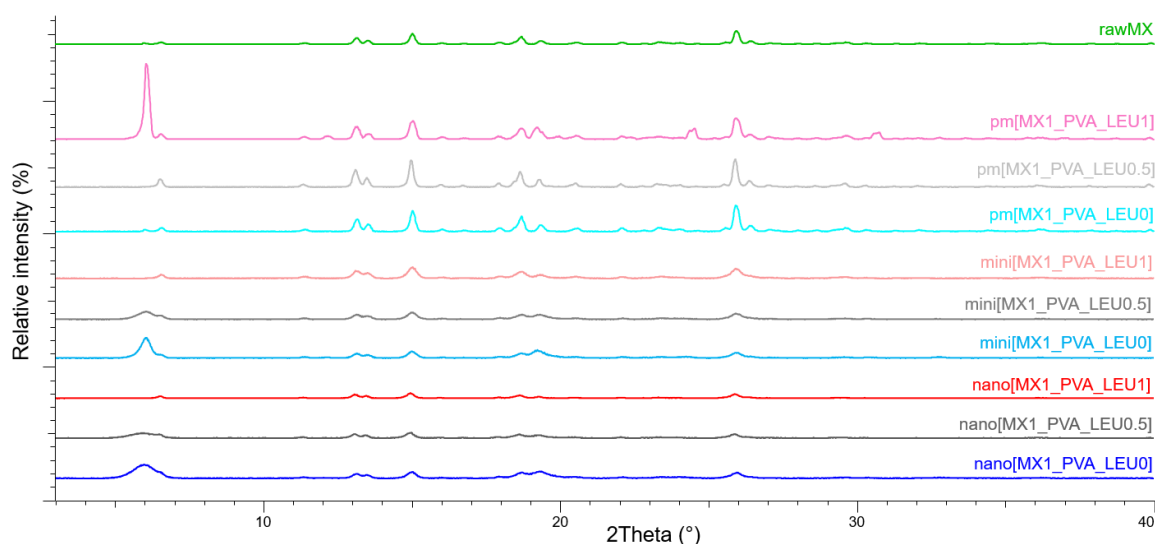


Figure 14. XRPD curves of the initial MX, PM and SPD samples.

9.5. Effects of the formulation on the solubility of MX

The initial solubility of the raw MX was 0.905 ± 0.005 mg/ml in artificial lung medium. As a result of the increased surface area of MX, the solubility of the mini and nano SPD samples improved in each case: 1.499 ± 0.012 mg/ml of mini[MX1_PVA_LEU0], 1.105 ± 0.001 mg/ml of mini[MX1_PVA_LEU0.5], 1.428 ± 0.000 mg/ml of mini[MX1_PVA_LEU1]. 2.025 ± 0.062 mg/ml of nano[MX1_PVA_LEU0], 1.501 ± 0.002 mg/ml of nano[MX1_PVA_LEU0.5] and 1.581 ± 0.029 mg/ml of nano[MX1_PVA_LEU1]. The reduction in drug particle size in the nano-range led to an increase in solubility, which predicted better dissolution properties [216].

9.6. Evaluation of the *in vitro* and *in silico* aerodynamic tests

9.6.1. Outcomes of the Andersen cascade impactor measurement

The *in vitro* aerodynamic investigation was carried out at different flow rates. The distribution of MX containing powders at 28.3 l/min is shown in Figure 15. Figure 16. showed the distribution of the deposited MX at 60 l/min. It can be concluded that the application of LEU decreased the remaining amount of powder in the capsules and the device and it also reduced the particle deposition in the induction port. The different API distributions are clearly observable at various flow rates.

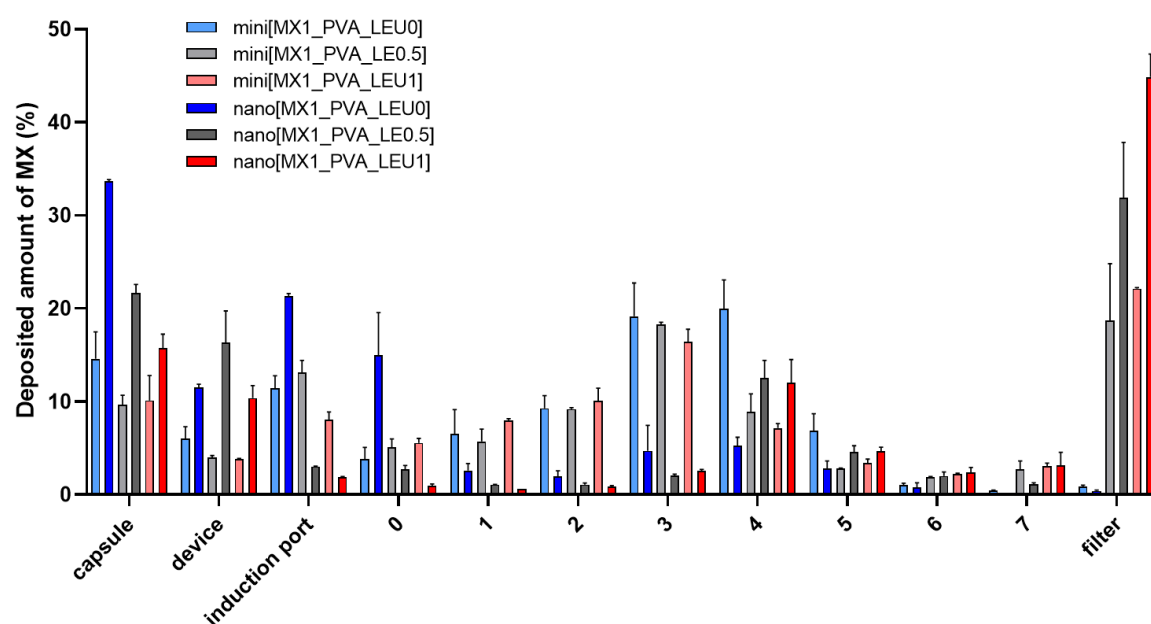


Figure 15. Distribution of DPIs at a flow rate of 28.3 l/min. Data are means \pm SD (n = 3 measurements).

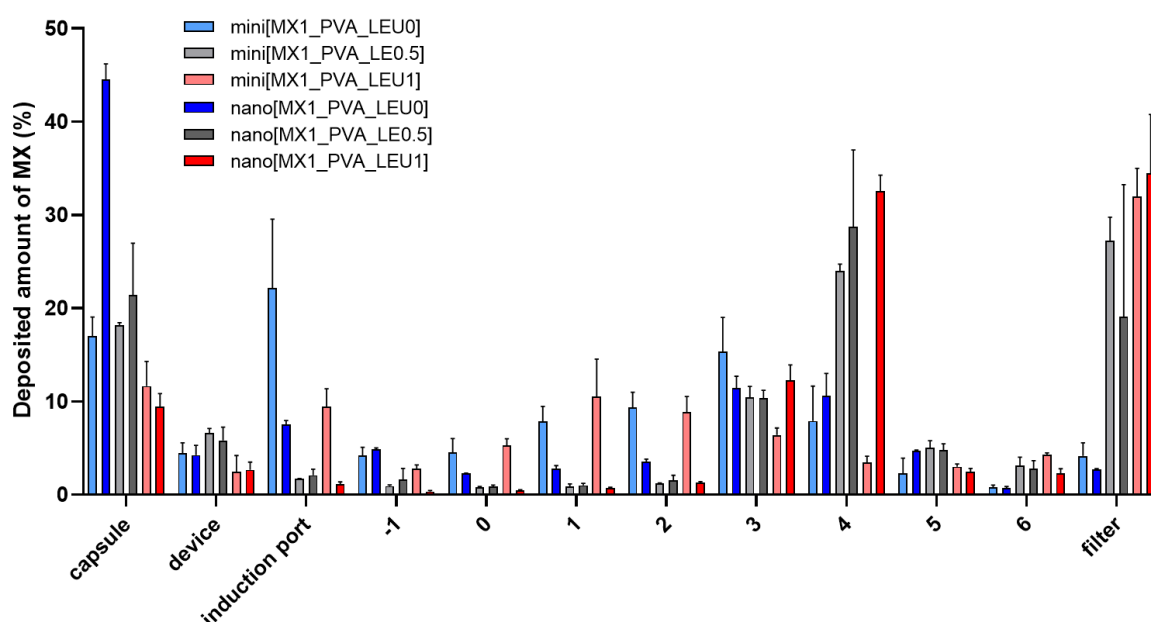


Figure 16. Distribution of the DPIs at a flow rate of 60 l/min. Data are means \pm SD (n = 3 measurements).

The *in vitro* aerodynamic results evaluated by the Inhalytix™ software are presented in Table 8. The MMAD values of the mini SPD samples were between 3.0-3.7 μm , which were appropriate to target the smaller conducting airways. The nano SPD samples containing LEU showed MMAD between 1.2 and 1.3 μm , which was preferable to reach the deeper parts of the airways [217]. There were MMADs smaller than 1 μm , which predicted the disintegration of the “nano-in-micro” formulations during inhalation. Interestingly, mini[MX1_PVA_LEU0.5] and mini[MX1_PVA_LEU1] showed this phenomenon at higher flow rates, compared to nano SPD samples. In the case of the LEU containing mini SPD samples, improved FPF values (up to 65%) were observed at both flow rates, indicating adequate drug delivery to patients with different lung conditions. The FPF values exceeded the commercially available DPI formulations in the Breezhale[®] device [218]. The nano SPD samples had FPF results between 87 and 95%, which was outstanding even in comparison to the formulations that are currently under development in the literature [83]. The EF values of the LEU containing samples were also larger, especially in the case of nano SPD samples, due to the improved aerosolization of the powder, owing to the reduced cohesion between the particles. Therefore, LEU guaranteed the improved liberation from the capsules compared to LEU free products. The results of ACI are promising in terms of therapeutic application, due to the currently available experimental data of inhalable nanoparticles suggesting a good correlation between *in vitro* cascade impactor measurements and clinical lung deposition [219,220].

Table 8. MMAD, FPF and EF of the DPIs at a flow rate of 28.3 and 60 l/min). Data are means \pm SD (n = 3 independent measurements).

Sample name	MMAD (μm)		FPF (%)		EF (%)	
	28.3 l/min	60 l/min	28.3 l/min	60 l/min	28.3 l/min	60 l/min
mini[MX1_PVA_LEU0]	3.63 ± 0.15	3.06 ± 0.62	68.82 ± 5.15	54.27 ± 14.41	72.42 ± 3.05	53.68 ± 15.68
mini[MX1_PVA_LEU0.5]	3.33 ± 0.35	0.88 ± 0.51	65.20 ± 4.84	72.16 ± 3.50	83.47 ± 1.33	61.48 ± 16.16
mini[MX1_PVA_LEU1]	3.37 ± 0.03	0.91 ± 0.40	67.03 ± 0.32	72.26 ± 2.57	75.22 ± 1.75	66.28 ± 12.25
nano[MX1_PVA_LEU0]	4.46 ± 0.65	2.17 ± 0.13	21.97 ± 4.98	62.62 ± 0.20	54.80 ± 0.46	28.02 ± 1.48
nano[MX1_PVA_LEU0.5]	0.51 ± 0.17	1.34 \pm 0.23	69.55 ± 4.29	86.16 ± 2.33	61.99 ± 2.48	54.29 ± 9.36
nano[MX1_PVA_LEU1]	0.33 ± 0.06	1.27 ± 0.07	82.93 ± 1.61	94.45 \pm 0.88	73.89 ± 2.86	92.42 ± 13.07

9.6.2. Findings of the *in silico* aerodynamic characterization

During the *in silico* characterization of the deposited and exhaled fractions of the samples, different breath holding times were determined (Table 9. and Table 10.). Extrathoracic deposition is lower for the LEU containing products, especially in the case of nano SPD samples (4-8 %), due to improved dispersity. Using a breath-holding time of 10 s, the deposition in the upper airways and the exhaled fraction decreased; therefore, the bronchial and acinar deposition improved in all cases. It was shown that the length of the breath holding had a significant impact on the deposited fraction [221], which is not taken into account during *in vitro* aerodynamic evaluation. Therefore, the combination of *in vitro* and *in silico* techniques is advantageous to provide a more informative analysis, which is practical before clinical trials [222]. Larger deposition values were obtained in the lungs in the case of mini SPD samples, and the exhaled fraction was larger in the case of the nano SPD samples. However, a longer breath holding time could decrease this exhaled fraction, therefore improving the deposition in smaller airways, especially in the acinar region of the products. Teaching the patients proper inhalation and breath holding techniques could improve the efficiency of the DPI and reach the smaller airways, as predicted by the ACI measurements. Therefore, the nano[MX1_PVA_LEU1] sample could be an impressive option in the therapy.

Table 9. *In silico* aerodynamic results of SPD samples at a flow rate of 28.3 l/min at a breath holding time of 5 and 10 s. Data are means \pm SD (n = 3 independent measurements).

Sample name	Extrathor. (%)		Bronchial (%)		Acinar (%)		Exhaled (%)	
	5 s	10 s	5 s	10 s	5 s	10 s	5 s	10 s
mini[MX1_PVA_LEU0]	20.75 ± 1.93	20.57 ± 1.93	14.54 ± 0.98	15.39 ± 1.00	33.65 ± 2.42	35.71 ± 2.40	10.48 ± 0.31	7.71 ± 0.26
mini[MX1_PVA_LEU0.5]	22.01 ± 2.30	21.86 ± 2.29	14.10 ± 0.85	14.69 ± 0.91	32.06 ± 0.94	35.06 ± 1.49	18.17 ± 3.43	14.72 ± 2.94
mini[MX1_PVA_LEU1]	18.82 ± 0.95	18.66 ± 0.95	14.32 ± 0.30	14.88 ± 0.31	32.65 ± 0.94	36.01 ± 1.03	20.25 ± 0.55	16.48 ± 0.44
nano[MX1_PVA_LEU0]	29.99 ± 2.31	29.92 ± 2.31	10.50 ± 0.48	10.77 ± 0.44	10.71 ± 1.61	11.42 ± 1.72	3.59 ± 0.72	2.69 ± 0.56
nano[MX1_PVA_LEU0.5]	6.64 ± 0.23	6.54 ± 0.22	6.15 ± 0.06	6.39 ± 0.12	25.93 ± 0.61	30.30 ± 0.96	23.24 ± 2.16	18.75 ± 1.86
nano[MX1_PVA_LEU1]	4.61 ± 0.28	4.51 ± 0.27	6.13 ± 0.40	6.33 ± 0.46	31.46 ± 1.56	37.20 ± 1.64	31.67 ± 0.62	25.85 ± 0.49

Table 10. *In silico* aerodynamic results of the SPD samples at a flow rate of 60 l/min at a breath holding time of 5 and 10 s. Data are means \pm SD (n = 3 independent measurements).

Sample name	Extrathor. (%)		Bronchial (%)		Acinar (%)		Exhaled (%)	
	5 s	10 s	5 s	10 s	5 s	10 s	5 s	10 s
mini[MX1_PVA_LEU0]	34.98 ± 8.09	34.53 ± 8.09	10.39 ± 0.05	10.39 ± 0.05	9.85 ± 1.76	12.80 ± 2.24	23.32 ± 7.35	20.68 ± 6.79
mini[MX1_PVA_LEU0.5]	20.36 ± 2.49	20.02 ± 2.48	7.99 ± 1.23	7.99 ± 1.23	13.98 ± 2.73	17.84 ± 3.47	33.11 ± 6.02	29.54 ± 5.35
mini[MX1_PVA_LEU1]	22.02 ± 2.62	21.56 ± 2.58	9.97 ± 0.65	9.97 ± 0.65	16.40 ± 0.81	20.92 ± 1.04	37.54 ± 0.82	33.46 ± 0.67
nano[MX1_PVA_LEU0]	16.41 ± 0.44	16.18 ± 0.43	6.15 ± 0.04	6.15 ± 0.04	7.16 ± 0.12	9.09 ± 0.13	21.49 ± 0.94	19.65 ± 0.92
nano[MX1_PVA_LEU0.5]	7.73 ± 2.06	7.57 ± 2.04	5.69 ± 0.52	5.69 ± 0.52	13.69 ± 2.56	17.11 ± 3.23	45.69 ± 4.17	42.18 ± 3.53
nano[MX1_PVA_LEU1]	6.06 ± 0.48	5.90 ± 0.47	6.16 ± 0.25	6.16 ± 0.25	18.18 ± 0.98	22.81 ± 1.22	57.49 ± 1.52	52.74 ± 1.29

Several commercially available DPIs were reported to have been tested with the stochastic lung model, demonstrating less sufficient lung deposition compared to the presented “nano-in-micro” DPI formulations [182,223].

9.6.3. Results of the characterization by Spraytec[®] device

LEU containing mini SPD and nano SPD formulations were chosen for further aerodynamic characterization. According to the Spraytec[®] test, the D [0.5] values of the samples were the following: 3.41 ± 0.05 μm of the mini[MX1_PVA_LEU0.5], 3.32 ± 0.01 μm of the mini[MX1_PVA_LEU1], 2.24 ± 0.03 μm of the nano[MX1_PVA_LEU0.5] and 1.92 ± 0.12 μm of the nano[MX1_PVA_LEU1]. The values were similar to the laser diffraction results in Section 9.1. The original goals in terms of particle size were achieved. However, LEU decreased the particle size such as the MMAD results of ACI. It demonstrated how LEU contributes to the dispersion and maintenance of particle uniqueness during aerosolization.

9.6.4. Particle size results according to particle counter

Formulations containing LEU were selected for additional aerodynamic characterization by particle counter. The geometric diameters of the particles are shown in Table 11. The particle size of the mini SPD particles was between 2 and 4 μm . The nano SPD DPI were below 2 μm , which corresponded to the definition of extra-fine particles ($d < 2$ μm) [59]. The results also met our initial particle size demand.

Table 11. The results of aerodynamic particle counting. Data are means \pm SD (n = 4 measurements).

Sample name	Number particle size (μm)	Surface particle size (μm)	Mass particle size (μm)
mini[MX1_PVA_LEU0.5]	1.552 ± 0.040	2.353 ± 0.058	2.912 ± 0.075
mini[MX1_PVA_LEU1]	1.625 ± 0.043	2.449 ± 0.089	3.017 ± 0.124
nano[MX1_PVA_LEU0.5]	1.043 ± 0.005	1.373 ± 0.007	1.594 ± 0.008
nano[MX1_PVA_LEU1]	0.986 ± 0.030	1.210 ± 0.039	1.330 ± 0.041

9.7. Results of the *in vitro* investigations of the pulmonary dosage form

9.7.1. Conclusion of the *in vitro* dissolution test

9.7.1.1. Outcomes of the conventional paddle method

During the *in vitro* drug release test, the amount of MX was the lowest for samples containing raw materials (Figure 17.). Approximately half of the drug was released from the mini SPD samples within the first 5 min compared to 5% from the reference samples. In the case of the nano SPD DPIs, in the first 5 min, up to 70% of the MX was released from the LEU containing samples, due to the smaller particle size and faster disintegration. These improvements are related to the higher specific surface area, enhanced solubility and amorphization of the MX in both cases. Hydrophilic PVA inhibited aggregation and increased polarity, LEU reduced the cohesion between the particles; therefore, a larger amount of MX was liberated. Additionally, faster drug release could be achieved in the presence of both excipients, due to their combined effect increasing the drug-solvent interactions [224]. The results are beneficial in local therapy, as it gives enough time to release the nanosized MX [73]. This sustained release can reduce the *in vivo* toxicity associated with the burst release effect [44].

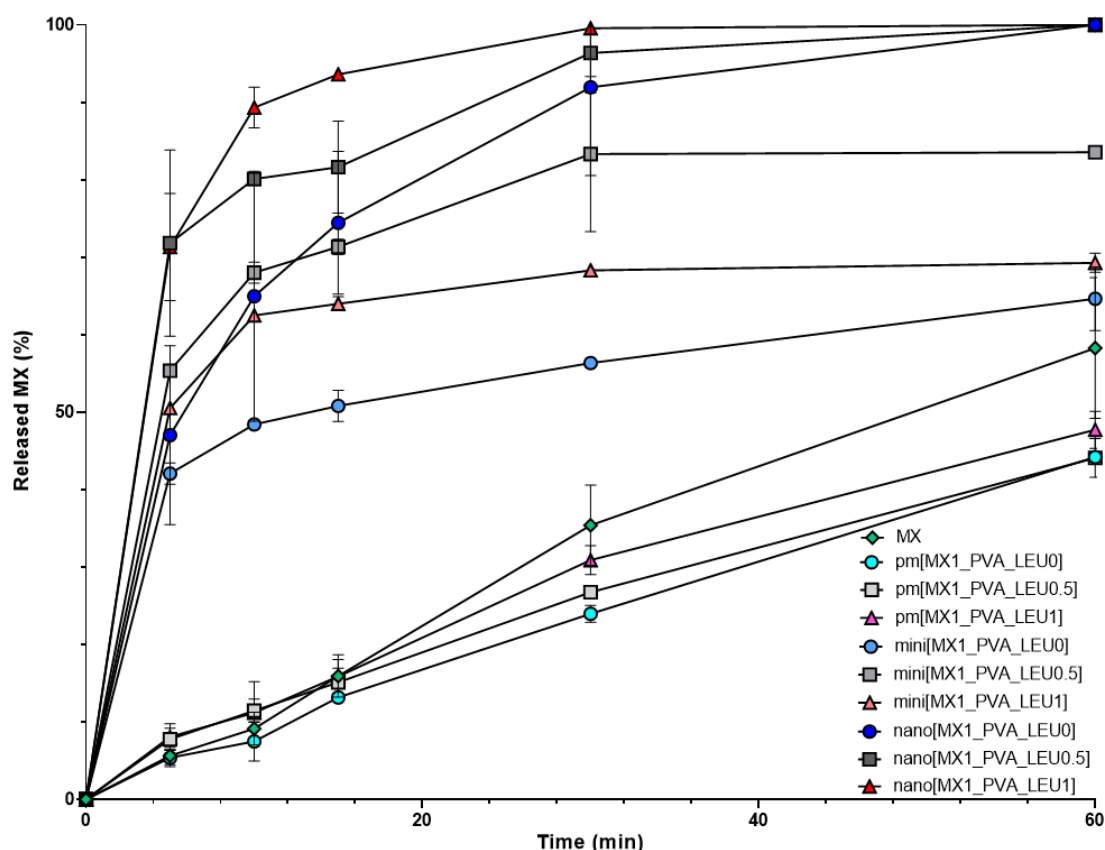


Figure 17. *In vitro* dissolution results of the DPIs containing the pulmonary dose of MX.

9.7.1.2. Findings of the dissolution test using paddle method combined with ACI

The released amount of MX of the largest LEU containing products was determined from the stage of the ACI, which collected the respirable fraction (mini[MX1_PVA_LEU1] and nano[MX1_PVA_LEU1]) and from the filter. The results were correlated with the ACI test and the conventional dissolution test (Figure 18.). Mini SPD DPIs showed a larger amount of dissolved API on the stage compared to the filter. In addition, almost 77% of the loaded API dose was released in the proper parts of the lung. In the case of nano SPD DPI, a smaller amount of MX was deposited on the stage; therefore, the released amount of MX was modest. However, an extensive amount of MX was found on the filter. Together, 85% of the pulmonary dose of MX was dissolved in the lung fluid.

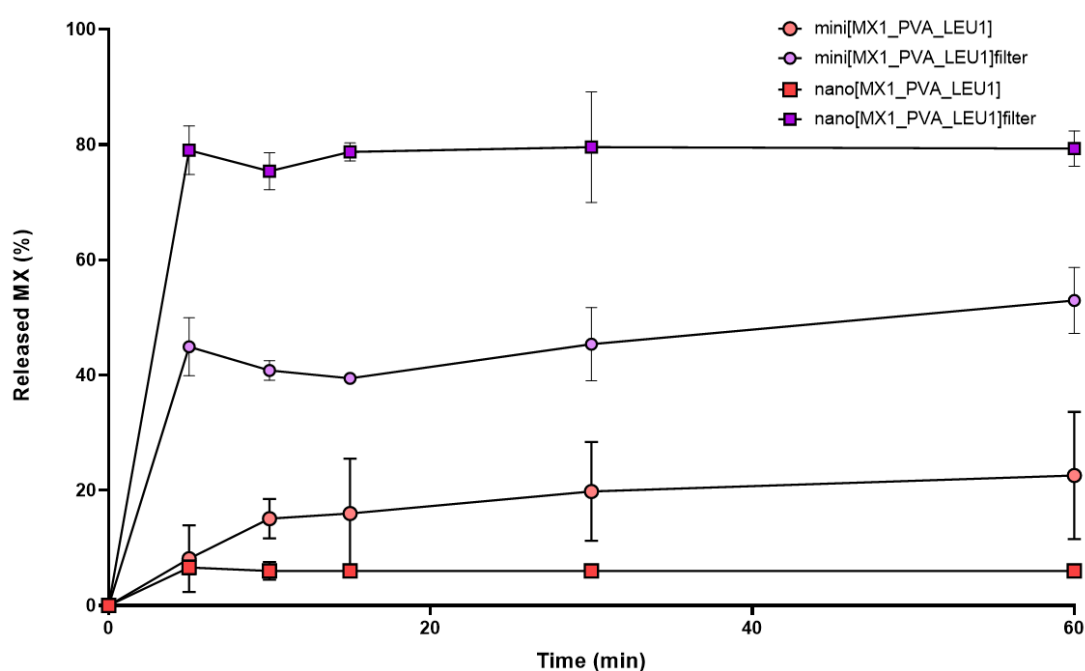


Figure 18. *In vitro* dissolution results of the DPIs containing the respirable fraction dose of MX.

9.7.2. Results of the *in vitro* permeability test

During the *in vitro* diffusion study, the high surface area achieved by the nanosized particles was the main factor that influenced the rate of passive diffusion. Diffusion of the API from the samples was larger in comparison to raw MX in all samples. The K_p values of the formulations significantly improved in five cases (0.37-0.65 cm/h). The products showed significantly increased J values in four cases (Figure 19.), compared to the PMs. The results were a remarkably high amount (60–110 $\mu\text{g}/\text{cm}^2$) if we take into account that the total surface of the lung is around 100 m^2 [225]. In overall, an increased amount of API could enter the epithelium using the SPD formulations.

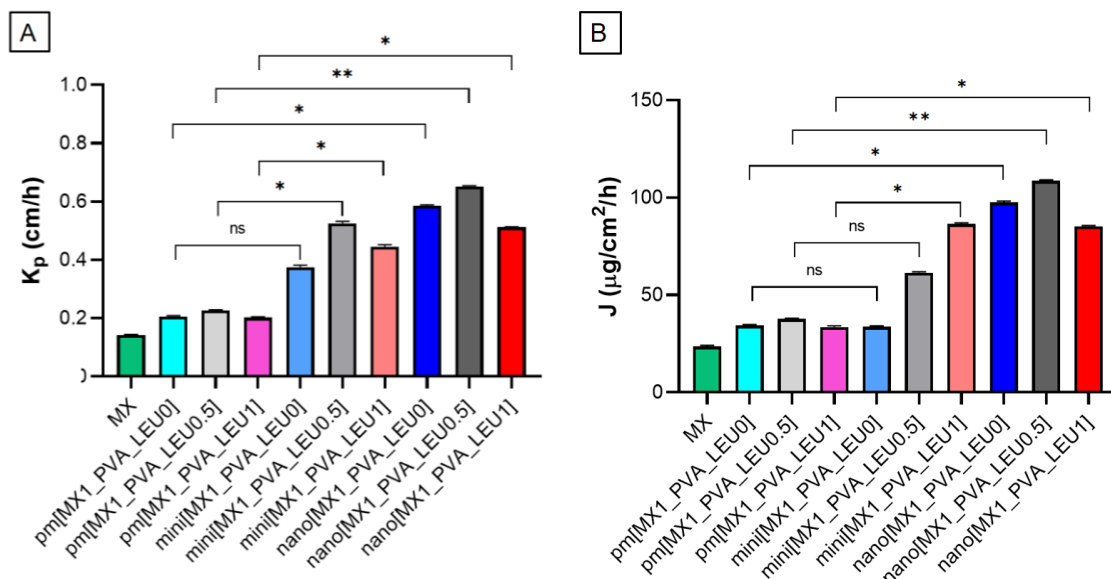


Figure 19. The results of the investigation of permeability. A: K_p results. B: J results. Data are means \pm S.D. ($n = 3$ independent measurements, level of significance: * $p < 0.05$, ** $p < 0.01$).

9.7.3. Consequences of the in vitro cell line investigations

9.7.3.1. Outcomes of the cytotoxicity measurement

The cytotoxicity test showed that all substances have a low cytotoxic effect at a concentration of 0.1 mg/ml. LPS did not have a cytotoxic effect. Cell viability was in order to MX, nano[MX1_PVA_LEU0], nano[MX1_PVA_LEU0.5], nano[MX1_PVA_LEU1] 91.97%, 90.32%, 80.38%, and 82.77%. The effect is not measurable at a concentration of 0.0125 mg. The findings were consistent with previous studies on the cytotoxicity effect of MX [226–228]. It can be concluded that the formulations are safe to administer pulmonary. The A549 cell lines showed similarities with type II alveolar epithelial cells, therefore, the results are valid to simulate the conditions of small airways [229].

9.7.3.2. Findings of the anti-inflammatory effect measurement

Nanosized MX containing samples inhibited IL-6 production on the translational level but not on the transcriptional level. LPS was used to increase IL-6 production in A549 cells [230]. LPS treated cells showed significantly higher relative expression compared to untreated cells; however, neither MX nor SPD formulation inhibited the increase of IL-6 (Figure 20.). Consequently, the level of IL-6 was checked *via* ELISA, and it was found that the expression of IL-6 increased significantly in LPS treated cells treated with LPS compared to cells untreated. Interestingly, MX and all SPD samples impeded IL-6 production (Figure 20.). IL-6 is a marker and target for the treatment of COVID-19. An increase in IL-6 concentration corresponds to respiratory failure and mortality, and its early reduction is promising for prolonged survival [231].

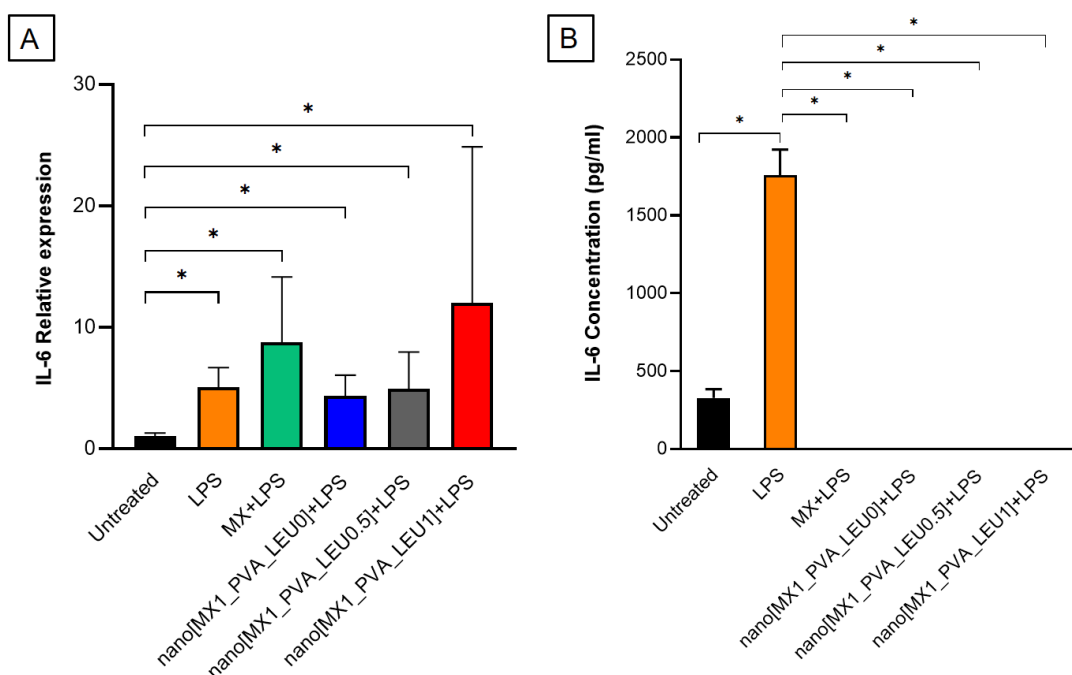


Figure 20. A: Relative expression of IL-6. A549 cells. B: Concentration of IL-6 in cell supernatants. The bars denote the standard for measurements made in triplicate. Level of significance: * $p < 0.05$).

9.8. Results of the stability test

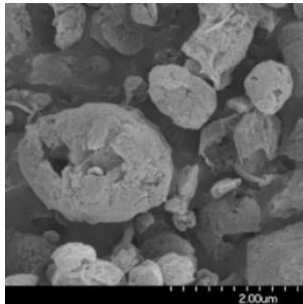
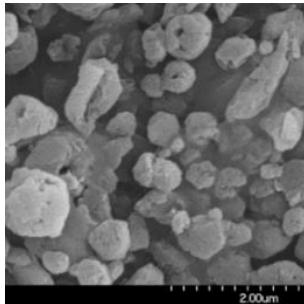
For the stability test, we had chosen the most promising nano[MX1_PVA_LEU1] (Table 12.). In addition to the proper characteristics of the samples, LEU has also stability-enhancing effect, mitigating moisture absorption with the hydrophobic shell [232].

According to laser diffraction measurement, there was no noticeable variation in size over the storage period, the particles remained within the required 1 to 5 μm range for lung delivery, proving that the particles did not agglomerate [53]. No significant changes occurred according to the DLS investigation. There was an increase in the Z-average, but it proved the disintegration of the system into nanoparticles. The ζ potential values did not increase significantly over time. Throughout the testing period, the formulation showed no signs of aggregation based on the SEM images. A slightly rougher surface can be observed due to air humidity, which was caused by a small amount of moisture absorption [233]. The DSC curves demonstrated that the partially amorphous characteristic of the samples persisted at 6 and 12 months. Fortunately, the results of the XRPD measurement supported the DSC findings because the recrystallization would have modified the other properties of the DPIs. According to the ACI test, beneficial aerodynamic properties were maintained. FPF values were above 90% and EF showed an only insignificant decrease. The *in silico* lung deposition was also similar to the initial data, using longer breath holding time the formulation would be outstandingly efficient. There was no change during *in vitro* drug

release from the samples over 12 months, nano[MX1_PVA_LEU1] preserved its advantageous dissolution properties.

As reported by the characterization, the developed DPI maintained its quality attributes for an extended period. However, further stability investigations could be required, such as a test in the final package.

Table 12. The results of the stability test for nano[MX1_PVA_LEU1].

Properties	6 months	12 months
D[0.5] (μm)	1.471 \pm 0.05	1.441 \pm 0.02
Span	1.562 \pm 0.47	1.357 \pm 0.01
Z average (nm)	548.57 \pm 35	657.37 \pm 46.9
ζ potential (mV)	-23.30 \pm 7.91	-22.23 \pm 0.55.
Morphology		
	Spherical form, Rough surface	Spherical form, Rough surface
Crystallinity (%)	42.51	41.89
FPF (%) (60 l/min)	92.90 \pm 0.80	93.85 \pm 0.31
<i>In silico</i> deposition (%)	Extrathoracic: 6.12 \pm 0.22	Extrathoracic: 5.46 \pm 0.32
10 s breath-holding time	Lung: 29.59 \pm 0.85	Lung: 28.51 \pm 0.50
	Exhaled: 48.45 \pm 2.11	Exhaled: 50.29 \pm 0.06
<i>In vitro</i> drug release	100 % in 30 min	100 % in 30 min

10. Conclusions

The purpose of the Ph.D. thesis was to develop an innovative, carrier-free “nano-in-micro” DPI system, that combines the advantages of the presence of nanosized API and the pulmonary drug delivery route. In addition to the organic-solvent free, combined preparation technique, a comprehensive investigation protocol for DPIs was developed. In line with the objectives of this dissertation, the following conclusions can be drawn:

- I. Based on a review of the literature, we pioneered the development of carrier-free “nano-in-micro” DPI formulations containing MX. To date, only a few studies have addressed the preparation of NSAID-containing DPIs, and none of them have discussed the pulmonary applicability of nanosized MX. As excipients, the combination of PVA and LEU was investigated for the first time with nanosized drug to achieve adequate lung deposition without the use of other additives.
- II. The nanosuspension was prepared using an organic solvent-free wet milling method in a planetary ball mill. The optimized process resulted in a monodisperse PSD and particle size of MX below 150 nm ($D[0.5] = 137.70 \pm 4.97$ nm according to laser diffraction and $D[0.5] = 124.90 \text{ nm} \pm 8.60$ nm according to NTA). The particle size and composition of the final suspension were suitable for further processing to create powders with a “nano-in-micro” structure.
- III. The nanosuspension was converted into a solid form by using two spray drying devices operating on different principles. It was found that both devices are capable of producing inhalation powders with suitable properties for pulmonary delivery, characterized by spherical shape and low density ($0.2\text{-}0.3 \text{ g/cm}^3$). The result of the mini spray drying was a “nano-in-micro” DPI, with particle size in the $3\text{--}4 \text{ }\mu\text{m}$ range to target the bronchiolar part of the airways. Nano spray dryer was utilized to create extra-fine particles smaller than $2 \text{ }\mu\text{m}$ to reach the alveolar region of the lungs. The main differences between the two drying devices were in the yield, the particle size achieved and consequently the deposition pattern. The yield of spray drying methods should be further improved in the future, especially in terms of scale-up. The incorporation of PVA contributed to the manufacture of a stable nanosuspension. It also preserved the individuality of the MX particles in their solid state. LEU enhanced the dispersibility of the powder mixture and modified the morphology of the particles, which was supported by the results of different particle size studies and SEM images. The *in vitro* and *in silico* aerodynamic

characterizations demonstrated that the aerodynamic properties of the samples could be favorably influenced by appropriate LEU concentrations. *In vitro* drug release and permeability were improved by reducing interparticle cohesion.

- IV. The outstanding lung deposition of the products ($\text{FPF} = 72.26 \pm 2.57\%$ of mini[MX1_PVA_LEU1] and $94.45 \pm 0.88\%$ of nano[MX1_PVA_LEU1]) was demonstrated by different aerodynamic measurements. The results of the various investigation techniques confirmed the appropriate particle size of the DPI systems to target different regions of the lung for pulmonary delivery. The mini SPD samples showed an aerodynamic diameter between 3 and 4 μm . The particle size of the nano SPD LEU containing samples were under 2 μm . The *in silico* investigation demonstrated the proper particle deposition in the bronchial (mini SPD DPI systems) and the acinar regions (nano SPD DPI systems). The prolonged breath holding time decreased the amount of API deposited in the extrathoracic areas and in the exhaled fraction.
- V. Based on the *in vitro* drug release study (77% and 85% of the pulmonary dose of MX in 60 min) and the *in vitro* permeability study (MX between 60-110 $\mu\text{g}/\text{cm}^2$ in 60 min), it was concluded that the formulations are suitable for pulmonary delivery. Due to the larger surface area, amorphization and the additives, dissolution was rapid in the artificial lung medium and the *in vitro* permeability of the DPIs was improved. We confirmed that the concentrations of the products applied in the lung were not toxic in A549 cell lines used to model human alveolar epithelium. According to the *in vitro* cell line test, formulations can assert a potent effect on the reduction of general inflammation by decreasing the concentration of IL-6.
- VI. The stability of a “nano-in-micro” system is crucial for future product development. It can be reported that the nano[MX1_PVA_LEU1] formulation was stable, showing no significant changes in its critical parameters for pulmonary application after 6 and 12 months.

Currently, a small number of carrier-free formulations are commercially available, but their beneficial properties are making them increasingly popular in therapy. In addition, the application of nanoparticles could further increase their effectiveness. DPI formulations with extremely high lung deposition could have the potential to improve the quality of life of millions of chronic lung patients, thereby mitigating serious social and economic problems.

11. Novelty and practical relevance of the work

The new findings and practical aspects of the work are summarized as follows.

- A novel ‘spray drying from nanosuspension’ technology was developed to design MX containing “nano-in-micro” DPIs, offering the benefits of a green manufacturing process and based on literature the possibility of scale-up.
- The DPIs presented are the first in the literature to contain nanosized MX.
- The effect of combining PVA and LEU without other excipients was investigated for the first time for “nano-in-micro” DPI systems.
- A detailed investigation protocol was developed to test “nano-in-micro” DPIs including particle size analysis (laser diffraction, DLS, NTA), drug release tests (two different *in vitro* dissolution test method), and aerodynamic assessments (Andersen cascade impactor, Spraytec[®] device), which could form the basis for the development of other DPI systems in the future.
- The formulations containing nanosized MX created by different spray drying methods exhibited excellent aerodynamic properties and better *in vitro* and *in silico* aerodynamic behavior than currently commercially available products.
- The “nano-in-micro” systems have been shown to be safe and effective according to cell line investigations and to have long-term stability.
- The novel MX containing “nano-in-micro” DPIs may offer new opportunities for the use of NSAIDs in inhalation therapy for the effective local treatment of diseases with pulmonary inflammation, such as pulmonary fibrosis, COPD, NSCLC and pneumonia caused by COVID-19 and it would be efficient for patients with weak breathing parameters.
- The preparation method could be beneficial for improving the bioavailability of other drugs with poor water-solubility, to expand the range of the treatable lung diseases (e.g. asthma, tuberculosis).

References

1. FDA Metered Dose Inhaler (MDI) and Dry Powder Inhaler (DPI) Products - Quality Considerations. *Cent. Drug Eval. Res. (CDER), Silver Spring* **2018**.
2. El-Gendy, N. et al. Scientific and Regulatory Activities Initiated by the U.S. Food and Drug Administration to Foster Approvals of Generic Dry Powder Inhalers: Quality Perspective. *Adv. Drug Deliv. Rev.* **2022**, *189*, 114519.
3. Soriano, J.B. et al. Prevalence and Attributable Health Burden of Chronic Respiratory Diseases, 1990–2017: A Systematic Analysis for the Global Burden of Disease Study 2017. *Lancet Respir. Med.* **2020**, *8*, 585–596.
4. Viegi, G. et al. Global Burden of Chronic Respiratory Diseases. *J. Aerosol Med. Pulm. Drug Deliv.* **2020**, *33*, 171–177.
5. Hanafi, N.S. et al. Chronic Respiratory Disease Surveys in Adults in Low- and Middle-Income Countries: A Systematic Scoping Review of Methodological Approaches and Outcomes. *J. Glob. Health* **2021**, *11*, 1–11.
6. Yıldız-Peköz, A. et al. Advances in Pulmonary Drug Delivery. *Pharmaceutics* **2020**, *12*, 1–7.
7. Strong, P. et al. Current Approaches to the Discovery of Novel Inhaled Medicines. *Drug Discov. Today* **2018**, *23*, 1705–1717.
8. Shahin, H.I. et al. A Comprehensive Overview of Dry Powder Inhalers for Pulmonary Drug Delivery: Challenges, Advances, Optimization Techniques, and Applications. *J. Drug Deliv. Sci. Technol.* **2023**, *84*, 104553.
9. Frijlink, H.W. et al. Dry Powder Inhalers for Pulmonary Drug Delivery. *Expert Opin. Drug Deliv.* **2004**, *1*, 67–86.
10. Shetty, N. et al. Physical Stability of Dry Powder Inhaler Formulations. *Expert Opin. Drug Deliv.* **2020**, *17*, 77–96.
11. Pilcer, G. et al. Formulation Strategy and Use of Excipients in Pulmonary Drug Delivery. *Int. J. Pharm.* **2010**, *392*, 1–19.
12. Woodcock, A. et al. Effects of Switching from a Metered Dose Inhaler to a Dry Powder Inhaler on Climate Emissions and Asthma Control: Post-Hoc Analysis. *Thorax* **2022**, 1187–1192.
13. Fulford, B. et al. Life-Cycle Assessment of the Breezhaler® Breath-Actuated Dry Powder Inhaler. *Sustain.* **2021**, *13*, 1–12.
14. Levy, M.L. et al. Understanding Dry Powder Inhalers: Key Technical and Patient Preference Attributes. *Adv. Ther.* **2019**, *36*, 2547–2557.
15. Liang, W. et al. Pulmonary Delivery of Biological Drugs. *Pharmaceutics* **2020**, *12*, 1–28.
16. Hebbink, G.A. et al. Recent Developments in Lactose Blend Formulations for Carrier-Based Dry Powder Inhalation. *Adv. Drug Deliv. Rev.* **2022**, *189*, 114527.
17. Benke, E. Development of Novel Formulated Ciprofloxacin Hydrochloride Containing Dry Powder Inhalation System, University of Szeged Faculty, 2023.
18. Lechanteur, A. et al. Influence of Composition and Spray-Drying Process Parameters on Carrier-Free DPI Properties and Behaviors in the Lung: A Review. *Pharmaceutics* **2020**, *12*, 1–22.
19. Chvatal, A. et al. Új Formulálási Stratégiák a Porinhalációs Készítmények Előállításában. *Gyógyszerészet* **2016**, 1–10.
20. Healy, A.M. et al. Dry Powders for Oral Inhalation Free of Lactose Carrier Particles. *Adv. Drug Deliv. Rev.* **2014**, *75*, 32–52.
21. Shahin, H.I. et al. A Comprehensive Overview of Dry Powder Inhalers for Pulmonary Drug Delivery: Challenges, Advances, Optimization Techniques, and Applications. *J. Drug Deliv. Sci. Technol.* **2023**, *84*, 104553.
22. Ye, Y. et al. The Future of Dry Powder Inhaled Therapy: Promising or Discouraging for Systemic Disorders? *Int. J. Pharm.* **2022**, *614*, 121457.
23. Liang, Z. et al. Recent Advances in Controlled Pulmonary Drug Delivery. *Drug Discov. Today* **2015**, *20*, 380–389.

24. Zillen, D. et al. Natural and Bioinspired Excipients for Dry Powder Inhalation Formulations. *Curr. Opin. Colloid Interface Sci.* **2021**, *56*, 101497.
25. Minne, A. et al. Optimization of the Aerosolization Properties of an Inhalation Dry Powder Based on Selection of Excipients. *Eur. J. Pharm. Biopharm.* **2008**, *70*, 839–844.
26. Prota, L. et al. Leucine Enhances Aerosol Performance of Naringin Dry Powder and Its Activity on Cystic Fibrosis Airway Epithelial Cells. *Int. J. Pharm.* **2011**, *412*, 8–19.
27. Simon, A. et al. Development of a Novel Dry Powder Inhalation Formulation for the Delivery of Rivastigmine Hydrogen Tartrate. *Int. J. Pharm.* **2016**, *501*, 124–138.
28. Li, L. et al. L-Leucine as an Excipient against Moisture on in Vitro Aerosolization Performances of Highly Hygroscopic Spray-Dried Powders. *Eur. J. Pharm. Biopharm.* **2016**, *102*, 132–141.
29. Tewes, F. et al. Development and Characterisation of Soluble Polymeric Particles for Pulmonary Peptide Delivery. *Eur. J. Pharm. Sci.* **2010**, *41*, 337–352.
30. Yang, M. et al. Design and Evaluation of Inhalable Chitosan-Modified Poly (DL-Lactic-Co-Glycolic Acid) Nanocomposite Particles. *Eur. J. Pharm. Sci.* **2012**, *47*, 235–243.
31. Iskandar, F. et al. Production of Morphology-Controllable Porous Hyaluronic Acid Particles Using a Spray-Drying Method. *Acta Biomater.* **2009**, *5*, 1027–1034.
32. Martinelli, F. et al. Engineered Sodium Hyaluronate Respirable Dry Powders for Pulmonary Drug Delivery. *Int. J. Pharm.* **2017**, *517*, 286–295.
33. Scalia, S. et al. Quercetin Solid Lipid Microparticles: A Flavonoid for Inhalation Lung Delivery. *Eur. J. Pharm. Sci.* **2013**, *49*, 278–285.
34. Mehta, P. Dry Powder Inhalers : A Focus on Advancements In. *J. od drug Deliv.* **2016**, *2016*, 1–17.
35. Lam, J. et al. Tobramycin Inhalation Powder (TIP): An Efficient Treatment Strategy for the Management of Chronic Pseudomonas Aeruginosa Infection in Cystic Fibrosis. *Clin. Med. Insights Circ. Respir. Pulm. Med.* **2013**, *7*, 61–77.
36. Li, H.Y. et al. The Use of Sodium Carboxymethylcellulose in the Preparation of Spray-Dried Proteins for Pulmonary Drug Delivery. *Eur. J. Pharm. Sci.* **2010**, *40*, 56–61.
37. Malamatar, M. et al. Preparation of Respirable Nanoparticle Agglomerates of the Low Melting and Ductile Drug Ibuprofen: Impact of Formulation Parameters. *Powder Technol.* **2017**, *308*, 123–134.
38. Möbus, K. et al. Zinc-Alginate Microparticles for Controlled Pulmonary Delivery of Proteins Prepared by Spray-Drying. *Eur. J. Pharm. Biopharm.* **2012**, *81*, 121–130.
39. Alipour, S. et al. Preparation and Characterization of Biodegradable Paclitaxel Loaded Alginate Microparticles for Pulmonary Delivery. *Colloids Surfaces B Biointerfaces* **2010**, *81*, 521–529.
40. Dellamary, L.A. et al. Hollow Porous Particles in Metered. **2000**, *17*, 168–174.
41. Ogienko, A.G. et al. Large Porous Particles for Respiratory Drug Delivery. Glycine-Based Formulations. *Eur. J. Pharm. Sci.* **2017**, *110*, 148–156.
42. Weers, J. et al. The PulmoSphere™ Platform for Pulmonary Drug Delivery. *Ther. Deliv.* **2014**, *5*, 277–295.
43. Makhlof, A. et al. Nanoparticles of Glycol Chitosan and Its Thiolated Derivative Significantly Improved the Pulmonary Delivery of Calcitonin. *Int. J. Pharm.* **2010**, *397*, 92–95.
44. Mukhtar, M. et al. Aerodynamic Properties and in Silico Deposition of Isoniazid Loaded Chitosan/Thiolated Chitosan and Hyaluronic Acid Hybrid Nanoplex DPIs as a Potential TB Treatment. *Int. J. Biol. Macromol.* **2020**, *165*, 3007–3019.
45. Angelo, R. et al. Technosphere® Insulin: Defining the Role of Technosphere Particles at the Cellular Level. *J. Diabetes Sci. Technol.* **2009**, *3*, 545–554.
46. Kim, D.H. et al. Solubility Enhancement and Application of Cyclodextrins in Local Drug Delivery. *J. Pharm. Investig.* **2020**, *50*, 17–27.
47. Karimi, K. et al. Physicochemical Stability and Aerosolization Performance of Dry Powder Inhalation System Containing Ciprofloxacin Hydrochloride. *J. Pharm. Biomed. Anal.* **2018**,

- 148, 73–79.
48. Parlati, C. et al. Pulmonary Spray Dried Powders of Tobramycin Containing Sodium Stearate to Improve Aerosolization Efficiency. *Pharm. Res.* **2009**, 26, 1084–1092.
 49. Yu, J. et al. Protective Effect of Sodium Stearate on the Moisture-Induced Deterioration of Hygroscopic Spray-Dried Powders. *Int. J. Pharm.* **2018**, 541, 11–18.
 50. ElKasabgy, N.A. et al. Respiratory Tract: Structure and Attractions for Drug Delivery Using Dry Powder Inhalers. *AAPS PharmSciTech* **2020**, 21, 12–15.
 51. Bennett, W.D. et al. Targeting Delivery of Aerosols to Different Lung Regions. *J. Aerosol Med.* **2002**, 15, 179–188.
 52. Liu, Q. et al. Physicochemical Properties Affecting the Fate of Nanoparticles in Pulmonary Drug Delivery. *Drug Discov. Today* **2020**, 25, 150–159.
 53. Darquenne, C. Aerosol Deposition in Health and Disease. *J. Aerosol Med. Pulm. Drug Deliv.* **2012**, 25, 140–147.
 54. Miller, D.P. et al. Targeting of Inhaled Therapeutics to the Small Airways: Nanoleucine Carrier Formulations. *Pharmaceutics* **2021**, 13.
 55. Chishti, N. et al. Nano-Embedded Microparticles Based Dry Powder Inhaler for Lung Cancer Treatment. *J. Res. Pharm.* **2020**, 24, 425–435.
 56. Heyder, J. Deposition of Inhaled Particles in the Human Respiratory Tract and Consequences for Regional Targeting in Respiratory Drug Delivery. *Proc. Am. Thorac. Soc.* **2004**, 1, 315–320.
 57. Thorley, A.J. et al. New Perspectives in Nanomedicine. *Pharmacol. Ther.* **2013**.
 58. Das, S.C. et al. *Nanomedicine in Pulmonary Delivery*; Elsevier Inc., 2021; ISBN 9780128204665.
 59. Hillyer, E. V. et al. Harmonizing the Nomenclature for Therapeutic Aerosol Particle Size: A Proposal. *J. Aerosol Med. Pulm. Drug Deliv.* **2018**, 31, 111–113.
 60. Jetzer, M.W. et al. Probing the Particulate Microstructure of the Aerodynamic Particle Size Distribution of Dry Powder Inhaler Combination Products. *Int. J. Pharm.* **2018**, 538, 30–39.
 61. Tse, J.Y. et al. Enhancement of the Extra-Fine Particle Fraction of Levofloxacin Embedded in Excipient Matrix Formulations for Dry Powder Inhaler Using Response Surface Methodology. *Eur. J. Pharm. Sci.* **2021**, 156, 105600.
 62. De Boer, A.H. et al. Can “extrafine” Dry Powder Aerosols Improve Lung Deposition? *Eur. J. Pharm. Biopharm.* **2015**, 96, 143–151.
 63. Potočník, J. Commission Recommendation of 18 October 2011 on the Definition of Nanomaterial. *Off. J. Eur. Union* **2011**.
 64. U.S. Food and Drug Administration Guidance for Industry Considering Whether an FDA-Regulated Product Involves the Application of Nanotechnology Available online: <https://www.fda.gov/media/88423/download>.
 65. Keck, C.M. et al. Drug Nanocrystals of Poorly Soluble Drugs Produced by High Pressure Homogenisation. *Eur. J. Pharm. Biopharm.* **2006**, 62, 3–16.
 66. Scherließ, R. et al. Particle Engineering in Dry Powders for Inhalation. *Eur. J. Pharm. Sci.* **2022**, 172.
 67. Muralidharan, P. et al. Inhalable Nanoparticulate Powders for Respiratory Delivery. *Nanomedicine Nanotechnology, Biol. Med.* **2015**, 11, 1189–1199.
 68. Hastedt, J.E. et al. Scope and Relevance of a Pulmonary Biopharmaceutical Classification System AAPS/FDA/USP Workshop March 16-17th, 2015 in Baltimore, MD. *AAPS Open* **2016**, 2, 1–20.
 69. Hastedt, J.E. et al. IBCS: 1. Principles and Framework of an Inhalation-Based Biopharmaceutics Classification System. *Mol. Pharm.* **2022**.
 70. Hastedt, J.E. et al. IBCS: 3. A Biopharmaceutics Classification System for Orally Inhaled Drug Products. *Mol. Pharm.* **2023**.
 71. Malamatar, M. et al. Spray Drying for the Preparation of Nanoparticle-Based Drug Formulations as Dry Powders for Inhalation. *Processes* **2020**, 8.
 72. Gaikwad, S.S. et al. Dry Powder Inhaler with the Technical and Practical Obstacles, and

- Forthcoming Platform Strategies. *J. Control. Release* **2023**, 355, 292–311.
73. Ruge, C.C. et al. Pulmonary Drug Delivery: From Generating Aerosols to Overcoming Biological Barriers-Therapeutic Possibilities and Technological Challenges. *Lancet Respir. Med.* **2013**, 1, 402–413.
 74. Wang, W. et al. Pulmonary Delivery Nanomedicines towards Circumventing Physiological Barriers: Strategies and Characterization Approaches. *Adv. Drug Deliv. Rev.* **2022**, 185, 114309.
 75. Donahue, N.D. et al. Concepts of Nanoparticle Cellular Uptake, Intracellular Trafficking, and Kinetics in Nanomedicine. *Adv. Drug Deliv. Rev.* **2019**, 143, 68–96.
 76. Torge, A. et al. The Influence of Mannitol on Morphology and Disintegration of Spray-Dried Nano-Embedded Microparticles. *Eur. J. Pharm. Sci.* **2017**, 104, 171–179.
 77. Bakand, S. et al. Toxicological Considerations, Toxicity Assessment, and Risk Management of Inhaled Nanoparticles. *Int. J. Mol. Sci.* **2016**, 17, 1–17.
 78. Hayes, A.J. et al. Toxicological Perspectives of Inhaled Therapeutics and Nanoparticles. *Expert Opin. Drug Metab. Toxicol.* **2014**, 10, 933–947.
 79. Kole, E. et al. Nanotherapeutics for Pulmonary Drug Delivery: An Emerging Approach to Overcome Respiratory Diseases. *J. Drug Deliv. Sci. Technol.* **2023**, 81.
 80. Ali, R. et al. Development and Clinical Trial of Nano-Atropine Sulfate Dry Powder Inhaler as a Novel Organophosphorous Poisoning Antidote. *Nanomedicine Nanotechnology, Biol. Med.* **2009**, 5, 55–63.
 81. Safety, Tolerability and Pharmacokinetics of Inhaled Nanoparticle Formulation of Remdesivir (GS-5734) and NA-831 (NEUROSIVIR) Available online: <https://clinicaltrials.gov/study/NCT04480333>.
 82. Inhaled Nanosilver Study Available online: <https://clinicaltrials.gov/study/NCT02408874>.
 83. Chan, H.W. et al. Inhalable Nanoparticle-Based Dry Powder Formulations for Respiratory Diseases: Challenges and Strategies for Translational Research. *AAPS PharmSciTech* **2023**, 24.
 84. Silva, A.S. et al. Sustainable Strategies for Nano-in-Micro Particle Engineering for Pulmonary Delivery. *J. Nanoparticle Res.* **2014**, 16.
 85. Haghighi, D.M. et al. Spray Freeze Drying to Solidify Nanosuspension of Cefixime into Inhalable Microparticles. *DARU, J. Pharm. Sci.* **2022**, 30, 17–27.
 86. Farhangi, M. et al. Optimization of a Dry Powder Inhaler of Ciprofloxacin-Loaded Polymeric Nanomicelles by Spray Drying Process. *Pharm. Dev. Technol.* **2019**, 24, 584–592.
 87. Yu, H. et al. Dry Powder Inhaler Formulation of High-Payload Antibiotic Nanoparticle Complex Intended for Bronchiectasis Therapy: Spray Drying versus Spray Freeze Drying Preparation. *Int. J. Pharm.* **2016**, 499, 38–46.
 88. Hu, X. et al. Docetaxel-Loaded Cholesterol-PEG Co-Modified Poly (N-Butyl) Cyanoacrylate Nanoparticles for Antitumor Drug Pulmonary Delivery: Preparation, Characterization, and in Vivo Evaluation. *Int. J. Nanomedicine* **2020**, 15, 5361–5376.
 89. Nemati, E. et al. Ethambutol-Loaded Solid Lipid Nanoparticles as Dry Powder Inhalable Formulation for Tuberculosis Therapy. *AAPS PharmSciTech* **2019**, 20.
 90. Satari, N. et al. Preparation and Evaluation of Inhalable Dry Powder Containing Glucosamine-Conjugated Gefitinib SLNs for Lung Cancer Therapy. *Drug Dev. Ind. Pharm.* **2020**, 0, 1265–1277.
 91. Party, P. et al. Preparation and Characterization of Ibuprofen Containing Nano - Embedded - Microparticles for Pulmonary Delivery. *Pharmaceutics* **2023**, 15, 1–16.
 92. Mukhtar, M. et al. Dry Powder Comprised of Isoniazid-Loaded Nanoparticles of Hyaluronic Acid in Conjugation with Mannose-Anchored Chitosan for Macrophage-Targeted Pulmonary Administration in Tuberculosis. *Pharmaceutics* **2022**, 14.
 93. Wan, K.Y. et al. Converting Nanosuspension into Inhalable and Redispersible Nanoparticles by Combined In-Situ Thermal Gelation and Spray Drying. *Eur. J. Pharm. Biopharm.* **2020**, 149, 238–247.

94. Porsio, B. et al. Inhalable Nano into Micro Dry Powders for Ivacaftor Delivery: The Role of Mannitol and Cysteamine as Mucus-Active Agents. *Int. J. Pharm.* **2020**, 582, 119304.
95. Banat, H. et al. A Novel Combined Dry Powder Inhaler Comprising Nanosized Ketoprofen-Embedded Mannitol-Coated Microparticles for Pulmonary Inflammations: Development, In Vitro–In Silico Characterization, and Cell Line Evaluation. *Pharmaceuticals* **2024**, 17.
96. El Baihary, D. et al. Pharmacokinetic/Pulmokinetic Analysis of Optimized Lung Targeted Spray Dried Ketotifen-Dextran Core Shell Nanocomplexes–in-Microparticles. *Int. J. Biol. Macromol.* **2019**, 139, 678–687.
97. Wang, Y. et al. A Comparison between Spray Drying and Spray Freeze Drying for Dry Powder Inhaler Formulation of Drug-Loaded Lipid-Polymer Hybrid Nanoparticles. *Int. J. Pharm.* **2012**, 424, 98–106.
98. Cheow, W.S. et al. Spray-Freeze-Drying Production of Thermally Sensitive Polymeric Nanoparticle Aggregates for Inhaled Drug Delivery: Effect of Freeze-Drying Adjuvants. *Int. J. Pharm.* **2011**, 404, 289–300.
99. Abdelrady, H. et al. Exploiting Gelatin Nanocarriers in the Pulmonary Delivery of Methotrexate for Lung Cancer Therapy. *Eur. J. Pharm. Sci.* **2019**, 133, 115–126.
100. Mohamed, A. et al. Polymeric Nanoparticles for the Delivery of MiRNA to Treat Chronic Obstructive Pulmonary Disease (COPD). *Eur. J. Pharm. Biopharm.* **2019**, 136, 1–8.
101. Puri, V. et al. Inhalation Potential of N-Acetylcysteine Loaded PLGA Nanoparticles for the Management of Tuberculosis: In Vitro Lung Deposition and Efficacy Studies. *Curr. Res. Pharmacol. Drug Discov.* **2022**, 3, 100084.
102. Rezazadeh, M. et al. Preparation and Characterization of Spray-Dried Inhalable Powders Containing Polymeric Micelles for Pulmonary Delivery of Paclitaxel in Lung Cancer. *J. Pharm. Pharm. Sci.* **2018**, 21, 200s-214s.
103. Kunda, N.K. et al. Pulmonary Dry Powder Vaccine of Pneumococcal Antigen Loaded Nanoparticles. *Int. J. Pharm.* **2015**, 495, 903–912.
104. Craparo, E.F. et al. Development of a Novel Rapamycin Loaded Nano- into Micro-Formulation for Treatment of Lung Inflammation. *Drug Deliv. Transl. Res.* **2022**, 12, 1859–1872.
105. Rawal, T. et al. Rifampicin Loaded Chitosan Nanoparticle Dry Powder Presents: An Improved Therapeutic Approach for Alveolar Tuberculosis. *Colloids Surfaces B Biointerfaces* **2017**, 154, 321–330.
106. Honmane, S. et al. Lung Delivery of Nanoliposomal Salbutamol Sulfate Dry Powder Inhalation for Facilitated Asthma Therapy. *J. Liposome Res.* **2019**, 29, 332–342.
107. Hu, J. et al. Spherical Agglomerates of Pure Drug Nanoparticles for Improved Pulmonary Delivery in Dry Powder Inhalers. *J. Nanoparticle Res.* **2013**, 15.
108. Dahmash, E.Z. et al. Novel Thymoquinone Nanoparticles Using Poly(Ester Amide) Based on L-Arginine-Targeting Pulmonary Drug Delivery. *Polymers (Basel)*. **2022**, 14.
109. Xu, Y. et al. Leucine Improves the Aerosol Performance of Dry Powder Inhaler Formulations of SiRNA-Loaded Nanoparticles. *Int. J. Pharm.* **2022**, 621.
110. Šimková, K. et al. Production of Fast-Dissolving Low-Density Powders for Improved Lung Deposition by Spray Drying of a Nanosuspension. *Eur. J. Pharm. Biopharm.* **2020**, 146, 19–31.
111. Bilgili, E. et al. Mechanistic Modeling of Wet Stirred Media Milling for Production of Drug Nanosuspensions. *AAPS PharmSciTech* **2021**, 22.
112. Seibert, K.D. et al. Milling Operations in the Pharmaceutical Industry. *Chem. Eng. Pharm. Ind.* **2019**, 861–879.
113. Singare, D.S. et al. Optimization of Formulation and Process Variable of Nanosuspension: An Industrial Perspective. *Int. J. Pharm.* **2010**, 402, 213–220.
114. Kumar, R. et al. Particle Size Reduction Techniques of Pharmaceutical Compounds for the Enhancement of Their Dissolution Rate and Bioavailability. *J. Pharm. Innov.* **2022**, 17, 333–352.
115. Van Eerdenbrugh, B. et al. Drying of Crystalline Drug Nanosuspensions-The Importance of

- Surface Hydrophobicity on Dissolution Behavior upon Redispersion. *Eur. J. Pharm. Sci.* **2008**, *35*, 127–135.
116. Li, X. et al. Nanoparticles by Spray Drying Using Innovative New Technology: The Büchi Nano Spray Dryer B-90. *J. Control. Release* **2010**, *147*, 304–310.
 117. Ordoubadi, M. et al. On the Physical Stability of Leucine-Containing Spray-Dried Powders for Respiratory Drug Delivery. *Pharmaceutics* **2023**, *15*, 1–26.
 118. Strojewski, D. et al. Spray Drying and Nano Spray Drying as Manufacturing Methods of Drug-Loaded Polymeric Particles. *Polim. medicina* **2022**, *52*, 101–111.
 119. Salama, A.H. Spray Drying as an Advantageous Strategy for Enhancing Pharmaceuticals Bioavailability. *Drug Deliv. Transl. Res.* **2020**, *10*, 1–12.
 120. European Medicines Agency ICH Q1A (R2) Stability Testing of New Drug Substances and Drug Products - Scientific Guideline Available online: <https://www.ema.europa.eu/en/ich-q1a-r2-stability-testing-new-drug-substances-drug-products-scientific-guideline>.
 121. Rabinow, B.E. Nanosuspensions in Drug Delivery. *Nat. Rev. Drug Discov.* **2004**, *3*, 785–796.
 122. Wu, L. et al. Physical and Chemical Stability of Drug Nanoparticles. *Adv. Drug Deliv. Rev.* **2011**, *63*, 456–469.
 123. Chang, R.Y.K. et al. Overcoming Challenges for Development of Amorphous Powders for Inhalation. *Expert Opin. Drug Deliv.* **2020**, *17*, 1583–1595.
 124. Szabó-Révész, P. Modifying the Physicochemical Properties of NSAIDs for Nasal and Pulmonary Administration. *Drug Discov. Today Technol.* **2018**, *27*, 87–93.
 125. Stigliani, M. et al. Non-Steroidal Anti-Inflammatory Drug for Pulmonary Administration: Design and Investigation of Ketoprofen Lysinate Fine Dry Powders. *Int. J. Pharm.* **2013**, *448*, 198–204.
 126. Yazdi, A.K. et al. Carrier-Free High-Dose Dry Powder Inhaler Formulation of Ibuprofen: Physicochemical Characterization and in Vitro Aerodynamic Performance. *Int. J. Pharm.* **2016**, *511*, 403–414.
 127. Jahangiri, A. et al. Carrier-Free Inhalable Dry Microparticles of Celecoxib: Use of the Electrospraying Technique. *Biomedicines* **2023**, *11*.
 128. Paclawski, A. et al. Development and Pharmacokinetics of a Novel Acetylsalicylic Acid Dry Powder for Pulmonary Administration. *Pharmaceutics* **2022**, *14*.
 129. Yazdi, A.K. et al. Hollow Crystalline Straws of Diclofenac for High-Dose and Carrier-Free Dry Powder Inhaler Formulations. *Int. J. Pharm.* **2016**, *502*, 170–180.
 130. Ceschan, N.E. et al. Carrier Free Indomethacin Microparticles for Dry Powder Inhalation. *Int. J. Pharm.* **2018**, *549*, 169–178.
 131. Meloxicam Available online: <https://pubchem.ncbi.nlm.nih.gov/compound/Meloxicam>.
 132. Meloxicam - Drugbank Available online: <https://go.drugbank.com/drugs/DB00814>.
 133. Bartos, C. et al. The Effect of an Optimized Wet Milling Technology on the Crystallinity, Morphology and Dissolution Properties of Micro- and Nanonized Meloxicam. *Molecules* **2016**, *21*.
 134. Bartos, C. et al. Optimization of a Combined Wet Milling Process in Order to Produce Poly(Vinyl Alcohol) Stabilized Nanosuspension. *Drug Des. Devel. Ther.* **2018**, *12*, 1567–1580.
 135. Pomázi, A. et al. Analysis of Co-Spray-Dried Meloxicam-Mannitol Systems Containing Crystalline Microcomposites. *J. Pharm. Biomed. Anal.* **2011**, *56*, 183–190.
 136. Benke, E. et al. Development of an Innovative, Carrier-based Dry Powder Inhalation Formulation Containing Spray-dried Meloxicam Potassium to Improve the in Vitro and in Silico Aerodynamic Properties. *Pharmaceutics* **2020**, *12*, 1–19.
 137. Chvatal, A. et al. Aerodynamic Properties and in Silico Deposition of Meloxicam Potassium Incorporated in a Carrier-Free DPI Pulmonary System. *Int. J. Pharm.* **2017**, *520*, 70–78.
 138. Chvatal, A. et al. Formulation and Comparison of Spray Dried Non-Porous and Large Porous Particles Containing Meloxicam for Pulmonary Drug Delivery. *Int. J. Pharm.* **2019**, *559*, 68–75.

139. Arafa, H.M.M. et al. Anti-Fibrotic Effect of Meloxicam in a Murine Lung Fibrosis Model. *Eur. J. Pharmacol.* **2007**, *564*, 181–189.
140. Weiss, A. et al. Chronic Obstructive Pulmonary Disease: A Palliative Medicine Review of the Disease, Its Therapies, and Drug Interactions. *J. Pain Symptom Manage.* **2020**, *60*, 135–150.
141. Suzuki, R. et al. A Phase II Study of Carboplatin and Paclitaxel with Meloxicam. *Lung Cancer* **2009**, *63*, 72–76.
142. da Silva, A.L. et al. New Perspectives in Nanotherapeutics for Chronic Respiratory Diseases. *Biophys. Rev.* **2017**, *9*, 793–803.
143. Yokouchi, H. et al. Cyclooxygenase-2 Inhibitors for Non-Small-Cell Lung Cancer: A Phase II Trial and Literature Review. *Mol. Clin. Oncol.* **2014**, *2*, 744–750.
144. Chen, J.S. et al. Cyclooxygenase-2 Is Induced by SARS-CoV-2 Infection but Does Not Affect Viral Entry or Replication. *bioRxiv* **2020**.
145. Meyer, K.C. et al. Regional Variability of Lung Inflammation in Cystic Fibrosis. *Am. J. Respir. Crit. Care Med.* **1997**, *156*, 1536–1540.
146. Mott, L.S. et al. Distribution of Early Structural Lung Changes Due to Cystic Fibrosis Detected with Chest Computed Tomography. *J. Pediatr.* **2013**, *163*, 243–248.e3.
147. Smith, B.M. et al. Location, Location, Location: Studying Anatomically Comparable Airways Is Highly Relevant to Understanding COPD. *Thorax* **2014**, *69*, 1049–1050.
148. Wang, C. et al. Progress in the Mechanism and Targeted Drug Therapy for COPD. *Signal Transduct. Target. Ther.* **2020**, *5*.
149. Ohara, T. et al. Comparison of Airway Dimensions in Different Anatomic Locations on Chest CT in Patients with COPD. *Respirology* **2006**, *11*, 579–585.
150. Lee, H.W. et al. Location of Stage I–III Non-Small Cell Lung Cancer and Survival Rate: Systematic Review and Meta-Analysis. *Thorac. Cancer* **2018**, *9*, 1614–1622.
151. Ashique, S. et al. Nano-Mediated Strategy for Targeting and Treatment of Non-Small Cell Lung Cancer (NSCLC). *Naunyn. Schmiedeberg's Arch. Pharmacol.* **2023**, *396*, 2769–2792.
152. Madas, B.G. et al. Deposition Distribution of the New Coronavirus (SARS-CoV-2) in the Human Airways upon Exposure to Cough-Generated Droplets and Aerosol Particles. *Sci. Rep.* **2020**, *10*, 1–8.
153. Chugh, H. et al. A Comprehensive Review on Potential Therapeutics Interventions for COVID-19. *Eur. J. Pharmacol.* **2021**, *890*, 173741.
154. Iwabuchi, K. et al. Therapeutic Potential of Ciclesonide Inhalation for COVID-19 Pneumonia: Report of Three Cases. *J. Infect. Chemother.* **2020**, *26*, 625–632.
155. Ong, S.W.X. et al. Safety and Potential Efficacy of Cyclooxygenase-2 Inhibitors in Coronavirus Disease 2019. *Clin. Transl. Immunol.* **2020**, *9*, 1–9.
156. Pomázi, A. et al. Effect of Polymers for Aerolization Properties of Mannitol-Based Microcomposites Containing Meloxicam. *Eur. Polym. J.* **2013**, *49*, 2518–2527.
157. Feng, A.L. et al. Mechanistic Models Facilitate Efficient Development of Leucine Containing Microparticles for Pulmonary Drug Delivery. *Int. J. Pharm.* **2011**, *409*, 156–163.
158. Poly-Vinyl-Alcohol 4–98 Available online: <https://pubchem.ncbi.nlm.nih.gov/compound/Polyvinyl-Alcohol>.
159. L-Leucine Available online: <https://pubchem.ncbi.nlm.nih.gov/compound/Leucine>.
160. Merisko-Liversidge, E. et al. Nanosizing: A Formulation Approach for Poorly-Water-Soluble Compounds. *Eur. J. Pharm. Sci.* **2003**, *18*, 113–120.
161. Loh, Z.H. et al. Overview of Milling Techniques for Improving the Solubility of Poorly Water-Soluble Drugs. *Asian J. Pharm. Sci.* **2014**, *10*, 255–274.
162. Bartos, C. Optimization of a Combined Wet Milling Process to Produce Nanosuspension and Its Transformation into Surfactant-Free Solid Compositions to Increase the Product Stability and Drug Bioavailability, 2019.
163. Yang, D.L. et al. Micro-Sized Nanoaggregates: Spray-Drying-Assisted Fabrication and Applications. *Particuology* **2024**, *85*, 22–48.

164. Meuri, M. BÜCHI Labortechnik AG Spray Drying. **2013**.
165. Sosnik, A. et al. Advantages and Challenges of the Spray-Drying Technology for the Production of Pure Drug Particles and Drug-Loaded Polymeric Carriers. *Adv. Colloid Interface Sci.* **2015**, 223, 40–54.
166. Seville, P.C. et al. Amino Acid-Modified Spray-Dried Powders with Enhanced Aerosolisation Properties for Pulmonary Drug Delivery. *Powder Technol.* **2007**, 178, 40–50.
167. Schmid, K. et al. Evaluation of the Nano Spray Dryer B-90 for Pharmaceutical Applications. *Pharm. Dev. Technol.* **2011**, 16, 287–294.
168. Arpagaus, C. et al. *10 - Nanocapsules Formation by Nano Spray Drying*; Elsevier Inc., 2017;
169. Piñón-Balderrama, C.I. et al. Encapsulation of Active Ingredients in Food Industry by Spray-Drying and Nano Spray-Drying Technologies. *Processes* **2020**, 8.
170. Arpagaus, C. Nano Spray Dryer B-90: Literature Review and Applications. *Büchi Inf. Bull.* **2011**, 8.
171. Van Eerdenbrugh, B. et al. A Screening Study of Surface Stabilization during the Production of Drug Nanocrystals. *J. Pharm. Sci.* **2008**, 98, 2091–2103.
172. 2.9.34. Bulk Density of Powders. In *European Pharmacopoeia 11.5*; 2024; pp. 5830–5833.
173. 2.9.36. Powder Flow. In *European Pharmacopoeia 11.5*; 2024; pp. 5382–5386.
174. Parlati, C. Respirable Microparticles of Aminoglycoside Antibiotics for Pulmonary Administration, University of Parma, 2008.
175. 2.9.18. Preparation for Inhalation: Aerodynamic Assessment of Fine Particles. In *European Pharmacopoeia 11.0*; 2024; pp. 369–382.
176. Chapman, K.R. et al. Delivery Characteristics and Patients' Handling of Two Single-Dose Dry-Powder Inhalers Used in COPD. *Int. J. COPD* **2011**, 6, 353–363.
177. Molimard, M. et al. Performance Characteristics of Breezhaler® and Aerolizer® in the Real-World Setting. *Clin. Drug Investig.* **2021**, 41, 415–424.
178. Clark, A.R. et al. The Confusing World of Dry Powder Inhalers: It Is All about Inspiratory Pressures, Not Inspiratory Flow Rates. *J. Aerosol Med. Pulm. Drug Deliv.* **2020**, 33, 1–11.
179. Hofmann, W. Modelling Inhaled Particle Deposition in the Human Lung-A Review. *J. Aerosol Sci.* **2011**, 42, 693–724.
180. Raabe., O.G. et al. Tracheobronchial Geometry: Human, Dog, Rat, Hamster - A Compilation of Selected Data from the Project Respiratory Tract Deposition Models. *U.S. Gov. Print. Off.* **1976**, 1–11.
181. Farkas, Á. et al. Computer Modelling as a Tool in Characterization and Optimization of Aerosol Drug Delivery. *Aerosol Air Qual. Res.* **2015**, 15, 2466–2474.
182. Farkas, Á. et al. Numerical Simulation of Emitted Particle Characteristics and Airway Deposition Distribution of Symbicort® Turbuhaler® Dry Powder Fixed Combination Aerosol Drug. *Eur. J. Pharm. Sci.* **2016**, 93, 371–379.
183. Levet, V. et al. Development of Controlled-Release Cisplatin Dry Powders for Inhalation against Lung Cancers. *Int. J. Pharm.* **2016**, 515, 209–220.
184. Abadelah, M. et al. Use of Inspiratory Profiles from Patients with Chronic Obstructive Pulmonary Disease (COPD) to Investigate Drug Delivery Uniformity and Aerodynamic Dose Emission of Indacaterol from a Capsule Based Dry Powder Inhaler. *Eur. J. Pharm. Sci.* **2019**, 134, 138–144.
185. Farkas, Á. et al. Establishment of Relationships between Native and Inhalation Device Specific Spirometric Parameters as a Step towards Patient Tailored Inhalation Device Selection. *Respir. Med.* **2019**, 154, 133–140.
186. Riley, T. et al. Challenges with Developing in Vitro Dissolution Tests for Orally Inhaled Products (OIPs). *AAPS PharmSciTech* **2012**, 13, 978–989.
187. Radivojev, S. et al. Searching for Physiologically Relevant in Vitro Dissolution Techniques for Orally Inhaled Drugs. *Int. J. Pharm.* **2019**, 556, 45–56.
188. 2.9.3. Dissolution Test for Solid Dosage Forms. In *European Pharmacopoeia 11.0*; 2024; pp. 348–355.

189. Fröhlich, E. et al. Measurements of Deposition, Lung Surface Area and Lung Fluid for Simulation of Inhaled Compounds. *Front. Pharmacol.* **2016**, 7, 1–10.
190. Tay, J.Y.S. et al. Dissolution of Fine Particle Fraction from Truncated Anderson Cascade Impactor with an Enhancer Cell. *Int. J. Pharm.* **2018**, 545, 45–50.
191. Gieszinger, P. et al. The Development of an in Vitro Horizontal Diffusion Cell to Monitor Nasal Powder Penetration Inline. *Pharmaceutics* **2021**, 13.
192. Virók, D.P. et al. A Direct Quantitative PCR-Based Measurement of Herpes Simplex Virus Susceptibility to Antiviral Drugs and Neutralizing Antibodies. *J. Virol. Methods* **2017**, 242, 46–52.
193. Hellemans, J. et al. QBase Relative Quantification Framework and Software for Management and Automated Analysis of Real-Time Quantitative PCR Data. *Genome Biol.* **2008**, 8.
194. Gieszinger, P. et al. Stability Study of Nasal Powder Formulation Containing Nanosized Lamotrigine. *Acta Pharm. Hung.* **2020**, 90, 27–31.
195. Benke, E. et al. Stability Test of Novel Combined Formulated Dry Powder Inhalation System Containing Antibiotic: Physical Characterization and in Vitro–in Silico Lung Deposition Results. *Drug Dev. Ind. Pharm.* **2019**, 45, 1369–1378.
196. Dubey, R. Impact of Nanosuspension Technology on Drug Discovery and Development. *Drug Deliv. Technol.* **2006**, 5, 67–71.
197. Powers, K.W. et al. Characterization of the Size, Shape, and State of Dispersion of Nanoparticles for Toxicological Studies. *Nanotoxicology* **2007**, 1, 42–51.
198. Hou, J. et al. Nanoparticle Tracking Analysis versus Dynamic Light Scattering: Case Study on the Effect of Ca²⁺ and Alginate on the Aggregation of Cerium Oxide Nanoparticles. *J. Hazard. Mater.* **2018**, 360, 319–328.
199. Salopek, B. et al. Measurement and Application of Zeta-Potential. *Rud. Zb.* **1992**, 4, 147–151.
200. Maguire, C.M. et al. Benchmark of Nanoparticle Tracking Analysis on Measuring Nanoparticle Sizing and Concentration. *J. Micro Nano-Manufacturing* **2017**, 5.
201. Vargaftik, N.B. et al. International Tables of the Surface Tension of Water. *J. Phys. Chem. Ref. Data* 1983, 12, 817–820.
202. Gliński, J. et al. Surface Properties of Aqueous Solutions of L-Leucine. *Biophys. Chem.* **2000**, 84, 99–103.
203. Muller, R.H. et al. Pharmaceutical Nanosuspension for Medicament Administration as Systems with Increased Saturation Solubility and Rate of Solution. *United States Pat.* 1999, 1–30.
204. Mangal, S. et al. Relationship between Surface Concentration of L -Leucine and Bulk Powder Properties in Spray Dried Formulations. *Eur. J. Pharm. Biopharm.* **2015**, 1–10.
205. Li, Q. et al. Interparticle van Der Waals Force in Powder Flowability and Compactibility. *Int. J. Pharm.* **2004**, 280, 77–93.
206. Dailey, L.A. et al. Surfactant-Free, Biodegradable Nanoparticles for Aerosol Therapy Based on the Branched Polyesters, DEAPA-PVAL-g-PLGA. *Pharm. Res.* **2003**, 20, 2011–2020.
207. Arpagaus, C. et al. Nano Spray Drying for Encapsulation of Pharmaceuticals. *Int. J. Pharm.* **2018**, 546, 194–214.
208. Pallagi, E. et al. New Aspects of Developing a Dry Powder Inhalation Formulation Applying the Quality-by-Design Approach. *Int. J. Pharm.* **2016**, 511, 151–160.
209. Ke, W. et al. Engineering the Right Formulation for Enhanced Drug Delivery. *Adv. Drug Deliv. Rev.* **2022**, 191, 114561.
210. Vehring, R. Pharmaceutical Particle Engineering via Spray Drying. *Pharm. Res.* **2008**, 25, 999–1022.
211. Sibum, I. et al. Dispersibility and Storage Stability Optimization of High Dose Isoniazid Dry Powder Inhalation Formulations with L-Leucine or Trileucine. *Pharmaceutics* **2020**, 12, 1–14.
212. Sou, T. et al. The Effect of Amino Acid Excipients on Morphology and Solid-State

- Properties of Multi-Component Spray-Dried Formulations for Pulmonary Delivery of Biomacromolecules. *Eur. J. Pharm. Biopharm.* **2013**, 83, 234–243.
213. Bosquillon, C. et al. Influence of Formulation Excipients and Physical Characteristics of Inhalation Dry Powders on Their Aerosolization Performance. *J. Control. Release* **2001**, 70, 329–339.
 214. Ave, G. Development of a Carrier Free Dry Powder Inhalation Formulation of Ketotifen for Pulmonary Drug Delivery. *Drug Res, Thieme* **2019**.
 215. Samet, Y. et al. Optical Properties of Meloxicam in the Far-Infrared Spectral Region. *Chem. Phys.* **2018**, 1–8.
 216. Böhm, B.H.L. et al. Lab-Scale Production Unit Design for Nanosuspensions of Sparingly Soluble Cytotoxic Drugs. *Pharm. Sci. Technol. Today* **1999**, 2, 336–339.
 217. Usmani, O.S. et al. Regional Lung Deposition and Bronchodilator Response as a Function of B2-Agonist Particle Size. *Am. J. Respir. Crit. Care Med.* **2005**, 172, 1497–1504.
 218. Chapman, K.R. et al. Delivery Characteristics and Patients' Handling of Two Single-Dose Dry-Powder Inhalers Used in COPD. *Int. J. COPD* **2011**, 6, 353–363.
 219. Bhavna et al. Nano-Salbutamol Dry Powder Inhalation: A New Approach for Treating Broncho-Constrictive Conditions. *Eur. J. Pharm. Biopharm.* **2009**, 71, 282–291.
 220. Kumar, N. et al. Edetate Calcium Disodium Nanoparticle Dry Powder Inhalation: A Novel Approach against Heavy Metal Decorporation. *Int. J. Pharm.* **2011**, 416, 376–383.
 221. Horváth, A. et al. Significance of Breath-Hold Time in Dry Powder Aerosol Drug Therapy of COPD Patients. *Eur. J. Pharm. Sci.* **2017**, 104, 145–149.
 222. Chvatal, A. Formulation and Aerodynamic Evaluation of Carrier-Free Dry Powder Inhalation Systems Containing Meloxicam, University of Szeged, 2019.
 223. Jókay, Á. et al. Computer Modeling of Airway Deposition Distribution of Foster® NEXThaler® and Seretide® Diskus® Dry Powder Combination Drugs. *Eur. J. Pharm. Sci.* **2016**, 88, 210–218.
 224. Sharif, S. et al. Impact of Leucine and Magnesium Stearate on the Physicochemical Properties and Aerosolization Behavior of Wet Milled Inhalable Ibuprofen Microparticles for Developing Dry Powder Inhaler Formulation. *Pharmaceutics* **2023**, 15.
 225. Das, S.C. et al. The Influence of Lung Surfactant Liquid Crystalline Nanostructures on Respiratory Drug Delivery. *Int. J. Pharm.* **2016**, 514, 465–474.
 226. Ambrus, R. et al. Cytotoxicity Testing of Carrier-Based Microcomposites for DPI Application. *Pharmazie* **2011**, 66, 549–550.
 227. Chvatal, A. et al. Cytotoxicity of Inhalable Dry Powders in A549 Human Lung Cancer Cell Line. *Farmacia* **2018**, 66, 172–175.
 228. Varga, P. et al. Physico-Chemical, in Vitro and Ex Vivo Characterization of Meloxicam Potassium-Cyclodextrin Nanospheres. *Pharmaceutics* **2021**, 13, 1–14.
 229. Forbes, B. Human Airway Epithelial Cell Lines for in Vitro Drug Transport and Metabolism Studies. *Res. Focus* **2000**, 3.
 230. Crestani, B. et al. Alveolar Type II Epithelial Cells Produce Interleukin-6 in Vitro and in Vivo. Regulation by Alveolar Macrophage Secretory Products. *J. Clin. Invest* **1994**, 94, 731–740.
 231. Copaescu, A. et al. The Role of IL-6 and Other Mediators in the Cytokine Storm Associated with SARS-CoV-2 Infection. *J. Allergy Clin. Immunol.* **2020**, 146, 518-534.e1.
 232. Alhajj, N. et al. Leucine as an Excipient in Spray Dried Powder for Inhalation. *Drug Discov. Today* **2021**, 26, 2384–2396.
 233. Sabuj, M.Z.R. et al. Stability of Inhaled Ciprofloxacin-Loaded Poly(2-Ethyl-2-Oxazoline) Nanoparticle Dry Powder Inhaler Formulation in High Stressed Conditions. *Pharmaceutics* **2022**, 15, 1–16.

Acknowledgement

Firstly, I would like to express my gratitude to my supervisor, **Dr. Rita Ambrus**, for all of her professional and emotional support, encouragement, and guidance.

I would like to sincerely thank **Prof. Dr. Ildikó Csóka**, Head of the Institute of Pharmaceutical Technology and Regulatory Affairs, for providing me the opportunity to work in this department and finish my doctoral research.

Also, I would like to thank **Prof. Dr. Piroska Szabó-Révész** for her scientific mentoring and **Dr. Anita Chvatal** for introducing me to the field of research as a student.

I am also grateful to my co-authors for their cooperation and invaluable help: **Dr. Csilla Balla-Bartos** from Institute of Pharmaceutical Technology and Regulatory Affairs, University of Szeged; **Dr. Árpád Farkas** from Centre for Energy Research Hungarian Academy of Sciences, **Dr. Dávid Kókai** and **Prof. Dr. Katalin Burián** from Department of Medical Microbiology, University of Szeged; **Prof. Dr. Béla Hopp** from Department of Optics and Quantum Electronics, University of Szeged; **Dr. Attila Nagy** from Wigner Research Centre for Physics, Hungarian Academy of Science.

I express appreciation to Erika Feczkoné Boda and Piroska Lakatosné Fekete for their outstanding technical help and to the undergraduate research students with whom I have worked. In addition, I would like to thank all members of the Institute of Pharmaceutical Technology and Regulatory Affairs for their help and kindness. I feel very fortunate to be able to work in such a collaborative environment.

I am thankful for my friends who supported me during the Ph.D. work: Fanni Falusi, Dorottya Németh, Szonja Plesz, Zsanett Pomaházi and Bence Sipos. I am grateful to my beloved parents, sister, niece and grandmother for their love and understanding throughout my studies. Finally, I would like to express my gratitude to Bálint Lőrinczi.


I acknowledge that the current thesis and other non-related projects were financially supported by Gedeon Richter's Talentum Foundation, Gedeon Richter Ltd., the ÚNKP-19-2-SZTE-101; ÚNKP-21-3-SZTE-258, ÚNKP-22-3-SZTE-157 and UNKP-23-3-SZTE-184 New National Excellence Program of the Ministry for Culture and Innovation from the source of the National Research, Development and Innovation Fund and by Project no. TKP2021-EGA-32 implemented with the support provided by the Ministry of Innovation and Technology of Hungary from the National Research, Development and Innovation Fund, financed under the TKP2021-EGA funding scheme and OTKA K_146148 project.

ANNEX

I.

Article

Formulation and In Vitro and In Silico Characterization of “Nano-in-Micro” Dry Powder Inhalers Containing Meloxicam

Petra Party ¹, Csilla Bartos ¹, Árpád Farkas ², Piroska Szabó-Révész ¹  and Rita Ambrus ^{1,*}

¹ Interdisciplinary Excellence Centre, Institute of Pharmaceutical Technology and Regulatory Affairs, University of Szeged, Eötvös street 6, 6720 Szeged, Hungary; party.petra@szte.hu (P.P.); bartos.csilla@szte.hu (C.B.); revesz@pharm.u-szeged.hu (P.S.-R.)

² Centre for Energy Research, Hungarian Academy of Sciences, Konkoly-Thege Miklós Street 29-33, 1121 Budapest, Hungary; farkas.arpad@energia.mta.hu

* Correspondence: ambrus.rita@szte.hu; Tel.: +36-62-545-572

Abstract: Pulmonary delivery has high bioavailability, a large surface area for absorption, and limited drug degradation. Particle engineering is important to develop inhalable formulations to improve the therapeutic effect. In our work, the poorly water-soluble meloxicam (MX) was used as an active ingredient, which could be useful for the treatment of non-small cell lung cancer, cystic fibrosis, and chronic obstructive pulmonary disease. We aimed to produce inhalable “nano-in-micro” dry powder inhalers (DPIs) containing MX and additives (poly-vinyl-alcohol, leucine). We targeted the respiratory zone with the microcomposites and reached a higher drug concentration with the nanonized active ingredient. We did the following investigations: particle size analysis, morphology, density, interparticular interactions, crystallinity, in vitro dissolution, in vitro permeability, in vitro aerodynamics (Andersen cascade impactor), and in silico aerodynamics (stochastic lung model). We worked out a preparation method by combining wet milling and spray-drying. We produced spherical, 3–4 µm sized particles built up by MX nanoparticles. The increased surface area and amorphization improved the dissolution and diffusion of the MX. The formulations showed appropriate aerodynamical properties: 1.5–2.4 µm MMAD and 72–76% fine particle fraction (FPF) values. The in silico measurements proved the deposition in the deeper airways. The samples were suitable for the treatment of local lung diseases.

Keywords: dry powder inhaler; nano; meloxicam; wet milling; spray-drying; Andersen cascade impactor; in silico assessment



Citation: Party, P.; Bartos, C.; Farkas, Á.; Szabó-Révész, P.; Ambrus, R. Formulation and In Vitro and In Silico Characterization of “Nano-in-Micro” Dry Powder Inhalers Containing Meloxicam. *Pharmaceutics* **2021**, *13*, 211. <https://doi.org/10.3390/pharmaceutics13020211>

Academic Editor: Fabio Sonvico

Received: 30 December 2020

Accepted: 28 January 2021

Published: 3 February 2021

Publisher’s Note: MDPI stays neutral with regard to jurisdictional claims in published maps and institutional affiliations.



Copyright: © 2021 by the authors. Licensee MDPI, Basel, Switzerland. This article is an open access article distributed under the terms and conditions of the Creative Commons Attribution (CC BY) license (<https://creativecommons.org/licenses/by/4.0/>).

1. Introduction

The main advantages of pulmonary delivery are the result of the huge surface area of the lung (100 m²) with a thin absorption layer (0.1–0.2 µm), as well as low metabolic activity. Targeted delivery of the drug could provide benefits such as achieving a greater local concentration at the target site with a reduced dose, resulting in reduced systemic side effects and adverse events [1]. Local delivery is especially effective in patients with serious pulmonary diseases such as asthma, cystic fibrosis (CF), chronic obstructive pulmonary (COPD) disease, and lung cancer [2].

For the application of inhaled medications, dry powder inhalers (DPIs) are more widely used compared with nebulizers or metered-dosed inhalers (MDIs). DPI products are solid-state; therefore, they have long-term stability. The delivery is driven by the inhalation flow, thus DPIs are environmentally friendly, and they do not require a compressor or propellant. The administration time is very short and the devices are cheap and portable [3]. Unfortunately, drug deposition in the pulmonary region is not sufficient with traditional carrier-based DPIs. In these systems, the active ingredient is attached to the surface of a carrier, which is usually lactose, although it could be mannitol or glucose too. The potentiality of the powders is proper dispersion in the respiratory system, so the aerosolization of the

products should be optimized. Hence, new carrier-free DPI systems have been developed to enhance the therapeutic effect. To reach efficient deposition, DPIs should contain a powder made of the active pharmaceutical ingredient (API) co-formulated with appropriate excipients, which are chosen based on their functions in the powder, leading to optimal aerodynamic properties [4]. Excipients approved for DPI formulations are, for example, hydrophobic additives (Mg-stearate) for protection against moisture, lipids (cholesterol) for coating, amino acids (leucine) for improved aerosol efficiency, and absorption enhancers (cyclodextrins, chitosan) and biodegradable polymers (poly(lactic-co-glycolic acid) (PLGA) for stability and released formulations [2].

Besides the components, the particle size and dispersibility of DPIs have a key role in the deposition pattern. There are three principal mechanisms of particle deposition in the lung. Inertial impaction affects particles that are larger than 5 μm . These particles are not able to follow the changes of gas flow direction in the upper airway and at the airway bifurcations. Therefore, the particles impact the upper airways walls, limiting the amount of API that can be delivered into the lung. Gravitational sedimentation is based on the settling of particles under the action of gravity and occurs in the smaller airways and where the distance is covered by the particles before they hit the wall of the airways. This deposition mechanism is the most effective for particles in the size range of 1–8 μm . DPIs in this size range are best suited to treat central and small airways. Random motions of the particles caused by their collisions with gas molecules result in deposition by Brownian diffusion. Unlike deposition by impaction and sedimentation, which increase with the increasing particle size, deposition by Brownian diffusion rises with decreasing particle size and becomes the dominant mechanism of deposition for particles less than 1 μm in diameter. These particles are effective in the alveolar region of the lung, where air velocities are low [5]. Particles under 1 μm usually are exhaled. In conclusion, the requested particle size range in pulmonary therapy is a particle diameter of 1–5 μm .

Nanoparticles are a beneficial formulation for Class II drugs of the Biopharmaceutics Classification System (BCS), where the dissolution rate is the rate-limiting step for absorption. The reduction of particle size can increase the dissolution rate as the amount of API dissolving over time is inversely correlated with the particle diameter. For this reason, nanoparticle formulations of API are being assessed for their potential to increase the drug dissolution rate as a result of a higher specific surface area. If we formulate the nanosized API into micrometric particles, we can target the proper parts of the airways and, when the powders come into contact with the lung lining fluid, the particles can disintegrate into their nano subunits and spread on the surface of the epithelium, resulting in a large surface area for drug dissolution, and thus increased absorption and more homogenous distribution [6]. A prosperous formulation for nanoparticle agglomerates is the preparation of nanosuspensions by wet milling followed by solidification, using spray-drying. They are reproducible, scalable, and cost- and time-effective preparation methods. We can combine the advantages of nanonized particles by preparing a nanosuspension (i.e., enhanced dissolution and solubility) with the benefits of solid formulations (i.e., stability, easier handling, and enhanced patient compliance) by producing microsized nanoparticle agglomerates suitable for pulmonary delivery [7].

Our research group had experiences with meloxicam (MX) as an API and different additives, such as polymers and amino acids. In this work, we used MX, which is a poorly water-soluble (in water, 7.15 mg/L at 25 °C), non-steroidal anti-inflammatory agent [8]. In pulmonary therapy, it could be useful to treat CF, COPD, and non-small-cell lung cancer [9–12]. Previous studies were about particle size reduction of meloxicam with wet milling using poly-vinyl-alcohol (PVA) solution as a dispersant [13]. In the presence of PVA, the particle size of the drug could be reduced to the nanometre range. In the case of co-spray-dried DPI formulations, PVA exerted an aggregation inhibitor effect, thereby providing individual particles [14]. L-leucine (LEU) was applied to enhance the dispersity of the particles, thereby improving the aerosolization and the flowability of the powders [15,16]. Our works correlated with the positive effect of LEU on the aerodynamic

properties, because LEU decreases the deposition in the upper airways and increases the emitted fraction during inhalation [17,18].

In the following work, we formulated micrometer-sized carrier-free DPIs using spray-drying, containing the previously nanonized active ingredient by wet milling. The novelty of the present work is the “nano-in-micro” structure of the DPI. We carried out morphology, rheology, structure, dissolution, diffusion, and aerodynamic characterization of the samples. We wanted to target the respiratory zone with micrometric particles. Thanks to the particle size reduction of the poorly water-soluble MX, and thus the increase of the specific surface area, we could improve the local dissolution in the lung fluid and permeability to the epithelium. Our product could provide an effective treatment for serious local pulmonary diseases.

2. Materials and Methods

2.1. Materials

Meloxicam (MX) (Egis Pharmaceuticals PLC., Budapest, Hungary) was used as an active ingredient. As additives, poly-vinyl-alcohol 3-88 (PVA) (ISP Customer Service GmbH, Cologne, Germany) and L-leucine (LEU) (AppliChem GmbH, Darmstadt, Germany) were applied.

2.2. Preparation Method

We used a two-step preparation protocol. First, the pre-nanosuspension was prepared by wet milling technology, using PVA and MX. The final microsized powders were obtained with co-spray drying of the diluted suspension and LEU (Figure 1).

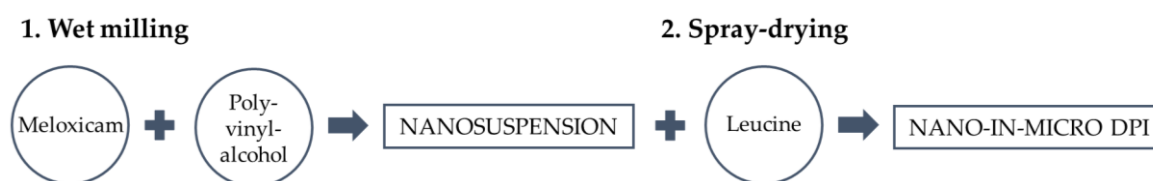


Figure 1. Two-step preparation method of the samples. DPI, dry powder inhaler.

2.2.1. Wet Milling

We applied a combined wet milling technique, which was optimized by our research group’s previous work [13]. We dissolved 2.5 g of PVA in purified water and the volume of the final solution was 100 mL. Then, 2.00 g of MX was suspended in 18.0 g of 2.5% (mass/volume) PVA solution. Moreover, 20.0 g of ZrO₂ beads was the milling medium in a planetary ball mill (Retsch Planetary Ball Mill PM 100 MA, Retsch GmbH, Haan, Germany). The milling parameters were as follows: 60 min and 500 rpm. As the result of the wet milling, we achieved a nanosized pre-suspension containing MX and PVA. The nanosuspension was diluted with purified water to 500 mL. The final concentration of the MX suspension was 4 g/L.

2.2.2. Co-Spray Drying

We prepared different compositions by adding a various amount of LEU, as shown in Table 1. A magnetic stirrer was used for sample homogenization (AREC.X heating magnetic stirrer, Velp Scientifica Srl, Usmate Velate, Italy). The inhalable microparticles were produced by spray-drying using a spray-dryer equipped with a two-fluid nozzle of 0.7 mm (Büchi Mini Spray Dryer B-191, Büchi, Flawil, Switzerland). Based on the preliminary experiments, the spray drying properties were as follows: inlet temperature: 165 °C, outlet temperature: 100 °C, aspirator capacity: 85%, airflow rate: 500 L/h, and feed pump rate: 10%. The yield was calculated as the ratio of the mass of the particles collected after spray-drying to the mass of the solid content of the initial nanosuspension. We

managed to increase the yield of spray-drying with the addition of LEU. Low spray-drying yields are indicative of cohesive powders. LEU reduced the cohesion between the particle, hence the improvement of the spray-drying yield [19].

Table 1. Composition of the samples and the yield of spray-drying. MX, meloxicam; PVA, poly-vinyl-alcohol; LEU, L-leucine.

Samples	MX (g/L)	PVA (g/L)	LEU (g/L)	Yield * (%)
nanoMX1_LEU0	4.00	0.90	0.00	45.41 ± 5.10
nanoMX1_LEU0.5	4.00	0.90	2.00	57.56 ± 1.36
nanoMX1_LEU1	4.00	0.90	4.00	58.43 ± 6.36

* Data are means ± SD (n = 3 independent measurements).

2.2.3. Physical Mixtures

We prepared physical mixtures of the raw materials. The compositions were the same as for the spray-dried samples (Table 2). During our measurements, we compared the properties of the spray-dried samples to the those of the physical mixtures.

Table 2. Composition of the physical mixtures.

Samples	MX (g)	PVA (g)	LEU (g)
pmMX1_LEU0	4.00	0.90	0.00
pmMX1_LEU0.5	4.00	0.90	2.00
pmMX1_LEU1	4.00	0.90	4.00

2.3. Determination of Particle Size and Distribution

Laser diffraction was used to determine the particle size and the particle size distribution of our samples (Malvern Mastersizer Scirocco 2000, Malvern Instruments Ltd., Worcestershire, UK). The wet dispersion unit was used to measure the particle size of the nanosuspension. We set the refractive index of MX (1.720) and measured it in purified water with 2000 rpm stirring. The dry dispersion unit was used to observe the spray-dried microcomposites. Approximately 0.5–1.0 g of product was loaded into the feeding tray. The dispersion air pressure was adjusted to 3.0 bar and 75% vibration feed was used. Each sample was measured in triplicate. The particle size distribution was characterized by the D[0.1] (10% of the volume distribution is below this value), D[0.5] (the volume median diameter is the diameter where 50% of the distribution is above and 50% is below), and D[0.9] (90% of the volume distribution is below this value) values. The size distribution Span was calculated according to Equation (1). A high Span value denotes a broad particle size distribution. The higher the Span value, the broader the particle size distribution [20]. We obtained the specific surface area (SSA) data, which predict the dissolution and permeability properties of the samples.

$$\text{Span} = \frac{D[0.9] - D[0.1]}{D[0.5]} \quad (1)$$

2.4. Investigation of Morphology

Scanning electron microscopy (SEM) (Hitachi S4700, Hitachi Scientific Ltd., Tokyo, Japan) was used to characterize the morphology of the spray-dried formulation. We applied a high voltage of 10 kV, an amperage of 10 mA, and an air pressure of 1.3–13.1 mPa. A high vacuum evaporator and argon atmosphere were used to make the sputter-coated samples conductive with gold-palladium (Bio-Rad SC 502, VG Microtech, Uckfield, UK). The thickness of the gold-palladium coating was approximately 10 nm. For the particle size analysis of the active ingredient, a public domain image analyzer software, ImageJ, was used (<https://imagej.nih.gov/ij/index.html>).

2.5. Density Measurement

The bulk and tapped densities of the formulations were measured using an Engelsmann Stampfvolumeter (Ludwigshafen, Germany) [21]. A 10 cm³ cylinder was filled with 1.5–2.0 cm³ of powder to calculate bulk density. Then, it was tapped 1000 times. The tapped density of the samples was calculated compared with the volume before and after the taps. We calculated the flow characters (Equations (2) and (3)) of the samples from the bulk (ρ_b) and tapped (ρ_t) density. All samples were measured in triplicate.

$$\text{Hausner ratio} = \frac{\rho_t}{\rho_b} \quad (2)$$

$$\text{Carr index} = \frac{\rho_t - \rho_b}{\rho_t} * 100 \quad (3)$$

2.6. Determination of the Interparticle Interactions

Around 0.10 g of the samples was pressed on a 1 ton hydraulic press (Perkin Elmer hydraulic press, Specac Inc., Waltham, MA, USA). Six pastilles were obtained from each sample. We did three parallel measurements with each composition. Three pastilles per sample were dripped with polar liquid (4.8 μ L of purified water) and the other three pastilles were dripped with non-polar solvent (2.0 μ L of diiodomethane). Contact angle was detected in an interval of 1 to 25 s with a Dataphysics OCA 20 apparatus (Dataphysics Instrument GmbH, Filderstadt, Germany) [22]. We obtained the contact angles of the two applied fluids. The surface free energy (γ_s) of the composites, which consists of the polar part (γ_s^p) and the disperse part (γ_s^d), so ($\gamma_s = \gamma_s^p + \gamma_s^d$), was calculated based on the Wu equation. The surface tension of the used liquids is known in the literature: distilled water $\gamma^p = 50.2$ mN/m, $\gamma^d = 22.6$ mN/m and diiodomethane $\gamma^p = 1.8$ mN/m, $\gamma^d = 49$ mN/m. We can express the Wu equation (Equation (4)), where θ = contact angle, γ = surface free energy, s = solid phase, l = liquid phase, d = dispersion component, and p = polar component.

$$(1 + \cos \theta)\gamma_l = \frac{4\gamma_s^d\gamma_l^d}{\gamma_s^d + \gamma_l^d} + \frac{4\gamma_s^p\gamma_l^p}{\gamma_s^p + \gamma_l^p} \quad (4)$$

Polarity (Pol) was calculated as the ratio of the surface free energy of the polar component and surface free energy multiplied by 100 (Equation (5)).

$$\text{Pol} = \frac{\gamma^p}{\gamma^s} * 100 \quad (5)$$

Cohesion work (W_c) was determined as twice the surface free energy (Equation (6)).

$$W_c = 2 * \gamma_s \quad (6)$$

2.7. Structural Analysis

To establish the crystalline character of the spray-dried samples, X-ray powder diffraction (XRPD) spectra were recorded with a BRUKER D8 Advance X-ray diffractometer (Bruker AXS GmbH, Karlsruhe, Germany). The radiation source was Cu K α 1 radiation ($\lambda = 1.5406$ Å). Measurement conditions were as follows: Cu target, Ni filter, 40 kV voltage, 40 mA current, time constant 0.1°/min, and angular step 0.010° over the interval 3–40°. We used the DIFFRACT plus EVA 28 software (Bruker AXS GmbH, Karlsruhe, Germany) for the evaluation.

2.8. Thermoanalytical Analysis

The differential scanning calorimetry (DSC) measurements were made with a Mettler Toledo DSC 821^e thermal analysis system with the STAR^e thermal analysis program V9.1 (Mettler Inc., Schwerzenbach, Switzerland). Approximately 2–5 mg of the samples was

examined in the temperature range between 25 °C and 300 °C. The heating rate was 5 °C/min. Argon was the carrier gas at a flow rate of 10 L/h during the investigation.

2.9. In Vitro Dissolution Test

No in vitro dissolution test for powders for inhalation exists in the current Pharmacopeia. We applied a modified paddle method (Hanson SR8 Plus, Teledyne Hanson Research, Chatsworth, CA, USA) from the European Pharmacopeia [23] to examine the release of MX from the samples. The capacity of the vessel was 100 mL instead of 1000 mL and the size of the stirrer was smaller. We designed the parameters of our measurement based on the circumstances of the human airways [24]. The medium was a simulated lung medium, which contained NaCl, NaHCO₃, CaCl₂, NaH₂PO₄, H₂SO₄, and glycine [25]. The volume of the medium was 50 mL based on the estimated volume of the lung fluid [26]. The pH of the medium was 7.4 ± 0.1. The temperature was set at 37 °C. The samples contained 1.5 mg of MX, which is one-tenth of the oral dose of the API. During pulmonary delivery, we can reduce the amount of API compared with the oral dose. We chose this amount of API based on a salbutamol dosage recommendation [27]. Applying these doses of our products is safe for use. Previous investigations proved that the API and the excipients had no cytotoxic effect on the concentration on the cells [28]. The paddle was rotated at 100 rpm and the sampling was performed up to 60 min. The total fraction of the samples was dispersed in the medium. We took 5 mL of the dissolution medium after 5, 10, 15, 30, and 60 min. The medium was replenished every time the sample was withdrawn. After filtration (pore size: 0.45 µm, Millex-HV syringe-driven filter unit, Millipore Corporation, Bedford, MA, USA) and dilution, the MX contents of the samples were determined by spectrophotometry at λ = 362 nm (ATI-UNICAM UV/VIS Spectrophotometer, Cambridge, UK). Three parallel measurements took place with the formulations.

2.10. In Vitro Diffusion Test

We would like to demonstrate the permeability from the lung fluid to the epithelial cells of the lung. A modified horizontal diffusion cell was used to investigate the in vitro permeability of the samples [26]. The donor phase (9 mL) was simulated lung medium (pH = 7.4). Phosphate buffer (pH = 7.4) was used as the acceptor phase (9 mL), modelling the circumstances of the epithelial cell. Between the two phases, there was a cellulose membrane (RC 55 Whatman™ GE Healthcare Life Sciences, Buckinghamshire, UK) impregnated with isopropyl myristate. The actual diffusion surface was 0.785 cm². The rotation of the stirring bar was set to 300 rpm. The temperature was 37 °C. We measured 1.5 mg MX contents of the samples. The API was first released in the simulated lung fluid, and then diffused through the membrane to the phosphate buffer. The amount of diffused MX was determined real-time at λ = 362 nm until 60 min with sonda (FDP-7UV200-VAR, Avantes, Apeldoorn, The Netherlands) spectrophotometer (Avaspec-ULS2048-USB2, Avantes, Apeldoorn, The Netherlands) in the acceptor phase [29]. The samples were measured three times.

The flux (J) [µg/cm²/h] of the active ingredient was calculated from the quantity of MX, which permeated through the membrane, divided by the surface of the membrane insert (A) and the duration (t) using the following Equation (7):

$$J = \frac{m}{A * t} \quad (7)$$

The permeability coefficient (K_p) [cm/h] was determined from the flux and the MX concentration in the donor phase (C_d) [µg/cm³], Equation (8):

$$K_p = \frac{J}{C_d} \quad (8)$$

2.11. In Vitro Aerodynamic Measurements

The aerosolization efficacy of the spray-dried formulations was assessed in vitro, using an Andersen cascade impactor (ACI) (Apparatus D, Copley Scientific Ltd., Nottingham UK) [30]. The inhalation flow rate was set to 28.3 ± 1 L/min (High-capacity Pump Model HCP5, Critical Flow Controller Model TPK, Copley Scientific Ltd., Nottingham, UK). Table 3 shows the cut-off aerodynamic diameter for stages of ACI at a flow rate of 28.3 L/min [31]. The actual flow rate through the impactor was measured by a mass flow meter (Flow Meter Model DFM 2000, Copley Scientific Ltd., Nottingham, UK). The inhalation time was 4 s for one inhalation. These parameters led to an inhalation volume of 1.89 L, which was similar to the inhalation volume of COPD patients [32]. Breezhaler[®] single dose devices (Novartis International AG, Basel, Switzerland) were used, with transparent size 3 gelatine capsules (Capsugel, Bornem, Belgium) filled with 2.0–2.5 mg of powder, which contained 1–2 mg of MX. Four capsules were inhaled during one measurement. The inhaler was actuated twice for each capsule. Each sample was measured in triplicate.

Table 3. Cut-off aerodynamic diameter for stages of Andersen cascade impactor (ACI) at a flow rate of 28.3 L/min.

ACI Stages	Cut-Off Diameter at 28.3 L/min (μm)
0	9.0–10.0
1	5.8–9.0
2	4.7–5.8
3	3.3–4.7
4	2.1–3.3
5	1.1–2.1
6	0.7–1.1
7	0.4–0.7
Filter	<0.4

To provide the pulmonary adhesive circumstances, the plates on the stages were coated with Span 85 and cyclohexane (1 + 99 $w/w\%$) mixture. After inhalation, the device, the capsules, the induction port, the collection plates, and the filter were washed with methanol and pH 7.4 phosphate buffer (60 + 40 $v/v\%$) to collect the deposited MX. The collected and dissolved MX was quantified by UV/vis spectrophotometry (ATI-UNICAM UV/VIS Spectrophotometer, Cambridge, UK) at a wavelength of $\lambda = 362$ nm.

The actual API content (%) of the spray-dried particles was measured by dissolving 1.0–1.1 mg of product in 25 mL of methanol/phosphate buffer (60:40 $w/w\%$), the solution of which was also used for the aerodynamic measurement. The solutions were mixed for 10 min at 600 rpm, and the API content was quantified by UV/vis spectrophotometry (ATI-Unicam UV/VIS Spectrophotometer, Cambridge UK) at a wavelength of 362 nm.

The aerodynamic properties were calculated from a plot of the cumulative percentage undersize of the API on log probability scale against the effective cut-off diameter using the KaleidaGraph program [31,33]. The mass of drug particles with a size under 5 μm was defined as a fine particle dose (FPD). The amount of drug leaving the device and reaching the impactor was considered as the emitted dose (ED). The fine particle fraction (FPF) was calculated as the percentage ratio between FPD and ED. The emitted fraction (EF) was expressed as a percentage of the ED divided by the initial amount of API. The aerodynamic diameter is influenced by the inhalation flow rate, density, and size and shape of the particle. The real size of the particle during inhalation is expressed with the MMAD (median mass aerodynamic diameter). The MMAD of the particles was determined from the same plot as the particle size corresponding to the 50% point of the cumulative distribution. For an inhalable and well-deposited powder, the MMAD should be in the 1–5 μm size range [34].

2.12. In Silico Characterization

The in silico simulations were performed by the stochastic lung deposition model, which tracks the inhaled particles until their deposition or exhalation and computes the fraction of the particles deposited in each anatomical part of the respiratory system, that is, extrathoracic, bronchial, and acinar regions [35]. The particle trajectories were simulated in an asymmetrical branching airway structure, mimicking the realistic airways by selecting morphometrical parameters from the database of Raabe et al. [36]. The inputs of the computational model are different parameters characterizing the aerosol particles like density, shape, or size, as well as the breathing parameters of the patient, such as inhaled volume, inhalation time, breath-hold time, exhalation time, and breathing mode (nasal or oral). A more detailed description of the numerical model can be found in Koblinger and Hofmann [37]. In our work, aerodynamic particle size distributions of the samples measured by the Andersen cascade impactor technique served as the inputs for the numerical airway deposition model. The inhalation parameters corresponded to a COPD patient inhaling through Breezhaler®, whose inhaled volume (IV) and inhalation time values ($IV = 1.7\text{ L}$, $t_{in} = 3.2\text{ s}$) matched the best flow rate of the current impactor measurements. The computational deposition model was validated for the case of aerosol drugs in our earlier works [38,39].

3. Results

3.1. Particle Size Distribution

We managed to prepare a nanosuspension using raw MX and 2.5% PVA dilution during the milling procedure. In the diluted suspension, the particle size of MX was $137.70\text{ nm} \pm 4.965\text{ nm}$ and the SSA was $43.65 \pm 5.318\text{ m}^2/\text{g}$. After spray-drying, the size of the particles was applicable for pulmonary delivery, as the $D[0.5]$ values were in the $1\text{--}5\text{ }\mu\text{m}$ range and the distribution was monodisperse (Table 4). The geometric diameter of spray-dried nanoMX1_LEU0 was around $3.2\text{ }\mu\text{m}$. Incorporating LEU in the formulations increased the geometric size of the spray-dried particles [40]. The distribution was monodisperse in all cases ($\text{Span} < 2.0$), which is essential for accurate dosing. The specific surface area (SSA) values increased compared with the raw materials, which predicted an improved dissolution profile.

Table 4. Particle size of the initial active pharmaceutical ingredient (API), the nanosuspension, the physical mixtures, and the final samples. SSA, specific surface area.

Samples	$D[0.1]^* (\mu\text{m})$	$D[0.5]^* (\mu\text{m})$	$D[0.9]^* (\mu\text{m})$	Span *	SSA * (m^2/g)
raw MX	2.719 ± 0.057	9.913 ± 0.371	29.49 ± 0.630	2.70 ± 0.043	1.09 ± 0.028
MX suspension	0.067 ± 0.001	0.138 ± 0.005	0.555 ± 0.310	3.584 ± 2.056	43.65 ± 5.318
pmMX1_LEU0	3.073 ± 0.030	13.10 ± 0.500	349.92 ± 34.86	26.47 ± 1.649	0.88 ± 0.025
pmMX1_LEU0.5	5.426 ± 0.631	91.22 ± 17.90	357.57 ± 168.2	3.86 ± 1.101	0.40 ± 0.066
pmMX1_LEU1	7.983 ± 0.092	110.67 ± 0.261	353.25 ± 47.24	3.12 ± 0.433	0.27 ± 0.002
nanoMX1_LEU0	1.497 ± 0.046	3.186 ± 0.019	6.481 ± 0.193	1.56 ± 0.068	2.22 ± 0.031
nanoMX1_LEU0.5	1.834 ± 0.007	3.800 ± 0.014	7.389 ± 0.030	1.46 ± 0.004	1.88 ± 0.024
nanoMX1_LEU1	1.977 ± 0.093	4.396 ± 0.032	8.903 ± 0.186	1.58 ± 0.075	1.71 ± 0.051

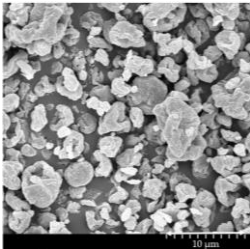
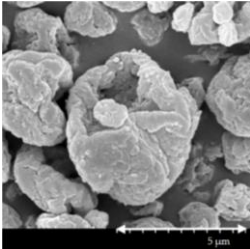
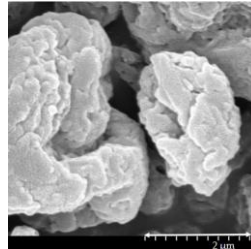
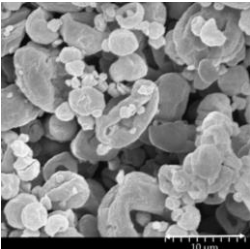
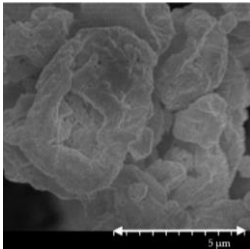
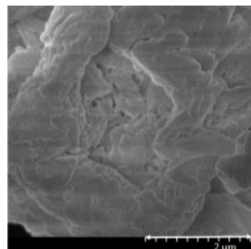
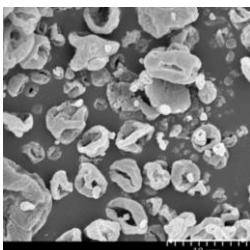
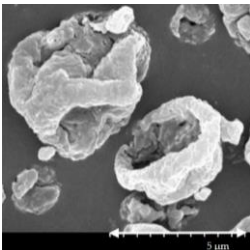
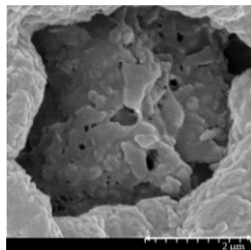
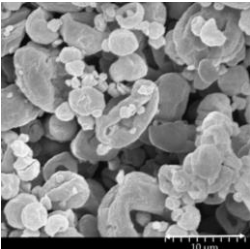
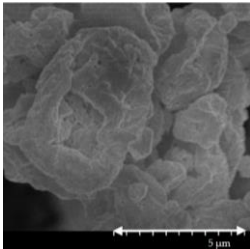
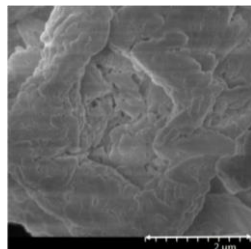
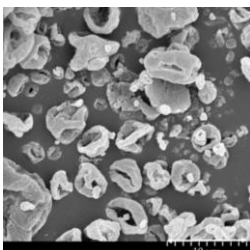
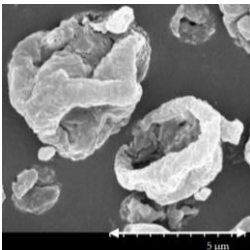
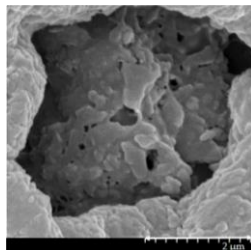
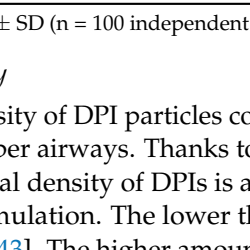
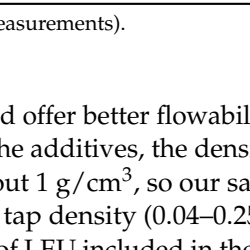
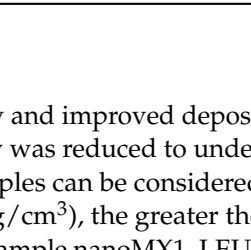
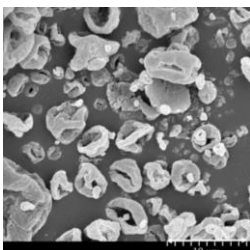
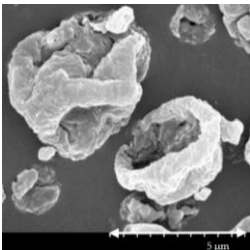
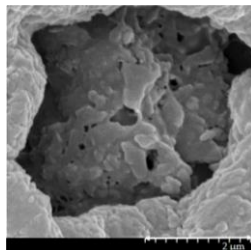
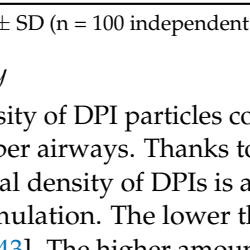
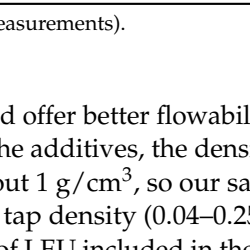
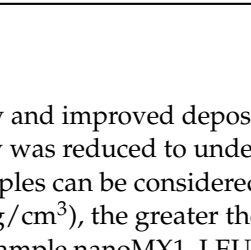
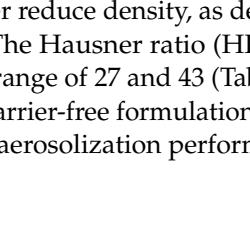
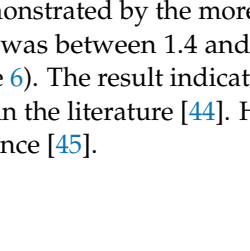
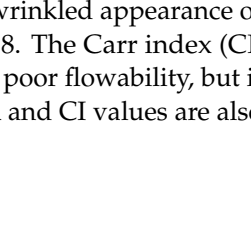
* Data are means \pm SD ($n = 3$ independent measurements).

3.2. Particle Morphology

The SEM pictures (Table 5) showed particles with a nearly spheroidal shape, which was the result of the optimized parameters of the co-spray-drying. The particles were produced from the droplets during the method, and the most stable shape for a droplet is the spherical form [41]. According to the SEM pictures, we observed that the presence of PVA prevented the aggregation. Particles were individually separated and displayed a regular size, which met the requirements for the formulation of a DPI [14]. The Peclet number of LEU is greater than 1, which led to a wrinkled particle morphology after spray-

drying. This rough surface improved the dispersion of the particles, reflecting low density and resulting in higher drug delivery into the low regions of the airways [18,40,42]. We could observe the nanosized active ingredient particles in the SEM pictures. We measured the diameter of the API with Image-J program. The size range of these was between 120 and 140 nm (Table 4). The diameter of the MX was correlated with the results of the nanosuspension. The images proved the “nano-in-micro” structure of the final powders.

Table 5. Diameter of the API in the products determined by Image-J analyses and the scanning electron microscopy (SEM) images of the spray-dried samples.

Samples	D * (nm)	SEM Pictures		
nanoMX1_LEU0	134.30 ± 23.07			
				
				
nanoMX1_LEU0.5	126.57 ± 27.26			
				
				
nanoMX1_LEU1	138.27 ± 42.57			
				
				

* Data are means \pm SD (n = 100 independent measurements).

3.3. Powder Rheology

The lower density of DPI particles could offer better flowability and improved deposition within the deeper airways. Thanks to the additives, the density was reduced to under 0.3 g/cm^3 . The usual density of DPIs is about 1 g/cm^3 , so our samples can be considered as low-density formulation. The lower the tap density ($0.04\text{--}0.25 \text{ g/cm}^3$), the greater the respirable fraction [43]. The higher amount of LEU included in the sample nanoMX1_LEU1 was found to further reduce density, as demonstrated by the more wrinkled appearance of the particles [17]. The Hausner ratio (HR) was between 1.4 and 1.8. The Carr index (CI) results were in the range of 27 and 43 (Table 6). The result indicates poor flowability, but it is similar to other carrier-free formulations in the literature [44]. HR and CI values are also responsible for the aerosolization performance [45].

Table 6. Rheology properties of the samples.

Samples	Bulk Density * (g/cm ³)	Tapped Density * (g/cm ³)	Hausner Ratio *	Carr Index *	Flowability
nanoMX1_LEU0	0.177 ± 0.020	0.262 ± 0.001	1.488 ± 0.048	32.39 ± 7.232	Very poor
nanoMX1_LEU0.5	0.156 ± 0.009	0.274 ± 0.004	1.759 ± 0.084	43.09 ± 2.704	Very, very poor
nanoMX1_LEU1	0.147 ± 0.013	0.204 ± 0.012	1.398 ± 0.209	27.65 ± 10.82	Very poor

* Data are means ± SD (n = 3 independent measurements).

3.4. Interparticular Interactions

Contact angle measurements were performed to calculate the polarity and the cohesive work (W_c) characteristic of the materials. The wettability study revealed that the microcomposites had a more hydrophilic character as compared with hydrophobic MX. With the use of PVA, the polarity increased, which predicted better dissolution results in simulated lung medium compared with raw MX. The highest polarity values were obtained with nanoMX1_LEU0. The lipophilic component LEU decreased the polarity of the samples. In the case of samples containing LEU, cohesivity decreased between the spherical, rough particles, so the presence of LEU caused the decrease in W_c (Table 7). The lower cohesivity of particles could result in more effective deposition properties.

Table 7. Surface free energy, cohesion work, and polarity values of the samples and their components.

Samples	γ^d * [mN/m]	γ^p * [mN/m]	γ * [mN/m]	W_c * [mN/m]	Pol * [%]
MX	45.49 ± 0.09	13.89 ± 0.13	59.38 ± 0.22	118.76 ± 0.44	23.39 ± 0.15
PVA	45.65 ± 0.10	36.89 ± 0.20	82.54 ± 0.30	165.08 ± 0.60	44.69 ± 0.11
LEU	30.00 ± 0.07	0.50 ± 0.17	30.50 ± 0.24	61.00 ± 0.48	1.639 ± 0.20
pmMX1_LEU0	42.62 ± 0.12	30.65 ± 0.48	73.27 ± 0.60	146.54 ± 1.20	41.83 ± 0.56
pmMX1_LEU0.5	36.57 ± 0.34	25.63 ± 0.27	62.20 ± 0.61	124.40 ± 1.22	41.21 ± 0.84
pmMX1_LEU1	34.01 ± 0.55	16.57 ± 0.36	50.58 ± 0.91	101.16 ± 1.82	32.76 ± 0.44
nanoMX1_LEU0	42.34 ± 0.08	31.03 ± 0.62	73.38 ± 0.70	146.76 ± 1.40	42.29 ± 0.44
nanoMX1_LEU0.5	36.15 ± 0.95	25.69 ± 0.45	61.84 ± 0.51	123.68 ± 1.02	41.54 ± 1.07
nanoMX1_LEU1	33.39 ± 0.86	16.59 ± 0.11	49.98 ± 0.97	99.96 ± 1.94	33.19 ± 0.43

* Data are means ± SD (n = 3 independent measurements).

3.5. X-ray Powder Diffraction Results

X-ray powder diffraction was used to characterize the crystalline state of MX after the preparation process. The XRPD pattern of the raw materials demonstrated the crystalline structure of MX and LEU, as expected. Raw MX has characteristic peaks with the highest intensities at 6.6°, 11.4°, 13.1°, 13.5°, 15.1°, 18.7°, 19.3°, 25.9°, and 26.4° 2-theta peaks, indicating its crystalline structure [46]. We detected the characteristic peaks of LEU at 6.12, 24.39, and 30.61 2-theta peaks [47]. In the case of the products, the intensities of the characteristic peaks decreased (Figure 2). The presence of PVA had no effect on the diffractograms. In the course of milling and spray-drying, a decrease in crystallinity was perceptible, which was determined via the mean of the decrease of the total area beneath the curve of the characteristic peaks compared with the physical mixtures. After treatment, ~71% of MX remained crystalline for nanoMX1_LEU0, ~52% for nanoMX1_LEU0.5, and ~53% for nanoMX1_LEU1. The other part of the active ingredient became amorphous during the preparation process. The preliminary stability test showed no changes in the structure after one month.

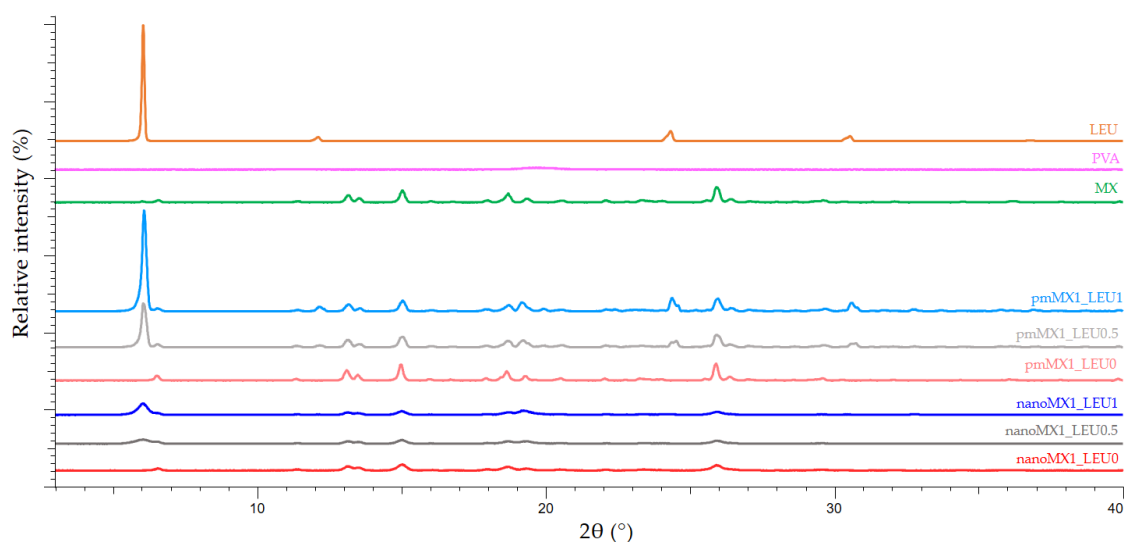


Figure 2. X-ray powder diffraction (XRPD) results of the raw materials (L-leucine (LEU), poly-vinyl-alcohol (PVA), and meloxicam (MX)), the physical mixtures (pmMX1_LEU0, pmMX1_LEU0.5, and pmMX1_LEU1), and the spray-dried samples (nanoMX1_LEU0, nanoMX1_LEU0.5, and nanoMX1_LEU1).

3.6. Thermoanalytical Results

DSC was employed to investigate the melting of PVA, LEU, and MX in the raw form, in the physical mixtures, and in the prepared products (Figure 3). PVA had no endothermic peak. LEU had an endothermic peak at 294.41 °C. The DSC curves of raw MX showed a sharp endothermic peak at 264.03 °C, reflecting its melting point and crystalline structure. After milling and spray drying, the DSC curves in all cases exhibited broader endothermic peaks of MX, indicating that the crystallinity of the drug decreased. The residual MX crystals in the products melted at a lower temperature than the crystals of raw MX owing to the smaller particle size and the increased degree of amorphization. This was promoted by PVA, which was softened at 85 °C as the glass transition temperature (T_g) value.

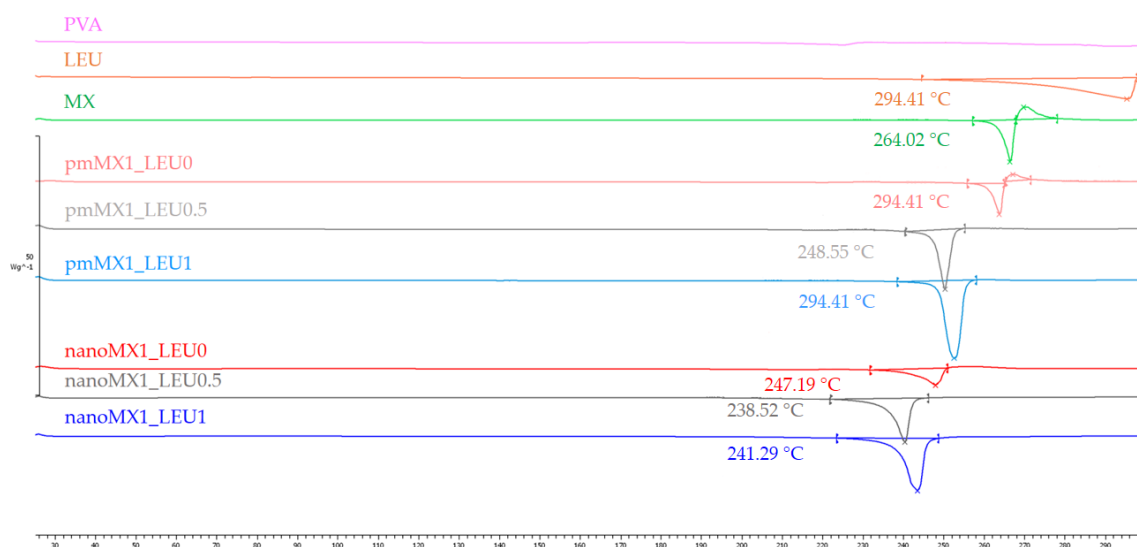


Figure 3. DSC results of the raw materials, (PVA, LEU, and MX), the physical mixtures (pmMX1_LEU0, pmMX1_LEU0.5, and pmMX1_LEU1), and the spray-dried samples (nanoMX1_LEU0, nanoMX1_LEU0.5, and nanoMX1_LEU1).

3.7. In Vitro Dissolution Results

The initial API showed poor water-solubility, as we mentioned above. The formulations were compared to raw MX and the physical mixtures. The results of the dissolution study confirmed our predictions (Figure 4). The released amount of MX was the lowest in the case of samples containing raw material during the investigation. The spray-dried samples showed enhanced drug release compared with the reference samples. Approximately half of the drug was released from the samples containing nanosized API within the first 5 min and 65–85% released within an hour. These improvements in dissolution profile could be related to nanosizing effects, higher specific surface area, and amorphization. The presence of PVA inhibited the aggregation and increased polarity, which helped to release the MX in the simulated lung medium. Applying LEU reduced the cohesion between the particles, so a larger amount of MX was liberated from the powder than without LEU. The highest amount of API was released from nanoMX1_LEU0.5, because the higher LEU concentration reduced the polarity of the products. The results of our formulations are promising in the local pulmonary therapy. The prolonged presence of the particles gives enough time to release the nanosized API. Therefore, the clearance mechanism of the lung will reduce the delivered drug dose by a lesser amount [6].

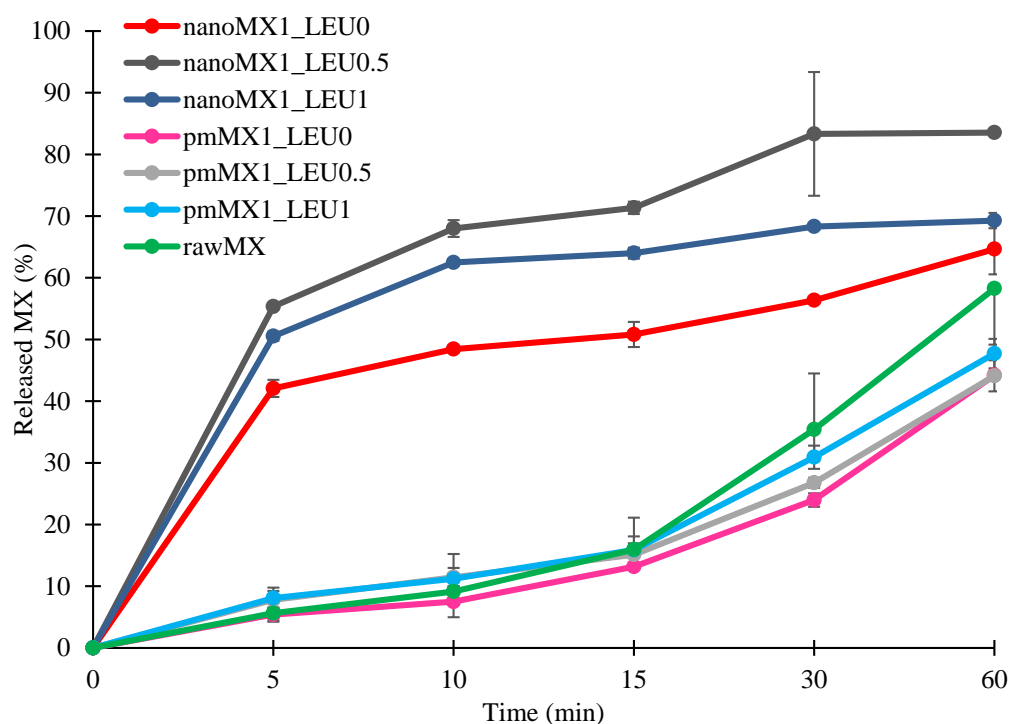


Figure 4. In vitro dissolution results of the active pharmaceutical ingredient (API) (rawMX), the physical mixtures (pmMX1_LEU0, pmMX1_LEU0.5, and pmMX1_LEU1), and the prepared samples (nanoMX1_LEU0, nanoMX1_LEU0.5, and nanoMX1_LEU1). Data are means \pm SD ($n = 3$ independent measurements).

3.8. In Vitro Permeability Results

We investigated the diffused amount of API from the simulated lung medium through a membrane to the epithelium. The high surface area achieved by the nanosized particles was the main factor affecting the rate of passive diffusion. Diffusion from the samples was faster and reached higher values than from raw MX and the physical mixtures (Figure 5). The diffused MX concentrations (60–90 $\mu\text{g}/\text{cm}^2$) were promising if we interpolate them to the total surface of the lung. We reached the highest values with the nanoMX1_LEU0.5 formulation, which was correlated with the result of the in vitro dissolution test. The products showed a significantly increased flux (J) and permeability coefficient (K_p) compared

with the raw materials (Table 8). The higher diffusion is connected to the higher surface area produced by the nanoparticles. A large amount of API could get into the epithelium with our spray-dried formulations; as a result of this, they could be effective in the local treatment of pulmonary diseases.

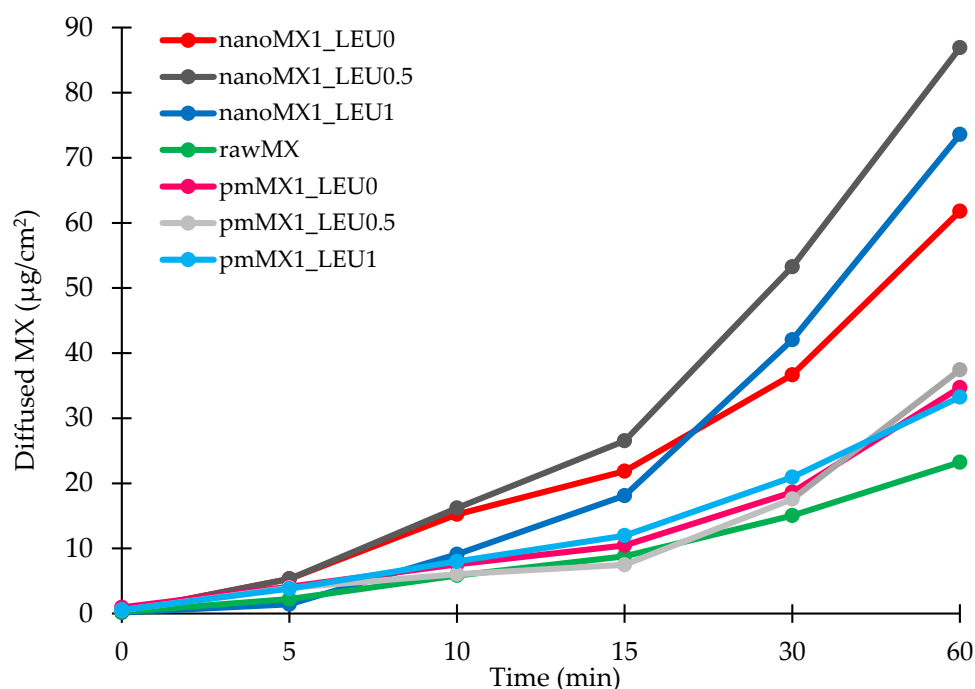


Figure 5. In vitro diffusion results of the API (rawMX), the physical mixtures (pmMX1_LEU0, pmMX1_LEU0.5, and pmMX1_LEU1), and the prepared samples (nanoMX1_LEU0, nanoMX1_LEU0.5, and nanoMX1_LEU1). SD < ±2% (n = 3 independent measurements).

Table 8. In vitro permeability results of the samples.

Samples	J (µg/cm ² /h)	Kp (cm/h)
rawMX	28.23	0.1394
pmMX1_LEU0	34.69	0.2081
pmMX1_LEU0.5	37.45	0.2247
pmMX1_LEU1	33.25	0.1995
nanoMX1_LEU0	61.80	0.3708
nanoMX1_LEU0.5	86.90	0.5214
nanoMX1_LEU1	73.58	0.4415

SD < ±2% (n = 3 independent measurements).

3.9. In Vitro Aerodynamic Results

The in vitro aerodynamic results are demonstrated in Table 9. The MMAD values were between 1.55 and 2.33 µm, wherewith we could target the deeper airways [48]. The samples had FPF values between 72 and 76%, which is higher than the FPF values of the Breezhaler formulations on the market [32]. We can see the distribution of the products on the stages of the Andersen cascade impactor (Figure 6). The nanoMX1_LEU0 sample had 15% deposition in the upper airways, and 25% and 27% deposited on the third and fourth stages. The FPF value here was the most outstanding (75.67%). The application of LEU improved the aerosolization of the products owing to the reduced cohesion between the particles, which de-aggregated during inhalation. The samples had smaller MMAD (nanoMX1_LEU0.5: 1.74 µm, nanoMX1_LEU1: 1.55 µm) and were flown deeper in the ACI, deposited on the filter. We achieved high FPF values (nanoMX1_LEU0.5: 72.81%, nanoMX1_LEU0.5: 73.63%). The emitted fraction (EF) in most of the samples was also

high (around 72–84%), indicating a weak adhesive character between the powder and the capsule, so a large amount of the product could be liberated from the device.

Table 9. In vitro aerodynamic properties of the “nano-in-micro” systems. FPD, fine particle dose; FPF, fine particle fraction; ED, emitted dose; EF, emitted fraction.

Samples	MMAD * (μm)	FPD * (mg)	FPF * (%)	ED * (mg)	EF * (%)	Loaded API * (mg)	API content * (%)
nanoMX1_LEU0	2.33 ± 0.08	4.52 ± 0.33	75.67 ± 3.46	5.98 ± 0.22	72.42 ± 3.05	8.26 ± 0.14	93.81 ± 2.99
nanoMX1_LEU0.5	1.74 ± 0.35	3.09 ± 0.31	72.81 ± 1.46	4.24 ± 0.34	83.47 ± 1.33	5.07 ± 0.33	55.48 ± 0.78
nanoMX1_LEU1	1.55 ± 0.06	2.51 ± 0.04	73.63 ± 0.96	3.40 ± 0.10	75.22 ± 1.75	4.53 ± 0.23	51.46 ± 0.66

* Data are means \pm SD (n = 3 independent measurements).

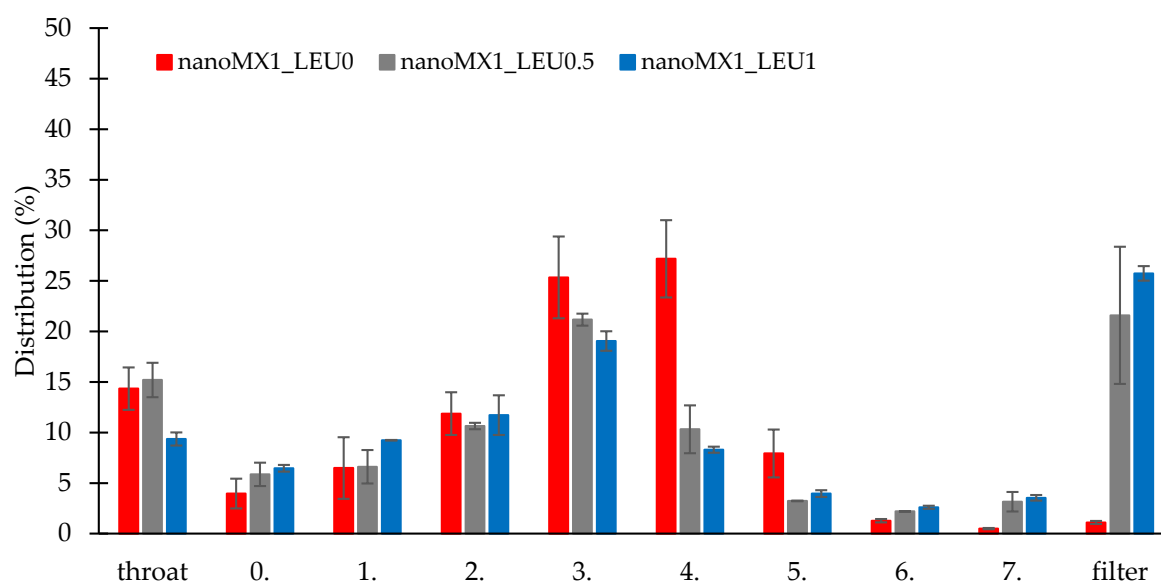


Figure 6. In vitro distribution of the samples (nanoMX1_LEU0, nanoMX1_LEU0.5, and nanoMX1_LEU1). Data are means \pm SD (n = 3 independent measurements).

3.10. In Silico Aerodynamic Results

Figure 7 shows the deposition fractions of the samples within the extrathoracic airways and within different regions of the lung; that is, the bronchial and acinar pulmonary regions. The results were calculated with breath-holding time after inhalation of 5 s and 10 s. Using a breath-holding time of 10 s, the deposited fraction improved in all cases. The extrathoracic deposition is lower for the LEU containing products, thanks to improved dispersity. The lower deposition in the lung was because this method was defined as the deposited amount on the filter, as an exhaled fraction. The nanoMX1_LEU0 reached the highest deposition (47.47%) in the lung (Table 10). In all cases, higher values were obtained in the acinar region than in the bronchial region, which proved the delivery into the lower parts of the lung. It is a more proper approach to the real distribution in the airways than the in vitro method. However, these data are also promising for us because, in various lung diseases, the airways are usually damaged, contracted, or obstructed.

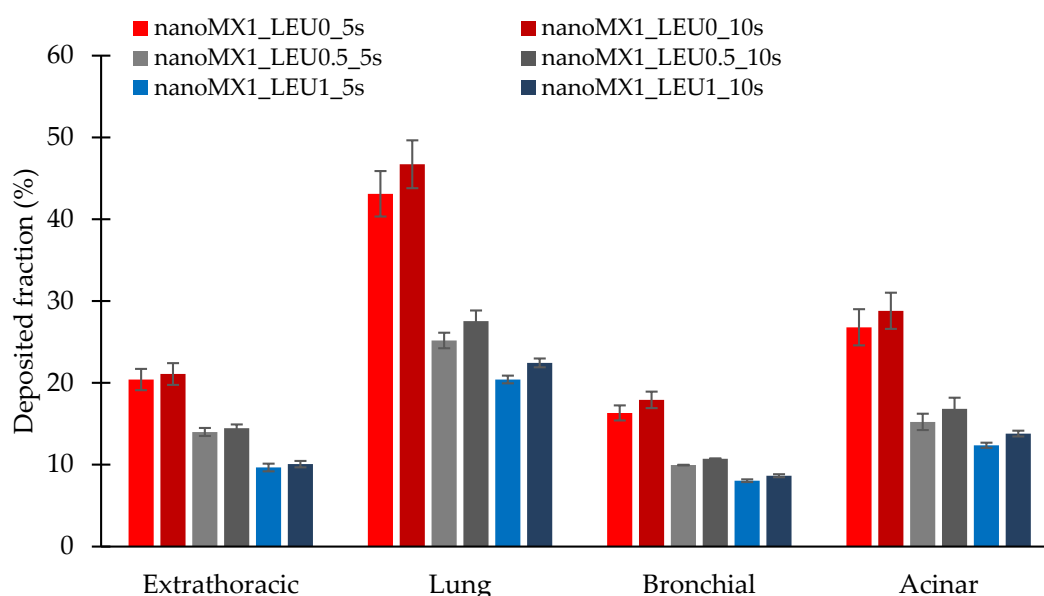


Figure 7. In silico aerodynamic results of the products (nanoMX1_LEU0, nanoMX1_LEU0_5s, nanoMX1_LEU0_10s, nanoMX1_LEU0.5_5s, nanoMX1_LEU0.5_10s, nanoMX1_LEU1_5s, and nanoMX1_LEU01_10s). Data are means \pm SD ($n = 3$ independent measurements).

Table 10. In silico aerodynamic properties with a breath-holding time of 10 s.

Samples	Deposited Fraction * (%)			
	Extrathoracic	Lung	Bronchial	Acinar
nanoMX1_LEU0	21.41 \pm 2.79	46.73 \pm 2.21	17.92 \pm 2.93	28.81 \pm 2.22
nanoMX1_LEU0.5	14.45 \pm 0.95	27.55 \pm 0.99	10.72 \pm 1.30	16.83 \pm 1.34
nanoMX1_LEU1	10.07 \pm 0.47	22.44 \pm 0.31	8.64 \pm 0.54	13.80 \pm 0.35

* Data are means \pm SD ($n = 3$ independent measurements).

4. Discussion

The purpose of our research work was to develop a carrier-free “nano-in-micro” DPI system including the advantages of a nanonized active ingredient. We successfully worked out a “nano-in-micro” structured particle preparation method. We nanonized the API by wet milling and prepared micrometric sized particles by spray-drying. The samples containing MX, stabilizing additive (PVA), and aerosolization adjuvant (LEU) were characterized. From the nanosuspension, which contained MX nanoparticles ($d = 137$ nm), we managed to prepare nearly spherical microparticles with a size of 3–4 μ m. By adding LEU, we could improve the yield (58%) of the spray-drying method. The specific surface area of the powders (1.7–2.2 m^2/g) increased compared with the raw materials. With the low density (0.20–0.27 g/cm^3) formulations, we achieved proper aerosolization properties. With the application of PVA, the polarity of the samples increased and, thanks to LEU, the cohesivity of the particles became lower. Part of the active ingredient was detected in an amorphous state according to the XRPD and DSC measurements. Owing to the particle size reduction, improved surface area, amorphization, and additives, dissolution was higher in the lung medium compared with the poorly water-soluble raw material, and the in vitro permeability of the samples also improved (61–87 $\mu\text{g}/\text{cm}^2/\text{h}$). The dissolution and permeability results were beneficial to local delivery. Samples showed good aerosolization properties during the in vitro aerodynamic measurements: FPF above 72%, MMAD between 1.55 and 2.33 μ m, and ED above 72%. The application of LEU increased the deposition in the deeper airways. The Andersen cascade impactor has limitations; that is, the data are usually higher than they could be in real circumstances [49]. The in silico aerodynamic values proved the deep deposition of the products in the respiratory airways.

They showed higher deposition in the acinar region than in the bronchial region. This method is also just an approximated translation to patients.

5. Conclusions

The presented DPI offers an effective local treatment for lung diseases to prove it; it should be tested in vivo soon. The execution of the stability measurement is also important because of the “nano-in-micro” structure and the partial amorphization of the active ingredient.

Author Contributions: Conceptualization and methodology, P.P., C.B., P.S.-R., and R.A.; investigation, P.P., R.A., and Á.F.; Evaluation, P.P.; writing—original draft, P.P.; writing—review and editing, C.B., Á.F., P.S.-R., and R.A.; supervision, R.A. All authors have read and agreed to the published version of the manuscript.

Funding: This research was funded by the University of Szeged Open Access Fund grant number 5062.

Institutional Review Board Statement: Not applicable.

Informed Consent Statement: Not applicable.

Acknowledgments: Gedeon Richter’s Talentum Foundation; this work was supported by Gedeon Richter Ltd.—GINOP project (2.2.1-15-2016-00007), EFOP 3.6.3-VEKOP-16-2017-00009, Ministry of Human Capacities, Hungary grant 20391-3/2018/FEKUSTRAT and TUDFO/47138-1/2019-ITM project is also acknowledged.

Conflicts of Interest: The authors declare no conflict of interest.

References

1. Sou, T.; Bergström, C.A.S. Contemporary formulation development for inhaled pharmaceuticals. *J. Pharm. Sci.* **2021**, *110*, 66–86. [CrossRef] [PubMed]
2. Pilcer, G.; Amighi, K. Formulation strategy and use of excipients in pulmonary drug delivery. *Int. J. Pharm.* **2010**, *392*, 1–19. [CrossRef] [PubMed]
3. Malamataris, M.; Charisi, A.; Malamataris, S.; Kachrimanis, K.; Nikolakakis, I. Spray drying for the preparation of nanoparticle-based drug formulations as dry powders for inhalation. *Processes* **2020**, *8*, 788. [CrossRef]
4. Lechanteur, A.; Evrard, B. Influence of composition and spray-drying process parameters on carrier-free DPI properties and behaviors in the lung: A review. *Pharmaceutics* **2020**, *12*, 55. [CrossRef]
5. Darquenne, C. Aerosol deposition in health and disease. *J. Aerosol Med. Pulm. Drug Deliv.* **2012**, *25*, 140–147. [CrossRef] [PubMed]
6. Ruge, C.C.; Kirch, J.; Lehr, C.M. Pulmonary drug delivery: From generating aerosols to overcoming biological barriers—therapeutic possibilities and technological challenges. *Lancet Respir. Med.* **2013**, *1*, 402–413. [CrossRef]
7. Malamataris, M.; Somavarapu, S.; Kachrimanis, K.; Buckton, G.; Taylor, K.M.G. Preparation of respirable nanoparticle agglomerates of the low melting and ductile drug ibuprofen: Impact of formulation parameters. *Powder Technol.* **2017**, *308*, 123–134. [CrossRef]
8. National Center for Biotechnology Information. 2021. Available online: <https://pubchem.ncbi.nlm.nih.gov/compound/Meloxicam> (accessed on 28 January 2021).
9. Szabó-Révész, P. Modifying the physicochemical properties of NSAIDs for nasal and pulmonary administration. *Drug Discov. Today Technol.* **2018**, *27*, 87–93. [CrossRef] [PubMed]
10. Arafa, H.M.M.; Abdel-Wahab, M.H.; El-Shafeey, M.F.; Badary, O.A.; Hamada, F.M.A. Anti-fibrotic effect of meloxicam in a murine lung fibrosis model. *Eur. J. Pharmacol.* **2007**, *564*, 181–189. [CrossRef] [PubMed]
11. Yokouchi, H.; Kanazawa, K.; Ishida, T.; Oizumi, S.; Shinagawa, N.; Sukoh, N.; Harada, M.; Ogura, S.; Munakata, M.; Dosaka-Akita, H.; et al. Cyclooxygenase-2 inhibitors for non-small-cell lung cancer: A phase II trial and literature review. *Mol. Clin. Oncol.* **2014**, *2*, 744–750. [CrossRef]
12. Weiss, A.; Porter, S.; Rozenberg, D.; O’Connor, E.; Lee, T.; Balter, M.; Wentlandt, K. Chronic obstructive pulmonary disease: A palliative medicine review of the disease, its therapies, and drug interactions. *J. Pain Symptom Manag.* **2020**, *60*, 135–150. [CrossRef]
13. Bartos, C.; Szabó-Révész, P.; Bartos, C.; Katona, G.; Jójárt-Laczovich, O.; Ambrus, R. The effect of an optimized wet milling technology on the crystallinity, morphology and dissolution properties of micro- and nanonized meloxicam. *Molecules* **2016**, *21*, 507. [CrossRef] [PubMed]
14. Pomázi, A.; Buttini, F.; Ambrus, R.; Colombo, P.; Szabó-Révész, P. Effect of polymers for aerolization properties of mannitol-based microcomposites containing meloxicam. *Eur. Polym. J.* **2013**, *49*, 2518–2527. [CrossRef]
15. Feng, A.L.; Boraey, M.A.; Gwin, M.A.; Finlay, P.R.; Kuehl, P.J.; Vehring, R. Mechanistic models facilitate efficient development of leucine containing microparticles for pulmonary drug delivery. *Int. J. Pharm.* **2011**, *409*, 156–163. [CrossRef]

16. Li, L.; Sun, S.; Parumasivam, T.; Denman, J.A.; Gengenbach, T.; Tang, P.; Mao, S.; Chan, H.K. L-Leucine as an excipient against moisture on in vitro aerosolization performances of highly hygroscopic spray-dried powders. *Eur. J. Pharm. Biopharm.* **2016**, *102*, 132–141. [\[CrossRef\]](#)
17. Chvatal, A.; Farkas, Á.; Balásházy, I.; Szabó-Révész, P.; Ambrus, R. Aerodynamic properties and in silico deposition of meloxicam potassium incorporated in a carrier-free DPI pulmonary system. *Int. J. Pharm.* **2017**, *520*, 70–78. [\[CrossRef\]](#) [\[PubMed\]](#)
18. Chvatal, A.; Ambrus, R.; Party, P.; Katona, G.; Jójárt-Laczkovich, O.; Szabó-Révész, P.; Fattal, E.; Tsapis, N. Formulation and comparison of spray dried non-porous and large porous particles containing meloxicam for pulmonary drug delivery. *Int. J. Pharm.* **2019**, *559*, 68–75. [\[CrossRef\]](#)
19. Seville, P.C.; Learoyd, T.P.; Li, H.Y.; Williamson, I.J.; Birchall, J.C. Amino acid-modified spray-dried powders with enhanced aerosolisation properties for pulmonary drug delivery. *Powder Technol.* **2007**, *178*, 40–50. [\[CrossRef\]](#)
20. Li, Q.; Rudolph, V.; Weigl, B.; Earl, A. Interparticle van der Waals force in powder flowability and compactibility. *Int. J. Pharm.* **2004**, *280*, 77–93. [\[CrossRef\]](#)
21. European Directorate for the Quality of Medicines and HealthCare. 2.9. Bulk density and tapped density of powders. In *European Pharmacopoeia 9.0*; European Directorate for the Quality of Medicines and HealthCare: Strasbourg, France, 2020; p. 359.
22. Ambrus, R.; Benke, E.; Farkas, Á.; Balásházy, I.; Szabó-Révész, P. Novel dry powder inhaler formulation containing antibiotic using combined technology to improve aerodynamic properties. *Eur. J. Pharm. Sci.* **2018**, *123*, 20–27. [\[CrossRef\]](#)
23. European Directorate for the Quality of Medicines and HealthCare. 2.9. Dissolution test for solid dosage forms. In *European Pharmacopoeia 9.0*; European Directorate for the Quality of Medicines and HealthCare: Strasbourg, France, 2010; p. 228.
24. Fröhlich, E.; Mercuri, A.; Wu, S.; Salar-Behzadi, S. Measurements of deposition, lung surface area and lung fluid for simulation of inhaled compounds. *Front. Pharmacol.* **2016**, *7*, 1–10. [\[CrossRef\]](#) [\[PubMed\]](#)
25. Parlatti, C. Respirable Microparticles of Aminoglycoside Antibiotics for Pulmonary Administration. Ph.D. Thesis, University of Parma, Parma, Italy, 2008.
26. May, S. Dissolution Testing of Powders for Inhalation. Ph.D. Thesis, Faculty of Natural Sciences and Technology, Saarbrücken, Germany, 2013; pp. 8–11.
27. Boarder, M.; Dixon, J.; Newby, D.; Navti, P.; Zetterström, T. *Pharmacology for Pharmacy and the Health Sciences*; Oxford University Press: Oxford, UK, 2010.
28. Chvatal, A.; Alzhrani, R.; Tiwari, A.K.; Ambrus, R.; Szabó-Révész, P.; Boddu, S.H.S. Cytotoxicity of inhalable dry powders in A549 human lung cancer cell line. *Farmacia* **2018**, *66*, 172–175.
29. Sipos, B.; Szabó-Révész, P.; Csóka, I.; Pallagi, E.; Dobó, D.G.; Béteky, P.; Kónya, Z.; Deák, Á.; Janovák, L.; Katona, G. Quality by design based formulation study of meloxicam-loaded polymeric micelles for intranasal administration. *Pharmaceutics* **2020**, *12*, 697. [\[CrossRef\]](#)
30. European Directorate for the Quality of Medicines and HealthCare. 2.9. Preparations for inhalation: Aerodynamic assessment of fine particles. In *European Pharmacopoeia 9.0*; European Directorate for the Quality of Medicines and HealthCare: Strasbourg, France, 2005; p. 323.
31. Buttini, F.; Colombo, G.; Kwok, P.C.L.; Wui, W.T. Aerodynamic assessment for inhalation products: Fundamentals and current pharmacopoeial methods. *Inhal. Drug Deliv. Tech. Prod.* **2013**, 91–119. [\[CrossRef\]](#)
32. Chapman, K.R.; Fogarty, C.M.; Peckitt, C.; Lassen, C.; Jadayel, D.; Dederichs, J.; Dalvi, M.; Kramer, B. Delivery characteristics and patients' handling of two single-dose dry-powder inhalers used in COPD. *Int. J. COPD* **2011**, *6*, 353–363. [\[CrossRef\]](#)
33. Benke, E.; Farkas, Á.; Szabó-révész, P.; Ambrus, R. Development of an innovative, carrier-based dry powder inhalation formulation containing spray-dried meloxicam potassium to improve the in vitro and in silico aerodynamic properties. *Pharmaceutics* **2020**, *12*, 535. [\[CrossRef\]](#)
34. Cunha, L.; Rodrigues, S.; da Costa, A.M.R.; Faleiro, M.L.; Buttini, F.; Grenha, A. Inhalable fucoidan microparticles combining two antitubercular drugs with potential application in pulmonary tuberculosis therapy. *Polymers* **2018**, *10*, 636. [\[CrossRef\]](#)
35. Hofmann, W. Modelling inhaled particle deposition in the human lung—A review. *J. Aerosol Sci.* **2011**, *42*, 693–724. [\[CrossRef\]](#)
36. Raabe, O.G.; Yeh, H.; Schum, G.M.; Phalen, R.F. *Tracheobronchial Geometry: Human, Dog, Rat, Hamster—A Compilation of Selected Data from the Project Respiratory Tract Deposition Models*; Lovelace Foundation for Medical Education and Research: Albuquerque, NM, USA, 1976; Volume 741, pp. 1–11.
37. Koblinger, L.; Hofmann, W. Monte Carlo modeling of aerosol deposition in human lungs. Part I: Simulation of particle transport in a stochastic lung structure. *J. Aerosol Sci.* **1990**, *21*, 661–674. [\[CrossRef\]](#)
38. Farkas, Á.; Jókay, Á.; Füri, P.; Balásházy, I.; Müller, V.; Odler, B.; Horváth, A. Computer modelling as a tool in characterization and optimization of aerosol drug delivery. *Aerosol Air Qual. Res.* **2015**, *15*, 2466–2474. [\[CrossRef\]](#)
39. Farkas, Á.; Jókay, Á.; Balásházy, I.; Füri, P.; Müller, V.; Tomisa, G.; Horváth, A. Numerical simulation of emitted particle characteristics and airway deposition distribution of Symbicort® Turbuhaler® dry powder fixed combination aerosol drug. *Eur. J. Pharm. Sci.* **2016**, *93*, 371–379. [\[CrossRef\]](#)
40. Mangal, S.; Meiser, F.; Tan, G.; Gengenbach, T.; Denman, J.; Rowles, M.R.; Larson, I.; Morton, D.A. Relationship between surface concentration of L-leucine and bulk powder properties in spray dried formulations. *Eur. J. Pharm. Biopharm.* **2015**, *94*, 160–169. [\[CrossRef\]](#)
41. Nandiyanto, A.B.D.; Okuyama, K. Progress in developing spray-drying methods for the production of controlled morphology particles: From the nanometer to submicrometer size ranges. *Adv. Powder Technol.* **2011**, *22*, 1–19. [\[CrossRef\]](#)

-
42. Focaroli, S.; Mah, P.T.; Hastedt, J.E.; Gitlin, I.; Oscarson, S.; Fahy, J.V.; Healy, A.M. A Design of Experiment (DoE) approach to optimise spray drying process conditions for the production of trehalose/leucine formulations with application in pulmonary delivery. *Int. J. Pharm.* **2019**, *562*, 228–240. [[CrossRef](#)]
 43. Bosquillon, C.; Lombry, C.; Pr  at, V.; Vanbever, R. Influence of formulation excipients and physical characteristics of inhalation dry powders on their aerosolization performance. *J. Control. Release* **2001**, *70*, 329–339. [[CrossRef](#)]
 44. Azari, F.; Ghanbarzadeh, S.; Safdari, R.; Yaqoubi, S.; Adibkia, K.; Hamishehkar, H. Development of a carrier free dry powder inhalation formulation of ketotifen for pulmonary drug delivery. *Drug Res.* **2020**, *70*, 26–32. [[CrossRef](#)]
 45. European Directorate for the Quality of Medicines and HealthCare. 2.9. Powder Flow. In *European Pharmacopoeia 9.0*; European Directorate for the Quality of Medicines and HealthCare: Strasbourg, France, 2010; Volume 3, p. 346.
 46. Aytekin, Y.S.; K  kt  rk, M.; Zaczek, A.; Korter, T.M.; Heilweil, E.J.; Esenturk, O. Optical properties of Meloxicam in the far-infrared spectral region. *Chem. Phys.* **2018**, *512*, 36–43. [[CrossRef](#)]
 47. Najafabadi, A.R.; Gilani, K.; Barghi, M.; Rafiee-tehrani, M. The effect of vehicle on physical properties and aerosolisation behaviour of disodium cromoglycate microparticles spray dried alone or with l -leucine. *Int. J. Pharm.* **2004**, *285*, 97–108. [[CrossRef](#)]
 48. Williams, R.O.; Carvalho, T.C.; Peters, J.I. Influence of particle size on regional lung deposition—What evidence is there? *Int. J. Pharm.* **2011**, *406*, 1–10. [[CrossRef](#)]
 49. Mitchell, J.; Newman, S.; Chan, H.K. In vitro and in vitro aspects of cascade impactor tests and inhaler performance: A review. *AAPS PharmSciTech* **2007**, *8*, 237–248. [[CrossRef](#)]

II.



Development of extra-fine particles containing nanosized meloxicam for deep pulmonary delivery: *In vitro* aerodynamic and cell line measurements

Petra Party^a, Dávid Kókai^b, Katalin Burián^b, Attila Nagy^c, Béla Hopp^d, Rita Ambrus^{a,*}

^a Institute of Pharmaceutical Technology and Regulatory Affairs, University of Szeged, Eötvös street 6., Szeged 6720, Hungary

^b Department of Medical Microbiology, Faculty of Medicine, University of Szeged, Dóm square 10., Szeged 6720, Hungary

^c Wigner Research Centre for Physics, Hungarian Academy of Sciences, Konkoly-Thege Miklós street 29-33., Budapest 1121, Hungary

^d Department of Optics and Quantum Electronics, University of Szeged, Dóm square 9., Szeged 6720 Hungary

ARTICLE INFO

Keywords:

Dry powder inhaler
Meloxicam
Nano spray-drying
Andersen cascade impactor
Aerodynamic particle counter
A549 cell line

ABSTRACT

Pulmonary drug administration provides a platform for the effective local treatment of various respiratory diseases. Application of nano-sized active ingredients results in higher bioavailability because of their large specific surface area. Extra-fine dry powder inhalers reach the smaller airways, further improving therapeutic efficiency. Poorly water-soluble meloxicam was the selected active ingredient. We aimed to decrease the particle size into the nano range by wet milling and producing extra-fine inhalable particles via nano spray-drying. The diameter of the drug was reduced to 138 nm. The particle size of the dry products was between 1.1 and 1.5 μm , and the dispersed diameter was between 500 and 800 nm. Owing to the excipients (poly-vinyl-alcohol, leucine), the spray-dried particles presented nearly spherical morphology. The drug became partially amorphous. Thanks to the improved surface area, the solubility and the released and the diffused amount of the meloxicam increased in artificial lung media. The *in vitro* aerodynamic measurements showed that the leucine-containing formulations had outstanding fine particle fraction (FPF) deposition with 1.3 μm mass median aerodynamic diameter (MMAD). The aerodynamic particle counter test also proved the extra-fine aerodynamic particle size. The *in vitro* cell line experiments revealed the non-cytotoxicity of the products and the suppression of the interleukin concentration. Overall, the powders are suitable for deep pulmonary delivery and the local treatment of lung inflammations.

1. Introduction

Nanotechnology is currently revolutionizing drug delivery, including the field of pulmonary administration. Its application allows combining the advantages of nanomaterials and the lung as a target. The definition of nanomaterials according to the European Union requires particles size under 100 nm (Potočník, 2011). Pharmaceutical nanoparticles are defined as individual particles with a size below 1 μm . Typically a mean particle diameter between 200 and 500 nm is applied (Keck and Müller, 2006), (Scherließ et al., 2022). The reduced size and hence larger specific surface area enhance the dissolution rate of poorly water-soluble drugs. Therefore, nanoparticles increase intracellular drug delivery and are better internalized by cells, resulting in higher bioavailability (Muralidharan et al., 2015). Proper formulation is indispensable for the efficient transport of the nanosized active ingredient to the respiratory system. In pulmonary therapy, the generally requested particle size

range is aerodynamic particle diameter between 1 and 5 μm . To reach the deeper lung parts, particles 0.5–1.5 μm in size are ideal, because of their very low deposition on their way to the targeted region and their large deposition in the small peripheral lung structures (Heyder, 2004; Thorley and Tetley, 2013; Das et al., 2021). Application of extra-fine particles (< 2 μm) built up nanosized active ingredient could be beneficial for the treatment of deeper lung segments (Hillyer et al., 2018; De Boer et al., 2015; Jetzer et al., 2018; Tse et al., 2021a; Scherließ et al., 2022). Harmonizing the advantages of nanoparticles with the aerodynamics of small microparticles could achieve an improved bioavailability and aerosolization behavior (Malamatari et al., 2020). The extra-fine particles deposit in the alveolar region, where the particles can disperse to nanoparticles. The liberated nano-sized active ingredient can effectively reach the epithelium, because they are not eliminated by the alveolar macrophages's size-dependent uptake (Thorley and Tetley, 2013; Ruge et al., 2013). However, drug delivery efficiency in the

* Corresponding author.

E-mail address: ambrus.rita@szte.hu (R. Ambrus).

<https://doi.org/10.1016/j.ejps.2022.106247>

Received 11 March 2022; Received in revised form 3 May 2022; Accepted 23 June 2022

Available online 25 June 2022

0928-0987/© 2022 The Authors. Published by Elsevier B.V. This is an open access article under the CC BY license (<http://creativecommons.org/licenses/by/4.0/>).

airways depends not only on the size of the formulations but also on particle morphology, density, and electrical charge (Muralidharan et al., 2015).

The deep respiratory deposition of drugs is important in the treatment of different lung inflammations. For example, in case of the new coronavirus (SARS-CoV-2) infection. When the aerosol particles contact the airways, the virus particles travel down into the acinar airways, resulting in a higher deposition fraction in the acinar airways than in the bronchi (Madas et al., 2020). The virus replicates in type II pneumocytes. After the release of the new virus, it activates alveolar macrophages. The virus also induces the release of proinflammatory cytokines, which leads to the common COVID-19 symptoms: acute respiratory distress syndrome, pneumonia, fever, multiple organ system failure, and coughing (Chugh et al., 2021). Since the virus replicates in alveolar epithelial cells, it is believed that inhaling as deeply as possible will enhance the therapeutic effect of the inhaled drug (Iwabuchi et al., 2020). The direct pulmonary delivery of medicines provides higher lung concentrations as well as reduces systemic toxicity in COVID-19 patients. Dry powder inhalers (DPIs) would be convenient in the therapy. DPIs offer several advantages including ease of use, non-invasiveness, no liquid propellant, an extended-release profile, improved tolerability, and long-term stability (Muralidharan et al., 2015). This approach would be ideal for the treatment of COVID-19 patients in an out-patient setting, especially if COVID-19 becomes a recurrent seasonal disease (Sun, 2020). For the treatment of lung inflammation, cyclooxygenase-2 (COX-2) inhibitors could be applied. SARS-CoV-2 infection induces COX-2 expression, which leads to inflammation. Meloxicam (MX) was chosen as an active ingredient during our work, because it is a selective COX-2 inhibitor non-steroidal anti-inflammatory drug (NSAID). The inhibition of COX-2 by MX does not affect viral entry or replication but may play a role in regulating the lung inflammation and injury observed in COVID-19 patients (Chen et al., 2020). Therefore, MX could be important in the adjuvant therapy of COVID-19 (Ong et al., 2020). Currently, the main indications of MX are arthritis and osteoarthritis in human therapy. MX is commercially available only in oral, intravenous, and intralesional delivery routes (Meloxicam Drugbank). The development of new delivery systems and/or changes in administration routes is an alternative way to reposition drugs. Drug repositioning is widely used by the pharmaceutical industry due to the notable cost and time reduction. An interesting alternative for COVID-19 treatment could be the identification of a suitable repositioned drug to be administered via pulmonary route. The local administration has shown positive results in the treatment of different lung diseases, which may be related to its rapid onset, low metabolic activity, and reduction of adverse effects (Sarcinelli et al., 2021). As previously mentioned, direct lung delivery could be the barely most efficient way to apply the poorly-water soluble MX. Our research group had a widespread experience in the DPI formulation of the drug. Carrier-based DPI-s (Pomázi et al., 2013; Palagi et al., 2016; Benke et al., 2020) and also carrier-free systems with different structures, such as porous formulations (Chvatal et al., 2019) and “nano-in-micro” particles (Party et al., 2021) were developed containing meloxicam and meloxicam-potassium. Porous formulation also can be delivered into the deeper lung region. They have low density, therefore they make small aerodynamic particle diameter during inhalation (Tse et al., 2021b; Alhajj et al., 2021). “Nano-in-micro” formulations combine the benefits of nanoparticles and microparticles, which leads to achieving better absorption and proper deposition in the lungs (Malamatari et al., 2020; Scherließ et al., 2022).

In the following work, we aimed to further develop our previous research work (Party et al., 2021). Now, we turned the focus to enhancing the water-solubility of the drug and targeting the smaller airways with the extra-fine particles. We selected wet milling to reduce the particle size of the poorly water-soluble MX, which increases the surface area, thus the solubility of the drug improves (Bartos et al., 2018). For the preparation of the inhalable extra-fine powders, we used a nano spray-drying technique. The preparation method is capable of

producing particles under 2 μm with narrow distribution and high yields (Li et al., 2010; Arpagaus et al., 2017). In addition, the combination of milling and spray-drying methods is scalable, cost-effective, and environmentally friendly. Besides the physico-chemical characterization and *in vitro* dosage form investigations, we extended the *in vitro* aerodynamic assessment to implement a more accurate characterization of the powders. We also wanted to prove the safety and efficiency of the formulations using *in vitro* cell line tests. Our final goal is to deliver a high percentage of the extra-fine particles into the deeper, alveolar region of the lung, where the nano-sized active ingredient could exert its anti-inflammatory effect. Therefore, we could provide new therapeutic applicability of the MX in the treatment of severe lung inflammation.

2. Materials and methods

2.1. Materials

The active pharmaceutical ingredient (API) was meloxicam (MX) (Egis Pharmaceuticals PLC., Budapest, Hungary). Poly-vinyl-alcohol 4–98 (PVA), (Aldrich Chemistry, Darmstadt, Germany) and L-leucine (LEU), (AppliChem GmbH, Darmstadt, Germany) were chosen as excipients.

2.2. Methods

2.2.1. Media milling

Firstly PVA was solved in purified water, which resulted in a solution with a 2.5% (w/w%) concentration. PVA is a polymer, which prevents the aggregation of the drug particles during the size reduction. It was followed by the preparation of a presuspension, which contained 2.00 g of pure MX and 18.0 g of 2.5% PVA solution, as a dispersant. A combined wet milling method was used, which was previously optimized by our research group (Bartos et al., 2018; Bartos et al., 2016). The milling medium was 20.00 g of ZrO_2 beads in a planetary ball mill (Retsch Planetary Ball Mill PM 100 MA, Retsch GmbH, Haan, Germany). The milling parameters were the following: 500 rpm, 60 min. After milling, the suspension was diluted to 500 ml with purified water (Party et al., 2021).

2.2.2. Nano spray-drying

Three different compositions were formulated from the MX nano-suspension by adding various amounts of LEU. The dry material contents of the final formulations are shown in Table 1. LEU is an amino acid, which enhances the dispersity of the spray-dried powders. A magnetic stirrer was used for its homogenization in the suspension (AREC. X heating magnetic stirrer, Velp Scientifica Srl, Italy). The inhalable powders were produced with a Büchi Nano Spray Dryer equipped with a small nebulizer (Büchi Nano Spray Dryer B-90 HP, Büchi, Flawil, Switzerland). Based on our preliminary experiments, the nano spray-drying settings were the following: inlet temperature: 80 °C, aspirator capacity: 100%, airflow rate: 120 ml/min, pump rate: 20%. In all cases, the yield of the nano spray-drying was around 62%. These results exceeded the yield of the traditional spray-drying method (Party et al., 2021).

Table 1

Final composition of the spray-dried samples and the yield of nano spray-drying and composition of the physical mixtures Data are means \pm SD ($n = 4$ independent measurements).

Sample name	MX (g)	PVA (g)	LEU (g)	Yield (%)
nano[MX1_PVA_LEU0]	2.00	0.45	0.00	61.44 \pm 3.34
nano[MX1_PVA_LEU0.5]	2.00	0.45	1.00	63.29 \pm 2.38
nano[MX1_PVA_LEU1]	2.00	0.45	2.00	62.44 \pm 5.86
pm[MX1_PVA_LEU0]	2.00	0.45	0.00	–
pm[MX1_PVA_LEU0.5]	2.00	0.45	1.00	–
pm[MX1_PVA_LEU1]	2.00	0.45	2.00	–

2.2.3. Preparation of the physical mixtures

Three physical mixtures were prepared from the initial materials. Their compositions were equivalent to the nano spray-dried samples (Table 1). During the investigations, the properties of the physical mixtures were compared to the spray-dried products.

2.2.4. Laser diffraction

Laser diffraction was used to determine the particle size, the particle size distribution, and the specific surface area of our samples (Malvern Mastersizer Scirocco 2000, Malvern Instruments Ltd., Worcestershire, United Kingdom). In both cases, the refractive index of MX was adjusted to 1.720. The wet dispersion unit was used to investigate the particle size of the suspension. The suspension was measured in purified water with stirring at 2000 rpm. The dry dispersion unit was used to observe the nano spray-dried powders. The dispersion air pressure was set to 3.0 bar and 75% vibration feed was applied. Each sample was measured in triplicate. The particle size distribution (PSD) was characterized by the values of D[0.1] (10% of the volume distribution is below this value), D [0.5] (50% of the volume distribution is below this value), and D[0.9] (90% of the volume distribution is below this value). Span values were revealed in the particle size distribution, the higher the Span value, the broader the distribution (Li et al., 2004). The specific surface area (SSA) was derived from the PSD data. The calculations were made under the assumption of spherical particles. SSA data predicted the dissolution and diffusion properties of the products.

2.2.5. Dynamic light scattering

The average hydrodynamic diameter (Z-average), polydispersity index (PdI), and zeta potential were analyzed via dynamic light scattering (DLS) using a Malvern Zetasizer Nano ZS (Malvern Instruments, Worcestershire, United Kingdom). The suspension was diluted, the spray-dried formulations were suspended in purified water and measured at 25 °C in folded capillary cells. The refractive index of MX was set to 1.720. Each measurement was carried out in triplicate.

2.2.6. Surface tension measurement

Surface tension measurements of the PVA solution and the MX nanosuspension were carried out using the pendant drop technique with an OCA 20 apparatus (Dataphysics Instrument GmbH, Filderstadt, Germany). The density values of the samples were measured and set for the surface tension calculations. Drop images were collected at 25 °C and the drop profiles were fitted using the Young-Laplace equation (van Eerdenbrugh et al., 2008). For each experiment, ten subsequent images were collected and the average surface tension was used. The experiment was performed in triplicate.

2.2.7. Scanning electron microscopy

Scanning electron microscopy (SEM), (Hitachi S4700, Hitachi Scientific Ltd., Tokyo, Japan) was used to define the morphology of the spray-dried formulations. The investigation conditions were the following: 10 kV high voltage, 10 mA amperage, and 1.3–13.1 mPa air pressure. A high vacuum evaporator and argon atmosphere were applied to make the sputter-coated samples conductive with gold-palladium (Bio-Rad SC 502, VG Microtech, Uckfield, United Kingdom). For the implementation of the particle diameter investigation, ImageJ a public domain image analyzer software was used (<https://imagej.nih.gov/ij/index.html>).

2.2.8. X-ray powder diffraction

For structural investigation, X-ray powder diffraction (XRPD) spectra were recorded with the help of the BRUKER D8 Advance X-ray diffractometer (Bruker AXS GmbH, Karlsruhe, Germany). The radiation source was Cu K α 1 radiation ($\lambda=1.5406$ Å). The parameters of the analysis were the following: Cu target, Ni filter, 40 kV voltage, 40 mA current, time constant 0.1°/min, angular step 0.010° over the interval of 3–40° DIFFRACT plus EVA 28 software (Bruker AXS GmbH, Karlsruhe,

Germany) was used for the evaluation. The crystallinity was calculated via the mean of the decrease of the total area beneath the curve of the characteristic peaks compared with the physical mixtures.

2.2.9. Differential scanning calorimetry

Thermoanalytical properties were determined by differential scanning calorimetry (DSC). The measurements were executed with a Mettler Toledo DSC 821e thermal analysis system with the STARE thermal analysis program V9.1 (Mettler Inc., Schwerzenbach, Switzerland). Approximately 2–5 mg of the samples were observed in the temperature range between 25 °C and 300 °C. The heating rate was 10 °C/min. The carrier gas was argon at a flow rate of 10 l/h during the investigations.

2.2.10. Solubility test

The solubility test of the spray-dried formulations was implemented in simulated lung fluid. It contains 0.68 g/l NaCl, 2.27 g/l NaHCO₃, 0.02 g/l CaCl₂, 0.1391 g/l NaH₂PO₄, 0.37 g/l glycine, and 5.56 ml/l 0.1 M H₂SO₄ (Parlati, 2008). The pH of the medium was 7.4 ± 0.1 . A known excess quantity, 15 mg of MX containing powders was added to the media. The samples were stirred with a magnetic stirrer (AREC. X heating magnetic stirrer, Velp Scientifica Srl, Italy) at 25 °C for 24 h and then filtered (pore size=0.45 μ m, Millex-HV syringe-driven filter unit, Millipore Corporation, Bedford, USA) and the dissolved drug content was analyzed spectrophotometrically (ATI-Unicam UV/VIS Spectrophotometer, Cambridge, United Kingdom) at a wavelength of 362 nm. The samples were measured in triplicate. Limit of detection (LOD) and limit of quantification (LOQ) was determined for the method as defined in International Conference on Harmonization (ICH) guidelines (ICH Harmonised Tripartite Guideline, 2005), (Prasad and Thireesha, 2018) (The formulas were the following $LOD = SD \cdot 3.3/S$ and $LOQ = SD \cdot 10/S$. SD is the standard deviation and S is the mean slope of the calibration curve. Based on these data, the LOD of MX was calculated to be 0.3786 μ g/ml ($n = 4$). The LOQ of MX was evaluated to be 1.147 μ g/ml ($n = 4$).

2.2.11. In vitro dissolution test

Currently, there are no regulatory requirements or established protocols for *in vitro* dissolution testing of inhaled products (Riley et al., 2012; Radivojevic et al., 2019). A modified paddle method (Hanson SR8 Plus, Teledyne Hanson Research, Chatsworth, CA, United States of America) from the European Pharmacopoeia (European Pharmacopoeia 10.0, 2019) was used to define the release of MX from the solid dosage form. The applied samples contained 1.5 mg of MX, which is the tenth of the highest oral dose of MX (Meloxicam Pubchem). This is the estimated dose of MX for pulmonary delivery. There is no optimal method to determine the exact volume of the lung lining fluid. The estimated value is between 10 and 70 ml (Fröhlich et al., 2016). Considering the limitation of the dissolution setup, 50 ml of the previously mentioned (Section 2.2.10) simulated lung medium was applied during the measurement (Tay et al., 2018; Parlati, 2008). The paddle was rotated at 100 rpm to continuously homogenize the media. The measurement was performed up to 60 min at 37 °C (Pomázi, 2013). 5 ml of the samples were taken out after 5, 10, 15, 30, and 60 min. The medium was replenished in every case. After filtration (pore size: 0.45 μ m, Millex-HV syringe-driven filter unit, Millipore Corporation, Bedford, United States of America) the dissolved quantity of MX was determined spectrophotometrically at a wavelength of 362 nm (ATI-UNICAM UV/VIS Spectrophotometer, Cambridge, United Kingdom). The measurement was executed three times.

2.2.12. In vitro permeability test

A modified horizontal diffusion cell was used to investigate the *in vitro* permeability of the samples. The diffusion cells are a 3D printed unique construction developed and validated by the research team (Gieszinger et al., 2021). The method is suitable for the investigations of alternative drug delivery routes. It provides a solution to measure the permeability properties of the samples in small volume and real-time.

The set-up of the apparatus is shown in [Fig. 1](#). 9 ml of simulated lung medium was used as the donor phase. As previously mentioned, the volume of the lung lining fluid is 10–70 ml ([Fröhlich et al., 2016](#)), which is divided into different lung generations, therefore 9 ml was the ideal choice to model the absorption in the alveolar region. 9 ml of phosphate buffer (pH=7.4) was the acceptor phase, simulating the circumstances of the lung epithelium. Between the two phases, a cellulose membrane (RC 55 Whatman™ GE Healthcare Life Sciences, Buckinghamshire, United Kingdom) was applied, which was impregnated with isopropyl myristate. The pore size of the membrane was 0.5 μm , its thickness was 0.75 μm . The diffusion surface was 0.785 cm^2 . The rotation of the stirring bar was set to 300 rpm. The magnetic stirring bars were moved by CS-DSD1 Digital Magnetic Stirrer (CS-Smartlab Devices Ltd., Kozármisleny, Hungary). The equipment was thermostated by a water jacket with the help of a circulator. The temperature was 37 °C during the investigation, which is the usual temperature inside the human lung. The diffusion model ensures a homogeneous distribution of pulmonary dry powder formulations by the continuous stirring of the donor phase and maintenance of temperature throughout the experiment. Samples containing 1.5 mg of MX were investigated, similarly to the dissolution test. The design of the chambers was suitable for real-time analysis with an immersion probe input. The amount of the diffused API to the acceptor phase was determined at the wavelength of 362 nm, for 60 min with the help of the spectrophotometric sonda (FDP-7UV200-VAR, Avaspec-ULS2048-USB2, Avantes, Apeldoorn, The Netherlands). Three parallel measurements were performed with the formulations. In case of the method, the LOD of MX was evaluated to be 0.7987 $\mu\text{g/ml}$ ($n = 4$). The LOQ of MX was calculated to be 2.421 $\mu\text{g/ml}$ ($n = 4$).

The flux (J) [$\mu\text{g}/\text{cm}^2/\text{h}$] of MX was calculated from the quantity of MX, which permeated through the membrane, divided by the surface of the membrane insert and the duration time (Eq. (1)):

$$J = \frac{m}{A_* t} \quad (1)$$

The permeability coefficient (Kp) [cm/h] was determined as a ratio of flux and the MX concentration in the donor phase [$\mu\text{g}/\text{cm}^3$] (Eq. (2)):

$$K_p = \frac{J}{Cd} \quad (2)$$

2.2.13. In vitro aerodynamic measurements

The aerosolization properties of the nano spray-dried formulations were assessed *in vitro*, using an Andersen Cascade Impactor (ACI), (Apparatus D, Copley Scientific Ltd., Nottingham, United Kingdom) (European Pharmacopoeia 10.0, 2019). The inhalation flow rate was set to 60 l/min (High-capacity Pump Model HCP5, Critical Flow Controller Model TPK, Copley Scientific Ltd., Nottingham, UK). The actual flow rate through the impactor was measured by a mass flow meter (Flow Meter Model DFM 2000, Copley Scientific Ltd., Nottingham, UK). The inhalation time was 4 s. The setting models the normal breathing pattern with a 4 l inhalation volume. Breezhaler®'s single-dose devices (Novartis International AG, Basel, Switzerland) were applied, with

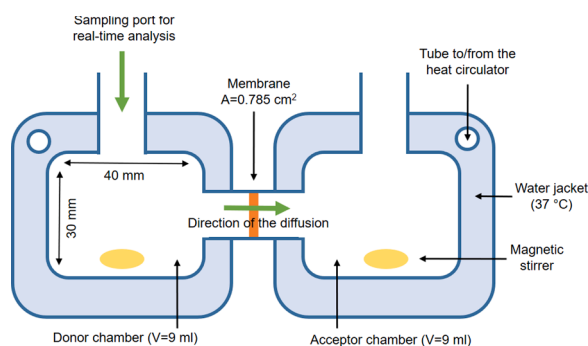


Fig. 1. The schematic set-up of the horizontal diffusion cells.

transparent, size 3 gelatine capsules (Capsugel, Bornem, Belgium) filled with the different powders. Between 2 and 3 mg of the dry samples were applied, therefore each capsule contained approximately 1.5 mg of the active ingredient. Four capsules were inhaled twice during one measurement. To simulate the pulmonary adhesive circumstances, the collection plates on the stages were coated with Span 85 and cyclohexane (1 + 99 w/w%) mixture. After inhalation, the device, the capsules, the induction port, the plates, and the filter were washed with methanol and pH 7.4 phosphate buffer (60+40 V/V%) to collect and dissolve the deposited amount of MX. The API was quantified by UV/Vis spectrophotometry (ATI-UNICAM UV/VIS Spectrophotometer, Cambridge, United Kingdom) at a wavelength of 362 nm. The *in vitro* aerodynamic properties were evaluated with the help of Inhalytix™ (Copley Scientific LTD., Nottingham, United Kingdom) data analysis software, which is a fully compliant, and validated aerodynamic particle size distribution data analysis solution. Fine particle fraction (FPF) and median mass aerodynamic diameter (MMAD) is the most widely used values. FPF is defined as the percentage of the mass of the active ingredient consisting of particles with an aerodynamic diameter of fewer than 5 µm divided by the emitted dose of the formulations. MMAD is influenced by the inhalation flow rate, density, size, and shape of the particle. The emitted fraction (EF) was also calculated, which is the released fraction from the DPI device.

2.2.14. Aerodynamic particle counter

The drug products were loaded into capsules and a Breezhaler® (Novartis International AG, Basel, Switzerland) dry powder inhalator device was used for the tests in the measurement setup shown in Fig. 2. The measurement setup consists of a breath simulator, an induction port representing the upper respiratory tract, a vacuum pump with a critical flow controller, and an Aerodynamic Particle Sizer (APS). A constant airflow Q2 was established in the system along the blue arrows using the

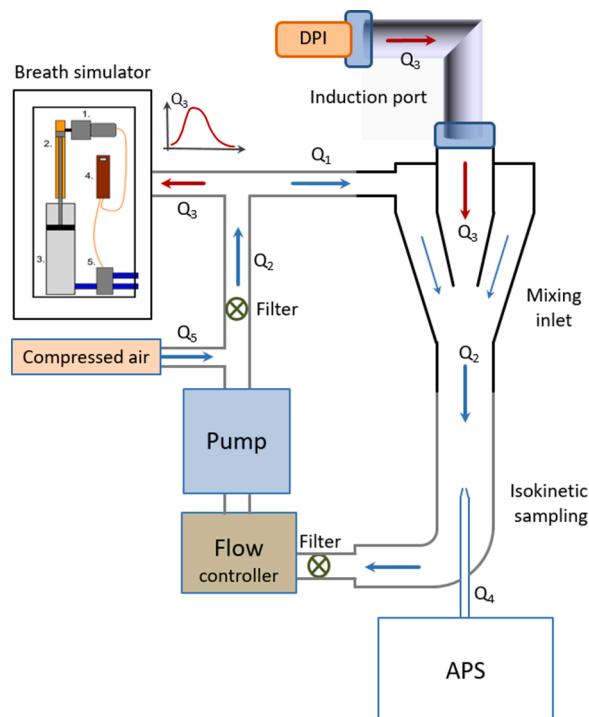


Fig. 2. The schematic design and components of the measurement setup: DPI, induction port, APS, vacuum pump with a critical flow controller, mixing inlet, and PWG. The pulmonary waveform generator consists of: 1-Servo motor; 2-Timing belt; 3-Piston pump; 4-PLC; 5-Valves (For interpretation of the references to color in this figure, the reader is referred to the web version of this article.).

pump (HCP5 High capacity pump; Copley Scientific Ltd., Nottingham, United Kingdom) and flow controller (TPK 2000; Copley Scientific Ltd., Nottingham, United Kingdom). The compressor compensates for the Q4 airflow taken by the particle counter and any losses. The airflow Q5 provided by the compressor was determined by measuring the airflow through the upper inlet of the mixing unit, in the inhaler side, in the default condition. During the measurements, the breathing simulator produced the flow profile Q3 activating the DPI unit through the mixing inlet (red arrows). The mixing inlet (Copley Scientific Ltd., Nottingham, United Kingdom) provides an interface between the flow that activates the DPI and the main stream that transfers the particles to the APS. The APS samples particles from the main stream by an isokinetic nozzle. A TSI 3321 (TSI Incorporated, Shoreview, Minnesota, United States of America) aerodynamic particle sizer was used for the measurements. The instrument measures the number size distributions of aerosol particles with aerodynamic diameters from 0.5 to 20 μm , in 52 channels. The instrument determines the aerodynamic size of the particles by time-of-flight measurement in an accelerated flow. The sample flow rate of the APS was 1 l/min and the sampling time was set to 5 s with no pause. Considering the length of the applied inhalation profile and the residence time of the particles in the measurement system the sampling time was set to 5 s during our investigations. As a breath simulator, we used an in-house developed pulmonary waveform generator. It uses a Piston pump driven by a PLC-controlled servo motor to generate the inhalation and exhalation air flows. The inhalation volume span from 0.1 cm³ to 6800 cm³. The time resolution of the inhalation profile can be set to 20, 50, and 100 ms. For the measurements, the inhalation waveform programmed into the breathing simulator was constructed based on literature data (Abadelah et al., 2019; Farkas et al., 2019). The flow controller was used to set a flow rate of 90 l/min, which was regularly checked during the measurements with a TSI 4000 thermal mass flow meter (TSI Incorporated, Shoreview, Minnesota, United States of America), which measuring range is 0.5–200 l/min.

2.2.15. Cytotoxicity measurement

Before the cell line investigation, the spray-dried samples were dissolved in dimethyl sulphoxide (DMSO) (VWR Chemicals, Leuven, Belgium). During the measurements, a concentration of 0.1 mg/ml was applied. This concentration of MX is adequate for pulmonary delivery, for 1.5 mg of drug dose in approximately 15 ml of lung fluid volume (Fröhlich et al., 2016). Diluted samples were also measured for further investigation. A concentration of 0.05 and 0.025 mg/ml were tested. Mitochondrial activity as a measure of cell viability was performed by MTT (3-(4,5-dimethylthiazol-2-yl)-2,5-diphenyltetrazolium bromide) assay in 96-well cell culture microplates using A549 (adenocarcinomic human alveolar basal epithelial cells) (ATCC). A549 cells were seeded at a density of 4×10^4 cells/well. The cells were treated with either MX or nano[MX1_PVA_LEU0] or nano[MX1_PVA_LEU0.5] or nano[MX1_PVA_LEU1]. The maximum concentration of the tested compounds was 0.1 mg/ml. Furthermore, 5 $\mu\text{g}/\text{ml}$ lipopolysaccharide (LPS; ThermoFisher Scientific Waltham, MA, USA) cytotoxicity was also measured. LPS was used to induce inflammation in the cells during the anti-inflammatory effect investigations (Crestani et al., 1994), therefore its cytotoxic effect was also tested (Section 2.2.16). Cells were incubated at 37 °C for 48 h. Later, 20 μl of thiazolyl blue tetrazolium bromide (Sigma, St. Louis, Missouri, USA) was added to each well. After additional incubation at 37 °C for 4 h, sodium dodecyl sulfate (Sigma, St. Louis, Missouri, USA) solution (10% in 0.01 M HCl) was added and incubated overnight. Cytotoxicity was then determined by measuring the OD at 550 nm (ref. 630 nm) with EZ READ 400 ELISA reader (Biochrom, Cambridge, United Kingdom). The assay was replicated four times for each concentration (Virók et al., 2017). Cell viability was concluded based on the following formula: $100 - ((\text{OD}_{\text{sample}} - \text{OD}_{\text{medium control}}) / (\text{OD}_{\text{cell control}} - \text{OD}_{\text{medium control}})) \times 100$.

2.2.16. Anti-inflammatory effect

The cells were propagated in minimum essential medium Eagle with Earle's salt (Sigma, St. Louis, MO, USA), and were supplemented with 25 $\mu\text{g}/\text{ml}$ gentamycin, 10% foetal calf serum, 0.5% wt/vol glucose, 0.3 mg/ml l-glutamine and 4 mM HEPES. A549 cells were seeded in 6-well plates at a density of 1×10^6 cells/well and treated with 0.1 mg/ml of MX and 5 $\mu\text{g}/\text{ml}$ of LPS or 0.1 mg/ml of nano[MX1_PVA_LEU0] and 5 $\mu\text{g}/\text{ml}$ of LPS or 0.1 mg/ml of nano[MX1_PVA_LEU0.5] and 5 $\mu\text{g}/\text{ml}$ of LPS or 0.1 mg/ml of nano[MX1_PVA_LEU1] and 5 $\mu\text{g}/\text{ml}$ of LPS or 5 $\mu\text{g}/\text{ml}$ of LPS or left untreated, then the cells were incubated for 48 h at 37 °C.

Total RNA extraction and cDNA synthesis. After 48 h of treatment, RNA was extracted using the TRI reagent (Sigma-Aldrich, St. Louis, Missouri, USA) according to the manufacturer's protocol. Subsequently, 0.1 μg of mRNA was reverse transcribed using Maxima Reverse Transcriptase according to the manufacturer's instructions using oligo(dT) primers (Thermo Fisher Scientific, Waltham, Massachusetts, USA).

qPCR amplification of IL-6, Actb. qPCR was performed using a Bio-Rad CFX96 real-time system with the 5x HOT FIREPol® EvaGreen® qPCR Supermix (Solis BioDyne, Tartu, Estonia) and the following human-specific primer pairs: IL-6: 5'-CAGCTATGAACCTCTTCTCCAC-3', and 5'-GCGGCTACATCTTTGGAATCT -3'; Actb: 5'-TTCTA-CATGAGCTGCGTGTGGCT-3', and 5'-TAGCACAGCCTGGA-TAGCAACGTA -3'. Primers were designed using the Primer Quest Tool software and synthesized by Integrated DNA Technologies Inc. (Montreal, Quebec, Canada). Melting curve analysis was performed to verify amplification specificity. Threshold cycles (Ct) were determined for IL-6 and Actb, and the relative gene expression was calculated via the 2-($\Delta\Delta\text{Ct}$) method. One-way analysis of variance with repeated measures (ANOVA RM) and planned comparisons was used to compare statistical differences in $\log_2(\Delta\Delta\text{Ct})$ values between infected and control samples, as described previously, with a level of significance of $P < 0.05$ (Hellemans et al., 2008).

Enzyme-linked immunosorbent assay (ELISA). After 48 h of treatment, the supernatant of the cells was collected and a standard sandwich human IL-6 ELISA kits Legend Max™ (BioLegend, San Diego, California, USA) was used to determine the IL-6 concentration. The supernatant of LPS-treated cells was diluted 10x. The assay was performed according to the manufacturer's instructions. The dynamic range of the kit was between 7.8 and 500 pg/ml. Plates were analyzed using the Biochrom Anthos 2010 microplate reader (Biochrom, Cambridge, United Kingdom). Samples were assayed in duplicate.

2.2.17. Statistical analysis

All described data indicate \pm SD of three parallel measurements ($n = 3$). Statistical analysis was performed by one-way analysis of variance (ANOVA) using GraphPad Prism 8.0.1. software (GraphPad Software, CA, United States of America). P -values < 0.05 indicated statistically significant differences.

3. Results and discussion

3.1. Laser diffraction

The initial diameter of the API was in the micrometric size range ($D[0.5] = 9.913 \pm 0.371 \mu\text{m}$), which successfully reached the nano range (Table 2). As a result of wet milling, the particle size of MX in the diluted suspension decreased to $D[0.5] = 137.70 \text{ nm} \pm 4.965 \text{ nm}$. SSA was increased from $1.09 \pm 0.028 \text{ m}^2/\text{g}$ up to $43.65 \pm 5.318 \text{ m}^2/\text{g}$. Size reduction and higher surface area of the nanoparticles as compared to the microparticles will lead to a higher rate of dissolution (Dubey, 2006). After nano spray-drying, the $D[0.5]$ values of the samples were

Table 2Particle size of the API, the suspension, and the nano spray-dried samples. Data are means \pm SD ($n = 3$ independent measurements).

Sample name	D[0.1] (μm)	D[0.5] (μm)	D[0.9] (μm)	Span	SSA (m^2/g)
MX	2.719 \pm 0.057	9.913 \pm 0.371	29.49 \pm 0.630	2.70 \pm 0.043	1.09 \pm 0.028
suspension[MX_PVA]	0.067 \pm 0.001	0.138 \pm 0.005	0.555 \pm 0.310	3.584 \pm 2.056	43.65 \pm 5.318
nano[MX1_PVA_LEU0]	0.441 \pm 0.004	1.168 \pm 0.004	6.770 \pm 1.722	5.422 \pm 1.488	6.600 \pm 0.028
nano[MX1_PVA_LEU0.5]	0.659 \pm 0.017	1.307 \pm 0.036	2.854 \pm 0.430	1.677 \pm 0.296	5.185 \pm 0.064
nano[MX1_PVA_LEU1]	0.789 \pm 0.017	1.429 \pm 0.088	3.400 \pm 0.503	1.586 \pm 0.116	4.385 \pm 0.007

between 1 and 1.5 μm . The result was correlated to our initial aim, which was to produce particles below 2 μm . The geometric diameter of spray-dried MX1_PVA_LEU0 was around 1.17 μm . Incorporating LEU, the geometric size of the spray-dried particles increased, which led to a decreasing SSA. The reason is that the particle–particle interaction forces alter the particle diameter (Mangal et al., 2015). The distribution was monodisperse in the case of LEU-containing products (Span < 2.0), which is important for accurate dosing (Chvatal et al., 2017).

3.2. Dynamic light scattering

During DLS investigations the average diameters of the diluted suspension and the dispersed powders were measured (Table 3). The test showed that the particle diameter of the suspension was 359.75 \pm 12 nm. The DLS results are more accurate than the laser diffraction in the nano range (Powers et al., 2007). In addition, we managed to reduce the diameter of the MX to under 500 nm. Therefore they can avoid the uptake by the alveolar macrophages (Thorley and Tetley, 2013). The average diameter of the dispersed spray-dried products was between 5 and 800 nm. This size results predict the behavior of the particles after deposition and disintegration in the airways. The polydispersity index (Pdl) values correlated with the Span values of laser diffraction. It decreased when more LEU was added. The zeta potentials of the samples ranged between -21 and -25 mV, which demonstrated that our samples constituted a stable suspension system (Salopek et al., 1992). Systems with negative zeta potential are more degradable in the lung, therefore do not cause further infection or fibrosis due to long retention (Dailey et al., 2003).

3.3. Surface tension

Considering surface tension, a variable lowering of the surface tension of water at 25 $^{\circ}\text{C}$ (71.99 \pm 0.36 mN/m) (Vargaftik et al., 1983), can be seen for the initial polymeric stabilizer. The surface tension of the 2.5% (w/V) PVA solution was 51.78 \pm 1.315 mN/m. The surface tension value of the nanosuspension was grown to 66.07 \pm 0.543 mN/m. Adding LEU could further increase the surface tension of the suspension (Gliński et al., 2000). The energy used by the mill to achieve particle size reduction can be defined as the collision energy. The collision energy is the sum of the kinetic energy of the beads acting perpendicular to the direction of the disk rotation and the collision heat generated by the milling components and the container wall (Bartos, 2016, 2019). That energy introduced during the particle size reduction process leads to an increase in surface tension of the suspension, which is associated with the increase in the dissolution pressure. The change in the surface tension can also lead to increased saturation solubility (Muller et al., 1999).

Table 3Average particle size, polydispersity index, and zeta potential of the suspension and the spray-dried products. Data are means \pm SD ($n = 3$ independent measurements).

Sample name	D (nm)	Pdl	Zeta potential (mV)
suspension[MX_PVA]	359.75 \pm 12	0.340 \pm 0.057	-23.70 ± 0.85
nano[MX1_PVA_LEU0]	676.70 \pm 47	0.543 \pm 0.055	-21.35 ± 5.27
nano[MX1_PVA_LEU0.5]	743.25 \pm 27	0.502 \pm 0.074	-23.30 ± 2.74
nano[MX1_PVA_LEU1]	526.90 \pm 20	0.381 \pm 0.031	-24.50 ± 1.47

However, a higher surface tension leads to a faster flow rate during nano spray-drying. Hence, a faster portion of fluid volume is delivered during the mesh vibration, leading to the formation of larger droplets (Arpagaus et al., 2017).

3.4. Scanning electron microscopy

According to the morphology investigation of the particles, a nearly spherical shape was observable (Fig. 3), which was due to the optimized nano spray-drying (Arpagaus et al., 2018). The particle diameter was measured based on the SEM pictures with the help of the Image-J program. The diameters were 692 \pm 157 nm of nano[MX1_PVA_LEU0], 838 \pm 307 of nano[MX1_PVA_LEU0.5] and 884 \pm 198 nm of nano[MX1_PVA_LEU1]. Data are means \pm SD ($n = 100$ independent measurements). The size results were correlated with the results of the previous particle size investigations. PVA prevented the aggregation of the particles, it makes a layer around the drug particles. This hydrophilic coat will also help the dissolution process of the API. Smooth surfaces are not preferred for pulmonary delivery since they tend to increase the interaction between particles while rough or wrinkled surfaces tend to increase the aerosolization efficiency. Changes in surface corrugation improve dispersibility by reducing contact points between particles, therefore achieving more separated particles. When LEU was present in the systems, preferable wrinkled, donut-like particles were established. Overall, the particles were forecasting a proper powder dispersion during inhalation, therefore higher drug delivery into the deeper regions of the lung (Sou et al., 2013; Chvatal et al., 2019; Party et al., 2021; Das et al., 2021).

3.5. X-ray powder diffraction

The XRPD pattern of the raw materials demonstrated, that MX and LEU had a crystalline structure. The presence of PVA did not affect the diffractograms, cause it had no crystalline properties. In the case of the products, the intensities of the characteristic peaks decreased (Fig. 4). Overall the wet milling and nano spray-drying procedures decreased crystallinity, which was determined via the mean of the decrease of the total area beneath the curve of the characteristic peaks compared with the physical mixtures. In nano[MX1_PVA_LEU0], nano[MX1_PVA_LEU0.5] and nano[MX1_PVA_LEU1] 68.19%, 66.11% and 54.04% of MX became amorphous, respectively (Bartos et al., 2016).

3.6. Differential scanning calorimetry

DSC was applied to determine the melting of PVA, LEU, and MX in the raw form, in the physical mixtures, and in the products (Fig. 5). PVA had no endothermic peak. LEU had an endothermic peak at 294.41 $^{\circ}\text{C}$, MX showed a sharper peak at 264.03 $^{\circ}\text{C}$, reflecting its melting point and crystalline structure. After the preparation method, the DSC curves showed broader endothermic peaks of MX, indicating a decrease in its crystallinity. The MX crystals remaining in the samples melted at a lower temperature than the crystals of raw MX because of particle size reduction. This was helped by PVA, which has the glass transition temperature (Tg) value at 85 $^{\circ}\text{C}$ (Bartos et al., 2018).

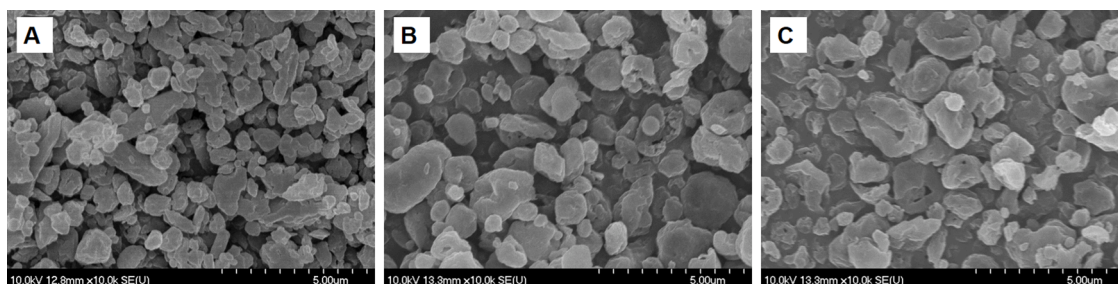


Fig. 3. SEM pictures of the spray-dried samples: A: nano[MX1_PVA_LEU0], B: nano[MX1_PVA_LEU0.5], C: nano[MX1_PVA_LEU1].

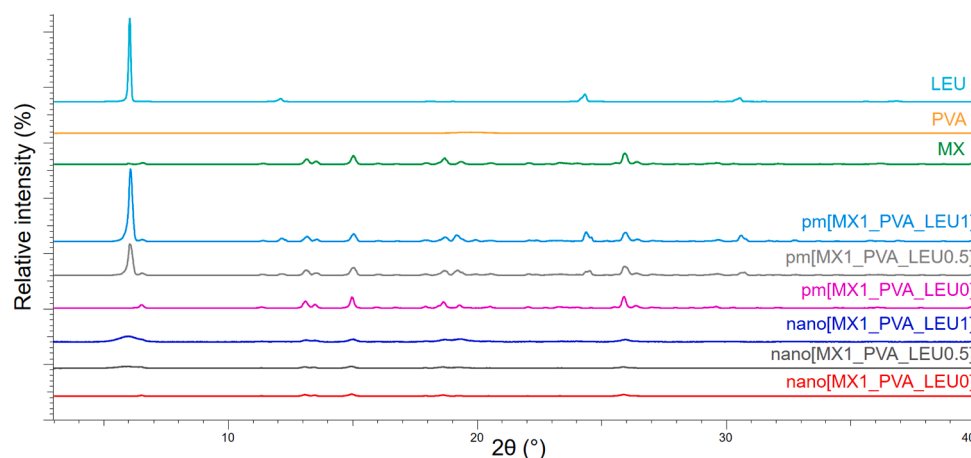


Fig. 4. XRPD results of the raw materials, (PVA, LEU, and MX), the physical mixtures (pm[MX1_PVA_LEU0], pm[MX1_PVA_LEU0.5], and pm[MX1_PVA_LEU1]), and the nano spray-dried samples (nano[MX1_PVA_LEU0], nano[MX1_PVA_LEU0.5], and nano[MX1_PVA_LEU1]).

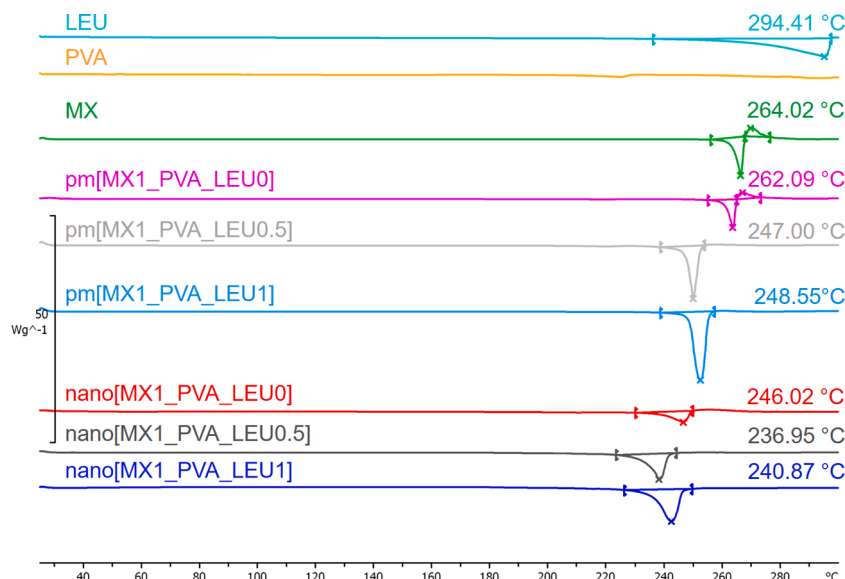


Fig. 5. DSC curves of the raw materials, (PVA, LEU, and MX), the physical mixtures (pm[MX1_PVA_LEU0], pm[MX1_PVA_LEU0.5], and pm[MX1_PVA_LEU1]), and the nano spray-dried samples (nano[MX1_PVA_LEU0], nano[MX1_PVA_LEU0.5], and nano[MX1_PVA_LEU1]).

3.7. Solubility test

The initial solubility of the raw MX was 0.502 ± 0.002 mg/ml in artificial lung media. As a result of the increased surface area of MX, the aqueous solubility of the nano spray-dried samples improved significantly in each case (Table 4 and Fig. 6). The reduction in the drug particle size in the nanometer range led to an increase in solubility,

which predicted better dissolution properties. Both are significant factors to enhance the bioavailability of poorly water-soluble drugs (Böhm and Müller, 1999). Amorphous pharmaceuticals are markedly more soluble, than crystalline forms. Our investigations also confirmed, even partially amorphous features can significantly increase the solubility (Hancock and Parks, 2000)

Table 4

Solubility results of the initial drug and the spray-dried products. Data are means \pm SD ($n = 3$ independent measurements).

Sample name	Solubility (mg/ml)
MX	0.905 \pm 0.005
nano[MX1_PVA_LEU0]	2.025 \pm 0.062
nano[MX1_PVA_LEU0.5]	1.501 \pm 0.002
nano[MX1_PVA_LEU1]	1.581 \pm 0.029

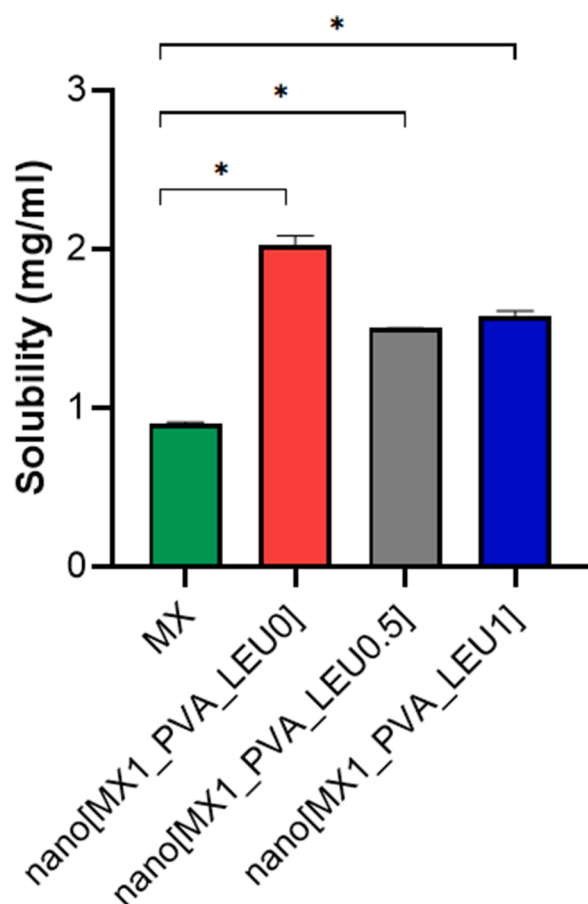


Fig. 6. Solubility results of the initial drug (MX), and the prepared samples (nano[MX1_PVA_LEU0], nano[MX1_PVA_LEU0.5], and nano[MX1_PVA_LEU1]). Data are means \pm SD ($n = 3$ independent measurements). Level of significance: * $p < 0.05$.

3.8. *In vitro* dissolution

The results of the dissolution test confirmed our predictions. The released amount of MX was the lowest for the samples containing raw materials because of the poor water solubility of MX (Fig. 7). In the first 5 min, $47.04 \pm 11.55\%$ of the MX was released from the nano[MX1_PVA_LEU0], $71.82 \pm 1.20\%$ from the nano[MX1_PVA_LEU0.5], and $71.31 \pm 6.91\%$ from the nano[MX1_PVA_LEU1]. All amount of the drug was released within an hour. The nano spray-dried samples showed significantly enhanced drug release compared to the physical mixtures (Fig. 8). These improvements could be related to the higher specific surface area, enhanced solubility, and the amorphization of the MX. The presence of PVA inhibited aggregation, and the use of LEU reduced the cohesion between the particles, therefore a larger amount of MX was liberated. The results of our formulations are advantageous in local therapy. The behavior of the particles gives enough time to release the nano-sized MX (Ruge et al., 2013). The sustained release can reduce the *in vivo* toxicity associated with the immediate burst release effect of the

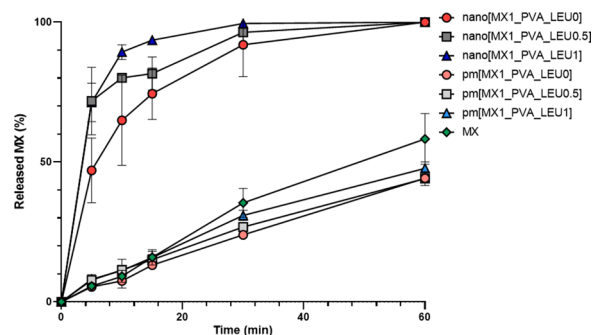


Fig. 7. *In vitro* dissolution results of the active ingredient (MX), the physical mixtures (pmMX1_PVA_LEU0, pmMX1_PVA_LEU0.5, and pmMX1_PVA_LEU1), and the prepared samples (nano[MX1_PVA_LEU0], nano[MX1_PVA_LEU0.5], and nano[MX1_PVA_LEU1]). Data are means \pm SD ($n = 3$ independent measurements).

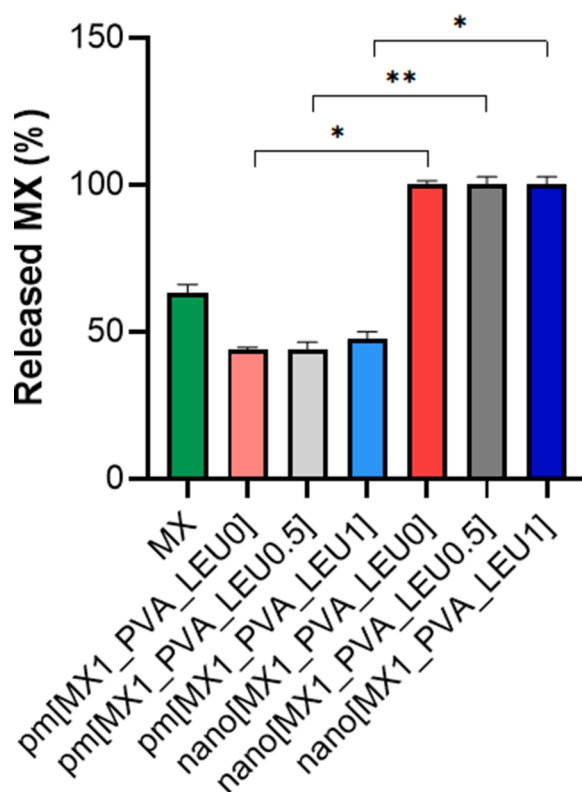


Fig. 8. *In vitro* dissolution results of the active ingredient (MX), the physical mixtures (pmMX1_PVA_LEU0, pmMX1_PVA_LEU0.5, and pmMX1_PVA_LEU1), compared to the spray-dried samples (nano[MX1_PVA_LEU0], nano[MX1_PVA_LEU0.5], and nano[MX1_PVA_LEU1]). Data are means \pm SD ($n = 3$ independent measurements). Level of significance: * $p < 0.05$, ** $p < 0.01$.

drug (Mukhtar et al., 2020).

3.9. *In vitro* permeability

During the permeability investigations, the high surface area provided by the nano-sized particles was the main factor affecting the rate of passive diffusion. Diffusion from the nano spray-dried samples reached higher values than from raw materials (Fig. 9). These results were a remarkably high amount ($85\text{--}110 \mu\text{g}/\text{cm}^2$) if we take into consideration that the total surface of the lung is around 100 m^2 (Das and Stewart, 2016). The products showed a significantly increased flux (J) and permeability coefficient (Kp) compared with the raw materials

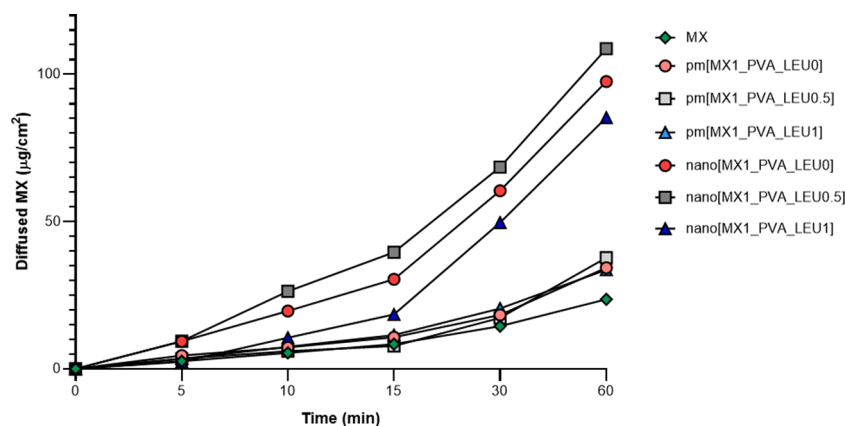


Fig. 9. *In vitro* permeability results of meloxicam (MX), the physical mixtures (pmMX1_PVA_LEU0, pmMX1_PVA_LEU0.5, and pmMX1_PVA_LEU1), and the prepared samples (nanoMX1_PVA_LEU0, nanoMX1_PVA_LEU0.5, and nanoMX1_PVA_LEU1). Data are means \pm SD ($n = 3$ independent measurements).

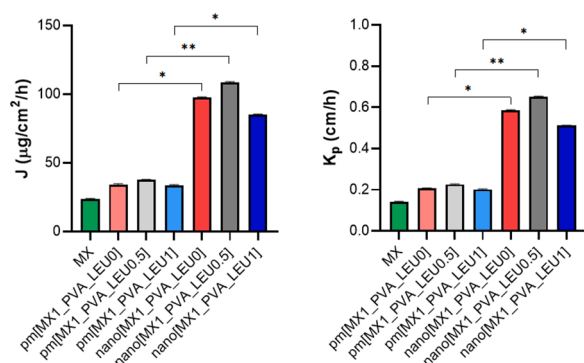


Fig. 10. The flux (J) and the permeability coefficient (K_p) results of meloxicam (MX), the physical mixtures (pmMX1_PVA_LEU0, pmMX1_PVA_LEU0.5, and pmMX1_PVA_LEU1), compared to the spray-dried samples (nanoMX1_PVA_LEU0, nanoMX1_PVA_LEU0.5, and nanoMX1_PVA_LEU1). Data are means \pm SD ($n = 3$ independent measurements). Level of significance: * $p < 0.05$, ** $p < 0.01$).

(Fig. 10). Therefore, an enhanced amount of API could get into the epithelium with the nano spray-dried formulations.

3.10. *In vitro* aerodynamic results

The distribution of the initial drug and the products were determined during the aerodynamic assessment. The deposition of the samples on different parts of the set was shown in Fig. 11. An insufficient quantity of raw MX reached the stages of the impactor. The drug remained in the capsule and a high amount was deposited on the induction port. The nanoMX1_LEU0 sample also mostly stayed in the capsule, but it reached the third and fourth stages. Those plates demonstrated the bronchial area. A small amount of the product reached the filter. The application of LEU improved the aerosolization of the products owing to the reduced cohesion between the particles. LEU-containing samples were liberated from the capsule in a larger amount, compared to the LEU-free products. Besides the deposition on the third and fourth stages, the largest amount reached the filter, which represented the alveolar region. The calculated *in vitro* aerodynamic results by Inhalytix™ software were presented in Table 5. The results of nanoMX1_LEU0.5 and nanoMX1_LEU1 are preferential. The MMAD values were between 1.2 and 1.3 μm . These extra-fine particles could target the deeper airways (Usmani et al., 2005). The samples had outstanding FPF results between 87 and 95%, which is

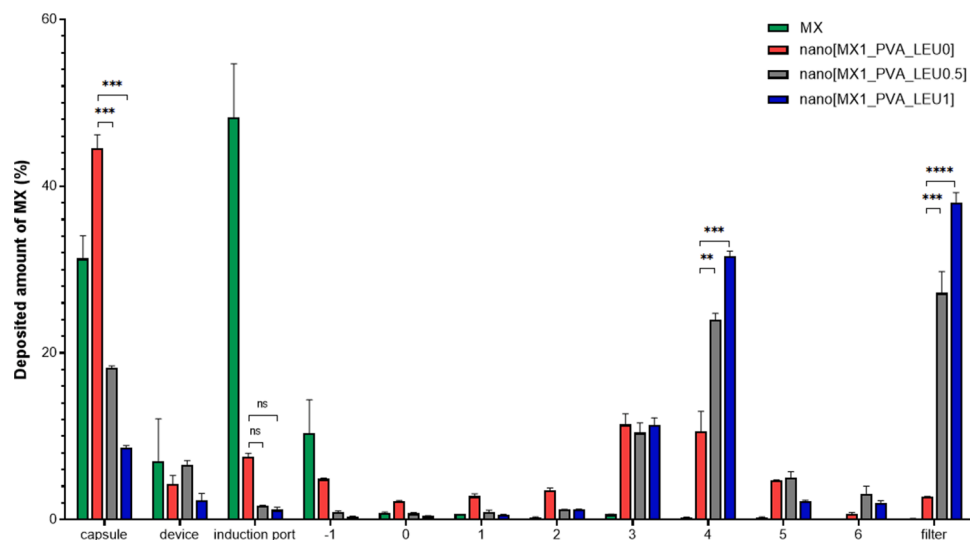


Fig. 11. *In vitro* aerodynamic distribution of the raw active ingredient and the gsamples at a flow rate of 60 l/min (MX, nano[MX1_PVA_LEU0], nano[MX1_PVA_LEU0.5], nano[MX1_PVA_LEU1]). Data are means \pm SD ($n = 3$ independent measurements). Level of significance: ** $p < 0.01$, *** $p < 0.001$, **** $p < 0.0001$).

Table 5

In vitro aerodynamic properties: mass median aerodynamic diameter (MMAD), fine particle fraction (FPF), and emitted fraction (EF) of the spray-dried samples at a flow 60 L/min.). Data are means \pm SD ($n = 3$ independent measurements).

Sample name	MMAD (μm)	FPF by size (%)	FPF by stage (%)	EF (%)
nano	2.151 \pm	62.62 \pm	65.93 \pm	30.50 \pm
[MX1_PVA_LEU0]	0.106	0.201	0.226	1.131
nano	1.344 \pm	86.16 \pm	86.99 \pm	58.77 \pm
[MX1_PVA_LEU0.5]	0.231	2.327	2.086	11.06
nano	1.265 \pm	94.45 \pm	94.91 \pm	80.90 \pm
[MX1_PVA_LEU1]	0.072	0.883	0.812	10.97

larger than the FPF values of the commercially available Breezhaler® formulations (Chapman et al., 2011). The emitted fraction (EF) was also higher in the LEU-containing products, indicating a weaker adhesive character between the powder and the gelatine capsule.

3.11. Aerodynamic particle counter investigation

The best formulation (nano[MX1_PVA_LEU1]) according to the ACI measurement was chosen for further aerodynamic characterization. Size results were determined based on the number, surface, and mass of the particles. The aerodynamic particles counter confirmed the particles' size between 1 and 1.4 μm (Table 6). These results also corresponded to the definition of extra-fine particles ($d < 2 \mu\text{m}$) (Hillyer et al., 2018), which was our initial goal.

3.12. Cytotoxicity measurement

Cytotoxicity studies represented that all the substances have a low cytotoxic effect in a concentration of 0.1 mg/ml. The cell viability was in order to MX, nano[MX1_PVA_LEU0], nano[MX1_PVA_LEU0.5], nano[MX1_PVA_LEU1] 91.97%, 90.32%, 80.38%, and 82.77%. The effect is not measurable at a concentration of 0.0125 mg/ml (Fig. 12). LPS had no cytotoxic effect at the highest concentration (data not shown). The results showed similarity to previous cytotoxicity effect investigations of MX (Ambrus et al., 2011; Chvatal et al., 2018; Varga et al., 2021). The formulations are safe for pulmonary administration. A549 cell lines exhibited similarities with type II. Alveolar epithelial cells, therefore the results are valid for imitating the circumstances of the small airways (Forbes, 2000).

3.13. Anti-inflammatory effect

Nano-sized MX solution inhibits IL-6 production on the translational level but not on the transcriptional level. LPS is a potent pro-inflammatory agent and increases IL-6 production in A549 cells (Cres-tani et al., 1994). LPS-treated cells showed significantly higher IL-6 relative expression compared to untreated cells (Fig. 13), however, neither MX solution nor nano-sized MX solutions inhibited the increase of IL-6 relative expression compared to LPS-treated cells (Fig. 14). Consequently, the IL-6 level was also checked via ELISA, and it was found that IL-6 expression increased significantly in LPS-treated cells

Table 6

The results of aerodynamic particle counting in case of nano[MX1_PVA_LEU1]. Data are means \pm SD ($n = 4$ independent measurements).

	Number particle size	Surface particle size	Mass particle size
Median (μm)	0.989 \pm 0.038	1.235 \pm 0.044	1.355 \pm 0.042
Mean (μm)	1.038 \pm 0.035	1.268 \pm 0.041	1.388 \pm 0.038
Geometric Mean (μm)	0.986 \pm 0.030	1.210 \pm 0.039	1.330 \pm 0.041
Mode (μm)	1.039 \pm 0.059	1.290 \pm 0.073	1.185 \pm 0.466
Geometric Standard Deviation	1.378 \pm 0.010	1.368 \pm 0.017	1.355 \pm 0.026

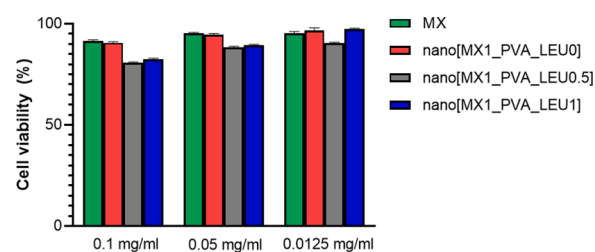


Fig. 12. Cell viability assay of substances on A549 cell line. A549 cells were treated with MX or nano[MX1_PVA_LEU0] or nano[MX1_PVA_LEU0.5] or nano[MX1_PVA_LEU1]. After an incubation period of 48 h, an MTT assay was performed to check the effect of the treatment on cell replication. Data are means \pm SD ($n = 3$ independent measurements).

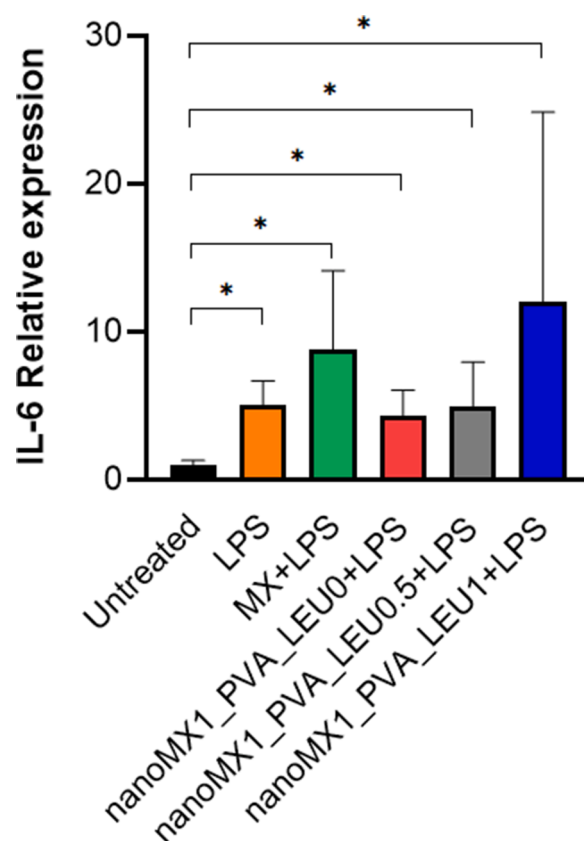


Fig. 13. Relative expression of IL-6. A549 cells were treated with 0.1 mg/ml nano[MX1_PVA_LEU0] and 5 $\mu\text{g/ml}$ LPS or 0.1 mg/ml nano[MX1_PVA_LEU0.5] and 5 $\mu\text{g/ml}$ LPS or 0.1 mg/ml nano[MX1_PVA_LEU1] and 5 $\mu\text{g/ml}$ LPS or 0.1 mg/ml MX and 5 $\mu\text{g/ml}$ LPS or 5 $\mu\text{g/ml}$ LPS or left untreated. After 48 h, RNA was extracted from the cells and gene expression was analyzed for IL-6 via RT-qPCR. Bars denote the mean and standard deviation of the expression level for triplicate measurements. Level of significance: * $p < 0.05$).

compared to untreated cells. Interestingly, MX solution and all of the nano-sized MX impeded IL-6 production (Fig. 10). IL-6 is a biomarker and a potential therapeutic target for patients infected with COVID-19. An increase in proinflammatory cytokine IL-6 concentration correlates with respiratory failure, poor outcomes, and mortality in SARS-CoV-2. The reduction of this and other cytokines at an early stage is promising in regards to moderating immune responses in acute SARS-CoV-2 infection (Copaescu et al., 2020).

4. Conclusion

The purpose of our research work was to develop a carrier-free dry

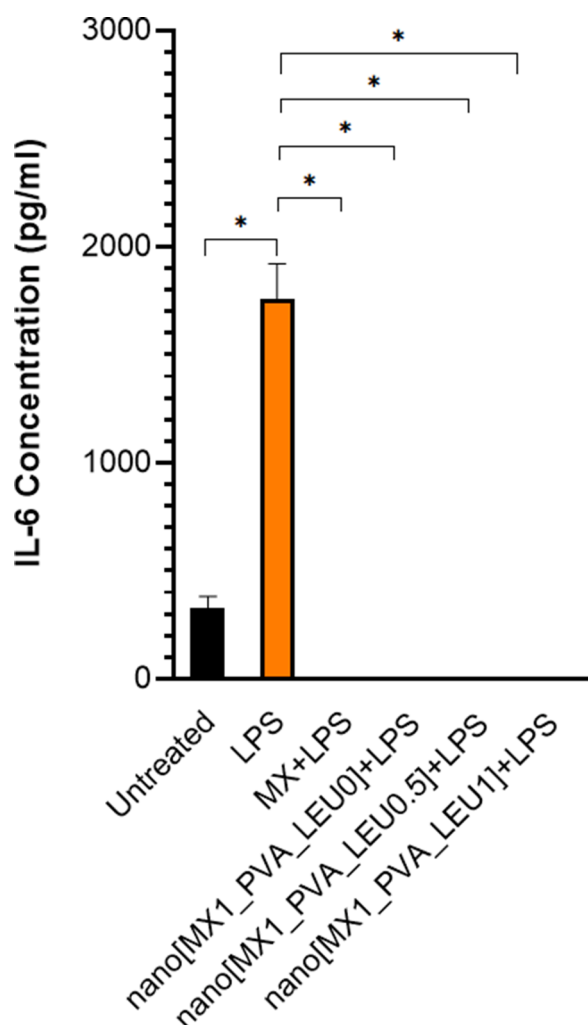


Fig. 14. Concentration of IL-6 in cell supernatants. Cells were treated with 0.1 mg/ml nano[MX1_PVA_LEU0] and 5 µg/ml LPS or 0.1 mg/ml nano[MX1_PVA_LEU0.5] and 5 µg/ml LPS or 0.1 mg/ml nano[MX1_PVA_LEU1] and 5 µg/ml LPS or 0.1 mg/ml MX and 5 µg/ml LPS or 5 µg/ml LPS or left untreated for 48 h. IL-6 concentration was measured via ELISA. Each bar denotes the mean standard deviation for triplicate measurements. Level of significance: * $p < 0.05$).

powder inhaler system combining the advantages of a nano-sized active ingredient and inhalable extra-fine powders. The particle size of the API was successfully reduced by wet milling and resulted in a nano-suspension ($d = 138$ nm). Nano spray-dried extra-fine inhalable powders were prepared from the nanosuspension. The final dry samples contained MX, stabilizing additive (PVA), and aerosolization adjuvant (LEU). The particles showed nearly spherical morphology and diameter between 1 and 1.5 µm. The particle size of the powders was complied with the definition of extra-fine particles. More than half of MX was detected in an amorphous state according to the XRPD measurements. The DSC investigations also demonstrated partial amorphization. Thanks to the particle size reduction, the solubility increased to 1.5–2.0 mg/ml. *In vitro* dissolution improved in the artificial lung medium compared to the initial material. *In vitro* permeability of the samples also got larger (85–110 µg/cm²/h). LEU-containing samples showed outstanding aerodynamic properties during the *in vitro* aerodynamic measurements: FPF around 90%, and MMAD around 1 µm. The aerodynamic particle counter method also proved the proper extra-fine particle size. The samples showed no cytotoxicity during the *in vitro* investigations and reduced the IL-6 concentration to zero. Based on the anti-inflammatory activities of meloxicam, the newly prepared

nanosized MX containing extra-fine microcomposites might be used in the local treatment of alveolar inflammation. Our formulating study makes good grounds for further investigations of the *in vivo* effectiveness and potential therapeutic use of MX in pulmonary therapy.

Funding

This research was funded by the University of Szeged Open Access Fund Grant No. 5674.

CRediT authorship contribution statement

Petra Party: Conceptualization, Methodology, Investigation, Data curation, Writing – review & editing, Visualization. **Dávid Kókai:** Methodology, Investigation, Data curation, Writing – review & editing. **Katalin Burián:** Supervision. **Attila Nagy:** Methodology, Investigation, Data curation, Writing – review & editing. **Béla Hopp:** Methodology, Investigation, Data curation, Writing – review & editing. **Rita Ambrus:** Conceptualization, Methodology, Investigation, Project administration, Supervision.

Declaration of Competing Interest

None.

Acknowledgments

Project no. TKP2021-EGA-32 has been implemented with the support provided by the Ministry of Innovation and Technology of Hungary from the National Research, Development and Innovation Fund, financed under the TKP2021-EGA funding scheme. This work was supported by the GINOP-2.3.2-15-2016-00036, Richter-GINOP-2.2.1-15-2016-00007, and by Gedeon Richter's Talentum Foundation, Gedeon Richter Ltd.

References

- Abadelah, M., Chrystyn, H., Larhib, H., 2019. Use of inspiratory profiles from patients with chronic obstructive pulmonary disease (COPD) to investigate drug delivery uniformity and aerodynamic dose emission of indacaterol from a capsule based dry powder inhaler. *Eur. J. Pharm. Sci.* 134, 138–144. <https://doi.org/10.1016/j.ejps.2019.04.018>.
- Alhajj, N., O'Reilly, N.J., Cathcart, H., 2021. Designing enhanced spray dried particles for inhalation: a review of the impact of excipients and processing parameters on particle properties. *Powder Technol.* 384, 313–331. <https://doi.org/10.1016/j.powtec.2021.02.031>.
- Ambrus, R., Pomázi, A., Réti-Nagy, K., Fenyvesi, F., Vecsernyés, M., Szabó-Révész, P., 2011. Cytotoxicity testing of carrier-based microcomposites for DPI application. *Pharmazie* 66, 549–550. <https://doi.org/10.1691/ph.2011.0378>.
- Arpagaus, C., Collenberg, A., Rütli, D., Assadpour, E., Jafari, S.M., 2018. Nano spray drying for encapsulation of pharmaceuticals. *Int. J. Pharm.* 546, 194–214. <https://doi.org/10.1016/j.ijpharm.2018.05.037>.
- Arpagaus, C., John, P., Collenberg, A., Rütli, D., 2017. 10 - Nanocapsules formation By Nano Spray drying. *Nanoencapsulation Technologies for the Food and Nutraceuical Industries*. Elsevier Inc. <https://doi.org/10.1016/B978-0-12-809436-5/00010-0>.
- Bartos, Csilla, 2016. Application of wet milling techniques to produce micronized and nanonized drug predispersion for the development of intranasal formulations. PhD Thesis.
- Bartos, Csaba, 2019. Optimization of a combined wet milling process to produce nanosuspension and its transformation into surfactant-free solid compositions to increase the product stability and drug bioavailability. PhD Thesis.
- Bartos, C., Jójárt-Laczkovich, O., Katona, G., Budai-Szűcs, M., Ambrus, R., Bocsik, A., Gróf, I., Deli, M.A., Szabó-Révész, P., 2018. Optimization of a combined wet milling process in order to produce poly(vinyl alcohol) stabilized nanosuspension. *Drug Des. Dev. Ther.* 12, 1567–1580. <https://doi.org/10.2147/DDDT.S159965>.
- Bartos, C., Szabó-Révész, P., Bartos, C., Katona, G., Jójárt-Laczkovich, O., Ambrus, R., 2016. The effect of an optimized wet milling technology on the crystallinity, morphology and dissolution properties of micro- and nanonized meloxicam. *Molecules* 21. <https://doi.org/10.3390/molecules21040507>.
- Benke, E., Farkas, Á., Szabó-Révész, P., Ambrus, R., 2020. Development of an innovative, carrier-based dry powder inhalation formulation containing spray-dried meloxicam potassium to improve the *in vitro* and *in silico* aerodynamic properties. *Pharmaceutics* 12, 1–19. <https://doi.org/10.3390/pharmaceutics12060535>.

- Böhm, Bernhard H.L., Müller, Rainer H., 1999. Lab-scale production unit design for nanosuspensions of sparingly soluble cytotoxic drugs. *Pharm. Sci. Technol. Today* 2 (8), 336–339. [https://doi.org/10.1016/S1461-5347\(99\)00177-7](https://doi.org/10.1016/S1461-5347(99)00177-7).
- Chapman, K.R., Fogarty, C.M., Peckitt, C., Lassen, C., Jadavay, D., Dederichs, J., Dalvi, M., Kramer, B., 2011. Delivery characteristics and patients' handling of two single-dose dry-powder inhalers used in COPD. *Int. J. COPD* 6, 353–363. <https://doi.org/10.2147/COPD.S18529>.
- Chen S, Jennifer, Alfajaro, Mia Madel, Wei, Jin, Chow, Ryan D., Filler, Renata B., Eisenbarth, Stephanie C., Wilen, Craig B., 2020. Cyclooxygenase-2 is induced by SARS-CoV-2 infection but does not affect viral entry or replication. *bioRxiv*. <https://doi.org/10.1101/2020.09.24.312769>.
- Chugh, H., Awasthi, A., Agarwal, Y., Gaur, R.K., Dhawan, G., Chandra, R., 2021. A comprehensive review on potential therapeutics interventions for COVID-19. *Eur. J. Pharmacol.* 890, 173741 <https://doi.org/10.1016/j.ejphar.2020.173741>.
- Chvatal, A., Alzhrani, R., Tiwari, A.K., Ambrus, R., Szabó-Révész, P., Boddu, S.H.S., 2018. Cytotoxicity of inhalable dry powders in A549 human lung cancer cell line. *Farmacia* 66, 172–175.
- Chvatal, A., Ambrus, R., Party, P., Katona, G., Jójárt-Laczovich, O., Szabó-Révész, P., Fattal, E., Tsapis, N., 2019. Formulation and comparison of spray dried non-porous and large porous particles containing meloxicam for pulmonary drug delivery. *Int. J. Pharm.* 559, 68–75. <https://doi.org/10.1016/j.ijpharm.2019.01.034>.
- Chvatal, A., Farkas, A., Balásházy, I., Szabó-Révész, P., Ambrus, R., 2017. Aerodynamic properties and *in silico* deposition of meloxicam potassium incorporated in a carrier-free DPI pulmonary system. *Int. J. Pharm.* 520, 70–78. <https://doi.org/10.1016/j.ijpharm.2017.01.070>.
- Copaescu, A., Smibert, O., Gibson, A., Phillips, E.J., Trubiano, J.A., 2020. The role of IL-6 and other mediators in the cytokine storm associated with SARS-CoV-2 infection. *J. Allergy Clin. Immunol.* 146, 518–534. <https://doi.org/10.1016/j.jaci.2020.07.001>.
- Crestani, B., Comillet, P., Dehoux, M., Rolland, C., Guenounou, M., Aubier, M., National, I., Sant, D., Medica, R., A., O.L.D.B., Bichat, F.X., 1994. Alveolar type II epithelial cells produce interleukin-6 *in vitro* and *in vivo*. Regulation by alveolar macrophage secretory products. *J. Clin. Invest.* 94, 731–740.
- Dailey, L.A., Kleemann, E., Wittmar, M., Gessler, T., Schmehl, T., Roberts, C., Seeger, W., Kissel, T., 2003. Surfactant-free, biodegradable nanoparticles for aerosol therapy based on the branched polyesters, DEAPA-PVAL-g-PLGA. *Pharm. Res.* 20, 2011–2020. <https://doi.org/10.1023/B:PHAM.0000008051.94834.10>.
- Das, S.C., Khadka, P., Shah, R., McGill, S., Smyth, H.D.C., 2021. Nanomedicine in Pulmonary delivery. Theory and Applications of Nonparenteral Nanomedicines. Elsevier Inc. <https://doi.org/10.1016/b978-0-12-820466-5.00014-4>.
- Das, S.C., Stewart, P.J., 2016. The influence of lung surfactant liquid crystalline nanostructures on respiratory drug delivery. *Int. J. Pharm.* 514, 465–474. <https://doi.org/10.1016/j.ijpharm.2016.06.029>.
- De Boer, A.H., Gjaltema, D., Hagedoorn, P., Frijlink, H.W., 2015. Can “extrafine” dry powder aerosols improve lung deposition? *Eur. J. Pharm. Biopharm.* 96, 143–151. <https://doi.org/10.1016/j.ejpb.2015.07.016>.
- Dubey, R., 2006. Impact of nanosuspension technology on drug discovery and development. *Drug Deliv. Technol.* 5, 67–71.
- European Pharmacopoeia 10.0, 2019. 2.9.3. Dissolution test for solid dosage forms. European Pharmacopoeia 10.0. EDQM Council of Europe.
- European Pharmacopoeia 10.0, 2019. 2.9.18. Preparations for inhalation: aerodynamic assessment of fine particles. European Pharmacopoeia 10.0. EDQM Council of Europe.
- Farkas, Á., Szipőcs, A., Horváth, A., Horváth, I., Gálffy, G., Varga, J., Galambos, K., Kugler, S., Nagy, A., Szalai, Z., 2019. Establishment of relationships between native and inhalation device specific spirometric parameters as a step towards patient tailored inhalation device selection. *Respir. Med.* 154, 133–140. <https://doi.org/10.1016/j.rmed.2019.06.021>.
- Forbes, Ben, 2000. Human airway epithelial cell lines for *in vitro* drug transport and metabolism studies. *Pharm. Sci. Technol. Today* 3 (1).
- Fröhlich, E., Mercuri, A., Wu, S., Salar-Behzadi, S., 2016. Measurements of deposition, lung surface area and lung fluid for simulation of inhaled compounds. *Front. Pharmacol.* 7, 1–10. <https://doi.org/10.3389/fphar.2016.00181>.
- Gieszinger, P., Kiss, T., Szabó-Révész, P., Ambrus, R., 2021. The development of an *in vitro* horizontal diffusion cell to monitor nasal powder penetration inline. *Pharmaceutics* 13. <https://doi.org/10.3390/pharmaceutics13060809>.
- Gliniński, J., Chavepeyer, G., Platten, J.K., 2000. Surface properties of aqueous solutions of l-leucine. *Biophys. Chem.* 84, 99–103. [https://doi.org/10.1016/S0301-4622\(99\)00150-7](https://doi.org/10.1016/S0301-4622(99)00150-7).
- Hancock, B.C., Parks, M., 2000. What is the true solubility advantage for amorphous pharmaceuticals? *Pharm. Res.* 17, 397–404. <https://doi.org/10.1023/A:1007516718048>.
- Hellemans, J., Mortier, G., De Paepe, A., Speleman, F., Vandesompele, J., 2008. qBase relative quantification framework and software for management and automated analysis of real-time quantitative PCR data. *Genome Biol.* 8 <https://doi.org/10.1186/gb-2007-8-2-r19>.
- Heyder, J., 2004. Deposition of inhaled particles in the human respiratory tract and consequences for regional targeting in respiratory drug delivery. *Proc. Am. Thorac. Soc.* 1, 315–320. <https://doi.org/10.1513/pats.200409-046TA>.
- Hillyer, E.V., Price, D.B., Chrystyn, H., Martin, R.J., Israel, E., van Aalderen, W.M.C., Papi, A., Usmani, O.S., Roche, N., 2018. Harmonizing the nomenclature for therapeutic aerosol particle size: a proposal. *J. Aerosol Med. Pulm. Drug Deliv.* 31, 111–113. <https://doi.org/10.1089/jamp.2017.1396>.
- ICH Harmonised Tripartite Guideline, 2005. Validation of Analytical Procedures: Text and Methodology. ICH Harmonised Tripartite Guideline.
- Iwabuchi, K., Yoshie, K., Kurakami, Y., Takahashi, K., Kato, Y., Morishima, T., 2020. Therapeutic potential of ciclesonide inhalation for COVID-19 pneumonia: report of three cases. *J. Infect. Chemother.* 26, 625–632. <https://doi.org/10.1016/j.jiac.2020.04.007>.
- Jetzer, M.W., Morrical, B.D., Schneider, M., Edge, S., Imanidis, G., 2018. Probing the particulate microstructure of the aerodynamic particle size distribution of dry powder inhaler combination products. *Int. J. Pharm.* 538, 30–39. <https://doi.org/10.1016/j.ijpharm.2017.12.046>.
- Keck, C.M., Müller, R.H., 2006. Drug nanocrystals of poorly soluble drugs produced by high pressure homogenisation. *Eur. J. Pharm. Biopharm.* 62, 3–16. <https://doi.org/10.1016/j.ejpb.2005.05.009>.
- Li, Q., Rudolph, V., Weigl, B., Earl, A., 2004. Interparticle van der Waals force in powder flowability and compactibility. *Int. J. Pharm.* 280, 77–93. <https://doi.org/10.1016/j.ijpharm.2004.05.001>.
- Li, X., Anton, N., Arpagaus, C., Belleiteix, F., Vandamme, T.F., 2010. Nanoparticles by spray drying using innovative new technology: the Büchi nano spray dryer B-90. *J. Control. Release* 147, 304–310. <https://doi.org/10.1016/j.jconrel.2010.07.113>.
- Madas, B.G., Füri, P., Farkas, Á., Nagy, A., Czitrovsky, K., Balásházy, I., Schay, G.G., Horváth, A., 2020. Deposition distribution of the new coronavirus (SARS-CoV-2) in the human airways upon exposure to cough-generated droplets and aerosol particles. *Sci. Rep.* 10, 1–8. <https://doi.org/10.1038/s41598-020-79985-6>.
- Malamataris, M., Charisi, A., Malamataris, S., Kachrimanis, K., Nikolakakis, I., 2020. Spray drying for the preparation of nanoparticle-based dry formulations as dry powders for inhalation. *Processes* 8. <https://doi.org/10.3390/pr8070788>.
- Mangal, S., Meiser, F., Tan, G., Gagenbach, T., Denman, J., Rowles, M.R., Larson, I., Morton, D.A.V., 2015. Relationship between surface concentration of l-leucine and bulk powder properties in spray dried formulations. *Eur. J. Pharm. Biopharm.* 1–10. <https://doi.org/10.1016/j.ejpb.2015.04.035>.
- Mukhtar, M., Pallagi, E., Csóka, I., Benke, E., Farkas, Á., Zeeshan, M., Burián, K., Kóki, D., Ambrus, R., 2020. Aerodynamic properties and *in silico* deposition of isoniazid loaded chitosan/thiolated chitosan and hyaluronic acid hybrid nanoplex DPIs as a potential TB treatment. *Int. J. Biol. Macromol.* 165, 3007–3019. <https://doi.org/10.1016/j.ijbiomac.2020.10.192>.
- Muralidharan, P., Malapit, M., Mallory, E., Hayes, D., Mansour, H.M., 2015. Inhalable nanoparticle powders for respiratory delivery. *Nanomed. Nanotechnol. Biol. Med.* 11, 1189–1199. <https://doi.org/10.1016/j.nano.2015.01.007>.
- Ong, S.W.X., Tan, W.Y.T., Chan, Y.H., Fong, S.W., Renia, L., Ng, L.F.P., Leo, Y.S., Lye, D. C., Young, B.E., 2020. Safety and potential efficacy of cyclooxygenase-2 inhibitors in coronavirus disease 2019. *Clin. Transl. Immunol.* 9, 1–9. <https://doi.org/10.1002/cti2.1159>.
- Pallagi, E., Karimi, K., Ambrus, R., Szabó-Révész, P., Csóka, I., 2016. New aspects of developing a dry powder inhalation formulation applying the quality-by-design approach. *Int. J. Pharm.* 511, 151–160. <https://doi.org/10.1016/j.ijpharm.2016.07.003>.
- Parlati, C., 2008. Respirable Microparticles of Aminoglycoside Antibiotics for Pulmonary Administration. University of Parma.
- Party, P., Bartos, C., Farkas, Á., Szabó-Révész, P., Ambrus, R., 2021. Formulation and *in vitro* and *in silico* characterization of “Nano-in-Micro” dry powder inhalers containing meloxicam. *Pharmaceutics* 13, 1–18. <https://doi.org/10.3390/pharmaceutics13020211>.
- Pomázi, Anita, 2013. Meloxikám tartalmú hordozó-alapú porinhalációs rendszer fejlesztése és vizsgálata lokális hatás elérése céljából. PhD Thesis.
- Pomázi, A., Buttini, F., Ambrus, R., Colombo, P., Szabó-Révész, P., 2013. Effect of polymers for aerolization properties of mannitol-based microcomposites containing meloxicam. *Eur. Polym. J.* 49, 2518–2527. <https://doi.org/10.1016/j.eurpolymj.2013.03.017>.
- Potocnik, J., 2011. Commission recommendation of 18 October 2011 on the definition of nanomaterial. *Off. J. Eur. Union.* <https://doi.org/10.7748/ns.24.26.6.s4>.
- Powers, K.W., Palazuelos, M., Moudgil, B.M., Roberts, S.M., 2007. Characterization of the size, shape, and state of dispersion of nanoparticles for toxicological studies. *Nanotoxicology* 1, 42–51. <https://doi.org/10.1080/17435390701314902>.
- Prasad, Ayya Rajendra, Thiresha, Bannaravuri, 2018. UV-spectrophotometric method development and validation for the determination of lornoxicam in microspores. *Int. J. Appl. Pharm.* 10 (1), 74–78. <https://doi.org/10.22159/ijap.2018v10i1.22357>.
- Radivojev, S., Zellnitz, S., Paudel, A., Fröhlich, E., 2019. Searching for physiologically relevant *in vitro* dissolution techniques for orally inhaled drugs. *Int. J. Pharm.* 556, 45–56. <https://doi.org/10.1016/j.ijpharm.2018.11.072>.
- R.H. Muller, R. Becker, B. Kruss, K. Peters, Berlin, all of, Germany, 1999. Pharmaceutical nanosuspensions for medicament administrations systems with increased saturation solubility and rate of solution. United States Pat. 1–30.
- Riley, T., Christopher, D., Arp, J., Casazza, A., Colombani, A., Cooper, A., Dey, M., Maas, J., Mitchell, J., Reiners, M., Sigari, N., Tougas, T., Lyapustina, S., 2012. Challenges with developing *in vitro* dissolution tests for orally inhaled products (OIPs). *AAAPS PharmSciTech* 13, 978–989. <https://doi.org/10.1208/s12249-012-9822-3>.
- Ruge, C.C., Kirch, J., Lehr, C.M., 2013. Pulmonary drug delivery: from generating aerosols to overcoming biological barriers-therapeutic possibilities and technological challenges. *Lancet Respir. Med.* 1, 402–413. [https://doi.org/10.1016/S2213-2600\(13\)70072-9](https://doi.org/10.1016/S2213-2600(13)70072-9).
- Salopek, Branko, Krasic, Dragan, Filipovic, Suzana, 1992. Measurement and application of zeta-potential. *Rudarsko-geolosko-naftni zbornik* 4, 147–151.
- Sarcinelli, M.A., Martins da Silva, T., Artico Silva, A.D., Ferreira de Carvalho Patricio, B., Mendes de Paiva, F.C., Santos de Lima, R., Leal da Silva, M., Antunes Rocha, H.V., 2021. The pulmonary route as a way to drug repositioning in COVID-19 therapy. *J. Drug Deliv. Sci. Technol.* 63 <https://doi.org/10.1016/j.jddst.2021.102430>.

- Scherließ, R., Bock, S., Bungert, N., Neustock, A., Valentin, L., 2022. Particle engineering in dry powders for inhalation. *Eur. J. Pharm. Sci.* 172 <https://doi.org/10.1016/j.ejps.2022.106158>.
- Sou, T., Kaminskas, L.M., Nguyen, T.H., Carlberg, R., McIntosh, M.P., Morton, D.A.V., 2013. The effect of amino acid excipients on morphology and solid-state properties of multi-component spray-dried formulations for pulmonary delivery of biomacromolecules. *Eur. J. Pharm. Biopharm.* 83, 234–243. <https://doi.org/10.1016/j.ejpb.2012.10.015>.
- Sun, D., 2020. Remdesivir for treatment of COVID-19: combination of pulmonary and IV administration may offer additional benefit. *AAPS J.* 22 <https://doi.org/10.1208/s12248-020-00459-8>.
- Tay, J.Y.S., Liew, C.V., Heng, P.W.S., 2018. Dissolution of fine particle fraction from truncated Anderson cascade impactor with an enhancer cell. *Int. J. Pharm.* 545, 45–50. <https://doi.org/10.1016/j.ijpharm.2018.04.048>.
- Thorley, A.J., Tetley, T.D., 2013. New perspectives in nanomedicine. *Pharmacol. Ther.* <https://doi.org/10.1016/j.pharmthera.2013.06.008>.
- Tse, J.Y., Kadota, K., Imakubo, T., Uchiyama, H., Tozuka, Y., 2021a. Enhancement of the extra-fine particle fraction of levofloxacin embedded in excipient matrix formulations for dry powder inhaler using response surface methodology. *Eur. J. Pharm. Sci.* 156, 105600 <https://doi.org/10.1016/j.ejps.2020.105600>.
- Tse, J.Y., Koike, A., Kadota, K., Uchiyama, H., Fujimori, K., Tozuka, Y., 2021b. Porous particles and novel carrier particles with enhanced penetration for efficient pulmonary delivery of antitubercular drugs. *Eur. J. Pharm. Biopharm.* 167, 116–126. <https://doi.org/10.1016/j.ejpb.2021.07.017>.
- Usmani, O.S., Biddiscombe, M.F., Barnes, P.J., 2005. Regional lung deposition and bronchodilator response as a function of β_2 -agonist particle size. *Am. J. Respir. Crit. Care Med.* 172, 1497–1504. <https://doi.org/10.1164/rccm.200410-1414OC>.
- van Eerdenbrugh, B., Vermant, J., Martens, J.A., Froyen, L., van Humbeeck, J., Augustijns, P., Van Den Mooter, G., 2008. A screening study of surface stabilization during the production of drug nanocrystals. *J. Pharm. Sci.* 98, 2091–2103. <https://doi.org/10.1002/jps>.
- Varga, P., Ambrus, R., Szabó-Révész, P., Kókai, D., Burián, K., Bella, Z., Fenyvesi, F., Bartos, C., 2021. Physico-chemical, *in vitro* and *ex vivo* characterization of meloxicam potassium-cyclodextrin nanospheres. *Pharmaceutics* 13, 1–14. <https://doi.org/10.3390/pharmaceutics13111883>.
- Vargaftik, N.B., Volkov, B.N., Voljak, L.D., 1983. International tables of the surface tension of water. *J. Phys. Chem. Ref. Data.* <https://doi.org/10.1063/1.555688>.
- Virók, D.P., Eszik, I., Mosolygó, T., Önder, K., Endrész, V., Burián, K., 2017. A direct quantitative PCR-based measurement of herpes simplex virus susceptibility to antiviral drugs and neutralizing antibodies. *J. Virol. Methods* 242, 46–52. <https://doi.org/10.1016/j.jviromet.2017.01.007>.
- <https://pubchem.ncbi.nlm.nih.gov/compound/Meloxicam>. (Accessed 27 June 2022).
- <https://go.drugbank.com/drugs/DB00814>. (Accessed 27 June 2022).

III.



Article

Investigation of Physico-Chemical Stability and Aerodynamic Properties of Novel “Nano-in-Micro” Structured Dry Powder Inhaler System

Petra Party and Rita Ambrus *

Faculty of Pharmacy, Institute of Pharmaceutical Technology and Regulatory Affairs, University of Szeged, Eötvös Street 6, 6720 Szeged, Hungary; party.petra@szte.hu

* Correspondence: ambrus.rita@szte.hu; Tel.: +36-62-545-572

Abstract: Pulmonary drug transport has numerous benefits. Large surface areas for absorption and limited drug degradation of the gastrointestinal system are provided through the respiratory tract. The administration is painless and easy for the patient. Due to their better stability when compared to liquid formulations, powders have gained popularity among pulmonary formulations. In the pharmaceutical sector, quality assurance and product stability have drawn a lot of attention. Due to this, it was decided to perform a long-term stability study on a previously developed, nanosized dry powder inhaler (DPI) formulation that contained meloxicam. Wet milling was implemented to reduce the particle size, and nano spray-drying was used to produce the extra-fine inhalable particles. The particle diameter was determined using dynamic light scattering and laser diffraction. Scanning electron microscopy was utilized to describe the morphology. X-ray powder diffraction and differential scanning calorimetry were applied to determine the crystallinity. In an artificial lung medium, the in vitro dissolution was studied. The Andersen Cascade Impactor was used to investigate the in vitro aerodynamic characteristics. The stability test results demonstrated that the DPI formulation maintained its essential qualities after 6 and 12 months of storage. Consequently, the product might be promising for further studies and development.

Keywords: nanotechnology; pulmonary delivery; dry powder inhaler; meloxicam; stability test



Citation: Party, P.; Ambrus, R. Investigation of Physico-Chemical Stability and Aerodynamic Properties of Novel “Nano-in-Micro” Structured Dry Powder Inhaler System. *Micromachines* **2023**, *14*, 1348. <https://doi.org/10.3390/mi14071348>

Academic Editors: Aiqun Liu, Guangsha Shi and Tianyu Yan

Received: 26 April 2023

Revised: 22 June 2023

Accepted: 28 June 2023

Published: 30 June 2023



Copyright: © 2023 by the authors. Licensee MDPI, Basel, Switzerland. This article is an open access article distributed under the terms and conditions of the Creative Commons Attribution (CC BY) license (<https://creativecommons.org/licenses/by/4.0/>).

1. Introduction

One of the first methods of medication administration identified is respiratory drug delivery [1]. The beneficial characteristics of the lung enable the administration of larger drug concentrations to the airways for enhanced efficacy and to limit adverse effects. These advantages include avoiding first-pass metabolism and enzymatic inactivation [2]. The administration is non-invasive, which enhances patient compliance. One of the most widely used methods for treating local respiratory conditions, such as chronic obstructive pulmonary disease, asthma, pneumonia, and chronic pulmonary infections, is pulmonary drug delivery [3,4].

Nebulizers, metered dosage inhalers (MDIs), soft mist inhalers (SMIs), and dry powder inhalers (DPIs) are the most frequently utilized pulmonary medication delivery devices. MDIs have a larger carbon footprint than DPIs. DPIs are also cost-effective compared to MDIs [5]. Hydrofluorocarbon propellants are used in MDIs, which are greenhouse gases that persist in the atmosphere for years. Since DPIs are absent of these propellants and produce 20 g CO₂ equivalent per dose compared to 500 g CO₂ equivalent for MDIs, they have lower greenhouse gas emission potential [6]. The inhalation helps the active ingredient to enter the respiratory tract. DPIs are also portable tools that make it simple for the patient to administer the formulation. On the other hand, education is essential for the correct usage of the products. Due to their solid form, DPIs have outstanding stability and do not require cold chain storage [4,7].

There is an increasing variety of commercially available dry powder inhalers, and these vary significantly in terms of their design, technical features, and other specific features. Some inhalers include properties that make them likely to be effective for a variety of patients, which may offer a certain level of ease for healthcare providers. However, there are numerous factors to take into consideration when choosing the most effective inhaler for individuals with lung disorders. In addition to the type of drug contained in the inhaler, factors such as the degree of clinical evidence supporting its efficacy and safety, doctor and patient preferences, technical features of the various inhalers, and the delivery and deposition of the fine particle dose to the lungs may be crucial to assisting the physician in choosing the best device for each patient in order to optimize their treatment [8].

Carrier-based and carrier-free systems are the two main categories into which DPIs can be categorized. Applying conventional carrier-based DPIs, drug deposition in the respiratory area is insufficient. The active ingredients in these systems are attached to the surface of a carrier, which is typically lactose. Optimizing the aerosolization of the products is essential since the potential of powders is the appropriate dispersion and deposition in the airways. To improve the therapeutic effect, novel carrier-free DPIs have been developed. In that case, a complex powder is formulated by combining the active pharmaceutical ingredient (API) with appropriate excipients [9].

The upper respiratory tract, which includes the mouth, larynx, and pharynx, and the lower respiratory tract, which includes the trachea, bronchi, and lungs, are the two primary divisions of the respiratory system. When moving from the trachea to the distal airways, the diameters of the airways decrease as they approach the lower region and alveoli of the lung, and their number simultaneously rises [1]. Generally, the lower part is the target for orally inhaled medications. Unwanted particle deposition in the upper area might have regional negative effects, such as localized discomfort, coughing, dysphonia, and infections [10]. Controlling the theoretical aerodynamic diameter at 1–5 μm is required for the successful transport of particles via the pulmonary route to the desired area in the lungs [11]. In the lower parts, regional deposition is also critical for effective drug delivery [10]. Extra-fine particles (1–2 μm) are suitable for reaching the deeper areas because they deposit significantly more in the smaller peripheral lung structures than in the upper regions [12,13].

Recently, attention has been focused on the inhalable, poorly water-soluble drugs, such as antibiotics and anti-inflammatory and antifungal agents, which would acquire elevated local concentration for improved therapeutic effectiveness. However, a poorly water-soluble drug cannot be efficiently absorbed in the lung since it dissolves slowly in the limited volume of the lining fluid. The undissolved particles may be removed through alveolar macrophage uptake and mucociliary clearance, which leads to a compromised therapeutic effect. Additionally, leftover particles that remain for a long time on the surface of the lung epithelium may cause lung irritation and inflammation [14].

The development of nano-embedded microparticles for pulmonary application has drawn a growing amount of attention in recent years [15]. The systems enable the combination of nano- and microparticle benefits. Nanoparticles have advantages for getting through biological barriers [16]. The overall dosage required is reduced due to the enhanced drug transport in mucus and biofilms [17]. Problems with pulmonary drug administration may be resolved by using nanoparticle delivery methods [18]. The application of innovative and effective products that contain nanoparticles may enhance various therapies [19,20]. Therefore, DPI formulation with enhanced dissolution and improved absorption is urgently required for the pulmonary delivery of water-insoluble drugs.

One of the most important factors for guaranteeing the safety and efficacy of pharmaceutical medicines is stability [21]. Drug nanoparticle stability issues, such as crystal formation, sedimentation, and agglomeration, may occur during production, storage, transportation, and application [22]. In general, liquid formulations are less stable than solid dosage forms. However, the potential of aggregation should be taken into consideration in the case of solid forms while using nanosized API. For efficient therapy, it is necessary

to maintain the quality-influencing properties of the products. Proper attention should be given to drug nanocrystal stability difficulties during the development of pharmaceutical products [23].

In our previous studies, wet milling and nano spray drying were used to prepare a carrier-free DPI product consisting of nanosized meloxicam (MX) [24]. The “nano-in-micro” DPI can target the smaller airways with the extra-fine particles ($<2\ \mu\text{m}$) and increase the water solubility of the drug. The alveolar section of the lung is where the nano-sized active ingredient may exert its anti-inflammatory effect; therefore, our goal is to deliver a high percentage of the extra-fine particles there. The combined preparation method can create particles under $2\ \mu\text{m}$ with narrow size distribution. The previous investigations of the product revealed that the nanosized MX particles are partially amorphized, improving drug release. In addition, the product demonstrated significant drug deposition in the lung in vitro. The present study focused on the long-term stability of the developed DPI powder that contains nanosized MX. A significant challenge related to the development of formulations in DPIs is their stability. Manufacturing processes, pharmaceutical engineering techniques, and storage conditions can significantly impact the physical and aerosol stability of inhalable particles. The physical stability of the DPIs is frequently overlooked in the literature even though they are critical to the quality and performance of the inhalation powders [4]. As a result of the extensive investigation, we could offer the MX a new, innovative therapeutic application in the management of severe lung inflammation.

2. Materials and Methods

2.1. Materials

Meloxicam (MX) (Egis Pharmaceuticals PLC., Budapest, Hungary) was used as the active ingredient. MX is a non-steroidal anti-inflammatory medication (NSAID) that selectively inhibits cyclooxygenase-2 (COX-2). MX is commercially available only in oral, intravenous, and intralesional delivery routes. In human therapy, osteoarthritis, and arthritis are currently the principal indications of MX [25]. However, COX-2 inhibitors could be used to treat pulmonary inflammation, such as SARS-CoV-2 infection, which induces the COX-2 expression and may help to control the lung inflammation and damage seen in COVID-19 patients [26–28]. It could be advantageous to improve and maintain the condition of patients with cystic fibrosis (CF), chronic obstructive pulmonary disease (COPD), and non-small-cell lung cancer (NSCLC) [29–32]. The pulmonary suitable additives were poly-vinyl-alcohol 4–98 (PVA), (Aldrich Chemistry, Darmstadt, Germany) and L-leucine (LEU), (AppliChem GmbH, Darmstadt, Germany). The list of potential excipients is limited to materials that are biocompatible or endogenous to the lung and can effectively be eliminated [33].

2.2. Preparation Method

A two-step preparation method was used. Firstly, the nanosuspension was prepared by wet-milling technology. The final micro-sized powders were obtained by spray drying the diluted suspension.

2.2.1. Wet Milling

Milling is a common scalable method used in the pharmaceutical industry for particle size reduction to improve the solubility and subsequently the bioavailability of poorly water-soluble APIs [34–36]. During wet milling, the drug is suspended in a liquid medium, such as surfactants or/and polymers, to stabilize the drug particles [37]. In this work, PVA was applied to maintain the stability and uniqueness of the MX particles. The MX particles are coated with PVA, which inhibits the drug particles from aggregating together during the size reduction process [38,39]. MX containing nanosuspension was prepared as follows: 2 g MX and 8 g of 2.5% (w/w%) PVA solution were added in a planetary ball mill (Retsch PM 100; Retsch GmbH, Haan, Germany). The following conditions were present: 20 g of zirconium-dioxide beads ($d = 0.3\ \text{mm}$), 500 rpm, 60 min. Due to the increased energy

supply during wet milling, the development of local amorphous regions is conceivable and thus could alter the surface properties. This metastable state may change during handling and over storage time, and it could induce re-crystallization of these amorphous regions and particle size changes post-production [40].

2.2.2. Spray Drying

Spray drying is a particle-engineering technique that is used to produce respirable powders for drug delivery to the deep lung [41], which is utilized in both laboratory and industrial environments. Compared to other popular drying methods, such as lyophilization, it attracted a lot of interest since it is less expensive, requires less time, and does not involve freezing, which is a high energy-consuming process [42]. One notable advantage of the nano spray dryer is its capacity to produce ultra-fine dry powder forms for a variety of materials, including heat-sensitive ones, with minimal damage. The advantages of a spray-dried powder include easy handling and storage as well as enhanced resistance to various environmental factors (such as light, oxidation, and temperature) [43]. LEU was incorporated into the MX nanosuspension to produce the dry powder. To enhance the aerosol characteristics, the administered dosage, and the overall efficacy of the product, LEU is frequently utilized as a dispersibility enhancer to minimize interparticle cohesion in DPIs. On the surface of spray-dried particles, LEU develops a crystalline layer, which reduces surface energy while enhancing surface rugosity [41]. The LEU enrichment at the surface of the particles can result in moisture protection, therefore improving their physical storage stability [44]. The inhalable powder was made by a Büchi Nano Spray Dryer (Büchi, Flawil, Switzerland) with a small nebulizer. Our preliminary research determined the following settings for the nano spray-drying process: inlet temperature of 80 °C, aspirator capacity of 100%, airflow rate of 120 mL/min, and pump rate of 20%. During the rapid drying of the method, the development of an amorphous form is possible and can lead to recrystallization. In the case of small-molecule drugs, such as MX, they tend to crystallize during spray drying [45].

2.2.3. Physical Mixture Preparation

A physical mixture (PM) was created from the raw materials. The composition of the PM was similar to the spray-dried sample. During the experiments, the different qualities of the spray-dried samples were compared to the PM. Table 1 shows the compositions of the physical mixture and the final formulation.

Table 1. The composition of the physical mixture and the spray-dried sample.

Sample	MX (g)	PVA (g)	LEU (g)
pm_MX_PVA_LEU	2.00	0.45	2.00
nano_MX_PVA_LEU	2.00	0.45	2.00

2.3. Stability Test

Stability tests were performed at 25 ± 2 °C with $50 \pm 5\%$ relative humidity to imitate room conditions in a desiccator. Throughout the testing period, samples were stored in a closed glass jar. Samples were taken and measured after 1 day, 6 months, and 12 months [46,47].

2.4. Particle Size and Morphology Characterization

2.4.1. Laser Diffraction

The particle sizes, the particle size distributions, and the specific surface areas of the samples were determined using laser diffraction (Malvern Mastersizer Scirocco 2000, Malvern Instruments Ltd., Worcestershire, UK). The refractive index of MX was adjusted to 1.720. MX was given a new refractive index of 1.720. The dry dispersion equipment was used to examine the nano spray-dried particles. The 3.0 bar of dispersion air pressure and 75% vibration feed were employed. Each sample was measured in triplicate. The

particle size distribution (PSD) was described using the values $D[0.1]$ (10% of the volume distribution is below this value), $D[0.5]$ (50% of the volume distribution is below this value), and $D[0.9]$ (90% of the volume distribution is below this value) (Equation (1)). Span values were indicated in the particle size distribution, the larger the span value, the broader the spread. The specific surface area (SSA) was calculated using the PSD data. The computations were performed assuming the particles were spherical.

$$\text{Span} = \frac{D[0.9] - D[0.1]}{D[0.5]}, \quad (1)$$

2.4.2. Dynamic Light Scattering (DLS)

Malvern Zetasizer Nano ZS (Malvern Instruments, Worcestershire, UK) was applied to analyze the average hydrodynamic diameter (d), polydispersity index (PDI), and zeta potential (ζ pot.) using DLS. The powders were dispersed in purified water and measured in folded capillary cells at 25 °C. A refractive index of 1.720 was assigned to MX. Each investigation was performed three times.

2.4.3. Scanning Electron Microscopy (SEM)

The shape and size of the particles were analyzed using SEM (Hitachi S4700; Hitachi Ltd., Tokyo, Japan) operating at a 10 kV voltage. Using a sputter coater (Bio-Rad SC502; VG Microtech, Uckfield, UK) and a 2.0 kV at 10 mA electric potential for 10 min, the samples received a 90-s gold-palladium coating. The range of air pressure was 1.3 to 13.0 mPa. ImageJ, a free and open-source image analyzer was used to perform the particle diameter analysis. (<https://imagej.nih.gov/ij/index.html>, accessed on 22 June 2023.).

2.5. Structural Investigation

2.5.1. Differential Scanning Calorimetry (DSC)

Thermal analyses of samples were performed using a Mettler Toledo TGA/DSC thermal analysis equipment (Mettler-Toledo GmbH, Greifensee, Switzerland). The DSC measurements were performed by analyzing 3–5 mg of samples heated to temperatures between 25 and 300 °C at a rate of 10 °C/min while maintaining a steady flow of argon at a rate of 10 L/h. The STAR^e program was used to analyze the data (Mettler-Toledo GmbH, Greifensee, Switzerland). The ratio normalized integrals were used to calculate the crystallinity indexes with the PM samples being considered as 100%.

2.5.2. X-ray Powder Diffraction (XRPD)

The crystal structure and level of crystallinity were measured using XRPD. Based on the X-ray diffraction concept, a sharp peak is seen when X-rays diffract from atoms that repeatedly appear in the same position within the unit cell (i.e., a crystalline structure). The BRUKER D8 advance X-ray powder diffractometer (Bruker AXS GmbH, Karlsruhe, Germany) and VNTEC-1 detector (Bruker AXS GmbH, Karlsruhe, Germany) were used to perform the XRPD measurement. The powder samples were placed on a slide of flat quartz glass with an etched square and measured. At 40 kV and 40 mA, samples were scanned. With a step time of 0.1 s and a step size of 0.007°, the angular range was 3–40°. The DIFFRACplus EVA program was used for all manipulations, including K2 stripping, background removal, and smoothing of the area under the diffractogram peaks. Based on Equation (2), the values for the crystallinity index (X_c) were determined. The PM sample was considered 100% crystalline. A symbolizes the area under the curve:

$$X_c = \frac{A_{\text{crystalline}}}{A_{\text{crystalline}} + A_{\text{amorphous}}} \times 100 \quad (2)$$

2.6. In Vitro Drug Release Study

Currently, there are no standardized methodologies or regulatory criteria to evaluate in vitro dissolution tests of inhaled powders [48]. Using a modified paddle method, the rate of drug release of powders was examined (Hanson SR8 Plus, Teledyne Hanson Research, Chatsworth, CA, USA). The analysis was performed under pulmonary circumstances (37 °C and pH: 7.4). The following components were included in 50 mL of artificial lung medium: 2.27 g/L NaHCO₃, 0.68 g/L NaCl, 0.1391 g/L NaH₂PO₄, 0.02 g/L CaCl₂, and 5.56 mL/L 0.1 M H₂SO₄ and 0.37 g/L glycine [49]. The sample preparation was completed after 5, 10, 15, 30, 45, and 60 min. The paddle rotated at 100 rotations per minute. To maintain the permanent volume constant, lung fluid was simultaneously added at every point of sampling to replace 5 mL of the sample. For filtering, cellulose ester membranes with 0.22 µm pore sizes were employed. Following filtration, spectrophotometry at 362 nm (Unicam UV/VIS Spectrophotometer, Cambridge, UK) was used to determine the drug content of the aliquots. The experiments were performed in three sets.

2.7. In Vitro Aerodynamic Performance

Using an Andersen Cascade Impactor (ACI, Apparatus D, Copley Scientific Ltd., Nottingham, UK), (Figure 1), which is authorized by the European Pharmacopoeia [50], it was determined how effectively the formulations in vitro aerosolized. The inhalation flow rate was set to 60 l/min (high-capacity pump model HCP5, critical flow controller model TPK, Copley Scientific Ltd., Nottingham, UK). To calculate the actual flow rate, a mass flow meter (flow meter model DFM 2000, Copley Scientific Ltd., Nottingham, UK) was utilized. There was a 4-s breathe-in. The setup imitates a regular, healthy breathing rhythm with a 4 L inhalation volume. The powders were delivered using Breezhaler® single-dose devices (Novartis International AG, Basel, Switzerland) and size 3 gelatin capsules (Capsugel, Bornem, Belgium). It is a breath-activated device that administers drugs for asthma and chronic obstructive pulmonary disease. To simulate the conditions of pulmonary adhesion, the collecting plates on the stages were coated with a mixture of Span 85 and cyclohexane (1 + 99 w/w%). Following inhalation, the apparatus, capsules, induction port, plates, and filter were rinsed with methanol and pH 7.4 phosphate buffer (60 + 40 V/V%) to collect and dissolve the deposited MX. The API was measured using an ATI-UNICAM UV/VIS Spectrophotometer (Cambridge, UK) at a wavelength of 362 nm. The in vitro aerodynamic properties were evaluated with the support of the data analysis tool, Inhalytix™ (Copley Scientific Ltd., Nottingham, UK), which is a completely approved and verified aero-dynamic particle size distribution data analysis solution. The most frequently employed parameter is fine particle fraction (FPF). FPF is calculated as the percentage of the mass of the active ingredient containing particles with an aerodynamic diameter of less than 5 µm divided by the emitted dose of the formulations. Additionally, the emitted fraction (EF), also known as the released fraction from the DPI device, was calculated.

2.8. Statistical Analysis

The statistical analysis was carried out using GraphPad Prism 8.0.1 (GraphPad Software, CA, USA). The Student's *t*-test was employed to assess the statistical significance. Changes were determined to be statistically significant at *p* = 0.05.

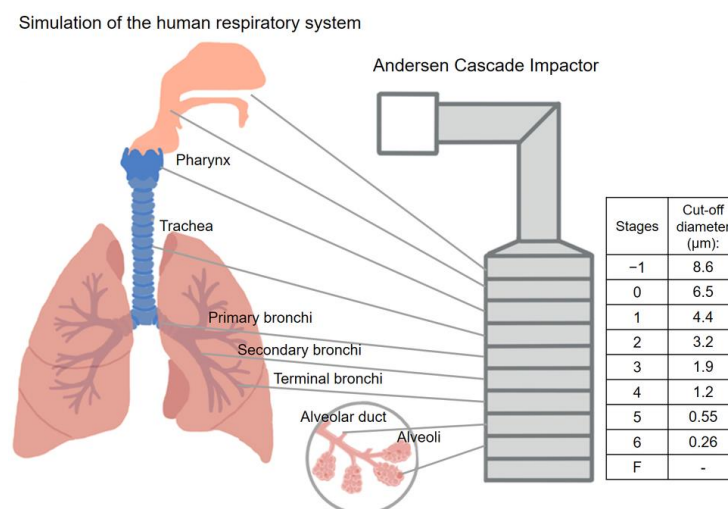


Figure 1. Correlation between the human respiratory system and the Andersen Cascade Impactor.

3. Results and Discussion

3.1. Characterization of Particle Size and Morphology

3.1.1. Laser Diffraction

The original particle of the MX was $D [0.5] = 9.913 \pm 0.371 \mu\text{m}$. As a result of wet milling, the particle size of API in the suspension decreased to $D [0.5] = 137.70 \text{ nm} \pm 4.965 \text{ nm}$. The reduced particle size and improved surface area of the particles lead to a faster dissolution rate [51]. After nano spray-drying, the $D [0.5]$ values of the samples were $1.429 \pm 0.09 \mu\text{m}$. For the treatment of deeper lung segments, the use of extra-fine built-up nanosized API could be advantageous [18,52]. According to the further particle size analysis, the particles of the products remained the same particle size during the testing period of the study (Table 2), proving that the particles did not agglomerate. The size was within the required 1 to 5 μm particle size range for pulmonary delivery [53]. The statistical analysis revealed that there was no noticeable variation in the particle size formulations over the storage period. The span values were between 1.3 and 1.6, which means that the distribution of the particles was monodisperse [54]. The monodisperse particle size distribution is crucial for proper lung deposition and dosage uniformity. The specific surface area (SSA) numbers slightly increased, suggesting that the dissolution of the drug may be improved.

Table 2. Particle sizes, spans, and SSA results of the samples.

Samples	D [0.1] (μm)	D [0.5] (μm)	D [0.9] (μm)	Span	SSA (m ² /g)
1 day	0.789 ± 0.02	1.429 ± 0.09	3.400 ± 0.50	1.586 ± 0.12	4.385 ± 0.01
6 months	0.800 ± 0.01	1.471 ± 0.05	3.110 ± 0.77	1.562 ± 0.47	4.445 ± 0.26
12 months	0.749 ± 0.01	1.441 ± 0.02	2.703 ± 0.03	1.357 ± 0.01	4.725 ± 0.06

Data are means ± SD ($n = 3$ independent measurements).

3.1.2. Dynamic Light Scattering

Table 2 shows the outcomes of the DLS investigation. DLS measured the liquid suspension of the particles. The particles were deagglomerated and resulted in decreased particle sizes compared to the laser diffraction. The diameters of the dispersed nano spray-dried particles were between 500 and 700 nm. It predicts that as the dry particles deposit into the lung fluid and disintegrate into nanoparticles, resulting in larger dissolution and cellular absorption [52]. Although there was an increase in particle diameter, the dry particle size is far more important in terms of lung deposition. Inhomogeneous distribution is shown by the relatively high PDI results ($\text{PDI} > 0.3$). However, it is not considered a problem if it does not negatively affect the drug release [39]. The ζ potential values were slightly decreased with time (Table 3). The systems are more degradable

and less retentive in the airways due to the negative ζ potential values of the spray-dried formulations. It is beneficial since the particles are unlikely to trigger further fibrosis, infection, or inflammation [55,56].

Table 3. Average particle diameter, polydispersity index, and ζ potential of samples.

Samples	d (nm)	PDI	ζ pot. (mV)
1 day	526.90 \pm 20.0	0.381 \pm 0.03	−24.50 \pm 1.47
6 months	548.57 \pm 35.9	0.382 \pm 0.03	−23.30 \pm 7.91
12 months	657.37 \pm 46.9	0.496 \pm 0.07	−22.23 \pm 0.55

Data are means \pm SD ($n = 3$ independent measurements).

3.1.3. Scanning Electron Microscopy

The stored samples were studied by SEM to understand the morphology of the particles. The SEM images of the spray-dried formulations showed spherical morphology (Figure 2). The optimized nano spray-drying created the spherical particle form [57]. The spray-dried spherical particles have a smaller contact area and a more uniform particle size distribution, which leads to a larger FPF compared to mechanically micronized drugs [58]. On the PVA surface, the MX nanoparticles were seen in a homogeneous distribution. The MX particles were covered with PVA, which helped their separation from one another [59]. Throughout the testing period, they showed no signs of aggregation. A slightly rougher surface can be observed because the humidity caused moisture absorption [60]. The results of the laser diffraction method were similar to the results of the ImageJ 1.53e software, which was utilized to determine the particle size based on the pictures (Table 4). The particle size of around 1 μ m is beneficial for deep pulmonary delivery.

3.2. Structural Investigation

3.2.1. Differential Scanning Calorimetry (DSC)

The DSC curves (Figure 3) throughout the testing period demonstrate that the partially amorphous characteristic of the samples did not change significantly. The original melting point of the MX was 246.55 $^{\circ}$ C; however, milling had the effect of lowering it to 240.87 $^{\circ}$ C. In the case of the DPI formulation, the character and size of the endothermic peak are nearly identical at each sample point (6 months: 238.46 $^{\circ}$ C, 12 months: 236.69 $^{\circ}$ C). The degrees of crystallinity of the samples ranged from 53 to 70% when compared to the PM, which was taken as 100% (Table 5).

Table 4. The particle sizes of the spray-dried samples according to the SEM images.

Samples	d (μ m)
1 day	1.106 \pm 0.29
6 months	1.240 \pm 0.40
12 months	1.060 \pm 0.19

Data are means \pm SD ($n = 100$ independent measurements).

Table 5. The crystallinity index (X_c) of the samples.

Samples	X_c (%)	
	DSC	XRPD
PM	100	100
1 day	69.92	49.81
6 months	53.91	42.51
12 months	53.67	41.89

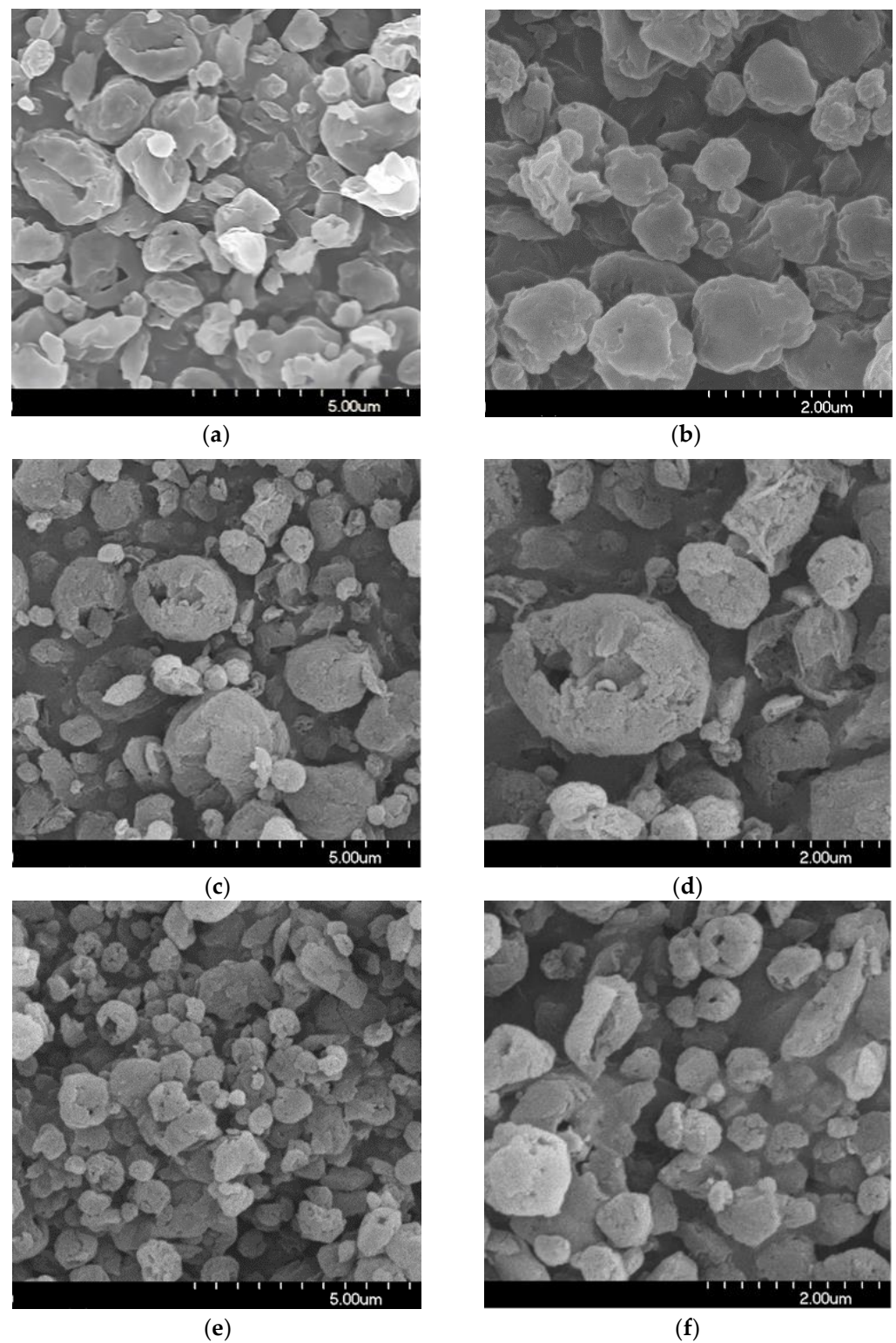


Figure 2. SEM records of the samples. (a) 1 day; (b) 1 day, (c) 6 months; (d) 6 months, (e) 12 months; (f) 12 months.

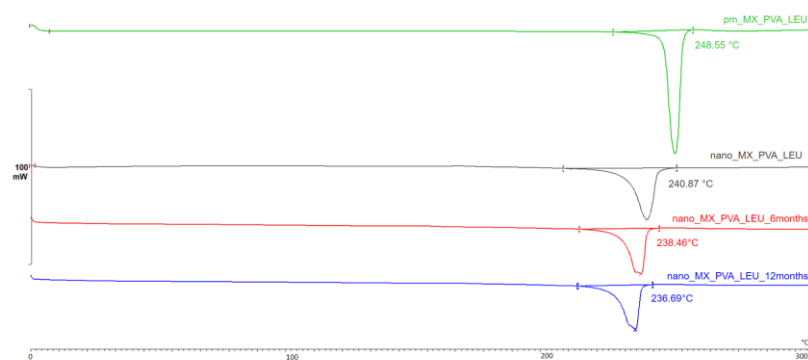


Figure 3. DSC curves of the samples.

3.2.2. X-ray Powder Diffraction (XRPD)

If the XRPD patterns of MX and the chosen excipients are known, XRPD can be used to observe the structural changes of the DPI samples throughout storage. Particularly, the properties of the active ingredient could be crucial because their crystalline or amorphous forms may result in morphological differences and affect the interactions between the particles, which could have an impact on the aerodynamic results. MX has characteristic peaks with the highest intensities at 6.6° , 11.4° , 13.1° , 13.5° , 15.1° , 18.7° , 19.3° , 25.9° , and 26.4° 2-theta peaks, indicating its crystalline structure. We detected the characteristic peaks of LEU at 6.12° , 24.39° , and 30.61° 2-theta peaks. The presence of PVA did not affect the diffractograms. The intensity of the peaks decreased in the 1-day sample as a result of the milling, and the crystallinity of the MX also decreased. This decreased crystallinity persisted at 6 and 12 months (Figure 4). The 1-day sample had a 49.81% crystallinity index, which did not change significantly throughout storage. The crystallinity indexes of the samples are shown in Table 5. The results of the measurement supported the DSC findings, indicating that the milling impact and the presence of PVA throughout the testing period caused the MX to become and remain partially amorphous.

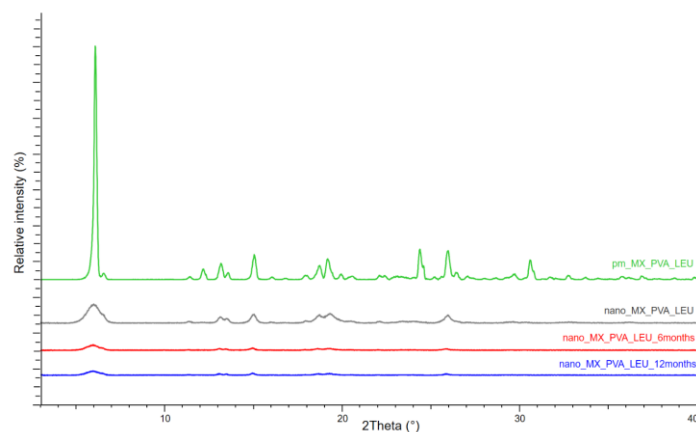


Figure 4. XRPD results of the samples.

3.3. In Vitro Drug Release Study

Figure 5 shows that the MX released quickly and in larger quantities in the case of the DPI samples than the PM. It is beneficial because the dissolution rate is the rate-limiting step for absorption of MX. The nanosized form, the increased surface area, and the partial amorphization of MX promoted a faster dissolution rate [61]. Furthermore, more API was released from the spray-dried samples than the PM because PVA prevented particle aggregation and LEU reduced cohesion between the particles. The rapid release was maintained. Furthermore, the drug release from stored samples was faster, possibly the water absorption on the surface helped the wettability of the particles. The outcomes

are beneficial in local treatment because the mucociliary clearance has minimal time to eliminate the particles [14,62].

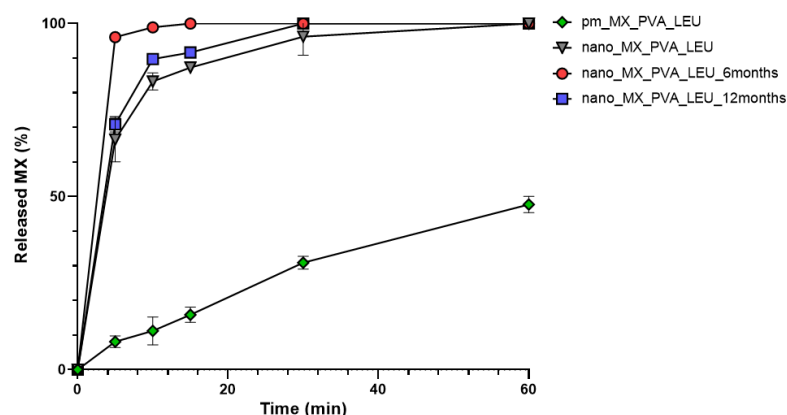


Figure 5. In vitro dissolution of the spray-dried samples and the physical mixture.

3.4. In Vitro Aerodynamic Properties

The distribution of the spray-dried samples was established during the aerodynamic analysis. Figure 6 illustrated how the samples were deposited on different areas of the set. An efficient MX deposition was on the third and fourth stages. The majority of the formulations reached the filter, which models the deeper lung region [63]. Successfully, the powder targeted the smaller airways even at the end of the stability study. The calculated in vitro aerodynamic results by Inhalytix™ V 2.0 software are presented in Table 6. The samples showed outstanding FPF values (93–95%), which exceed the FPF values of the commercially available formulations in the Breezhaler® inhalator. The high emitted fraction (EF) showed an insignificant decrease. The application of LEU improved the aerosolization of the products owing to the increased cohesion between the particles of the powder and the adhesion between the powder and the gelatine capsule.

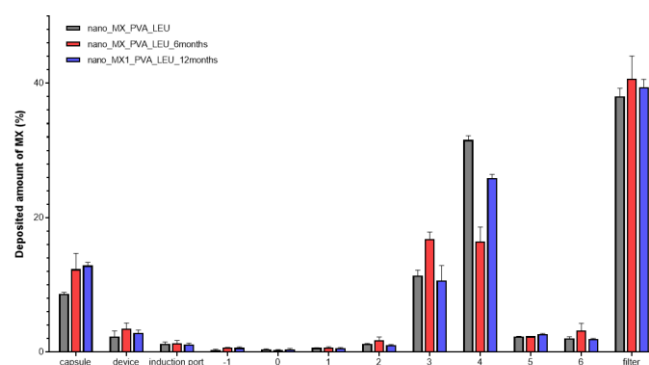


Figure 6. Distribution of the deposited MX in the ACI.

Table 6. FPF and EF of the spray-dried samples.

Samples	FPF by Size (%)	FPF by Stage (%)	EF (%)
1 day	94.94 ± 0.39	95.35 ± 0.39	89.04 ± 1.08
6 months	92.90 ± 0.80	93.39 ± 0.71	84.17 ± 3.20
12 months	93.85 ± 0.31	94.28 ± 0.38	84.27 ± 0.88

Data are means ± SD ($n = 3$ independent measurements).

4. Conclusions

In this study, the stability test of a carrier-free, novel DPI sample containing nanosized, non-steroidal, anti-inflammatory drug was examined at normal room conditions. After the

storage, the formulation presented advantageous characteristics, thanks to the technological steps and the compositions. Wet media milling is one of the most popular methods in the pharmaceutical field to produce stable nanosuspension of poorly water-soluble APIs. To optimize time and cost considerations and accurately predict milling performance at higher scales, a variety of modeling techniques could be used in the industry. The spray-drying technique has also been successfully applied at both laboratory and industrial scales. The advantages of a spray-dried powder include easy use and long shelf-life stability. The development of novel delivery methods can be a strategy for repositioning medications; therefore, it saves money and time for the pharmaceutical industry. The pulmonary route of MX could be an intriguing solution for treating different lung inflammation, which can be caused by SARS-CoV-2 infection, CF and COPD, and NSCLC. The excipients were pulmonary-approved materials. During the testing period, the particle size remained unchanged, while the particle size of MX in the formulation increased but did not differ significantly. Furthermore, the partially amorphous property of MX persisted throughout the stability examination. The outcomes of the dissolution test demonstrated that the initially large amount of drug was released from the samples in the examination time. The results suggest that PVA might inhibit the particles from aggregation and crystallizing. The aerosol performance of the formulated DPIs did not deteriorate. The sample has beneficial FPF and EF results after 12 months. The addition of LEU enhanced the aerosolization of the products. The outcome of this study demonstrates that the “nano-in.micro” DPI can maintain its quality for an extended period. According to ICH guidelines, further stability investigations are required, such as a test of the final package.

Author Contributions: Conceptualization and methodology, P.P. and R.A.; investigation, P.P.; evaluation, P.P.; writing—original draft, P.P.; writing—review and editing, R.A.; supervision, R.A. All authors have read and agreed to the published version of the manuscript.

Funding: The work was supported by Gedeon Richter’s Talentum Foundation, UNKP-21-3-SZTE-157 New National Excellence Program of the Ministry for Culture and Innovation from the source of National Research, Development and Innovation Fund and EFOP-3.6.2-16-2017-00006.

Data Availability Statement: We declare the real scientific content of our data.

Conflicts of Interest: The authors declare no conflict of interest.

References

1. ElKasabgy, N.A.; Adel, I.M.; Elmeligy, M.F. Respiratory Tract: Structure and Attractions for Drug Delivery Using Dry Powder Inhalers. *AAPS PharmSciTech* **2020**, *21*, 238. [\[CrossRef\]](#) [\[PubMed\]](#)
2. Yıldız-Peköz, A.; Ehrhardt, C. Advances in pulmonary drug delivery. *Pharmaceutics* **2020**, *12*, 911. [\[CrossRef\]](#) [\[PubMed\]](#)
3. Frijlink, H.W.; De Boer, A.H. Dry powder inhalers for pulmonary drug delivery. *Expert Opin. Drug Deliv.* **2004**, *1*, 67–86. [\[CrossRef\]](#) [\[PubMed\]](#)
4. Shetty, N.; Cipolla, D.; Park, H.; Zhou, Q.T. Physical stability of dry powder inhaler formulations. *Expert Opin. Drug Deliv.* **2020**, *17*, 77–96. [\[CrossRef\]](#)
5. Woodcock, A.; Janson, C.; Rees, J.; Frith, L.; Löfdahl, M.; Moore, A.; Hedberg, M.; Leather, D. Effects of switching from a metered dose inhaler to a dry powder inhaler on climate emissions and asthma control: Post-hoc analysis. *Thorax* **2022**, *77*, 1187–1192. [\[CrossRef\]](#)
6. Fulford, B.; Mezzi, K.; Whiting, A.; Aumônier, S. Life-cycle assessment of the breezhaler® breath-actuated dry powder inhaler. *Sustainability* **2021**, *13*, 6657. [\[CrossRef\]](#)
7. Levy, M.L.; Carroll, W.; Izquierdo Alonso, J.L.; Keller, C.; Lavorini, F.; Lehtimäki, L. Understanding Dry Powder Inhalers: Key Technical and Patient Preference Attributes. *Adv. Ther.* **2019**, *36*, 2547–2557. [\[CrossRef\]](#)
8. Demoly, P.; Hagedoorn, P.; De Boer, A.H.; Frijlink, H.W. The clinical relevance of dry powder inhaler performance for drug delivery. *Respir. Med.* **2014**, *108*, 1195–1203. [\[CrossRef\]](#)
9. Lechanteur, A.; Evrard, B. Influence of composition and spray-drying process parameters on carrier-free DPI properties and behaviors in the lung: A review. *Pharmaceutics* **2020**, *12*, 55. [\[CrossRef\]](#)
10. Miller, D.P.; Tarara, T.E.; Weers, J.G. Targeting of inhaled therapeutics to the small airways: Nanoleucine carrier formulations. *Pharmaceutics* **2021**, *13*, 1855. [\[CrossRef\]](#)
11. Chishti, N.; Dehghan, M.H. Nano-embedded microparticles based dry powder inhaler for lung cancer treatment. *J. Res. Pharm.* **2020**, *24*, 425–435. [\[CrossRef\]](#)

12. Thorley, A.J.; Tetley, T.D. New perspectives in nanomedicine. *Pharmacol. Ther.* **2013**, *140*, 176–185. [\[CrossRef\]](#) [\[PubMed\]](#)
13. Tse, J.Y.; Kadota, K.; Imakubo, T.; Uchiyama, H.; Tozuka, Y. Enhancement of the extra-fine particle fraction of levofloxacin embedded in excipient matrix formulations for dry powder inhaler using response surface methodology. *Eur. J. Pharm. Sci.* **2021**, *156*, 105600. [\[CrossRef\]](#)
14. Lin, L.; Quan, G.; Peng, T.; Huang, Z.; Singh, V.; Lu, M.; Wu, C. Development of fine solid-crystal suspension with enhanced solubility, stability, and aerosolization performance for dry powder inhalation. *Int. J. Pharm.* **2017**, *533*, 84–92. [\[CrossRef\]](#)
15. Malamataris, M.; Charisi, A.; Malamataris, S.; Kachrimanis, K.; Nikolakakis, I. Spray drying for the preparation of nanoparticle-based drug formulations as dry powders for inhalation. *Processes* **2020**, *8*, 788. [\[CrossRef\]](#)
16. Wang, W.; Huang, Z.; Huang, Y.; Zhang, X.; Huang, J.; Cui, Y.; Yue, X.; Ma, C.; Fu, F.; Wang, W.; et al. Pulmonary delivery nanomedicines towards circumventing physiological barriers: Strategies and characterization approaches. *Adv. Drug Deliv. Rev.* **2022**, *185*, 114309. [\[CrossRef\]](#)
17. Torge, A.; Grützmacher, P.; Mücklich, F.; Schneider, M. The influence of mannitol on morphology and disintegration of spray-dried nano-embedded microparticles. *Eur. J. Pharm. Sci.* **2017**, *104*, 171–179. [\[CrossRef\]](#)
18. Das, S.C.; Khadka, P.; Shah, R.; McGill, S.; Smyth, H.D.C. *Nanomedicine in Pulmonary Delivery*; Elsevier Inc.: Amsterdam, The Netherlands, 2021; ISBN 9780128204665.
19. Weers, J.G.; Miller, D.P. Formulation Design of Dry Powders for Inhalation. *J. Pharm. Sci.* **2015**, *104*, 3259–3288. [\[CrossRef\]](#)
20. Huang, Z.; Kłodzińska, S.N.; Wan, F.; Nielsen, H.M. Nanoparticle-mediated pulmonary drug delivery: State of the art towards efficient treatment of recalcitrant respiratory tract bacterial infections. *Drug Deliv. Transl. Res.* **2021**, *11*, 1634–1654. [\[CrossRef\]](#)
21. European Medicines Agency ICH Q1A (R2) Stability Testing of New Drug Substances and Drug Products—Scientific Guideline. Available online: <https://www.ema.europa.eu/en/ich-q1a-r2-stability-testing-new-drug-substances-drug-products-scientific-guideline> (accessed on 22 June 2023).
22. Rabinow, B.E. Nanosuspensions in drug delivery. *Nat. Rev. Drug Discov.* **2004**, *3*, 785–796. [\[CrossRef\]](#)
23. Wu, L.; Zhang, J.; Watanabe, W. Physical and chemical stability of drug nanoparticles. *Adv. Drug Deliv. Rev.* **2011**, *63*, 456–469. [\[CrossRef\]](#) [\[PubMed\]](#)
24. Party, P.; Kókai, D.; Burián, K.; Nagy, A.; Hopp, B.; Ambrus, R. Development of extra-fine particles containing nanosized meloxicam for deep pulmonary delivery: In vitro aerodynamic and cell line measurements. *Eur. J. Pharm. Sci.* **2022**, *176*, 106247. [\[CrossRef\]](#) [\[PubMed\]](#)
25. Meloxicam—Drugbank. Available online: <https://go.drugbank.com/drugs/DB00814> (accessed on 22 June 2023).
26. Chen, J.S.; Alfajaro, M.M.; Wei, J.; Chow, R.D.; Filler, R.B.; Eisenbarth, S.C.; Wilen, C.B. Cyclooxygenase-2 is induced by SARS-CoV-2 infection but does not affect viral entry or replication. *bioRxiv* **2020**. [\[CrossRef\]](#)
27. Ong, S.W.X.; Tan, W.Y.T.; Chan, Y.H.; Fong, S.W.; Renia, L.; Ng, L.F.P.; Leo, Y.S.; Lye, D.C.; Young, B.E. Safety and potential efficacy of cyclooxygenase-2 inhibitors in coronavirus disease 2019. *Clin. Transl. Immunol.* **2020**, *9*, e1159. [\[CrossRef\]](#) [\[PubMed\]](#)
28. Sarcinelli, M.A.; Martins da Silva, T.; Artico Silva, A.D.; Ferreira de Carvalho Patricio, B.; Mendes de Paiva, F.C.; Santos de Lima, R.; Leal da Silva, M.; Antunes Rocha, H.V. The pulmonary route as a way to drug repositioning in COVID-19 therapy. *J. Drug Deliv. Sci. Technol.* **2021**, *63*, 102430. [\[CrossRef\]](#)
29. Szabó-Révész, P. Modifying the physicochemical properties of NSAIDs for nasal and pulmonary administration. *Drug Discov. Today Technol.* **2018**, *27*, 87–93. [\[CrossRef\]](#)
30. Arafa, H.M.M.; Abdel-Wahab, M.H.; El-Shafeey, M.F.; Badary, O.A.; Hamada, F.M.A. Anti-fibrotic effect of meloxicam in a murine lung fibrosis model. *Eur. J. Pharmacol.* **2007**, *564*, 181–189. [\[CrossRef\]](#)
31. Yokouchi, H.; Kanazawa, K.; Ishida, T.; Oizumi, S.; Shinagawa, N.; Sukoh, N.; Harada, M.; Ogura, S.; Munakata, M.; Dosaka-Akita, H.; et al. Cyclooxygenase-2 inhibitors for non-small-cell lung cancer: A phase II trial and literature review. *Mol. Clin. Oncol.* **2014**, *2*, 744–750. [\[CrossRef\]](#)
32. Weiss, A.; Porter, S.; Rozenberg, D.; O'Connor, E.; Lee, T.; Balter, M.; Wentlandt, K. Chronic Obstructive Pulmonary Disease: A Palliative Medicine Review of the Disease, Its Therapies, and Drug Interactions. *J. Pain Symptom Manag.* **2020**, *60*, 135–150. [\[CrossRef\]](#)
33. Pilcer, G.; Amighi, K. Formulation strategy and use of excipients in pulmonary drug delivery. *Int. J. Pharm.* **2010**, *392*, 1–19. [\[CrossRef\]](#)
34. Bilgili, E.; Guner, G. Mechanistic Modeling of Wet Stirred Media Milling for Production of Drug Nanosuspensions. *AAPS PharmSciTech* **2021**, *22*, 2. [\[CrossRef\]](#)
35. Seibert, K.D.; Collins, P.C.; Luciani, C.V.; Fisher, E.S. Milling operations in the pharmaceutical industry. In *Chemical Engineering in the Pharmaceutical Industry*; John Wiley & Sons, Inc.: Hoboken, NJ, USA, 2019; pp. 861–879. [\[CrossRef\]](#)
36. Singare, D.S.; Marella, S.; Gowthamrajan, K.; Kulkarni, G.T.; Vooturi, R.; Rao, P.S. Optimization of formulation and process variable of nanosuspension: An industrial perspective. *Int. J. Pharm.* **2010**, *402*, 213–220. [\[CrossRef\]](#)
37. Kumar, R.; Thakur, A.K.; Chaudhari, P.; Banerjee, N. Particle Size Reduction Techniques of Pharmaceutical Compounds for the Enhancement of Their Dissolution Rate and Bioavailability. *J. Pharm. Innov.* **2022**, *17*, 333–352. [\[CrossRef\]](#)
38. Party, P.; Bartos, C.; Farkas, Á.; Szabó-Révész, P.; Ambrus, R. Formulation and In Vitro and In Silico Characterization of “Nano-in-Micro” Dry Powder Inhalers Containing Meloxicam. *Pharmaceutics* **2021**, *13*, 211. [\[CrossRef\]](#)
39. Party, P.; Klement, M.L.; Révész, P.S.; Ambrus, R. Preparation and Characterization of Ibuprofen Containing Nano-Embedded-Microparticles for Pulmonary Delivery. *Pharmaceutics* **2023**, *15*, 545. [\[CrossRef\]](#)

40. Müller, T.; Krehl, R.; Schiewe, J.; Weiler, C.; Steckel, H. Influence of small amorphous amounts in hydrophilic and hydrophobic APIs on storage stability of dry powder inhalation products. *Eur. J. Pharm. Biopharm.* **2015**, *92*, 130–138. [\[CrossRef\]](#)
41. Ordoubadi, M.; Shepard, K.B.; Wang, H.; Wang, Z.; Pluntze, A.M.; Churchman, J.P.; Vehring, R. On the Physical Stability of Leucine-Containing Spray-Dried Powders for Respiratory Drug Delivery. *Pharmaceutics* **2023**, *15*, 435. [\[CrossRef\]](#)
42. Strojewski, D.; Krupa, A. Spray drying and nano spray drying as manufacturing methods of drug-loaded polymeric particles. *Polim. Med.* **2022**, *52*, 101–111. [\[CrossRef\]](#)
43. Salama, A.H. Spray drying as an advantageous strategy for enhancing pharmaceuticals bioavailability. *Drug Deliv. Transl. Res.* **2020**, *10*, 1–12. [\[CrossRef\]](#)
44. Sibum, I.; Hagedoorn, P.; Kluitman, M.P.G.; Kloezen, M.; Frijlink, H.W.; Grasmeijer, F. Dispersibility and storage stability optimization of high dose isoniazid dry powder inhalation formulations with L-leucine or trileucine. *Pharmaceutics* **2020**, *12*, 24. [\[CrossRef\]](#)
45. Vehring, R. Pharmaceutical particle engineering via spray drying. *Pharm. Res.* **2008**, *25*, 999–1022. [\[CrossRef\]](#) [\[PubMed\]](#)
46. Gieszinger, P.; Katona, G.; Szabó-Révész, P.; Ambrus, R. Stability study of nasal powder formulation containing nanosized lamotrigine. *Acta Pharm. Hung.* **2020**, *90*, 27–31. [\[CrossRef\]](#)
47. Benke, E.; Farkas, Á.; Balásházy, I.; Szabó-Révész, P.; Ambrus, R. Stability test of novel combined formulated dry powder inhalation system containing antibiotic: Physical characterization and in vitro–in silico lung deposition results. *Drug Dev. Ind. Pharm.* **2019**, *45*, 1369–1378. [\[CrossRef\]](#) [\[PubMed\]](#)
48. Shahin, H.I.; Chablani, L. A comprehensive overview of dry powder inhalers for pulmonary drug delivery: Challenges, advances, optimization techniques, and applications. *J. Drug Deliv. Sci. Technol.* **2023**, *84*, 104553. [\[CrossRef\]](#)
49. Parlati, C. *Respirable Microparticles of Aminoglycoside Antibiotics for Pulmonary Administration*; University of Parma: Parma, Italy, 2008.
50. European Directorate for the Quality of Medicines. Section 2.9. 18—Preparations for Inhalation: Aerodynamic Assessment of Fine Particles. In *European Pharmacopoeia 10.0*; Council of Europe: Strasbourg, France, 2019; p. 354. ISBN 9789287189127.
51. Dubey, R. Impact of nanosuspension technology on drug discovery and development. *Drug Deliv. Technol.* **2006**, *5*, 67–71.
52. Scherließ, R.; Bock, S.; Bungert, N.; Neustock, A.; Valentin, L. Particle engineering in dry powders for inhalation. *Eur. J. Pharm. Sci.* **2022**, *172*, 106158. [\[CrossRef\]](#)
53. Darquenne, C. Aerosol deposition in health and disease. *J. Aerosol Med. Pulm. Drug Deliv.* **2012**, *25*, 140–147. [\[CrossRef\]](#)
54. Chvatal, A.; Farkas, Á.; Balásházy, I.; Szabó-Révész, P.; Ambrus, R. Aerodynamic properties and in silico deposition of meloxicam potassium incorporated in a carrier-free DPI pulmonary system. *Int. J. Pharm.* **2017**, *520*, 70–78. [\[CrossRef\]](#)
55. Dailey, L.A.; Kleemann, E.; Wittmar, M.; Gessler, T.; Schmehl, T.; Roberts, C.; Seeger, W.; Kissel, T. Surfactant-Free, Biodegradable Nanoparticles for Aerosol Therapy Based on the Branched Polyesters, DEAPA-PVAL-g-PLGA. *Pharm. Res.* **2003**, *20*, 2011–2020. [\[CrossRef\]](#)
56. Jones, R.M.; Neef, N. Interpretation and prediction of inhaled drug particle accumulation in the lung and its associated toxicity. *Xenobiotica* **2012**, *42*, 86–93. [\[CrossRef\]](#)
57. Arpagaus, C.; Collenberg, A.; Rütli, D.; Assadpour, E.; Jafari, S.M. Nano spray drying for encapsulation of pharmaceuticals. *Int. J. Pharm.* **2018**, *546*, 194–214. [\[CrossRef\]](#)
58. Aspragus, C.; Schafroth, N.; Meuri, M. Laboratory Scale Spray-Drying of Lactose: A Review. Available online: https://www.researchgate.net/publication/267830231_Laboratory_scale_spray-drying_of_lactose_A_review (accessed on 22 June 2023).
59. Bartos, C.; Ambrus, R.; Sipos, P.; Budai-Szucs, M.; Csányi, E.; Gáspár, R.; Márki, Á.; Seres, A.B.; Sztojok-Ivanov, A.; Horváth, T.; et al. Study of sodium hyaluronate-based intranasal formulations containing micro- or nanosized meloxicam particles. *Int. J. Pharm.* **2015**, *491*, 198–207. [\[CrossRef\]](#)
60. Sabuj, M.Z.R.; Rashid, M.A.; Dargaville, T.R.; Islam, N. Stability of Inhaled Ciprofloxacin-Loaded Poly(2-ethyl-2-oxazoline) Nanoparticle Dry Powder Inhaler Formulation in High Stressed Conditions. *Pharmaceutics* **2022**, *15*, 1223. [\[CrossRef\]](#)
61. Tang, B.C.; Dawson, M.; Lai, S.K.; Wang, Y.Y.; Suk, J.S.; Yang, M.; Zeitlin, P.; Boyle, M.P.; Fu, J.; Hanes, J. Biodegradable polymer nanoparticles that rapidly penetrate the human mucus barrier. *Proc. Natl. Acad. Sci. USA* **2009**, *106*, 19268–19273. [\[CrossRef\]](#)
62. Ruge, C.C.; Kirch, J.; Lehr, C.M. Pulmonary drug delivery: From generating aerosols to overcoming biological barriers—therapeutic possibilities and technological challenges. *Lancet Respir. Med.* **2013**, *1*, 402–413. [\[CrossRef\]](#)
63. Chapman, K.R.; Fogarty, C.M.; Peckitt, C.; Lassen, C.; Jadayel, D.; Dederichs, J.; Dalvi, M.; Kramer, B. Delivery characteristics and patients’ handling of two single-dose dry-powder inhalers used in COPD. *Int. J. Chronic Obstr. Pulm. Dis.* **2011**, *6*, 353–363. [\[CrossRef\]](#)

Disclaimer/Publisher’s Note: The statements, opinions and data contained in all publications are solely those of the individual author(s) and contributor(s) and not of MDPI and/or the editor(s). MDPI and/or the editor(s) disclaim responsibility for any injury to people or property resulting from any ideas, methods, instructions or products referred to in the content.